Supercritical Water Gasification of Biomass

Daniele Castello

UNIVERSITÀ DEGLI STUDI DI TRENTO

**Dipartimento di Ingegneria Civile,
Ambientale e Meccanica**

2013

Doctoral thesis in **Environmental Engineering, 25th cycle**

Department of Civil, Environmental and Mechanical Engineering, **University of Trento**

Academic year **2012/2013**

Supervisor: **Dr. Luca Fiori, DICAM**

University of Trento

Trento, Italy

February 2013

To my parents

In memory of granny Lina

***Nothing is lost,
nothing is created:
everything is transformed.***

*Antoine A. Lavoisier
(1743 - 1794)*

Contents

List of Figures

List of Tables

Acknowledgments

The scientific work carried out in this three-year period has been possible thanks to several people and organizations, to whom I would like to express all my personal reconnaissance.

First of all, I would like to thank the University of Trento for having funded my PhD scholarship. I am particularly grateful to my supervisor, Dr. Luca Fiori, who has believed in this project and has always given me large autonomy of work. I would like to say "thank you" not only for having been my mentor, but also for his human attitude, which resulted in a friendly work relationship. The things I learnt by him in these three years will guide me for all my future working experiences.

I would like also to acknowledge all the staff of the Institute of Catalysis Research and Technology, at the Karlsruhe Institute of Technology (Germany), for the nine-month period I spent there as a visiting PhD candidate. Special thanks go to the team leader: Prof. Andrea Kruse. I really enjoyed the possibility to perform on-field research and to have interesting talks with an experienced researcher as her. Nonetheless, this experience abroad has been possible thanks to the financial support of the European Commission, through the mobility program "Erasmus", which I would like to equally thank.

A person I would like to acknowledge is my master thesis advisor, Dr. Mario Iamarino from the University of Basilicata. He first introduced me to the world of research and transmitted me this great passion. If I decided to enroll in a PhD program after graduating, I owe it to him.

The greatest and absolute acknowledgment goes to my parents. I would like to say them "thank you" because they gave me the possibility to study up to the PhD, always supporting my choices even though they meant going 1,000 km away from home. Thank you, because you have always been there when I was in the need. This thesis, which is the result of three years of train travels, food packages and Skype calls at night, is dedicated to you.

Finally, I would like to thank God for everything He has given to me. I ask Him to bless also this thesis, which is the fruit of my work. I put it in His hands and I hope He could grow, from this small seed, a big harvest to be shared with many other people.

Summary

Renewable energy is gaining a more and more important role during the last few years. Global warming issues are in fact pushing the economies towards newer and more respectful technologies which could have a reduced impact on the environment. Moreover, fossil fuels are experiencing a large shortage. The cost of oil derived fuels is increasing on an almost daily basis. Furthermore, fossil resources are not well distributed all over the world, which sometimes results in socio-economical conflicts. Thus, the need to find an energy source with small impact on the environment, renewable and possibly well-distributed is becoming increasingly more important.

Biomass can fulfill all of these requirements. If it is grown in an appropriate way, biomass is fully renewable and it can have limited or even no impact on the environment. The carbon released in the atmosphere by its thermal processing is the same stored in the organic tissues during the living being's life: the net balance is then neutral. Furthermore, biomass is much more homogeneously diffused in the world than fossil resources. On the other hand, common thermo-chemical technologies for biomass exploitation usually require dry biomass in order to ensure process sustainability and profitability. They thus drop out wet biomass, which represents a huge part of the overall amount: organic waste and agro-industrial byproducts are included in this category. A technology to treat such feedstock would thus be extremely beneficial, allowing to convert an abundant and inexpensive material into energy, with great economic and environmental advantages.

This work analyzes a novel technology for biomass energy valorization: supercritical water gasification (SCWG). Such process consists in reacting biomass with supercritical water, that is water above its critical point (T>374.15°C; P>221 bar). Unlike common gasification technologies, SCWG can provide significant advantages. First of all, it is able to treat wet biomass, since water is a reactant itself. Moreover, SCWG is able to greatly reduce char and tar formation, thus minimizing clogging and plugging problems and increasing gasification yields. Furthermore, under appropriate process conditions, hydrogen production can be greatly enhanced.

An overview of thermo-chemical processes for biomass energy valorization is given in Chapter 1. Special focus is given to hydrothermal processes, which are the class of technologies involving biomass processing with hot pressurized water. Aqueous phase reforming, hydrothermal carbonization and hydrothermal liquefaction are shortly described and compared, highlighting their specific issues, advantages and disadvantages. The attention is then shifted to supercritical water, whose unique properties (e.g. density, dielectric constant, ionic product) are presented. Processes involving biomass and supercritical water are outlined: supercritical water oxidation (SCWO) and supercritical water gasification (SCWG). A comprehensive state of the art of the latter is provided by classifying the existing literature into four areas: studies with model compounds, studies with real biomass, catalysis, mathematical modeling and reactor technology.

The attention is then shifted to thermodynamic equilibrium modeling. Such aspect allows understanding which is the system composition at equilibrium and investigating how process parameters like temperature, pressure and biomass concentration affect the process outputs. In Chapter 2 a thermodynamic non-stoichiometric model, based on Gibbs free energy minimization, is presented. Such model is able to deal with the formation of a gaseous phase and of a solid phase at equilibrium. The model, validated by means of literature data, enables to state the influence of several process variables (e.g. temperature, pressure and biomass concentration) on the gas composition and the formation of solids at equilibrium. The model also allows performing an analysis of the energy needs of the process, which shows that supercritical water gasification can be an auto-thermal or even exothermal process.

Chapter 3 focuses on chemical kinetics modeling. This is a pioneer field, since only a few works have been presented in the literature so far. In this work, detailed modeling for methanol SCWG is presented. This compound was selected because it is one of the simplest organic compounds and its kinetics could be still described in terms of elementary reactions. Nevertheless, such analysis helps to understand the main reaction mechanisms involved in SCWG, with general conclusions that can be extended also to other feedstock. Three different models, which have been originally conceived for oxidative processes (SCWO or simple combustion) are presented and implemented for methanol SCWG. Results show that good accordance with literature experimental data can be found. The kinetics model also allows drawing the main reaction mechanisms, which help to understand the

main phenomena involved in SCWG. Some improvements to the models are provided as well.

Thermodynamics and kinetics modeling can be seen as a tool helping to understand which are the main phenomena involved in SCWG. On the other hand, in order to develop an industrial process, not only the study of the SCWG reactions is useful, but a series of unit operations must be arranged to achieve process performances and sustainability. This is the aim of Chapter 4, which is devoted to process modeling. A process conceptual design for a throughput of 1000 kg/h is presented and implemented through the commercial process simulator Aspen Plus®. The goal of the proposed process is to produce pure hydrogen in order to feed fuel cells or a fuelling station. The process design is intended to maximize such production achieving, at the same time, the complete energy sustainability (i.e. no additional fuel has to be utilized to run the process). Technical constraints are taken into account as well, for example the impossibility to recover all the process heat and the necessity to dispose of the waste heat in an economically reasonable way. The simulation, conducted for different types of biomass, revealed that solid matter concentrations in the feed of at least 15-20% can reasonably guarantee process sustainability.

The work goes on with the report of experimental tests conducted at the laboratories of the Karlsruhe Institute of Technology (KIT). Chapter 5 focuses on batch SCWG tests performed on model compounds. Such tests are carried out in micro-autoclaves, which allow safe and fast operations. Solid, liquid and gaseous products are collected and analyzed. The different behavior of glucose (model compound for cellulose) and glucose-phenol mixtures (phenol can be considered as a model compound for lignin) is investigated. Tests are conducted at different temperatures, both in supercritical and subcritical water. Moreover, all the tests are performed with micro-autoclaves made of different materials: stainless steel, Inconel® 625. The results show that the reactor material has remarkable influence on syngas composition. Scanning electron microscope (SEM) images of the inner parts of the reactors are taken in order to try to explain the observed differences.

Chapter 6 adopts a similar methodology applied to real biomass. In this case, different substrates are considered, ranging from ligno-cellulosic biomass to municipal organic wastes and agro-industrial byproducts. The Chapter is divided into three sections. The first one involves experiments on beech sawdust – a ligno-cellulosic biomass – following the same procedure used for glucose in the previous Chapter. The second section involves the supercritical water gasification of hydrothermal char, that is the product of the HTC (Hy-

dro Thermal Carbonization) process. For such biomass, tests with different residence time were performed and SEM observations of the solid samples obtained after gasification were conducted, in order to see how reaction modifies the structure of the feedstock. The third section involves long-time testing with four different biomasses: besides beech sawdust and hydrothermal char, municipal waste and malt spent grains were used for SCWG tests involving 16 hours of residence time. The results were compared with thermodynamic equilibrium models forecasts. For these tests, a ceramics reactor was also adopted. An alkali catalyst (K_2CO_3) was added in order to improve gasification yields.

After batch experiments, SCWG continuous processes are also considered, which are closer to the process conditions of possible industrial-scale applications. Chapter 7 is dedicated to the tests performed with a continuous tubular reactor, operated at 400°C. Different tests are made, using glucose and glucose/phenol mixtures, with increasing relative content of phenol. The experimental plant is operated at steady state at 400°C, and residence times in the range of 10-240 seconds are adopted. The effect of phenol, which lowers the gasification yields, is clearly seen. Gas and liquid compositions are also determined. Finally, some issues about the role of phenol and the formation of intermediates in the liquid phase are discussed.

Chapter 1

Biomass and Supercritical Water

In this Chapter, a general overview of the core topic of the present work is provided. First, the importance of biomass as an energy source is presented, along with the technologies for its energetic exploitation. The focus is then moved to hydrothermal processes and, especially, to supercritical water gasification. After presenting the most relevant physical and chemical properties of supercritical water, the state of the art in SCWG is drawn. Finally, the aims of the present work are stated.

1.1. Biomass as a renewable energy source

The development of renewable energy sources in order to face the world's future problems is acquiring growing importance on account of several factors. First of all, a significant shortage of fossil fuels (oil, gas and carbon) is foreseen for the next few decades as a result of growing worldwide demand, boosted by developing countries. Secondly, fossil fuels are located to a great extent in politically and socially unstable regions, which makes their exports subject to fluctuations in prices and supply. Finally, global warming issues, mostly related to CO_2 releases in the atmosphere caused by thermo-electric power plants and, more generally, by combustion plants utilizing fossil fuels, have called on many national governments to look for alternative and more environmental-friendly ways to produce energy.

One of the ways for renewable energy production is represented by biomass. Biomass can be defined as the «biological material from living, or recently living organisms, most often referring to plants or plant-derived materials» [1]. Inside this widespread definition, a huge number of compounds are comprised: vegetables, wood, algae, organic wastes, agro-industrial byproducts are only some of the materials that can fall under the definition "biomass".

Biomass presents two main advantages with respect to conventional fossil energy resources. One thing making it very popular is the fact that it can be considered carbon neutral. This means that, when burned or decomposed, biomass releases in the atmosphere the same quantity of carbon, as CO_2, that was stored in it during the living being's life cycle.

This implies that biomass constitutes a sort of "closed loop" of carbon and it does not contribute to CO_2 emission, which are claimed of being one of the most important causes of global warming.

Though these considerations are true in general, it must be paid attention that biomass is factually carbon neutral if and only if it is grown and exploited in an appropriate way. For instance, if biomass is harvested in a place located at large distance from the energy conversion plant, the impact of transportation may overcome the advantages of using a renewable fuel. Moreover, if an increased usage of biomass results in huge deforestation, the impact on atmospheric CO_2 would be still negative, in case even worse than fossil fuels [2]. The environmental impacts on air emissions, resource depletion and land use change should be thus carefully investigated case by case. Hence, it is more correct to say that biomass is a carbon neutral renewable source only if it is grown and managed in a proper (sustainable) way.

Another fundamental advantage of using biomass as an energy source is represented by its widespread diffusion. An examination of the world's proved reserves of coal, crude oil and natural gas and their regional locations shows that well over half of the world's crude oil and natural gas supplies are located in the Middle East and Russia, while North America, the Far East and Russia have over 70% of the coal reserves [3]. This means that fossil resources are concentrated only in some areas of the world. This state of fact is problematic, since the supply of these resources resents of the geopolitical situation of the producing states. This can result in economic speculations or sometimes in geopolitical conflicts among the nations.

Biomass distribution is much more equal than the one of fossil resources. It can be said that in every part of the (populated) world there is biomass, though in different forms: forests, agricultural residues, algae, grass, etc. Improving the capacity of exploiting an increasing portion of the overall biomass would be greatly beneficial in order to guarantee a global access to energy.

Finally, the most important concern about traditional fossil fuel is represented by their shortage. The rate of consumption of fossil fuels, and especially of oil and natural gas, is steadily increasing as world's population and developing countries' economic conditions rise. On the other hand, fossil hydrocarbons need extremely long time scales to be regenerated. The process of oil formation takes place along geological eras, while the "oil age" has started since no more than 150 years.

It is thus very reasonable to foresee that, in a finite number of years, the available fossil resources will be depleted. To this purpose, it is worthy to recall Hubbert's peak theory, which foresees that global production of oil and other fossil resources follows a bell-like trend, with a peak of maximum production. Updated calculations, based on Hubbert's approach, can be found in [4] and are visually reported in Figure 1.1. It can be seen that oil peak will be achieved in only a few years. Natural gas and coal peaks occur later, but still in the first half of this century.
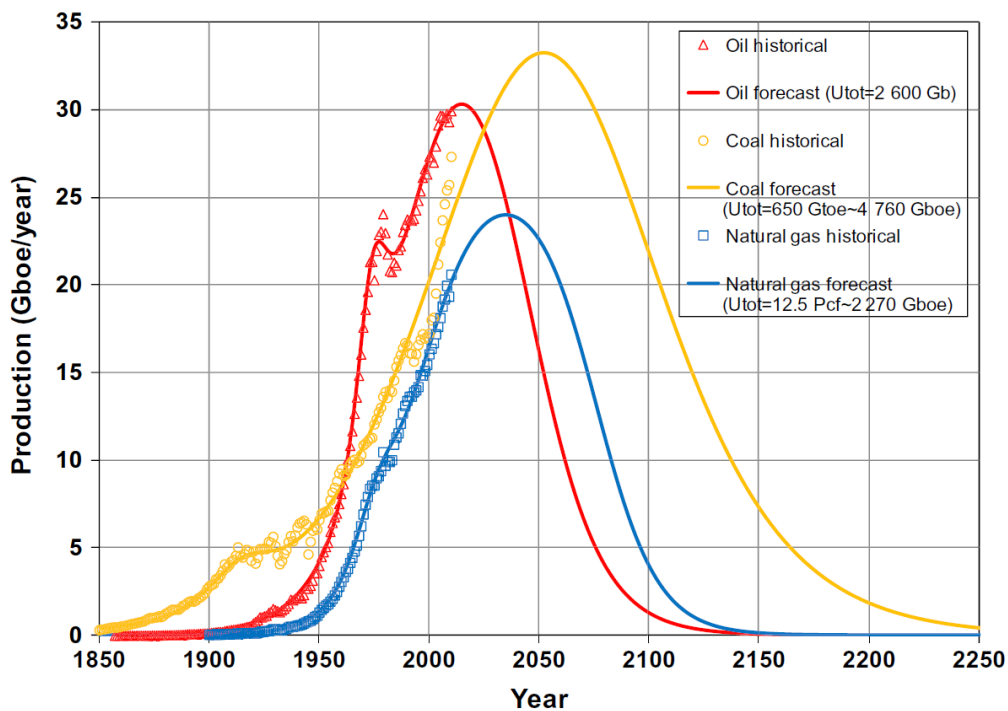
Figure 1.1 – Foreseen trend of fossil fuel production in the mid-long term according to Maggio and Cacciola [4].

By the way, it must be stated that, well before the complete run out of oil and natural gas, their prices will progressively increase, according to the law of supply and demand. Providing efficient fuels with a considerably lower regeneration time to substitute oil in the mid-long term is thus necessary.

1.1.1. Biomass conversion into energy

The usage of biomass as an energy source dates back to time immemorial. It can be reasonably thought that the first way man used to produce heat for its necessities was to put wood on fire. Quite soon, mankind learnt to perform more efficient ways of firing biomass, for example by converting it into charcoal. Firing wood or charcoal had been the

main way of producing energy for many centuries, at least up to the industrial revolution, when coke and, later, fossil oil and gas were used to power mechanical machines. Although it lost its favored role, biomass has still conserved an important role in thermal energy production up to nowadays, especially in rural areas.

Besides direct combustion, there are many other different ways to produce energy from biomass and they can be classified into two main branches, according to the nature of the transformations: biochemical processes and thermochemical processes.

Biochemical technologies involve biomass transformations operated by bacteria and micro-organisms. The most popular technology in this field is anaerobic fermentation. In this process, a pool of specific bacteria is able to assimilate some biomass substrates in order to grow and reproduce, in absence of oxygen. The metabolic activity of such microorganisms causes the production of a mixture of carbon dioxide and methane, which has a limited but acceptable heating power. The resulting gas can be burned in internal combustion engines or turbines to provide both thermal and electrical energy.

Such technology is very useful, since it can deal with waste biomass, also with high moisture content. Additionally, the technology involved is relatively simple if compared to the thermochemical ones. This has allowed a widespread diffusion of anaerobic fermentation, in special way in the field of wastewater sludge, organic waste and manure treatment.

The other large area of biomass-to-energy technologies is represented by thermochemical processes. This kind of processes are conducted under high temperature conditions. High temperatures, possibly with addition of an oxidant, are able to convert biomass into solid, liquid or gaseous products. Direct combustion falls in this category.

It was already mentioned the carbonization process, aimed at production a solid fuel from biomass. Here, biomass undergoes a pyrolysis, that is heating in absence of oxygen. In particular, to achieve carbonization pyrolysis is conducted very slowly. This treatment causes the solid product to enrich in carbon, since the most volatile oxygenated compounds migrate to the gas phase. As a result, a lower mass of solid fuel is obtained, but with much higher energy density.

Thermochemical technologies can also serve to produce liquid fuels. This role is achieved by means of fast pyrolysis, where the feedstock is reacted at high temperature in absence of oxygen, but with a very fast heating rate. Under such conditions, biomass is mainly converted into a liquid, usually defined "bio-oil" or "bio-crude". It is a black and

viscous liquid, composed by a high number of organic oxygenated compounds, which can be burned or further refined to other fuels and chemicals.

Table 1.1 – Biomass availability in the European Union (27 countries) [5].

Feedstock type	Available quantity [kt/y]	Energy potential [ktoe/y]		
		2000	2010	2020
Agricultural biomass				
Solid agricultural residues	76,128	32,729	36,153	39,936
Wet manure	65,808	14,145	15,623	17,260
Dry manure	10,630	2,226	2,459	2,716
Forest biomass				
Forest by-products	40,692	17,494	19,325	21,346
Refined wood fuels	57,200	24,592	27,164	30,006
Industrial biomass				
Solid industrial residues	30,103	12,942	14,296	15,792
Black liquor	44,265	10,573	11,679	12,901
Sewage sludge	9,945	2,135	2,362	2,609
Waste biomass				
Biodegradable municipal waste				
Landfill gas		5,072	4,675	2,489
Incineration		7,116	19,010	33,708
Demolition wood	13,585	5,841	6,452	7,127
TOTAL		**134,865**	**159,198**	**185,890**

When the aim is to convert biomass into a fuel gas, the process is named "gasification". Gasification is one of the most promising technologies [6, 7], as it provides a gaseous product which can be directly burnt in engines or turbines to produce electrical power. Standard gasification technologies are based on the partial oxidation of biomass, i.e. a reaction where oxygen is supplied below the stoichiometric amount. A gaseous mixture, whose main compounds are H_2, CO and CO_2 is produced through such operations. An alternative solution is that of processing biomass through steam, thus achieving a steam reforming reaction. In this case, H_2 and CH_4 are produced in higher amounts, although the process re-

quires large quantities of energy [6]. Other options have been proposed, for instance the usage of an air-CO_2 mixture as gasifying agent [8].

A major drawback, common to all these thermochemical technologies, is that they are practically limited to dry or almost dry biomass, such as wood, straw, etc. A high moisture content would considerably lower the energy performance of the process, since the presence of water in the feedstock results in a further demand of thermal energy, to ensure its evaporation [6]. This is a strong limitation, since wet biomass represents a large portion of the available biomass resources. In this category, indeed, the largest part of agro-industrial wastes, vegetables and municipal waste are included. It can be observed in Table 1.1, which reports the biomass potential in the European Union, that wet biomass represents a very large amount of the total biomass potential. Nonetheless, these biomass materials are often associated to environmental issues, since they are many times observed as waste material to be disposed of in some way.

In order to provide effective energy valorization of waste biomass, a novel class of thermochemical processes has been developed, based on the idea of turning the high water content from a drawback to an advantage. These processes are commonly named "hydrothermal processes", as they take place in hot, pressurized water.

1.2. Hydrothermal processing of biomass

One of the thermochemical routes to produce energy and, possibly, chemicals from biomass is represented by the so called hydrothermal processes. These are processes carried out using hot pressurized water. For these processes, it is necessary to operate with higher pressures than the atmospheric one, since they are normally conducted with liquid water. The boiling temperature of water, indeed, rises as pressure is increased.

Hydrothermal processes are usually classified according to the their final product. Thus, we have: hydrothermal carbonization (HTC), hydrothermal liquefaction (HTL), aqueous phase reforming (APR) and supercritical water gasification (SCWG). In this paragraph, the first three processes will be briefly presented, while SCWG will be the focus of the subsequent Paragraph 1.4.

1.2.1. Aqueous phase reforming

Aqueous phase reforming (APR) is a process intended to produce a fuel gas from biomass, especially from carbohydrates and polyols (e.g. methanol, ethylene glycol, glycerol). It

can be considered as an upgrade of the traditional steam reforming process, where water is utilized in its vapor phase.

APR involves the utilization of liquid water at moderate temperature, around 220°C, with pressures in the range of 15-50 bar. This combination of temperature-pressure corresponds to the range in which water-gas shift reaction is favorable, thus allowing to enhance H_2 production and eliminate the production of CO. These important objectives can be achieved in a single-step process, unlike conventional multi-reactor processes, necessary for steam reforming [9].

Some substrate have been used for APR experiments. Results show that methanol exhibits a very high selectivity towards H_2 when a Pt/Al_2O_3 catalyst is adopted [10].

Catalysts are needed for the APR process. The optimal choice would be a material able to promote C-C bond cleavage, in order to decompose biomass, and the removal of CO by means of water-gas shift reaction. Commonly used catalysts are made of platinum and nickel, on a silica support [11].

1.2.2. Hydrothermal carbonization

When operating at relatively low temperatures, a solid product can be obtained from wet biomass. In this case, the main objective is to obtain a solid product where most carbon of the original feedstock could be stored. The resulting process is named "hydrothermal carbonization" (HTC). The evidence that organic materials, such as cellulose, could be converted into char through a hydrothermal treatment has been known since longtime. The first documented experiments were presumably carried out by F. Bergius in 1913 [12].

This technology has been applied to different ligno-cellulosic substrates, operating at a temperature range of 170-250°C. Reaction times are relatively long: they go from a few hours to one day. The process takes place effectively only in water and is exothermic and proceeds spontaneously [13].

Several advantages can be envisaged by the application of such technology. First of all, the process is relatively simple and it can be performed very easily with a modest technical effort. Most practical experiences take place in batch autoclaves and usually do not require any catalysts. Moreover, practically any kind of biomass can be used to the purpose. This makes HTC a viable process for waste disposal and valorization.

The carbonaceous materials resulting from the process can have several interesting applications. As far as energy applications are concerned, HTC is able to produce a coal-like

product that can be used for combustion. In the literature, there are some experiences of co-combustion of HTC derived char with low rank coals [14]. This is considered one of the most viable ways, since it combines low risk, low expenditure and is a short term option for realizing biomass energy utilization [15]. Biomass, indeed, poses a lot of problems when it is burned for energy generation. Its high moisture and oxygen content lower the combustion temperature, causing less net energy production and an increase in CO emissions, which is a serious pollutant. The relatively high concentrations of alkali and alkali-earth metals can cause fouling and agglomeration inside boilers. A prior carbonization treatment would be able to overcome these issues. Moreover, carbonization is able to increase biomass energy density: this would result in lower transport costs and lower expense for combustors building.

The usage of HTC as a valuable pre-treatment can be particularly appreciated for very wet biomass, such as algae. With moderate conditions of temperature (< 200°C) and residence time of approximately 30 minutes, it is possible to obtain a product of bituminous coal quality from microalgae. Such product can be utilized for subsequent syngas and chemicals production, or even for soil nutrient amendment [13].

Besides energy applications, HTC char can be also a value-added product. With proper reaction conditions and feedstock materials, biomass can be converted into functional carbonaceous materials with very important applications. In particular, nanostructured materials can be obtained for applications in crucial fields such as separations, energy conversion and catalysis. HTC would thus constitute a green process to produce solid particles or high surface area scaffolds with polar functional groups, thus making them hydrophilic and functional [16].

1.2.3. Hydrothermal liquefaction

A way to valorize wet biomass in an energy sense would be the production of liquid energy carriers. The resulting hydrothermal process is thus named "hydrothermal liquefaction" (HTL). Such process could be seen as the "hydrothermal equivalent" of flash pyrolysis, where biomass is processed without any oxidant for very short time in order to produce a combustible liquid named bio-oil. HTL was first conceived as a technology to produce liquid products from coal. Subsequently, such technology has been applied to biomass, especially to agricultural by-products and algae.

Hydrothermal liquefaction is generally carried out at 280-370°C and between 10 and 25 MPa. Water is kept at subcritical state, since supercritical conditions favor gasification reactions [17]. An average reaction time is around 20 minutes, variable over a range of 3-120 minutes. Though HTL has been mainly implemented on lab- or bench-scale, some examples of practical applications are present: e.g. HTU® (HydroThermal Upgrading), CatLiq® and TDP® (Thermo-Depolymerization).

The aim of the process is to produce a liquid product, which is often called bio-oil or bio-crude. This is a mixture of oxygenated organics with an oily consistency, usually with a relatively low polarity which makes them only partly soluble in water but typically solvable in acetone. Bio-oils are usually dark brown, free-flowing liquids with a distinctive smoky odor. Unlike petroleum derived oils, bio-oils are mixtures of several hundreds of organic compounds, mainly including acids, alcohols, aldehydes, esters, ketones, phenols and lignin-derived oligomers [18].

During a HTL treatment, some basic reactions take place: *(a)* depolymerization of biomass; *(b)* Decomposition of biomass monomers through cleavage, dehydration, decarboxylisation and deammination; *(c)* Recombination of reactive fragments. Possibly, catalysts are added to promote the production of certain products. In the literature, examples of different catalysts are present. Usually, they are alkali carbonates or hydroxides (homogenous catalysts) or metals like nickel and ruthenium (heterogeneous catalysts). The reasons for utilizing such catalysts are different. In some cases, they are utilized to directly increase oil yields or to reduce solid char formation, which is an unwanted product. They can also be adopted to obtain some specific reactions, like enhancing decarboxylisation or glucose isomerization. Some typical gasification catalysts, for example nickel, which promotes water-gas shift, are also used. Though gasification represents a product loss for liquefaction purposes, it is beneficial to some extent. Gasification helps removing oxygen from the feedstock, thus it allows to obtain a higher heating value and lower polarity product.

1.2.4. Hydrothermal oxidation

Hydrothermal oxidation treatment (HOT) can be seen as a combustion carried out under hydrothermal conditions. Here, an oxidant is added to water in order to achieve the conversion of organic material into water and carbon dioxide. As a consequence, a non-

combustible flue gas is produced, along with a relatively large amount of heat. Commonly used oxidants range from air to pure oxygen, including also ozone and hydrogen peroxide.

There are two kinds of hydrothermal oxidation treatments, depending on the used temperature range. If subcritical conditions are adopted, the process is commonly referred as "wet oxidation". If supercritical conditions are achieved, the process is named "supercritical water oxidation" (SCWO).

Wet oxidation has been usually applied in the fields of wastewater treatment, especially to dispose of sewage sludge or to efficiently treat some kinds of toxic industrial wastewater which turned out to be refractory to common biological treatments [19]; incineration is a viable alternative only for those effluents having more than 100 g/l of COD [20]. Among wet oxidation processes, wet air oxidation (WAO) is one of the most promising. In this case, air or pure oxygen are used as oxidizing agent. This allows performing less expensive operations compared to H_2O_2 or O_3. Typical reaction temperatures are in the range of 125-320°C, with pressures between 0.5 and 20 MPa, necessary to keep water in its liquid phase. By using WAO, the organic pollutants are either partially oxidized into biodegradable intermediates or mineralized to carbon dioxide, water and innocuous end products [20].

When temperatures exceeding 374.1°C (water critical temperature) are adopted, SCWO is performed. Such technology has found applications in treating many organic effluents, but also high-risk wastes including military by-products. Such technology allows much higher oxidation efficiencies since it is able to use the unique properties of supercritical water, such as the possibility to conduct all reactions under a homogenous phase and the very high gas diffusivity. All these properties will be better presented in the following Paragraph 1.3.

SCWO was developed since some compounds (e.g. acetic acid or m-xylene) are not oxidized under WAO process conditions. Furthermore, WAO is often not able to achieve the 99.9% destruction efficiencies that many current regulations require [21].

From an energy point of view, SCWO has been mainly investigated for coal processing. Energy efficiencies higher than conventional coal power plants were calculated [22]. Although, it was demonstrated that a SCWO process applied to diluted wastewater treatment is able to operate under energetically self-sufficient operations [23]. This gives clues that, as well as for coal, biomass SCWO could be also proposed as a technology for heat production.

1.2.5. Hydrothermal gasification

When no oxidant is added to the reaction environment, but temperatures higher than 350°C are used, the resulting process is called hydrothermal gasification (HTG). Such process, rather than producing heat and an inert flue gas, is aimed at producing a valuable flue gas. The gaseous product can be, according to the different reaction conditions, rich in hydrogen or in methane.

As in case of hydrothermal oxidation, we can distinguish between subcritical technologies, which will be addressed as generic hydrothermal gasification (HTG) and supercritical ones. Subcritical hydrothermal gasification is however performed around the critical point. Some examples are represented by the works of Knezevic *et al.* [24, 25], where glucose and real biomass were reacted in hot compressed water (350°C) or the work by Azadi *et al.* [26], where near-critical gasification yields were improved by adding a heterogeneous catalyst.

When water is used at its supercritical state, the technology is more properly called "supercritical water gasification" (SCWG). As for SCWO, the choice to operate the process under supercritical condition is crucial, because the reaction environment can benefit of unique characteristics able to achieve high gas yields, minimizing some drawbacks of the traditional gasification processes.

Traditional gasification technologies, indeed, have encountered a number of major difficulties hampering their development. One of the factors that really limit the diffusion of gasification is represented by the low quality of the product gas usually produced, since the syngas is often contaminated by impurities like char and tar. Such aspect causes important troubles to normal operations, especially related to pipes clogging and damages to the mechanical parts of the energy conversion devices (e.g. engines and turbines) where the gas has to be burned. Therefore, in order to avoid too discontinuous operations due to frequent maintenance tasks, gas purification is needed to achieve the required quality standard, resulting in further costs and plant complication [27]. The problem of gas purification is considered one of the main factors that limit biomass gasification only to niche applications, hampering a more widespread utilization of this extremely interesting technology [28].

Supercritical water gasification is able to significantly limit these issues. SCWG is based on the usage of supercritical water, i.e. water above its critical point (temperature and pressure higher than 374.15°C and 220.64 bar, respectively), as a gasifying agent. Under these conditions, water exhibits properties which are intermediate between a liquid and a gas,

with high density but also low viscosity and high diffusivity. Furthermore, the behavior of supercritical water is even more unique. When supercritical conditions are achieved, water changes its nature from a polar compound to an almost non-polar substance [29]. This enables water to solvate many organic substances, including those responsible for the formation of char and tar (mainly polycyclic aromatic hydrocarbons). As a result, many experiments of SCWG show nearly no formation of char and tars [30, 31]. Moreover, thanks to the aqueous environment, SCWG can boost steam reforming and water-gas shift reactions, thus allowing to obtain a syngas very rich in hydrogen. These features will be more extensively presented in the next Paragraphs.

1.3. Supercritical water

All the technologies that have been reviewed in the previous paragraph involved the usage of liquid water. When pressure is increased, water stays in the liquid state even at quite high temperatures. In Figure 1.2, the phase diagram of water is shown.
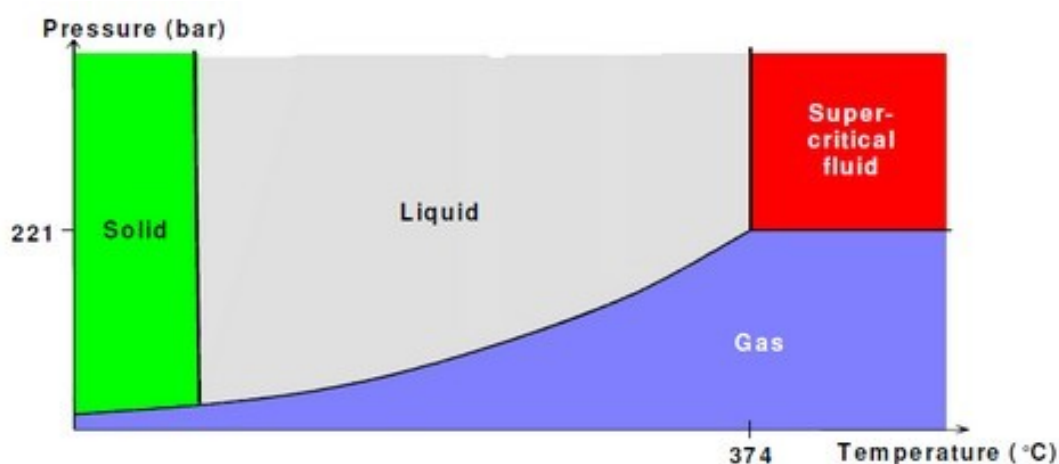
Figure 1.2 – Phase diagram of water.

It is possible to observe that, if a pressure higher than the critical one, that is of 22.1 MPa, is adopted, water stays always in its liquid state. This happens as long as the temperature is kept below the critical point of 374.1°C.

When both critical pressure and critical temperature are exceeded, water is not a liquid anymore, since no liquid phase is possible when the critical temperature is overcome. However, water is not even able to be a gas, since no gas phase is possible at pressures above the critical one. As a consequence, a completely new state is reached, which is called "supercritical state".

Supercritical water is therefore something halfway between a liquid and a gas. In fact, some of its physical properties are closer to those of a gas, while some other properties match those of a liquid. Like a liquid, for example, the density of supercritical water is relatively high [32]. In Figure 1.3, water density as a function of temperature and pressure is displayed. First, it can be noticed that below the critical pressure (221 bar) a phase change occurs. This is witnessed by the straight vertical lines, indicating a sudden drop of density, as water passes from the liquid to the vapor state. This temperature (boiling temperature) increases as pressure is raised.

In the supercritical region, no straight line can be seen. Water density varies continuously and, even though around the critical point its value diminishes, its values are much higher than at room conditions. For instance, at 400°C supercritical water at 300 bar exhibits a density 200 times higher than atmospheric water vapor.
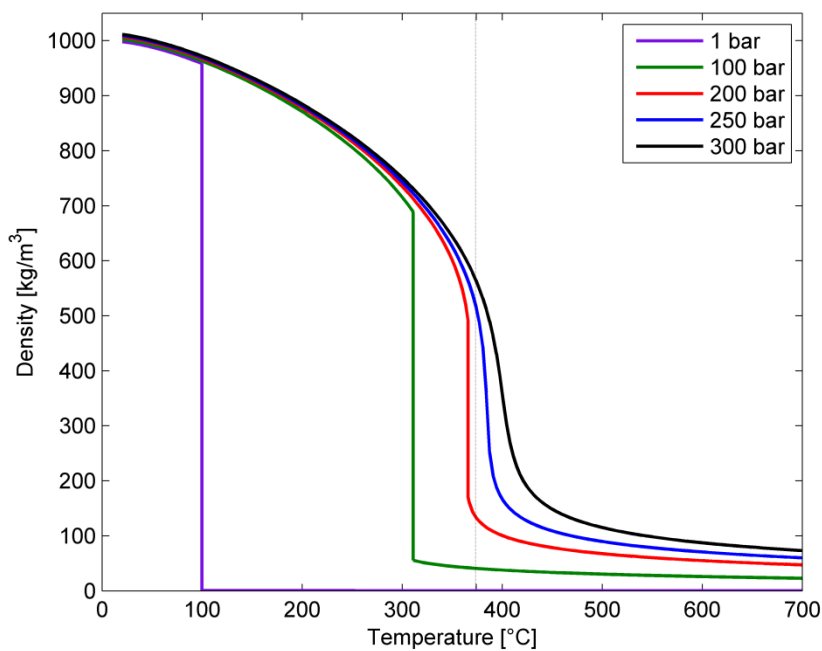
Figure 1.3 – Density of water as a function of temperature and pressure.

An important thing that must be stated is that all the physical properties show a very high variability around the critical point. Around this region, a very small variation in temperature causes an important change in the properties of the fluid. This is particularly evident when considering the case of the isobaric heat capacity c_p.
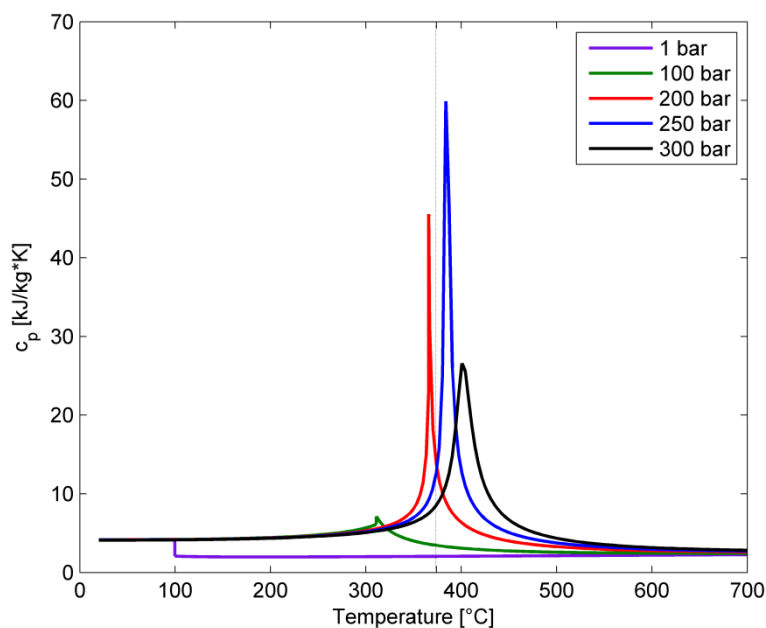
Figure 1.4 – Isobaric heat capacity of water as a function of temperature and pressure.

It can be noticed in Figure 1.4 that around the critical point a sudden change of the isobaric heat capacity is present. This behavior remembers what happens during the passage of state, when the heat capacity tends to infinite.

The considerations made so far are of general value for all the substances when heated and compressed above their critical point. However, water shows also some further important characteristics that considerably affect its behavior at the supercritical state. A remarkable behavior is the trend of the static dielectric constant ε. This parameter expresses the polarity of a solvent, that is its ability of its molecules to form dipoles. This property determines whether a certain substance can be dissolved in a certain solvent or not. A polar solvent can dissolve polar solutes, while non-polar solutes get dissolved in non-polar solvents.

Water at room temperature has a dielectric constant of around 80, which makes it a quite strong polar solvent. When it is heated and compressed up to the supercritical state, the dielectric constant drops to values typical of non-polar solvent. In Figure 1.5 the trend of the dielectric constant is reported, calculated according to [33].
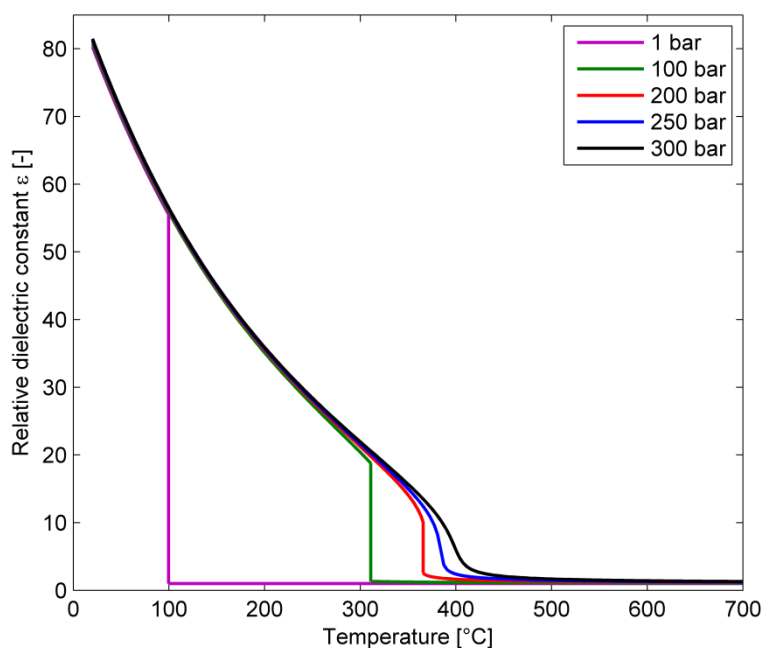
Figure 1.5 – Dielectric constant (ε) of water as a function of temperature and pressure.

Polarity change makes the usage of supercritical water as a solvent very interesting [34]. In fact, supercritical water is able to solvate substances that commonly require organic non-polar solvents to be dissolved, like hexane or toluene. This becomes very interesting when dealing with hydrothermal processing of biomass. It is known by the experiences carried out with traditional gasification technologies, that biomass produces water insoluble intermediates during high temperature treatment: these are called tars. When reactions are conducted in supercritical water, these intermediates are completely solubilized. This enhances reaction rates, since single-phase reactions can be carried out. On the other hand, the transition of water to non-polar behavior caused the salts to precipitate, since they become hardly soluble. On the technical point of view, this results in problems since the precipitated salts may cause reactor clogging, which damages the process.

Finally, another important feature of supercritical water is its ionic product. Such quantity is defined as the product between the molar concentration of ions H_3O^+ and OH^- which are in equilibrium with non-dissociated water molecules. At room conditions, the ionic product of pure water K_w is $1 \cdot 10^{-14}$ M or, in other words, its pK_w is 14. This gives a measure of how many ions are present, which is determining for acid-base equilibria and for the selectivity towards certain types of reaction (for example, ionic pathways). Figure

1.6 shows the trend of pK_w for water at sub- and supercritical conditions, estimated by means of the interpolation formula of [35].
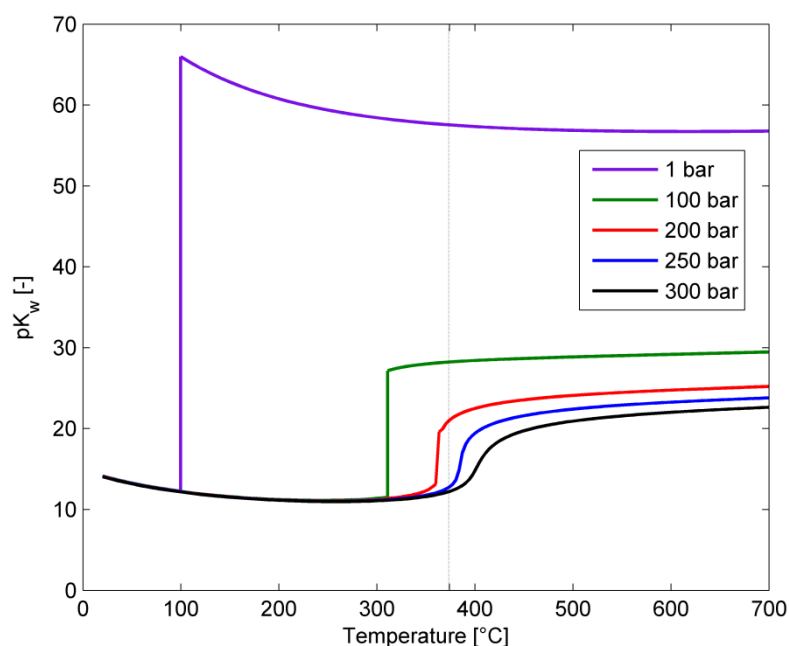
Figure 1.6 – Value of pK_w (-logK_w) of water as a function of temperature and pressure.

It can be observed that, around the critical point, pKw is lower than at room conditions, implying that water is more dissociated. Such fact has important consequences, especially for corrosion issues, since salts experience an enhanced dissociation. On the other hand, for temperatures higher than the critical one, water is considerably less dissociated than at room conditions. This causes lower solubility of many substances. Many ionic salts, which are commonly soluble in water, now precipitate and they can cause clogging problems to the reactors. Moreover, strong acids/bases experience lower dissociations, becoming weak acid/bases. Supercritical water thus offers a unique reaction environment, with many interesting potential applications.

1.4. Supercritical water gasification of biomass: state of the art

The first experience in supercritical water gasification dates back to 1985 with the work of Modell [36], who first experimented the possibility to gasify biomass feedstock by means of water in supercritical state. In his work, he plunged maple wood sawdust in supercritical water, noticing its fast decomposition without the formation of char.

Since then, much research has been devoted to this new technology. It can be affirmed, however, that research is still in an initial phase and is mainly concentrated on the

laboratory scale. All over the world, only a few research groups are permanently operating in this field and a regular research activity was established only in the last decade [37].

Supercritical water gasification of biomass is generally indicated as a promising technology for an efficient energy valorization of wet biomass [38]. Nonetheless, there are still some challenges to be overcome through further research. According to Kruse [39], they include: biomass pumpability to high pressures, reactor plugging due to salts deposition, energy efficiency of the process, materials resistance to corrosion and catalysts poisoning.

In the present Paragraph, the current state of the art in supercritical water gasification is reviewed. The different studies on the topic were grouped in five main areas: *(a)* experimental studies with model compounds; *(b)* Tests with real biomass; *(c)* Tests involving catalysts; *(d)* Mathematical modeling; *(e)* Reactor concepts.

1.4.1. Experimental studies with model compounds

Many research activities in the SCWG field have been performed by studying the behavior of some simple model compounds instead of real biomass; this choice has been made in order to overcome the difficulty of taking into account a complex matter like biomass, whose composition is not homogeneous and counts many different substances. This simplifying choice allows analyzing the process in a precise and reproducible way. Usually, glucose is used in order to model cellulose, one of the most important constituents of vegetal biomass, because it is the monomer unit of cellulose; lignin, the other main constituent of biomass, is often modeled through phenol, whose aromatic structure is one of the building blocks of such macro-molecule.

The way glucose and fructose react in sub- and supercritical water to form reaction intermediates is the subject of the fundamental work by Kabyemela *et al.* [40]. The authors performed experiments in the range 300-400°C, with pressures comprised between 25 and 40 MPa and sketched a comprehensive mechanism through which glucose is converted into compounds such as glyceraldehyde, dihydroxyacetone, glycolaldehyde, anhydroglucose, pyruvaldehyde and organic acids (Figure 1.7). On the basis of their results, they also wrote a kinetics model describing the process.
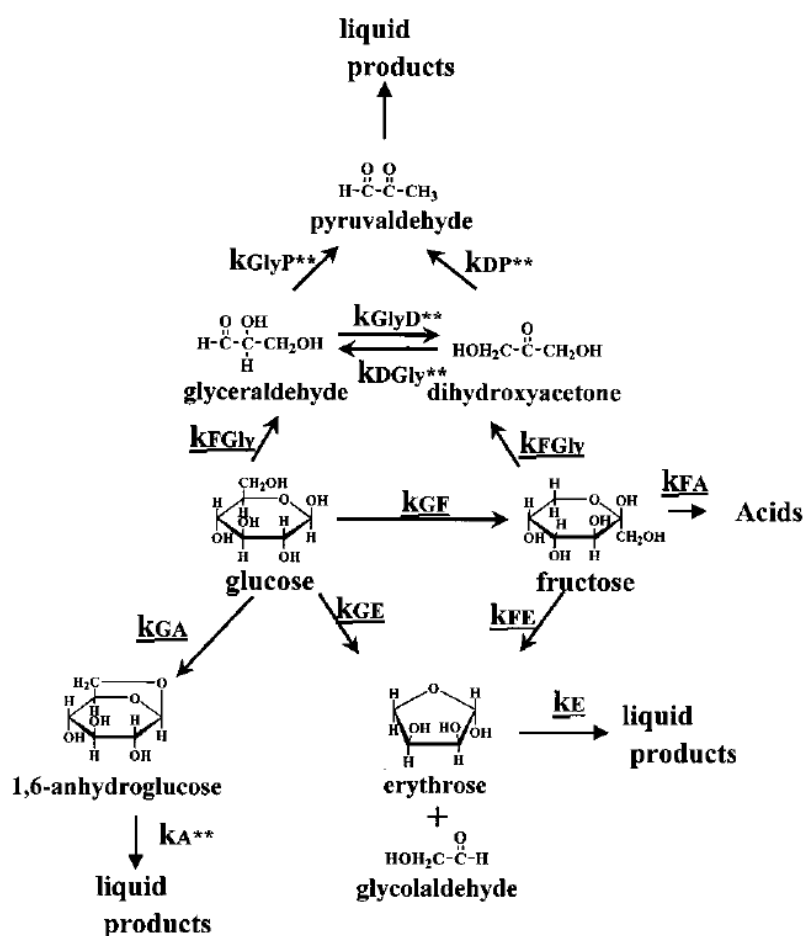
Figure 1.7 – Mechanism of glucose degradation in supercritical water as proposed by Kabyemela *et al.* [40].

A systematic experimental study on glucose SCWG was the one by Hao *et al.* [41], performed at the State Key Laboratory of Multiphase Flow (SKLMF) at Xi'an University (China). In this work, 30 experimental tests are performed by using an aqueous solution of glucose in different concentrations and varying residence time, temperature, pressure, reactor internal diameter. The results show that, with a residence time of less than 4 minutes and at approximately 650°C, almost complete glucose conversion is achieved, without any formation of char and tar.

Another systematical study about glucose SCWG is the one by Lee *et al.* [42]. Here, higher temperatures were used (480-750°C at 28 MPa), with residence time of 10-50 s. Glucose was fed at 0.6 M, corresponding to 10.6% wt. The reaction window was fully investigated, highlighting the effect of temperature and residence time on gasification yields. Among the results, they reported complete gasification (i.e. 100% carbon efficiency) at

700°C and a decrease of CO production at higher temperature, probably due to water-gas shift.

Williams and Onwudili also performed SCWG studies on glucose as a model compound for biomass. In their work [43], they investigated gasification in the range 330-380°C, with reaction times up to 120 minutes. However, for some of their experimental runs, they added hydrogen peroxide to the reacting mixture, in order to enhance feedstock conversion at lower temperatures. A significant result they reported, is the scarce influence of reaction time on gasification yields.

An insight in reaction order is offered by the work of Matsumura *et al.* [44]. Here, glucose was gasified between 175-400°C at 25 MPa. Though it is often assumed that reactions are of first order, the authors demonstrated that, at temperatures around 250°C, the reaction order of glucose decomposition reduces from 1.0 to around 0.7. This could be a consequence of the switch from an ionic mechanism to a radicalic one.

Gasification at very high temperature was carried out by Hendry *et al.* in a recent work [45]. Reaction temperatures of 750-800°C were adopted, which allowed to operate at very reduced reaction times (4-6.5 s). Carbon efficiencies varied from 52.7% in the worst conditions (highest glucose concentration, lowest temperature and residence time) to 100% in the best ones (lowest concentration, highest temperature and residence time).

High temperature glucose SCWG was also performed by Susanti *et al.*, without adding catalysts [46], in a continuous reactor operating between 600-767°C. In the most favorable conditions they reported hydrogen productions of 11.5 mol/mol_{GLU}, which are very close to equilibrium.

The study of the interactions between glucose and phenol are of outstanding importance, since they schematize the two main constituents of ligno-cellulosic biomass. This is the aim of the experimental work by Weiss-Hortala *et al.* [47], who performed SCWG tests of glucose, phenol and glucose/phenol mixtures in a continuous tubular reactor. Their work demonstrated that phenol plays a inhibiting role on gasification. Indeed, even a small amount of phenol, indeed, is able to dramatically lower the efficiency of the solution's conversion.

A similar philosophy was adopted by Goodwin and Rorrer, from the Oregon State University (USA). In their work [48], they performed supercritical water gasification of xylose and xylose-phenol mixtures in an isothermal microtube (inner diameter < 1.0 mm) flow reactor. Here, xylose is considered as a model compound for hemicellulose, the third

constituent of biomass after cellulose and lignin. Also here, phenol is reported as more difficult to gasify and it considerably lowers gas productions.

Many works actually deal with methanol. Though it cannot be strictly defined as a model compound for biomass, methanol can also be considered a model molecule for alcohols in general. Moreover, it is one of the simplest species of organic oxygenated compounds, and this makes its usage quite practical for more general studies.

Gadhe and Gupta performed methanol gasification [49] in an Inconel® tubular reactor at 700°C. They reported that methane formation is favored when long residence times and high biomass concentrations are used. Since their aim was to increase selectivity towards hydrogen, they proposed three strategies to suppress CH_4 formation: operation at low residence time, addition of an alkali catalyst (KOH) and utilization of the catalytic effect of the reactor walls made of Ni-Cu alloys.

Another work in methanol gasification is the one perfomed by Boukis et al. [50] at the Karlsruhe Institute of Technology (Germany). In this study, methanol was gasified from 400°C to over 600°C in an Inconel® tubular reactor. Feedstock was employed also at high loads, up to 64% wt. Results showed that, at 600°C, methanol is fully converted after only a few seconds of reaction. Gas composition anyway overcomes some important changes due to water-gas shift and CO methanation reactions. Similar experiments were carried out by van Bennekom et al. [51], who also proposed a reaction scheme for both methanol and glycerol SCWG.

Some works with model compounds have been also devoted to understand how certain reaction intermediates influence gasification products. Large attention, for example, was paid to 5-HydroxyMethylFurfural (5-HMF), a glucose gasification intermediate which is thought to be the most important precursor of char formation. To this purpose, a series of works was published by Chuntanapum and Matsumura [30, 52, 53], from the University of Hiroshima (Japan). Through direct gasification of 5-HMF in water, the authors concluded that, at least in their experimental conditions, no char was formed. On the other hand, they remarked that 5-HMF is effectively a char precursor, but it is not active when alone; the interaction between 5-HMF and organic compounds from glucose gasification is crucial. An interesting point is that they only detected char formation at subcritical conditions. At supercritical temperatures, char-free glucose gasification was achieved.

Investigations about char formation are also the object of the work by Müller and Vogel [54]. They conducted their experiments in batch reactors in both sub- and supercritical

ranges, using glucose and glycerol as feedstock. They stated that the maximum production of char occurs in the range of 350-370°C and identified phenol and hydroquinone as precursors for the formation of coke.

1.4.2. Tests with real biomass

Besides model compounds, also several types of real biomasses have been gasified in supercritical water. Now, things are generally more complicated, since the composition of the feedstock is much more complex. Moreover, practical problems, such as pumpability or salts deposition, start being of relevant importance. We already mentioned the pioneer work by Modell, who first gasified maple sawdust in supercritical water [36].

Another important work involving real biomass SCWG is that of Antal *et al.*, which was carried out at the University of Hawaii (USA) [55]. Antal, starting from Modell's results, made several experiments using several types of biomass like cornstarch, poplar wood sawdust, potato starch and potato waste. For this work, the authors used a tubular reactor heated by a furnace and they fed the different biomasses by means of a cement pump, after making an aqueous suspension at 4% wt. Results, which were in good accordance with equilibrium calculations, showed that, at high temperature, extraordinary gas yields (more than 2 l/g) were obtained, with a hydrogen molar content of 57%. Tars and char were not produced in a significant amount, though the reactor got clogged after some hours of operation.

As for model compounds, much work has been carried out at the SKLM (China) also by using real biomass [56, 57]. This research group made tests with several kinds of substrates, like cellulose, lignin, xylane, sawdust, straw, rice shells, sorghum stalk and corn cob. They carried out a comprehensive analysis, investigating the effect of the main process variables, such as temperature, pressure and residence time; nonetheless, they also tested the influence of reactor geometry, catalytic walls, heat exchange and biomass particle size. They reported that pressure influences the reaction mechanism at supercritical conditions. They also proposed some strategies to overcome reactor plugging issues: high temperature processing, high heat transfer at the entrance of the reactor, the usage of a catalyst and innovative reactor designs.

The gasification of industrial organic wastes was the topic of the work by Garcìa Jarana et al. [58]. They processed two wastewater streams having a possible energy potential: cutting oil wastes, that are oleaginous wastewater from metalworking industries, and vinasses,

alcohol distillery wastewater. The authors operated with a continuous plant, with the possibility of oxygen addition. They reported that the maximum yields occurred at 550°C (the maximum temperature tested), adding oxidant with an equivalence ratio of 0.1 and in presence of KOH.

Chakinala *et al.* gasified microalgae and glycerol using batch quartz capillaries and continuous flow reactors at 400-700°C and with reaction times of 1-15 minutes [59]. Complete gasification of algae was only attained at high temperatures with excess amounts of Ru/TiO_2 catalyst. A possible explanation, which was practically tested in this study, was the presence of proteins in algae, resulting in higher coke and liquid intermediates production.

Several experimental activities were carried out at the Karlsruhe Institute of Technology (Germany) by the group of A. Kruse. The influence of dry matter content was investigated through gasification of a chopped mixture of carrots and potatoes in both CSTR and batch reactors [60]. The study underlined that an increased dry matter content causes an increase in gas yields only in the CSTR; such effect was not present in the batch reactor, where higher biomass concentrations implied higher coke and tar yields. The authors tried to explain this referring to the faster heating up of the CSTR and to back-mixing, which leads to the presence of active hydrogen during every step of biomass degradation. Back-mixing was more deeply investigated in a subsequent work [61], where also the effect of salts was taken into account. Here, cellulose was gasified in a batch reactor, a CSTR and a PFR. CSTR produced better results, thanks to its capability to enhance back-mixing. Active hydrogen is, indeed, a late reaction product and, in a tubular reactor, it has no possibility to react with fresh biomass at the inlet. The authors thus proposed a process scheme composed of a CSTR, for fast biomass mixing and heating, followed by a PFR, to achieve the residence time required for complete conversion. Other experimental tests concerned ligno-cellulosic and tannery waste gasification, concluding that not only cellulose and lignin influence gasification yields; a major role was, indeed, played by chromium residues in tannery wastes [62].

A matter which has been investigated in SCWG is the influence of the heating rate on gasification performances. Matsumura *et al.* [63] studied this effect on the gasification of glucose and cabbage slurry. They found out that, in the range 10-30 K/s, carbon gasification efficiency improved as the heating rate increased.

An interesting perspective in SCWG is represented by the production of the so-called "green gas", also called "synthetic natural gas" (SNG). This was the aim of the work carried

out at the Energy Research Centre of the Netherlands [64]. While most studies actually aim at producing a hydrogen-rich syngas from SCWG, if SNG is the desired product the process is focused mainly on methane production. This choice allows much lower temperature operations, resulting in lower process costs. By the way, the authors stated that the process can be economically affordable only if a negative-value feedstock (i.e. wastes) is considered. This is mainly due to the high investment and maintenance costs of the process, compared to other SNG production technologies.

A number of studies have dealt with supercritical gasification of waste materials, especially of the wet ones. In this category, wastewater and agricultural residues are included. Sometimes, the process is more focused on achieving the highest organic reductions than on the quality of the product gas.

An example of such approach is the interesting study by Di Blasi *et al.* [65] concerning the supercritical gasification of wastewater from traditional updraft wood gasifiers. In this work, operations were conducted at 500-600°C, with residence times between 46-114 s. The process was able to achieve TOC reductions from 30% to 70%.

As far as agro-industrial waste are concerned, Demirbas investigated the aqueous conversion of whole fruit shells to hydrogen rich gas under low temperature conditions (380-530°C) [66]. Williams and Onwudili [67] gasified cellulose, starch, glucose and Cassava waste in both sub- and supercritical conditions, finding that cellulose produced the highest amounts of char and Cassava waste, though yielding similar amounts of char as starch, produced less hydrogen. Gasification of straw, wood and sewage sludge was carried out by Schmieder *et al.* [68]. They found that, operating at 600°C and 25 MPa, complete gasification can be achieved by adding KOH or K_2CO_3.

Xu et al. studied the feasibility of the direct gasification of dewatered sludge in supercritical water, by operating at 400°C for 60 minutes in an autoclave [69], adopting solid matter concentrations ranging from 75% to 95%. They observed that a reduced water content favors carbonization and affects CO_2 yields significantly; a slighter effect was instead noticed on H_2 and CH_4 productions.

Penninger and Rep [70] performed gasification of aqueous condensates deriving from beech sawdust pyrolysis. By operating at 650°C and 28 MPa, they reported successful conversion of the feedstock into a hydrogen-rich gas. They also observed that H_2 is mainly a late product, originated by water-gas shift reaction. Furthermore, the authors stated that

pressure plays an important role, since low pressure promotes coke formation, which can be avoided at higher pressures.

1.4.3. Catalysis

Another field of interest is represented by catalysis, which is fundamental in order to reduce the energy required by the process and to increase the selectivity towards the desired products. Both homogenous and heterogeneous catalysis approaches are followed. The former is usually achieved by means of alkali hydroxides or carbonates, the latter uses metals like nickel, ruthenium and palladium on adequate supports.

One of the first works dealing with catalytic decomposition of biomass at hydrothermal conditions is the one by Minowa *et al.* [71]. Although this study was only performed at subcritical conditions, it provides useful information about catalytic mechanisms determining cellulose hydrolysis. The authors concluded that alkali catalysts avoid char formation by stabilizing the oily products, while nickel promotes steam reforming of reaction intermediates, as well as the methanation reaction.

The positive effect of alkali compounds, like KOH and $KHCO_3$, has been investigated by the group of A. Kruse, at the Karlsruhe Institute of Technology (Germany). In one work [72], catalytic SCWG of pyrocatechol, a model compound for lignin, was performed in presence of potassium hydroxide, observing an increase in hydrogen production and a decrease in methane formation. In a subsequent work [73], potassium carbonate was used for glucose SCWG. Again, increased hydrogen production was observed, as well as an increase in phenol formation.

Another work by the same group [74] investigated the effect of several catalysts on ligno-cellulosic materials and tannery waste. Here, the addition of natural products or residues, like Trona ($NaHCO_3 \cdot Na_2CO_3 \cdot 2H_2O$) and red mud (a by-product of aluminum production rich in iron oxides), was compared to commercial catalysts like K_2CO_3 and Raney nickel at 500°C. In order to promote hydrogen production, Trona and red mud was found to be satisfactory, allowing a cheap option for catalysis.

The way to improve gasification yields by using low-cost catalysts is also the aim of the work by Rönnlund *et al.*, concerning paper sludge gasification [75]. Here, the authors found that adding black liquor, another by-product of paper mills, resulted in similar catalytic effect as alkali salts. This allows beneficial effects for the process economy.

Guan and co-workers [76] studied cellulose SCWG between 450-500°C, with both K_2CO_3 and $Ca(OH)_2$. An interesting result they obtained is that the synergic use of both catalysts allowed obtaining higher H_2 yields than with one catalyst alone.

Gasification of phenol, which is quite refractory to hydrothermal treatment, can be achieved through catalytic partial oxidative gasification. Xu *et al.* performed tests with this technology, adopting Na_2CO_3 [77].

A number of works have been devoted to heterogeneous catalysis by means of metallic reactors. First of all, some studies focused on determining the intrinsic reaction rates, operating in a non-catalytic environment able to exclude any catalytic wall effect. Such approach was introduced by the group of the University of Twente, where a methodology based on quartz capillaries was developed [78]. Through this technique, glucose and wood were gasified; inserting catalyst inside the capillary, the catalytic influence of ruthenium was clearly observed and distinguished from the non-catalyzed behavior [79].

A similar approach was followed by DiLeo and Savage [80], who performed the SCWG of methanol. They conducted their experiments in sealed quartz cylinders to avoid any catalytic influence. In a second time, they added to the cylinders a nickel wire and, in this way, they were able to clearly identify the effect of the added catalyst in terms of enhanced conversion. They also observed catalyst deactivation after a few experimental runs.

By using a similar methodology, the same group investigated the influence of catalysts on lignin SCWG [81]. This time, several metallic catalysts were added to the quartz reactors: nickel, iron, copper, zinc, zirconium, ruthenium and Raney-nickel. Nickel and copper turned out to be the most effective in catalyzing H_2 production at 500°C. No relevant effects on CH_4 yields were observed.

Azadi *et al.* [26] performed gasification of glucose in near-critical water (340-380°C) using different metal catalysts. They found out that Raney-nickel shows the highest catalytic activity. By the way, results were not so different among Raney-nickel, ruthenium and Raney-copper. Furthermore, changes in catalyst loads in the range 30-100% did not lead to any appreciable difference in the results.

Several metallic catalysts were also tested by Youssef *et al.* [82] in hog manure gasification at 500°C. They found that palladium catalyst was the best performing one in terms of hydrogen production, while NaOH was the worst one. On the other hand, if COD reduction was considered, the efficiencies were completely reversed: NaOH was the most effective catalyst, while Pd led to the worst results. Platinum can also be a good catalyst for

SCWG: Fang *et al.* [83] reported the positive effect of a Pt/Al_2O_3 catalyst on the gasification of cellulose and glucose.

Byrd *et al.* successfully implemented heterogeneous catalysis for glycerol SCWG by using Ru/Al_2O_3 [84]; the results showed high yields, near to equilibrium predictions, also when highly concentrated biomass were used. In a subsequent work [85], the same research group applied catalytic gasification to switchgrass biocrude, that is a product from biomass liquefaction. They tested several catalysts (Ni, Co, Ru) and find out that Ni/ZrO_2 catalyst was able to give the highest hydrogen yields. However, they also reported that all materials suffered significant area losses due to sintering and charring occurred in the lower temperature zone at the entrance of the reactor.

May *et al.* [86] investigated catalytic gasification of 5% wt. glycerol in supercritical water at 510-550°C in a bed of inert zirconia and in a bed of 1% Ru/ZrO_2 catalyst. They achieved complete glycerol conversion after 8.5 s at 510°C and after 5 s at 550°C, in catalyzed experiments. They observed that catalyst was able to promote glycerol degradation to reaction intermediates, but was not active enough to achieve complete gasification. The authors hypothesize this would be due to carbon deposition.

The role of the catalyst support emerges from the work by Lu *et al.* [87]. Here, tests with glucose were carried out using two different nickel-based catalysts: the former supported on γ-alumina, the latter on γ-alumina and ceria. The Ni/CeO_2-$γAl_2O_3$ catalyst turned out to behave better than the other, since Ce is thought to inhibit carbon deposition and coking.

Carbon supported catalysts were adopted by Sato *et al.* for the gasification of bean curd refuse at mild temperature conditions (200-400°C) [88]. According to their experiments, Ru/C catalysts were the most performing ones. They also underlined the importance of rapid heating to prevent the formation of heavier compounds.

An original way for catalysis in supercritical water is the one presented by Gadhe and Gupta [89]. In their work, they used the peculiarities offered by supercritical water to generate *in situ* particles of copper which exhibit high catalytic activity. They fed the reactor with a solution of water, methanol and cupric acetate. In supercritical water, such compound is able to form nanometric copper particles, exhibiting extremely high catalytic activity due to both their low dimensions and freshness of the surface. Moreover, since particles are continuously generated, poisoning by sulfur is not an issue, since poisoned materials are continuously ejected from the reactor.

General exhaustive reviews concerning catalysis applied to SCWG can be found in [90] and [91]. A review about heterogeneous catalysts can be found in [92].

1.4.4. Mathematical modeling

Some efforts have been also made in the field of mathematical modeling. This field is of outstanding importance, since it provides the theoretical basis to understand the way the process works and how operating parameters determine its outputs. Here, the attention has been focused on four main topics: thermodynamic equilibrium, kinetics, process simulation, computational fluid dynamics (CFD).

Thermodynamic equilibrium modeling is aimed at stating the system composition at equilibrium and at evaluating the theoretical yields and energy requirements of the process. In this field, two main approaches can be identified: stoichiometric and non-stoichiometric.

The stoichiometric approach is based on reaction equilibria. In other words, a certain number of independent reactions involving the different species are considered. Calculations are then performed in order to find the equilibrium among the reactions examined. This approach has the advantage of making the contribution of each reaction easily identifiable. On the other hand, the reactions involved in the conversion of biomass have to be known in advance. This approach was implemented in the work of Letellier *et al.* [93], where a system consisting of a SCWG reactor and an atmospheric pressure separator was modeled, taking into account seven independent reactions. In a subsequent work [94], the same research group applied the same model in order to study the energy features of the process. The authors concluded that, when an oxidizing agent is fed to the reactor, an "autothermal" operational regime can be obtained without any external energy input to the system.

The other family of methods is called non-stoichiometric. Here no reactions have to be defined, but the equilibrium composition is calculated according to Gibbs free energy minimization. In order to apply this family of models, the species expected in the products need to be defined. Subsequently, the distribution of the products enabling to reach the minimum value of Gibbs free energy is calculated. Although no reference to real reactions is made, this approach has the great advantage of being extremely flexible and preventing that important reactions in the scheme are neglected. It was successfully applied in a study by Tang and Kitagawa [95] where Peng-Robinson equation of state (EoS) was used to predict the behavior of a supercritical mixture. Their analysis showed that high temperature,

low pressure and low concentration of biomass in the feed are the ideal conditions for hydrogen production through SCWG, in good accordance with experimental data.

A similar approach was adopted by Yan *et al.* [96], who used Duan's EoS, which is considered more effective when dealing with supercritical mixtures. In this work, the authors also introduced a carbon conversion efficiency coefficient to take into account that equilibrium is not completely achieved in practice. As a result, the conversion of the feedstock is not complete even after a long residence time. Another similar approach is that of Voll *et al.* [97], who implemented a simplified model in order to overcome some computational difficulties and improve reliability. In all these works, anyway, only one-phase (the supercritical phase) is considered and the energy requirements of the process are not analyzed.

Thermodynamic equilibrium modeling is very important for the evaluation of parameters influence and process energy needs. By the way, such approach provides no information about the transient state, where intermediate compounds form. Furthermore, thermodynamics is not sufficient for reactor sizing and design, as it does not account for the time required by the development of each step of the process. All these aims could be achieved by means of a kinetics model.

Kinetics mathematical modeling of SCWG is poorly developed and, at the actual state, a comprehensive simulation program has not been implemented yet. In the literature, some models can be found which were developed for SCWO. In this field, an extensive work has been performed by the group of J. W. Tester at the Massachusetts Institute of Technology, resulting in models for methane, methanol and CO oxidation in supercritical water [98-100]. Another research group active in this field is that of P. E. Savage, at Michigan State University. They also developed a mathematical model [101] based on elementary reactions (actually 148 elementary reactions involving 22 species), aimed at describing the supercritical water oxidation of some simple compounds like methane and methanol as well as hydrogen, taking also into account the effect of pressure-dependent kinetics.

Another kinetics model for reactions in supercritical water is the one by Ederer *et al.* [102]. They tried to describe the pyrolysis (i.e. production of liquid intermediates) in supercritical water of tert-butylbenzene; the model involves 67 species and 171 elementary reactions. In the work by Bühler *et al.* [103], kinetic modeling of radical and ionic pathways for glycerol SCWG was executed and the simulations were compared with experimental results. This approach allowed stating that radical and ionic reaction schemes are competing

pathways in SCWG: the former is preferred at higher temperatures, while near-critical conditions are more favorable for the latter.

In the field of SCWG, most works have only tried to express kinetics through simple correlations, rather than by structured reaction-based kinetics models [42]. Some kinetics models have been proposed to generally predict the production of certain intermediates and to model the overall gas productions [30, 40]. These models are effective in interpreting the reaction mechanism, in order to understand the relative importance of the intermediate reactions leading to certain intermediates. On the other hand, none of them is able to describe the SCWG process to give information about the composition of the product gas.

An important step ahead in the mathematical modeling of SCWG was represented by the work of Resende and Savage [104]. They described the SCWG of cellulose and lignin, the main constituents of ligno-cellulosic biomass. Such model abandons the idea of elementary reactions, which can hardly be applied to complex organic molecules, in favor of a more "engineering" approach based on a few lumped reactions. In the proposed model, only 11 reactions and 7 components are present. In this way, the main reaction steps, ranging from hydrolysis to intermediate formation and eventual gasification, are modeled.

Another typology of models which is gaining an increasing importance is the family of the so-called "process models". All the studies reported so far, indeed, only focus on the SCWG reaction itself. They aim at describing how the reactions involved in SCWG works but they do not take into account the inclusion of SCWG inside a real process. In other words, they consider SCWG as a standalone unit operations, without taking into account, for example, the devices to heat up water, to compress it to the reaction conditions, to condense the reaction products and so on.

Such kind of modeling is crucial for engineering, because it enables to calculate the actual energy needs of the process, a piece of information that is of outstanding importance to analyze its practical feasibility. Some preliminary studies in this field were conducted by Feng *et al.* In their two works [105, 106], the authors performed a thermodynamic study of SCWG comparing Statistical Associating Fluid Theory (SAFT), Peng-Robinson and Soave-Redlich-Kwong equations of state. They also used the obtained data to propose a simple process layout, involving thermal recovery and hydrogen separation through membranes; CO_2 separation by means of 1-hexanol was also proposed to increase the gas heating value. Another work is the one by Lu *et al.* [107], who applied their thermodynamic analysis to a system involving reactors, heat exchangers and water recovery.

The work of Gutierrez Ortiz *et al.* [108] is the first in-depth study aimed at designing and optimizing a complex process scheme for SCWG. The idea is to produce power by expanding the high pressure syngas exiting the SCWG reactor in a turbine. The syngas is then burned with air in a combustor to provide the heat needed to sustain the SCWG reaction. The process accounts for several heat recoveries designed with a view to optimizing the process itself. It is intended to treat a feed stream consisting of a water-glycerol mixture.

Another typology of modeling activity is represented by computational fluid dynamics (CFD). This kind of modeling combines information about the process chemistry with the physical behavior of fluids in a given reactor geometry. The information obtained is of outstanding importance, especially for engineering purposes. It thus allows to carefully design the reactors and to optimize them in order to get the maximum efficiency. One work in this field is by Yoshida and Matsumura, who developed a reactor for glucose (4.9% wt.) SCWG at 400°C [109]. Through CFD techniques, Goodwin and Rorrer [110] modeled a microchannel reactor used for xylose gasification, focusing on the improved heat exchange, made possible by this innovative technology (see Paragraph 1.4.5).

1.4.5. Reactor concepts and technology

Most of the works that can be found in the literature deal with small bench-scale experiments which are normally aimed at studying the physical and chemical fundamentals of the supercritical water gasification process. These experiments have been performed in both continuous and batch reactors. Anyway, some works also deal with possible full scale applications of the supercritical water gasification technology by presenting reactor design concepts.

In the field of possible large-scale applications of SCWG, Matsumura's group patented a biomass SCWG system based on the production of a biomass slurry able to be pumped into the reactor [111, 112]. The supercritical water gasification of sewage sludge in order to obtain hydrogen is instead the object of a patent application by Wang and Yang [113], who propose to feed a tubular reactor with a slurry consisting of sludge plus an alkali or alkali-earth hydroxide. The problem related to supplying energy to the process is, instead, the object of the patent applications by Guo *et al.*, who propose a reactor driven by solar energy [114-116].

As concerns tubular reactors, an interesting work is that of Susanti *et al.* [117], where a concept for a full scale tubular reactor is presented. The proposed reactor is divided into

distinct zones where optimal conditions for mixing, reaction and cooling down are provided.

On the basis of their kinetics studies, Kruse *et al.* proposed (and patented) a reactor scheme foreseeing a CSTR reactor followed by a PFR reactor [61, 118]. This choice was made in order to exalt back-mixing, which is said to have a very positive effect on gasification efficiencies. This seems caused by active hydrogen, which is able to enhance the degradation of the organic compounds to permanent gases. Active hydrogen is a late reaction product, thus a CSTR configuration is the best way to enhance back-mixing. The successive PFR reactor is intended to complete the reaction.

One of the most interesting alternatives to tubular reactors is represented by fluidized bed reactors, which can treat solid biomass in an efficient way, avoiding the problems related to clogging and plugging of tubular reactors. The work of Matsumura and Minowa [119] gives some fundamental parameters useful for the design of a fluidized reactor operated with supercritical water, such as fluidization regime, minimum fluidization velocity and terminal velocity. Lu *et al.* [120] implemented a fluidized bed for SCWG, designed for temperatures up to 700°C and pressures up to 30 MPa. They reported continuous and stable gasification of corn cob (17% wt.) and glucose (30% wt.) without plugging.

Attention has also been paid to smaller applications, for example in order to provide hydrogen to small fuel cell powering electronic devices. In this context, Taylor presents a compact supercritical water reformer powered with methanol [121] based on a tubular Inconel® reactor followed by a heat exchanger, achieving a product gas composition close to the equilibrium composition.

A novel approach is represented by the utilization of micro-scale techniques in order to carry out SCWG reactions in a safe and efficient way. The first interest in microreactors for SCWG applications starts with the fundamental work of Potic et al. [122], who performed a large number of batch tests using tiny glass capillaries filled with a water-glucose solution. The choice was strategic, because it assures a very cheap and safe testing technique, which allows also to visually monitor the reactions occurring in the capillaries. Glass capillaries were also utilized in a subsequent work [123] to simulate the behavior of a biomass bed fluidized by supercritical water.

Recently, Goodwin and Rorrer explored the potentialities of supercritical water gasification of glucose by using a very small stainless steel microreactor (4.5 x 4.0 x 0.4 cm) [124]. This device is formed by a network of microchannels arranged into 25 layers with 21

parallel channels; each channel has a section of 75x500 μm. Though the device is not optimized for the SCWG process and no catalyst is used, the results are extremely promising: at 750 °C the gas composition foreseen by thermodynamics equilibrium is achieved. In a subsequent work [125] the authors investigate the SCWG of xylose by using a single microtube reactor (internal diameter: 762 μm).

In the optics of evaluating the feasibility of supercritical water gasification, Y. Matsumura [126] conducted an analysis to compare biomass SCWG and biomethanation in Japan. The output of his work highlighted that, though SCWG looks more effective than biomethanation, the cost of the produced syngas is still higher than the cost of city gas in Tokyo. His analysis highlighted that the bottleneck of the SCWG process is represented by thermal recovery. Such aspect can be overcome by improving the heat exchanger efficiency, thus reducing the cost of the final product.

A crucial problem in SCWG reactors is represented by corrosion. Indeed, supercritical water provides a very harsh reaction environment. The materials used for reactor manufacturing are thus subjected to impressive corrosion phenomena. This is one the major drawbacks for SCWG and hydrothermal treatment in general, especially when acid feedstock is processed.

Much research has been done to find a solution to this issue. The work by Marrone and Hong [127] reviews the corrosion control methods for SCWG. They report that the main corrosion phenomena in supercritical water gasification are: general corrosion, dealloying, pitting, stress corrosion cracking and under-deposit corrosion. All these phenomena have pushed to adopt corrosion-resistant materials, such as nickel alloys (e.g. Inconel®, Hastelloy, etc.). Besides the adoption of such materials, the authors also propose other strategies: the use of vortex/circulating flow reactors to prevent the fluid to stay in contact with metallic surfaces; a pretreatment to neutralize acidic and basic feedstock fed to the reactor; a general optimization of process conditions.

Since metallic surfaces encounter such extensive corrosion issues, ceramic compounds were considered for reactors manufacturing and/or coating, also for economic reasons. Nevertheless, even ceramics can suffer corrosion at SCWG reaction condition. The work by Richard *et al.* [128] tested several technical ceramics, like alumina, zirconia, aluminosilicate, etc., finding poor corrosion resistance. On the other hand, other ceramic materials, like graphite and glassy carbon, show good resistance to harsh reaction environments.

Another problem with supercritical water gasification is represented by salts deposition, since they are not soluble in supercritical water. Kruse *et al.* [129] proposed a method to avoid reactor plugging due to salts precipitation in the reactors. The method is based on a second salt-rich phase, the so-called "hydrothermal brine", used to catch the salts precipitating inside the reactor. By operating in this way, it was possible to continuously extract salts from the reactor, thus achieving more stable and continuous gasification operations.

Integration of SCWG with pulp and paper production industry is the subject of the analysis by Myreen *et al.* [130]. They analyzed two possibilities of integration, based on mass and energy calculations and laboratory experiments, concluding that the integration of SCWG would facilitate the transformation of pulp and paper mills into modern-day biorefineries.

1.5. Aims and scopes of the present work

Moving from the current state of the art, this work aims at extending knowledge in supercritical water gasification. The work can be divided into two parts: the former related to mathematical modeling (Chapters 2-4), the latter dealing with experimental activities (Chapters 5-7). The goal of this work is to provide knowledge which could have technical significance, being possibly useful for a concrete application of the SCWG technology.

The first part, focused on mathematical modeling activities, is aimed at:

1. The development of a two-phase thermodynamic model for biomass SCWG, able to foresee the reaction products when a generic biomass is fed and certain pressure-temperature combinations are chosen. The model should be able to predict the formation of a solid phase at equilibrium, which is important to understand the application limits of the process;

2. The evaluation of the energy performance of SCWG reaction, enabling to understand if this process is endothermal or exothermal, and if the energetic behavior is significantly influenced by the process conditions;

3. The development of a kinetics model, in order to describe what happens during the transient state eventually leading to thermodynamic equilibrium. The model should be developed using a white-box philosophy, that is with rigorous modeling of the single elementary reactions involved in SCWG;

4. The development of a "process" model, that is the simulation of a possible real-life process for SCWG. This includes the development of a layout involving reactors, pumps,

heat exchangers, separators, etc. This simulation is useful to assess the technical feasibility of the process, especially dealing with its self-sustainability on the energy point of view.

The second part of the work reports the results of experimental activities carried out with model compounds and real biomass. The aims of such activities are:

1. Understanding the influence of long reaction times (up to 16 hours) on gasification performances for both model compounds and real biomass;

2. Evaluating the significance of the catalytic effect of reactor walls made of different metallic materials, highlighting the consequences on syngas composition;

3. Evaluating the effect of sub- and supercritical conditions, comparing experimental tests carried out at 350°C (subcritical) and 400°C (supercritical);

4. Comparing the experimental behavior of different categories of real biomass, including forestry residues, municipal waste, agro-industrial byproducts;

5. Evaluating the effect of an alkali catalyst (K_2CO_3) on gasification yields;

6. Performing short-time gasification of glucose/phenol mixtures in a continuous tubular device to simulate a real-scale process. During this activity, the inhibiting behavior of phenol should be investigated.

Chapter 2[*]

Thermodynamic equilibrium modeling

In this Chapter, a thermodynamic equilibrium analysis of the supercritical water gasification process is carried out by means of a non-stoichiometric model based on Gibbs free energy minimization. The model was validated through literature data and employed to simulate the influence of process parameters such as temperature, pressure and biomass concentration. The model, which is also able to deal with the formation of a solid phase, was used to state under which conditions solid char is formed at equilibrium for each kind of biomass. Finally, an isothermal energy analysis of SCWG was carried out, highlighting the process conditions under which such reaction is exothermal.

2.1. Introduction

Thermodynamic equilibrium modeling provides information about the composition which is reached by the system at equilibrium. Every system tends to equilibrium. Theoretically, equilibrium should be reached after an infinite reaction time; in practice, after a period of time long enough to allow all the reactions to completely take place. Since it can happen that some reactions are extremely slow or that kinetic constraints are present, it could happen that equilibrium is never reached in reality. Anyway, if high temperature reactions are considered, where very high reaction rates are observed, thermodynamic equilibrium gives a very realistic idea of the actual system composition.

Thermodynamic equilibrium analysis is also very important in order to understand how the process parameters affect the yields. This gives important information to understand which parameters should be changed, and in which measure, in order to obtain the desired outputs. Furthermore, such approach is also fundamental in energy evaluations, to state if a certain process is energetically sustainable or not. Even though real conditions could be very different, thermodynamics provides a theoretical limit, which cannot be climbed over.

In the field of thermodynamic equilibrium modeling, two main approaches can be identified: stoichiometric and non-stoichiometric. The stoichiometric approach is based on reaction equilibria. In other words, a certain number of independent reactions involving the different species are considered. Calculations are then performed in order to find the equilibrium among the reactions examined. This approach has the advantage of making the contribution of each reaction easily identifiable. On the other hand, the reactions involved in the conversion of biomass have to be known in advance.

The other family of methods is called non-stoichiometric. Here no reactions have to be defined, but the equilibrium composition is calculated according to Gibbs free energy minimization. In order to apply this family of models, the species expected in the products need to be defined. Subsequently, the distribution of the products enabling to reach the minimum value of Gibbs free energy is calculated. Although no reference to reactions is made, this approach has the great advantage of being extremely flexible and preventing that important reactions in the scheme are neglected. In all the state-of-art works, anyway, only one-phase (the supercritical phase) is considered and the energy requirements of the process are not analyzed (see Paragraph 1.4.4).

In this chapter, a non-stoichiometric, two-phase model for SCWG is developed and implemented. This new model is able to predict the system equilibrium composition not only considering the supercritical phase, but also the possibility for a solid phase to form. This enables to foresee the formation of solid carbon among the reaction products. Another innovative aspect is that biomass is not modeled just as a compound made of carbon, hydrogen and oxygen, but nitrogen is also considered, thus allowing for the occurrence of NO_x compounds.

By means of this model, the conditions leading to the formation of solid carbon were investigated as a function of the different process parameters (temperature, pressure, biomass concentration and biomass typology). An interesting issue is that of energy implications, and thus the calculation of the process heat duty, which is a fundamental piece of information to state the real profitability of SCWG. According to the state of the art (see Chapter 1), this work is the first one delivering an energy analysis by means of a non-stoichiometric model.

2.2. Model description

The thermodynamic model proposed here is based on Gibbs free energy minimization. This condition implies that the system has reached an equilibrium state.

Gibbs free energy of the system (G) can be calculated as the sum of each component's chemical potential (μ_i) multiplied by the same component's number of moles (n_i):

$$G = \sum_{i=1}^{N} n_i \mu_i \tag{2.1}$$

The chemical potential is a function of temperature and pressure, according to:

$$\mu_i(T,P) = \mu_{0,i}(T) + RT \ln \frac{f_i}{f_{0,i}} \tag{2.2}$$

$\mu_{0,i}$ is the chemical potential under standard pressure conditions (101,325 Pa). It can be calculated as a function of enthalpy and entropy of formation, which are only dependent on temperature, through the following formula:

$$\mu_{0,i}(T) = \Delta H_{f,i}^0 + \int_{298}^{T} c_{p,i}(T) dT - T\Delta S_{f,i}^0 - T \int_{298}^{T} \frac{c_{p,i}(T)}{T} dT \tag{2.3}$$

In order to calculate the isobaric heat capacity c_p, the NASA polynomial formula was adopted: eq. (2.4) [131]. For each chemical species, this formula foresees two sets of five coefficients, one for the low temperature range (i.e. up to 1000 K) and another for the high temperature range (i.e. from 1000 to 6000 K). The generic formula can be expressed as:

$$\frac{c_{p,i}}{R} = q_1 + q_2 T + q_3 T^2 + q_4 T^3 + q_5 T^4 \tag{2.4}$$

Coefficients q_1,..., q_5 for a large number of compounds can be found in [131].

The second term after the equal sign in eq. 2.2 takes into account the dependence on pressure by introducing the fugacity of the ith component, which is a state variable with units of pressure and is defined as:

$$f_i = P\varphi_i x_i \tag{2.5}$$

Actually, eq. 2.2 considers the ratio between the fugacity of the ith component in the mixture (f_i) and the fugacity of pure component i at standard pressure conditions ($f_{0,i}$; $f_{0,i} = P_0$).

Term φ_i is called fugacity coefficient, it is dimensionless and can be calculated through an EoS. The Peng-Robinson EoS was chosen, which has been extensively used [95, 97] on account of its capability of dealing effectively with supercritical fluids.

Peng-Robinson EoS describes the link between system pressure, temperature and molar volume by resorting to parameters derived from critical properties of the substances, such as critical temperature T_c, critical pressure P_c and acentric factor ω. For a pure substance, it has the following form:

$$P = \frac{RT}{\widetilde{V} - b} - \frac{a}{\widetilde{V}^2 + 2b\widetilde{V} - b^2} \tag{2.6}$$

Parameters a and b depend on the critical properties and are defined as follows:

$$a = \frac{0.45724R^2T_c^2}{P_c}\left[1 + \left(0.37464 + 1.54226\omega - 0.26992\omega^2\right)\left(1 - \sqrt{\frac{T}{T_c}}\right)\right]^2 \tag{2.7}$$

$$b = \frac{0.07780RT_c}{P_c} \tag{2.8}$$

Equation 2.6 can also be expressed in a different way by introducing the dimensionless compressibility factor Z:

$$Z = \frac{P\widetilde{V}}{RT} \tag{2.9}$$

Thus, a third grade polynomial is obtained:

$$Z^3 - \left(1 - \frac{bP}{RT}\right)Z^2 + \left(\frac{aP}{R^2T^2} - 2\frac{bP}{RT} - 3\frac{b^2P^2}{R^2T^2}\right)Z - \left(\frac{abP^2}{R^3T^3} - \frac{b^2P^2}{R^2T^2} - \frac{b^3P^3}{R^3T^3}\right) = 0 \tag{2.10}$$

Solving eq. 2.10 for Z, three solutions are obtained. When two phases are present, all the solutions are real. The minimum value is referred to the liquid phase and the maximum value to the gaseous phase; the middle value has no physical meaning. Above the critical point, only one value is physically meaningful.

To deal with a mixture, rather than a pure compound, van der Waals' binary mixing rules were introduced. These rules enable to calculate a_m and b_m, which are the a and b parameters appearing in eq. 2.10 but with reference to a mixture of N components, each having the molar fraction x, in the following way:

$$a_m = \sum_{i=1}^{N}\sum_{j=1}^{N} x_i x_j a_{ij} \tag{2.11}$$

$$b_m = \sum_{i=1}^{N}\sum_{j=1}^{N} x_i x_j b_{ij} \tag{2.12}$$

Where:

$$a_{ij} = \left(1 - k_{ij}\right)\sqrt{a_i a_j}$$ (2.13)

$$b_{ij} = \left(1 - \eta_{ij}\right)\frac{b_i + b_j}{2}$$ (2.14)

Parameters k_{ij} and η_{ij} are called interaction parameters and express the interaction between species i and j. They can be seen as the elements of matrices **K** and **E**, which are symmetrical and have null elements on the diagonal.

Elements $k_{i,j}$ in matrix **K** were calculated according to Poling *et al.*, 2007:

$$k_{i,j} = 1 - 8\frac{\sqrt{\widetilde{V}_{c,i} \cdot \widetilde{V}_{c,j}}}{\left(\sqrt[3]{\widetilde{V}_{c,i}} + \sqrt[3]{\widetilde{V}_{c,j}}\right)^3}$$ (2.15)

Matrix **E** is assumed to be null, thus neglecting the effect of η_{ij}, as suggested by McHugh and Krukonis [132].

Once Z for the whole mixture is calculated, the resulting value can be used to determine the fugacity coefficient φ_i of the ith component of the mixture:

$$\ln(\varphi_i) = \frac{b_i{}^*}{b_m}(Z - 1) - \ln(Z - B) - \frac{A}{2.828B}\left(\frac{2\sum_{j=1}^{N} x_j a_{i,j}}{a_m} - \frac{b_i{}^*}{b_m}\right)\ln\frac{Z + 2.414B}{Z - 0.414B}$$ (2.16)

Where

$$A = \frac{a_m}{R^2 T^2}P$$ (2.17)

$$B = \frac{b_m}{RT}P$$ (2.18)

$$b_i{}^* = 2\sum_{j=1}^{N} x_j b_{ij} - b_m$$ (2.19)

The model accounts for the presence of a solid phase, represented by graphitic carbon and indicating char formation. In order to calculate the chemical potential for the solid phase, equation 2.2 must be revised, since it has been derived for a gas.

From the definition of Gibbs free energy:

$$\mu(T, P) = \mu_0(T) + \int_{P_0}^{P} \widetilde{V}dP$$ (2.20)

For a solid, the molar volume $\tilde{v}$ can be reasonably considered to be constant, thus it can be taken outside the sign of integration. Moreover, since the volume is constant, the critical volume $\tilde{v}_c$ can be used. The integration is, then, immediate:

$$\mu(T,P) = \mu_0(T) + \tilde{V}_c(P - P_0) \tag{2.21}$$

Table 2.1 – Chemical species considered in the model, along with their critical parameters (NIST-TRC databank).

		T_c [K]	P_c [Pa]	$\tilde{V}_c$ [m³/kmol]	ω [-]
Oxygen	O_2	154.644	5042190	0.07351871	0.0213195
Hydrogen	H_2	33.172	1239720	0.06473499	-0.232001
Water	H_2O	647.296	22140200	0.05629781	0.343897
Solid Carbon	C	6810	223000000	0.0188	0.326841
Methane	CH_4	190.562	4607790	0.09925631	0.0106362
Carbon monoxide	CO	134.464	3774230	0.09062499	0.0370708
Carbon dioxide	CO_2	304.169	7378280	0.0942549	0.224877
Nitrous oxide	N_2O	309.565	7241650	0.09778602	0.1611
Ammonia	NH_3	405.6	11277473	0.072362166	0.25
Nitric oxide	NO	180	6484800	0.057693375	0.607
Nitrogen dioxide	NO_2	431.4	10132500	0.16990837	0.86
Nitrogen	N_2	128.464	3094240	0.08616066	0.04
Propane	C_3H_8	369.859	4255660	0.1986718	0.152919
Ethane	C^2H_6	305.367	4885500	0.1461753	0.100161
Ethylene	C_2H_4	282.345	5042360	0.1310267	0.0864047
Methanol	CH_3OH	512.658	8012950	0.1165915	0.55967
Acethylene	C_2H_2	308.341	6239770	0.1190043	0.185731
Methyl-acethylene	C_3H_4	401.564	5625550	0.1614438	0.209058
Propylene	C_3H_6	364.933	4594260	0.1830666	0.14218
Benzene	C_6H_6	561.99	4897390	0.2566344	0.21047
Naphthalene	$C_{10}H_8$	748.191	4081640	0.4075999	0.307871
Formaldehyde	CH_2O	418	6853840	0.1043348	0.201805

2.3. Model implementation and validation

The model was implemented by using the MatLab® software (The Mathworks, Inc.). In order to perform the minimization of Gibbs free energy, the routine FMINCON was used. This routine is based on the method of Lagrange multipliers, which enables to solve a minimization problem subject to constraints.

In this case, the problem consists in finding a composition for the system which corresponds to the minimum value for *G*. This problem is subject to two constraints: *(a)* mass conservation, insofar as the amount of each element (C, H, O, N) must be the same in the input (reagents) and output (products) streams; *(b)* non-negativity of the number of moles n_i. The latter is very important, since to obtain a solution which can respect the mass balance is numerically possible but completely meaningless owing to the negative number of moles.

The input stream composition is only useful in order to define the mass balances and to calculate its enthalpy. All the simulations foresee an input stream composed of water, biomass and, possibly, pure oxygen (O_2) as oxidizing agent.

Most analyses are conducted with glycerol ($C_3H_8O_3$). Glycerol can be considered a model compound for common biomass, since its molecule reproduces typical ratios of carbon, hydrogen and oxygen, which are the most important constituents of biomass. Glycerol also plays a major role as the most abundant co-product in biodiesel production plants. As a result of the biodiesel industry expansion, glycerol world production has increased from 500,000 tons in 1991 to currently 2,500,000 tons a year. Today, the biodiesel industry accounts for 70% of worldwide glycerol production [133]. This enormous quantity of glycerol is difficultly absorbed through traditional channels (e.g. cosmetics, pet food). Therefore, glycerol has become an industrial waste. SCWG could be an effective way to dispose of this substance and, at the same time, convert it into a valuable gas with a high H_2 content. Finally, experimental data about glycerol SCWG are available in the literature, thus a model validation can be performed for this compound.

In addition, some analyses were conducted on microalga *Spirulina*, a blue-green alga which is very common as a dietary supplement for both humans and animals. Algae are biomass with a great potential for exploitation, since they can be easily grown by only using water, CO_2 and solar energy. They can also be cultivated resorting to municipal or agro-industrial wastewater. Moreover, since algae normally possess a high water content, they

seem particularly suitable for hydrothermal treatment, while traditional gasification technologies, which require dry biomass, seem less applicable to them [134].

Microalga *Spirulina* was modeled as a pseudo-compound whose formula is $C_xH_yO_zN_w$. Coefficients x, y, z and w were computed according to the dry ash-free ultimate analysis, which was provided by the database "Phyllis" [135], where x was considered equal to 1. As a result, microalga *Spirulina* was modeled as a compound whose molecular formula is $C_1H_{1.8655}O_{0.5893}N_{0.1275}$.

Among the output compounds, 22 different species were selected as representative of the the main categories of compounds which can be reasonably found in the output stream. Besides the standard products like H_2O, H_2, CO, CO_2 and CH_4, C_{2-4} hydrocarbons and PAH were considered, as well as N_2, NH_3 and nitrogen oxides. The complete list of output compounds, along with their critical parameters, is reported in

Table 2.1.

The model results were compared with the experimental data by Byrd *et al.* [84], who carried out a study on the SCWG of glycerol with a Ru/Al_2O_3 catalyst. The results of model testing are shown in Figure 2.1, where the syngas composition is reported as a function of the feed concentration expressed in weight basis. To mention an example, a feed concentration of 20% corresponds to a feed consisting of water (80%) and dry glycerol (20%).
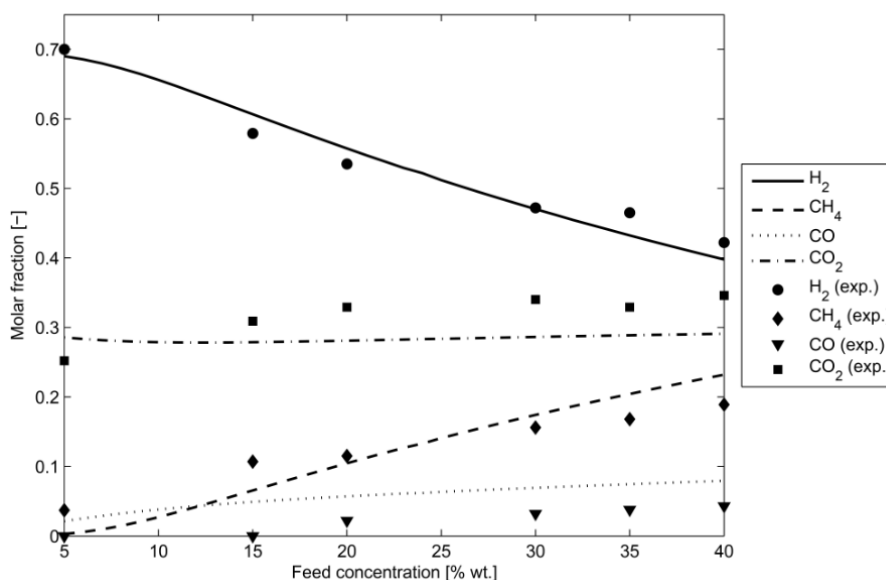
Figure 2.1 – Model validation with experimental data from Byrd *et al.* [84].

In order to compare model predictions and experimental results quantitatively, Pearson's correlation coefficient *r* was used, where a value of 0 stands for no correlation and a value of 1 means optimal correlation.

As far as hydrogen is concerned, the agreement between experimental data and model predictions is found to be very good (*r=0.988*), which demonstrates that the model is able to predict hydrogen yields in a very effective way.

The situation is slightly different for other gaseous species (methane, carbon monoxide and carbon dioxide). In this case, the agreement between model and experimental results is acceptable, the model output and the experimental data follow approximately the same trend, but the fitting is not perfect. The correlation coefficient is still high for methane (*r*=0.984), lower but tolerable for carbon dioxide (*r*=0.728), very low for carbon monoxide (*r*=0.469).

In general, it is possible to state that the model implemented provides results which are in good accordance with experimental data and, therefore, the model is a valuable tool for predicting the thermodynamics constraints of the SCWG process.

2.4. Results and discussion

Two different types of analysis were performed through the model proposed. The first class is aimed at describing the two-phase behavior of the reacting system, i.e. the process conditions that cause the output stream containing solid carbon. The second approach is focused on energy aspects, with a view to investigating the reaction energy requirements and the amount of energy contained in the product gas.

2.4.1. Char formation

The model was first run to state the dependence of the composition of the reaction products (syngas and possibly solid carbon) as a function of the biomass concentration in the feed.
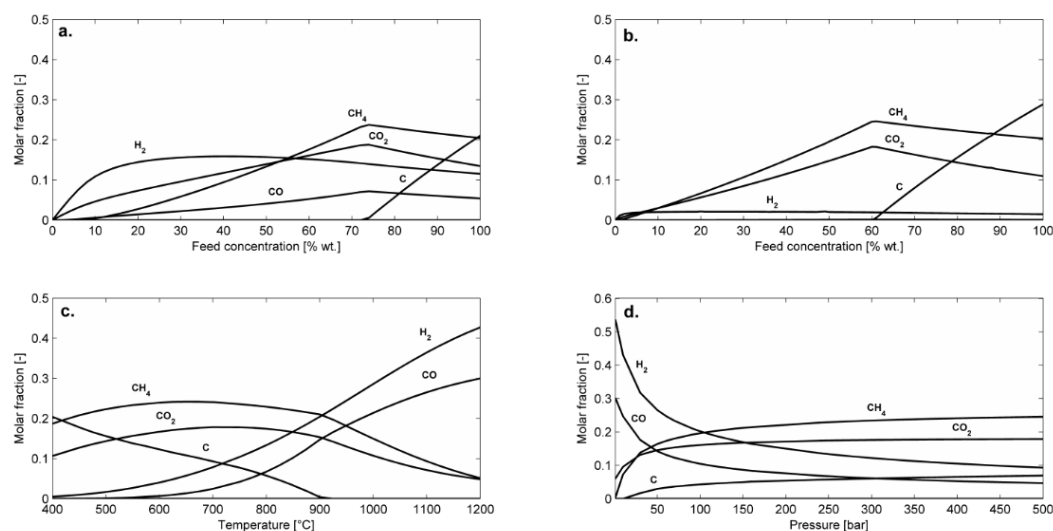
Figure 2.2 – Model results for the SCWG of glycerol under different operating conditions. (a) Equilibrium composition versus feed concentration (T=800°C, P=250 bar); (b) Equilibrium composition versus feed concentration (T=500°C, P=250 bar); (c) Equilibrium composition versus temperature (P=250 bar, feed concentration = 80%); (d) Equilibrium composition versus pressure (T=800°C, feed concentration = 80%).

Figure 2.2a shows the composition of the syngas produced through the SCWG of glycerol at 800 °C and 250 bar. Water was excluded from the plot in order to improve its readability. Clearly, the syngas composition significantly varies with the feed concentration (expressed in weight basis as for Figure 2.1). At low feed concentrations, the products preferred, besides water, are hydrogen and carbon dioxide. Up to a feed concentration of 10%, H_2, CO_2 and H_2O are almost the only products at equilibrium. When the feed concentration increases, CH_4 and CO form at equilibrium. Hydrogen production reaches its maximum at a feed concentration of about 40% and subsequently starts to decrease, while methane production increases. All trends are quite regular up to a feed concentration of 72%, the minimum concentration at which solid carbon is expected at equilibrium. At this point a noticeable change in the slope of all curves involving gaseous carbon compounds occurs, and their molar fraction starts to decrease.

The situation is completely different when working at a lower temperature. Figure 2.2b shows the equilibrium behavior resulting from the SCWG of the same compound at the same pressure, but with a temperature of 500 °C. Significantly, hydrogen production is far lower than in the previous case, while methane is also found at low feed concentrations. Carbon monoxide is almost absent at equilibrium. In this case an evident change in the slope can also be observed by the time solid carbon forms at equilibrium. However, at low-

er temperatures, solid carbon forms at lower feed concentrations: at 500 °C it forms with a feed concentration of 60%.

Figure 2.2c shows the equilibrium composition as a function of temperature for the SCWG of glycerol at 250 bar and feed concentration of 80%. Water was not included in the diagram for the sake of readability. An increase in temperature plays a favorable role for hydrogen and carbon monoxide formation, while methane and carbon dioxide are preferred at medium-low temperatures. Similar trends were observed in the case of atmospheric pressure steam gasification of pine sawdust [136]. The formation of solid carbon is thwarted at high temperature. Indeed char is found up to 900 °C.

High pressure is favorable for char formation, as shown in Figure 2d. Below 10 bar no char is expected at 800 °C for an 80% wt. feeding stream. The effect of pressure is that of minimizing the overall volume of the system. Therefore, a solid, whose specific volume is normally far lower than that of a gas, is definitely advantaged.

The same analyses were conducted on microalga *Spirulina*: see Figure 2.3. All analyses point to trends which are very similar to those observed in studies on glycerol (Figure 2.2). On the other hand, it is evident that the conditions leading to formation of a solid phase for microalgae are substantially different than for glycerol. Solid carbon forms at lower feed concentrations and pressure and at higher temperatures. The formation of a solid phase seems to be "easier" for this type of biomass, i.e. for a substance with this specific ratios of carbon, hydrogen and oxygen.
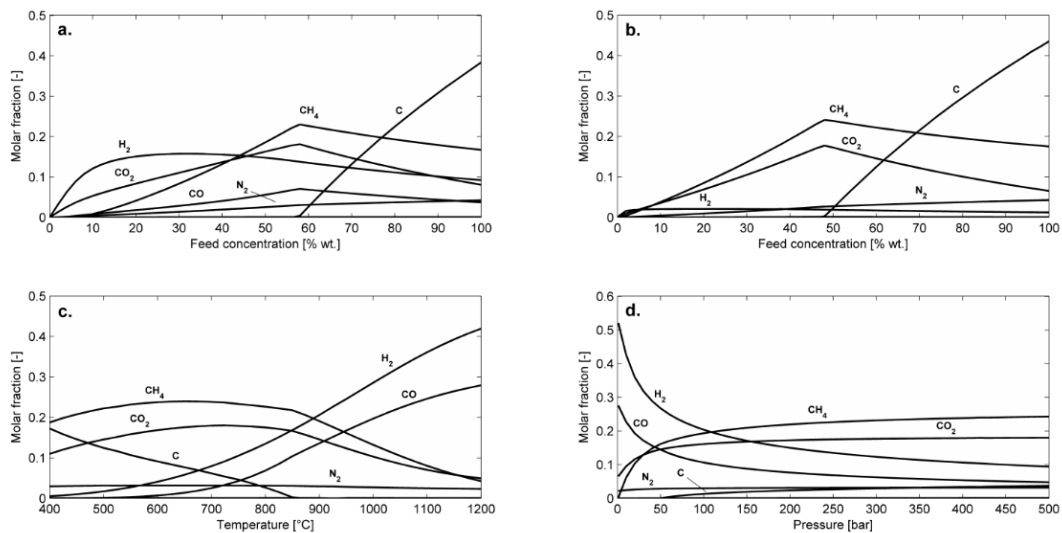
Figure 2.3 – Model results for the SCWG of microalga *Spirulina* under different operating conditions. (a) Equilibrium composition versus feed concentration (T=800°C, P=250 bar); (b) Equilibrium composition versus feed concentration (T=500°C, P=250 bar); (c) Equilibrium composition

versus temperature (P=250 bar, feed concentration = 60%); (d) Equilibrium composition versus pressure (T=800°C, feed concentration = 60%).

While Figure 2.3a and Figure 2.3b can be directly compared with Figure 2.2a and Figure 2.2b (temperatures and pressures coincide), this does not apply to other Figures. Figure 2.3c and Figure 2.3d were, indeed, obtained with a feed concentration of 60% (with 40% of the feed consisting of water and 60% of dry biomass $C_1H_{1.8655}O_{0.5893}N_{0.1275}$). This highlights the shift from a situation where only the supercritical phase is found at equilibrium to one where solid carbon is also found at equilibrium. In the case of microalga S*pirulina*, with a feed concentration of 80% (value utilized for the SCWG of glycerol, see Figure 2.2c and Figure 2.2d) solid carbon is found at equilibrium in the whole range of temperature analyzed.

The analysis with microalga *Spirulina* also enables to account for the presence of nitrogen compounds. Looking at Figure 2.3a to d, nitrogen is only found as N_2 in the product gas. Its molar fractions in the syngas seem to be solely determined by the biomass concentration in the feed. Neither temperature nor pressure appear to influence N_2 concentrations significantly.

A parameter significantly influencing the formation of char in the SCWG process is the elemental composition of the biomass used, as demonstrated by comparing the model results for glycerol with the ones for microalga *Spirulina*.

In order to account for different types of biomass, a representation based on ternary diagrams was adopted. In this depiction, each of the three axes of the diagram stands for the molar fraction of C, H and O in the biomass pseudo-molecule, represented by the simplified formula $C_xH_yO_z$ (nitrogen was neglected for this purpose). With this schematization, each biomass is represented by a point in the ternary diagram.
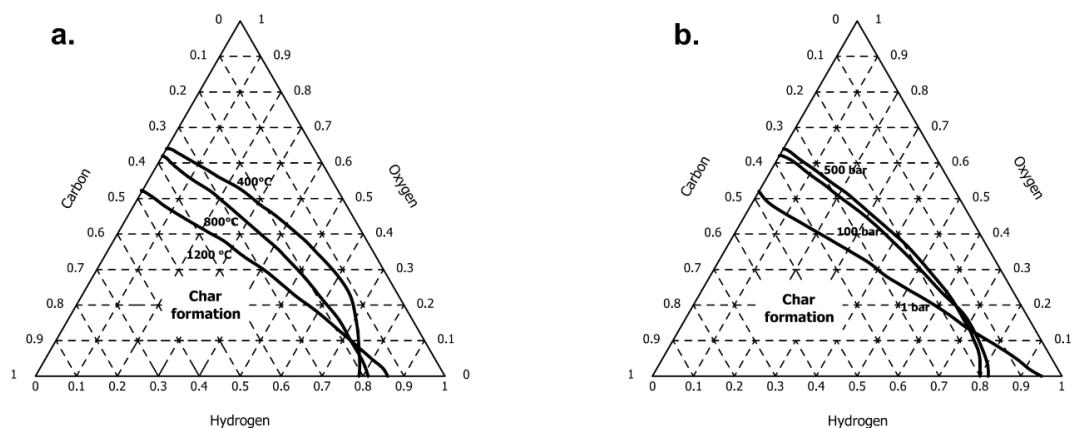
Figure 2.4 – Ternary diagrams for a generic biomass schematized by the pseudo-molecule $C_xH_yO_z$. Values on the axes refer to the molar ratios of C, H and O in the biomass molecule. (a) Char formation at varying temperature (P=250 bar); (b) Char formation at varying pressure (T=800°C).

Each axis of the ternary plot was divided into 50 intervals. For each point inside the triangle, a different run of the model was then performed to verify whether, for that particular biomass composition, graphitic carbon had been expected or not at equilibrium. Thus, these simulations are representative of a biomass concentration of 100%, which is the most favorable condition for char formation.

Figure 2.4a shows the results of the analysis when the system temperature was changed, holding the pressure constant at 250 bar. It is possible to see that, in general, biomass with a high oxygen content (upper zone of the diagram) does not cause the formation of solid carbon. This is also true for low carbon content feedstock.

The region where solid carbon is found is that in the bottom-left part of the triangle. However, the boundaries of this region are influenced by temperature. High temperature discourages carbon formation, as more energy is available for carbon to perform reforming reactions. Figure 2.4a reflects this statement, inasmuch as the "char formation" region is slightly wider at 400 °C than at 800 °C and 1200 °C. On the other hand, there is a small region around H=0.8 and O between 0 and 0.1 where the three curves invert their order, thus allowing for a char production favored by an increase in temperature.

Figure 2.4b shows the results of the same analysis conducted under different pressure conditions, while temperature was kept at 800 °C. Pressure plays an important role in char formation, as char formation is facilitated by high pressure. This can be easily explained from a thermodynamic perspective, since high pressure favors reactions determining a decrease in the total volume of the system. Under high pressure conditions solids are therefore favored, as also demonstrated by Figure 2.2d and Figure 2.3d. Figure 2.4b reveals that

the "char formation" region significantly enlarges when increasing pressure from 1 to 100 bar. However, in the typical pressure range of hydrothermal treatments, the effect of pressure on char formation is very limited: looking at Figure 4b, the curves corresponding to 100 and 500 bar almost overlap.

Interestingly, these ternary plots can also be used for a generic biomass feed with an arbitrary water/biomass ratio. It is just necessary to consider the amount of water in the calculation of the stoichiometric index x, y and z. The new point in the plot will then represent the SCWG of the considered biomass at the concentration desired. This is possible because the equilibrium composition of the system is determined by the relative amount of C, H and O supplied with the reagent stream, regardless of its actual composition.

2.4.2. Energy analysis

Another series of simulations were performed to evaluate the energy needs of the SCWG process. The process heat duty was calculated under different process conditions, i.e. by varying biomass concentration and temperature.

In order to calculate the process heat duty, isothermal operations were considered. Therefore, reagents and products are at the same temperature and the heat produced or required for the reaction (ΔH) is calculated as the difference between the enthalpy of the products and that of the reagents. In order to gain information on the quality of the product gas, its high heating value (HHV) was calculated, neglecting its water content.

Importantly, this approach only considers the amount of thermal energy required for (or provided by) the reaction itself. The energy required for the whole process is normally higher, because the input stream has to be heated up to the reaction temperature and it is not possible to recover all the sensible heat of the product stream to warm up the reagent stream.

Moreover, the possibility of using an oxidizing agent like O_2 was taken into account, in order to simulate the effect of a partial oxidation of the biomass. The amount of oxidizing agent was expressed in terms of equivalence ratio (ER), i.e. the ratio between the quantity of O_2 which is used and the amount of O_2 required for the complete stoichiometric oxidization of the considered biomass. Starting from the stoichiometric reaction for biomass combustion, ER was defined as:

$$ER = \frac{n_{O2}}{\left(x + \dfrac{y}{4} - \dfrac{z}{2}\right) \cdot n_{bio}} \qquad (2.22)$$

Figure 2.5 shows the heat duty and the HHV of the product gas for SCWG of glycerol at a concentration of 10% on weight basis, at varying temperatures and equivalence ratios (ERs). If no oxidizing agent is used, SCWG is weakly exothermic for temperatures below 680 °C and weakly endothermic above 680°C. If oxygen is added to the reagent stream, exothermic operations result in the whole range of temperatures analyzed, even with slight amounts of O_2. As ER increases, the HHV of the product gas decreases. At ER=1, the product gas shows a null heating value, since all combustible gases are oxidized.

Similar considerations apply also to the energy analysis conducted for the SCWG of microalga *Spirulina* (the model results are not reported for sake of brevity).
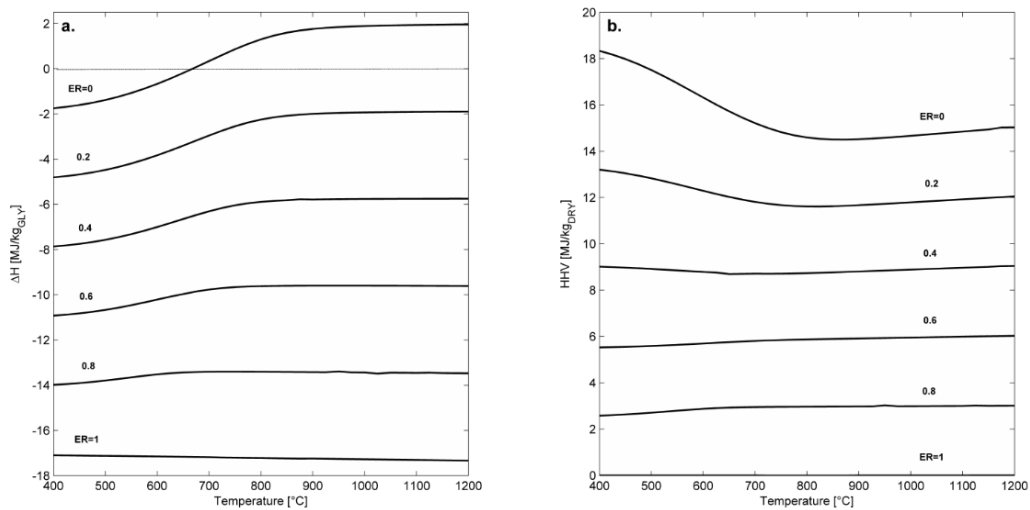
Figure 2.5 – Energy analysis for the SCWG of glycerol as a function of temperature and equivalence ratio ER (-) (P=250 bar, feed concentration = 10%). (a) Reaction heat duty; (b) HHV of the product gas on dry basis.

A similar analysis was performed where ER was kept null and glycerol concentration in the feed was increased from 5% to 100%. Results are presented in Figure 2.6. Figure 2.6a shows that, as temperature increases, the reaction requires more energy. Operations are exothermic at lower temperature and then become endothermic as temperature rises. It is possible to observe a temperature at which the reaction is energetically neutral: above it, operations are endothermic, while below it they are exothermic. For a feedstock concentration of 5%, this temperature is of approximately 580°C; for a 100% glycerol feed, this temperature is 1050°C. This suggests that the energy demand of the reaction decreases as the

feed concentration increases. On the other hand, it is possible to observe that, at high temperature, a higher glycerol concentration leads to slightly higher energy needs for the process (see the upper-right portion of Figure 2.6a where the curves cross). In any case, the amount of energy which the isothermal SCWG process provides or consumes is small, being below 2 MJ/kg$_{GLYCEROL}$.
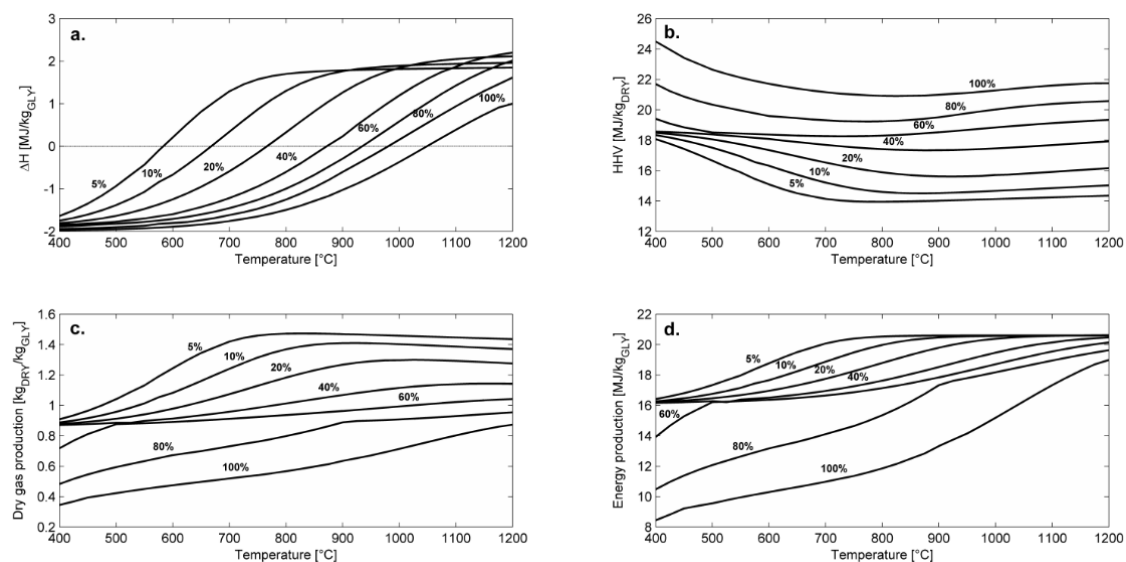
Figure 2.6 – Energy analysis for the SCWG of glycerol as a function of temperature and feed concentration (P=25 MPa, ER=0). (a) Reaction heat duty; (b) HHV of the product gas on dry basis; (c) Product gas yields per unit mass of fed glycerol; (d) Energy yields for the complete oxidation of the product gas derived by a unit mass of fed glycerol.

Figure 2.6b shows that, by increasing the feedstock concentration, the gas HHV rises, too. Anyway, it is important to focus on the amount of dry gas which can be produced, since at high glycerol concentrations considerable amounts of solid carbon are yielded. Figure 2.6c reports the specific production of dry gas per unit mass of feedstock. Gas production generally rises as temperature increases and glycerol concentration decreases. For highly concentrated streams (60% and 80%), a sudden change is observed in the slopes of the curves, corresponding to the formation of solid carbon, which lowers the specific gas yields.

Figure 2.6d shows the energy associated with the gas produced from 1 kg of glycerol. Given the results presented in Figure 6d (which stem from a combination of the results of Figure 2.6b and c), energy production is higher for diluted streams than for highly concentrated ones. Clearly, temperature does not play a significant role in this regard. Indeed, even though the gas HHV is higher at lower temperatures (Figure 2.6b), the specific gas produc-

tion is higher at higher temperatures (Figure 2.6c), thus playing a sort of "compensation" effect.

Some general remarks could be inferred from the energetic results obtained for the SCWG of glycerol (Figure 2.5 and Figure 2.6) and microalga *Spirulina* (not reported data). The isothermal SCWG process is weakly endothermic or energetically neutral in the temperature range 700-900 °C and for feed concentration between 10 and 20%, which are probably the most reasonable conditions for real applications of the process. In addition, for these conditions no char is expected at equilibrium (see Paragraph 2.4.1). Thus, to make the process energetically (and therefore economically) sustainable, the fundamental point is not represented by the energy necessary for the SCWG reaction itself but, instead, by the energy necessary to heat the reagents up to the reaction temperature. Actually, it is worth to underline that the reagent stream consists of biomass and huge amount of water. An optimal plant design becomes mandatory to make the SCWG process profitable, with efficient heat exchangers capable to transfer the sensible heat from the process product stream to the reagent stream. In addition to this, the results reported in Figure 2.5a suggest another possibility. The whole process could become energetically self-sustainable by adding to the reagent stream an oxidizing agent like O_2. Obviously, in this case the calorific value of the syngas produced would decrease, but not dramatically as testified by Figure 2.5b.

Future efforts in the SCWG field should cover, among the others (reaction kinetics, catalyst development, reactor material resistance testing), the design and optimization of the whole process: in this field nowadays only a few examples are at disposal in the literature [106].

2.5. Conclusions

A non-stoichiometric two-phase equilibrium model for the SCWG has been developed. This model enables to foresee the process conditions leading to char formation and the energy needs of the process.

Char formation is only relevant when processing concentrated streams, especially at low temperatures and when the carbon content of the chosen biomass is particularly high.

Isothermal energy analysis applied to glycerol shows that SCWG is weakly exothermic for temperatures below 680 °C and weakly endothermic above 680°C. But if a small amount of O_2 is added (ER=0.2), SCWG becomes exothermic in the whole temperature range analyzed (400-1200 °C).

2.6. Nomenclature

A dimensionless form for a

a Peng-Robinson attraction parameter (N m^4 mol^{-2})

B dimensionless form for b

b Peng-Robinson repulsion parameter (m^3 mol^{-1})

b^* term in Peng-Robinson EoS (m^3 mol^{-1})

c_p isobaric heat capacity (kJ mol^{-1} K^{-1})

$\mathbf{E}$ matrix whose elements are η_{ij}

f fugacity (Pa)

G Gibbs' free energy (kJ mol^{-1})

ΔH enthalpy change (kJ mol^{-1})

HHV   high heating value (kJ kg^{-1})

k_{ij} binary mixture parameter for intermolecular interactions

$\mathbf{K}$ matrix whose elements are k_{ij}

N number of components

n number of moles (mol)

P pressure (Pa)

$q_1,...,q_5$ Coefficients for c_p calculation

r Pearson's correlation coefficient

R universal gas constant (J mol^{-1} K^{-1})

ΔS entropy change (kJ mol^{-1} K^{-1})

T temperature (K)

$\widetilde{V}$ molar volume (m^3 mol^{-1})

x molar fraction

Z compressibility factor

Greek symbols

φ fugacity coefficient

μ chemical potential (kJ mol^{-1})

η_{ij} binary mixture parameter for packing of unlike components

ω acentric factor

Subscripts and superscripts

0 standard

c critical

f formation

m mixture

x stoichiometric index for carbon

y stoichiometric index for hydrogen

z stoichiometric index for oxygen

w stoichiometric index for nitrogen

Chapter 3[*]

Kinetics modeling

While the last Chapter dealt with thermodynamic equilibrium, this Chapter focuses on kinetics modeling. Such approach is able to describe the dynamic behavior of the system, that is the reactions transforming the original reactants into intermediates and then final products. Three models from the literature, developed for combustion or supercritical water oxidation, were implemented and run at conditions typical of SCWG. The models were compared with literature data and the one by Webley and Tester was selected as the most performing one. The main reaction pathways were identified and outlined.

3.1. Introduction

Thermodynamic modeling focuses on equilibrium, that is the situation in which the system composition remains constant. It is very important, since it is able to state which are the reaction final products and which is the energy behavior of the process. On the other hand, such approach provides no information of the transient state that leads from the reactants to the products.

More in deep, thermodynamics is not able to predict which are the reaction intermediates and which are the reaction chains leading from reactants to products. Above all, it does not provide any information about time. In other words, though we know which is the system equilibrium composition, we do not know how much time will be required to obtain that composition. This item is of outstanding importance for engineering and design. In order to properly size a reactor, indeed, it is fundamental to know the rates of the reactions to be carried out in it. This allows to state the optimal residence time, which determines the volume of the reactor.

The literature (see Paragraph 1.4.4) presents kinetics models which mainly address combustion or supercritical water oxidation (SCWO). In particular, these models are based on detailed kinetics, where a large number of elementary reactions is taken into account. It can be hypothesized that the reactions presented in these models are basically the same as those involved in SCWG. Thus, if these models are applied to a mixture fuel/water rather than a mixture fuel/oxidizing agent, they should allow for a successful interpretation of the experimental data.

The aim of this chapter is to apply the same elementary reaction models utilized for SCWO and combustion to SCWG of methanol, which can be considered a model compound for more complex alcohols. Moreover, methanol has a great importance on its own, since it can be used as an energy carrier, easier to handle than hydrogen. Some studies have thus used the term "methanol economy" to describe a possible scenario of widespread usage of this alcohol as energy carrier [137]. Such approach is completely new in the state-of-the-art literature. Three different models were chosen, implemented and then run. The models were also compared with literature experimental data. Finally, the main reaction pathways were identified.

3.2. Structure of the mathematical models

Each kinetics model is composed of a certain number j of components, i.e. chemical species, and a certain number i of elementary reactions. An elementary reaction describes the actual physical event leading to the transformation of the reagents into the products and, consequently, it normally involves a limited number of molecules (in general one or two). For example, for the generic i-th reversible elementary reaction:

$$\alpha A + \beta B \leftrightarrow \gamma C + \delta D \tag{3.1}$$

net reaction rate r_i can be expressed as the difference between forward and backward reaction rates:

$$r_i = k_i \, C_A^\alpha C_B^\beta - k_{-i} \, C_C^\gamma C_D^\delta \tag{3.2}$$

Where term k_i is the kinetics constant of the forward reaction, k_{-i} is that of the backward one and C_j is the molar concentration of specie j. The forward reaction kinetics constant can be calculated through the modified Arrhenius expression:

$$k_i = k_{o,i} T^{m_i} \exp\left(-\frac{E_{act,i}}{RT}\right) \tag{3.3}$$

Where $k_{o,i}$ is the pre-exponential factor, m_i is an exponent for the dependence on the temperature T, $E_{act,i}$ is the reaction activation energy and R is the universal gas constant.

Following this procedure, all the forward reaction rates can be calculated. To calculate the backward ones, thermodynamic considerations can be used. Indeed, at thermodynamic equilibrium the rates of forward and backward reactions are equal. As a consequence, for a generic reaction i:

$$k_i C_A^\alpha C_B^\beta = k_{-i} C_C^\gamma C_D^\delta \tag{3.4}$$

Thus:

$$\frac{k_i}{k_{-i}} = \frac{C_C^\gamma C_D^\delta}{C_A^\alpha C_B^\beta} = \prod_j C_j^{\nu_{j,i}} = Y_i \tag{3.5}$$

where $\nu_{j,i}$ is the stoichiometric coefficient of component j in reaction i (positive if j is a product, negative if j is a reactant). Term Y_i is called reaction quotient and it represents the product between the reactant and product concentrations at equilibrium, each elevated to its stoichiometric coefficient. Relating Y_i to the reaction equilibrium constant and assuming ideal gas behavior, Y_i can be calculated as reported in eq. (3.6):

$$Y_i = \prod_j C_j^{\nu_{j,i}} = \left(\frac{P_o}{RT}\right)^{\sum_j \nu_{j,i}} \exp\left(-\frac{\Delta G^o}{RT}\right) \tag{3.6}$$

where ΔG° is the difference of Gibbs free energy between products and reactants at reference pressure P_o (101,325 Pa).

Thus, the kinetics constant for the backward reaction is straightly determined as:

$$k_{-i} = \frac{k_i}{Y_i} \tag{3.7}$$

It is worth mentioning that the assumption of ideal behavior for the supercritical phase is made only for the computation of the kinetics constant for the backward reactions, in accordance with all the three reference models detailed in Paragraph 3.3. The utilization of a more complex and reliable equation of state (EoS), such as Peng-Robinson EoS, cannot be addressed for this scope considering that critical temperature, critical pressure and acentric factor are not available for the radical species present in the models. Peng-Robinson EoS is instead utilized to calculate total molar concentration (see Paragraph 3.3).

3.2.1. Reactions with pressure-dependent rates

Some reactions in the models show pressure-dependent rates. They are often represented by dissociation reactions and they are modeled following the Lindemann's approach.

Considering a generic dissociation reaction, by which a species A converts into a species P:

$$A \rightarrow P \tag{3.8}$$

It can be assumed that reaction (3.8) is the overall reaction of a mechanism made up of two elementary reactions. In the former, a single molecule of A collides with another molecule in the system to form activated complex $A*$

$$A + M \xleftrightarrow{\,1\,} A* + M \tag{3.9}$$

In the latter, $A*$ forms final product P

$$A* \xrightarrow{\,2\,} P \tag{3.10}$$
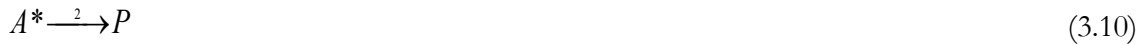
The molar balance of P can thus be expressed as:

$$\frac{dC_P}{dt} = k_2 C_{A*} \tag{3.11}$$

At steady state, considering reaction (3.10) irreversible:

$$\frac{dC_{A*}}{dt} = k_1 C_A C_M - k_{-1} C_{A*} C_M - k_2 C_{A*} = 0 \tag{3.12}$$

Thus:

$$C_{A*} = \frac{k_1 C_A C_M}{k_{-1} C_M + k_2} \tag{3.13}$$

Substituting eq. (3.13) into eq. (3.11):

$$\frac{dC_P}{dt} = \frac{k_1 k_2 C_M}{k_{-1} C_M + k_2} C_A = k_{eff} C_A \tag{3.14}$$

where

$$k_{eff} = \frac{k_1 k_2 C_M}{k_{-1} C_M + k_2} \tag{3.15}$$

Notably, if the pressure is high, the concentration of M is correspondingly high. In this case, k_{eff} can be approximated as:

$$k_{eff} = \frac{k_1 k_2}{k_{-1}} = k_\infty \tag{3.16}$$

Reaction (3.8) is thus first-order. On the other hand, at low pressures, it is unlikely that a molecule of *A* collides with a third body. Equation (3.15) becomes:

$$k_{eff} = k_1 C_M = k_0 C_M \tag{3.17}$$

Reaction (3.8) will be thus second-order. For intermediate pressures, then, this type of reactions show an order intermediate between 1 and 2. Sometimes, the overall reaction rate is also corrected by means of a factor *F*, the so-called "broadening parameter", which is derived from RRKM calculations. The final expression for k_{eff} is thus:

$$k_{eff} = F \frac{k_0 k_\infty C_M}{k_0 C_M + k_\infty} \tag{3.18}$$

Kinetics constants k_0 and k_∞ depend on the temperature as a result of an Arrhenius-like relation; broadening parameter *F* also has a temperature dependence.

3.2.2. Reactor

To perform mass balances for each of the components involved in the model and compare the results with the literature data provided by Boukis *et al.* [50], the kinetics scheme was implemented for an isothermal and isobaric continuous plug-flow reactor (PFR).

The PFR is assumed to consist of a tube with cross-sectional area *S* and longitudinal coordinate ξ. The steady-state molar balance for generic component *j* for infinitesimal control volume *dV* between the sections at ξ and $\xi+\mathrm{d}\xi$ gives:

$$C_j \frac{dQ}{d\xi} + Q \frac{dC_j}{d\xi} = S \sum_i v_{j,i} r_i \tag{3.19}$$

Where *Q* is the volumetric flow rate.

Apparent residence time τ at coordinate ξ can be defined as the ratio between the reactor volume up to that coordinate and volumetric flow rate Q_0 at the reactor inlet:

$$\tau = \frac{S\xi}{Q_0} \tag{3.20}$$

Importantly, to calculate the actual residence time (time spent by a fluid element inside the reactor) the volumetric flow rate variability (due to a variable number of moles owing to reactions) should be considered along the reactor. On the other hand, a simpler definition

of the apparent residence time is useful to draw a comparison with experimental data, since the experimental literature normally uses it for the sake of simplicity. Taking the differential of (3.20):

$$d\tau = \frac{S}{Q_0} d\xi$$ (3.21)

Then, substituting this expression into (3.19), the molar balance equation for generic component j becomes:

$$\frac{dC_j}{d\tau} = \frac{Q_0}{Q} \sum_i v_{j,i} r_i - \frac{C_j}{Q} \frac{dQ}{d\tau}$$ (3.22)

This formula expresses the molar balance for generic component j as a function of residence time τ.

Since the system pressure and temperature are constant, total molar concentration C_T (in other words: the system molar density) can be assumed to be constant as well. The system composition variation, which takes place along the reactor, does not reasonably have a significant impact on molar density – this would be strictly exact for a mixture of ideal gases. Thus, if a total molar balance is written, the time derivative of C_T will be null. Indicating with r_T the total molar generation rate (which is obtained summing up all the molar generation rates of the various components), the following is achieved:

$$\frac{dQ}{d\tau} = \frac{Q_0 r_T}{C_T}$$ (3.23)

The expression of the molar balance for the j-th component thus becomes:

$$\frac{dC_j}{d\tau} = \frac{Q_0}{Q} \sum_{i=1} v_{j,i} r_i - \frac{C_j Q_0 r_T}{Q C_T}$$ (3.24)

The model output is then the solution of the system of j non-linear ODEs in the form of eq. (3.24) plus eq. (3.23). To perform the calculations, a set of initial conditions must be established, which are the concentration of each species at time zero and the flow rate at the reactor inlet, whose value can be chosen arbitrarily (for simplicity, it was assumed to be equal to 1 [m³/s]).

Table 3.1 – Principal characteristics of the analyzed kinetics models: number of reactions, number of components and species involved (● indicates that the species is involved in the model).

	GRI-Mech	**Brock and Savage**	**Webley and Tester**
Reactions	215	148	66
Components	34	22	17
Species			
O	●	●	●
O_2	●	●	●
H	●	●	●
OH	●	●	●
H_2	●	●	●
HO_2	●	●	●
H_2O_2	●	●	●
CH	●	●	
CO	●	●	●
CH_2	●	●	
HCO	●	●	●
$CH_2(s)$	●		
CH_2O	●	●	●
CH_3	●	●	●
CH_4	●	●	●
CO_2	●	●	●
CH_2OH	●		●
CH_3O	●	●	●
CH_3OH	●	●	●
C_2H	●		
C_2H_2	●		
HCCO	●		
C_2H_3	●		
CH_2CO	●		
C_2H_4	●		
C_2H_5	●		
C_2H_6	●		
H_2O	●	●	●
C	●		
HCOOH	●		
CH_2CHO	●		
CH_3CHO	●		
C_3H_8	●		
C_3H_7	●		
CH_2OH		●	
CH_3O_2		●	
CH_3O_2H		●	
HOCO		●	

3.3. Overview of the models and implementation

In the present work, three different models were analyzed. Each of them involves a certain number of components, i.e. chemical species, and a certain number of reactions. All the models provide a set of kinetics parameters: for each reaction, k_0, m and E_{act} are given for the forward reaction. Backward reaction rates are calculated in the way described in Paragraph 3.2.

The three models which were chosen for the analyses are GRI-Mech 3.0 [138], Brock and Savage's model [101] and Webley and Tester's model [99]. Each of these models accounts for gas-phase radical mechanisms. Radical reactions can be assumed to be the only reactions that take place in supercritical water at high temperature and pressure. Under such conditions, the ionic product of water is extremely low, thus ionic reactions can be reasonably ignored [101]. An overview about each model's properties, including the list of the components involved, is given in Table 3.1.

GRI-Mech 3.0 [138] is a model developed to describe the combustion of air/methane mixtures; however, its application can also be extended to the combustion of other light hydrocarbons. GRI-Mech 3.0 is one of the most used kinetics models for gas-phase oxidative processes. It was included in the analysis due to the large number of radical chemical reactions involved and to the possibility to handle different pressures. In its original form, it consists of 325 reactions and 53 components. However, since many reactions are intended to describe the formation of nitrogen compounds in combustion reactions, which are not relevant to the present work, a subset of the model was considered. It comprises 215 reactions and 34 components.

Brock and Savage's model [101] was conceived for the supercritical water oxidation of methane, hydrogen and C_1 compounds. It is based on 148 reactions with 22 components. All the elementary reactions were taken from existing literature data about combustion and atmospheric chemistry.

Webley and Tester's model [99] was also developed for methane SCWO and predicts 66 reactions with 17 components. As well as for Brock and Savage's model, the model parameters were taken from existing chemical kinetics literature.

It is worth noticing that neither Brock and Savage's nor Webley and Tester's models were calibrated by their authors to fit the experimental data better. On the other hand, GRI-Mech 3.0 was optimized for CH_4 combustion, thus its reliability is questionable outside its standard application field.

The models were implemented by means of the computing package MatLab®. Thermodynamic data were taken from NASA polynomials [131]. The resulting system of ODEs gave rise to a stiff problem, which was solved through the routine ODE15S, that can deal effectively with such numerical problems. Among the initial conditions, total molar concentration C_T was calculated through the Peng-Robinson EoS.

The three models were run at a temperature of 600°C and a pressure of 250 bar, with a methanol concentration of 50% on a weight basis, corresponding to 36% on a molar basis, the remaining part being water. These operational conditions are the same as those utilized in the experimental work of Boukis *et al.* [50], who gasified methanol in supercritical water by means of a reactor made of a nickel-based alloy. A comparison between model outputs and experimental results was then drawn. Webley and Tester's model was also tested at 600°C, 250 bar and a methanol weight concentration of 26.2% and 64%, which are other experimental conditions implemented in the above-mentioned work by Boukis *et al.* [14].

3.4. Results and discussion

First of all, each model was run in order to assess its specific behavior. Then, a comparison regarding methanol conversion rate and principal gaseous products output was drawn. Furthermore, the main reaction networks for Webley and Tester's model are presented. Finally, a highly-simplified model improvement is proposed.

3.4.1. Model runs

Figure 3.1 shows the model results obtained by means of GRI-Mech 3.0. In the diagram, a logarithmic time scale was adopted, in order to highlight the reactions occurring very slowly and, as a result, quite late. On the other hand, this choice also emphasizes the processes taking place in the first seconds of the reaction.
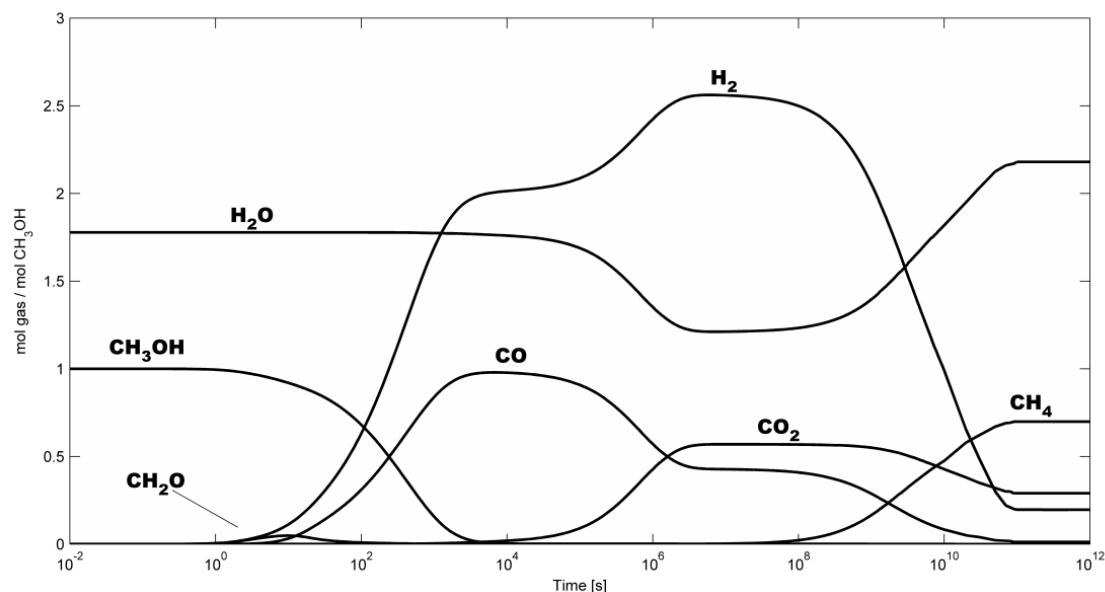
Figure 3.1 – Gas composition vs. time as predicted by the model GRI-Mech 3.0. Process conditions: 600°C, 250 bar, CH_3OH 50%wt. in the feed. X-axis in logarithmic scale.

GRI-Mech 3.0 exhibits quite slow reactions, which take place over a relatively long time scale. Among the products, only H_2 and CO are present in significant amounts after the first few hours; formaldehyde is also present as a reaction intermediate in the first seconds.

The apparent steady-state, which is achieved after approximately 2000 s of run time, is determined by the dissociation reaction of methanol into two moles of hydrogen and one mole of carbon monoxide. Therefore, the ratio of H_2 to CO is 2:1. Water plays nearly no role in the reaction mechanism.

However, if the simulation is performed for at least 10^4-10^6 s, the effect of the water-gas shift (WGS) reaction becomes visible. Water starts to play an active role, since it reacts with carbon monoxide to yield more hydrogen, along with carbon dioxide:

$$CO + H_2O \rightarrow H_2 + CO_2 \qquad (3.25)$$

After more time, hydrogen ceases to form and begins to be consumed instead. At the same time, water and methane form, while carbon monoxide continues to decrease. These are the effects of the methanation reaction, which can be written in the following way:

$$CO + 3H_2 \rightarrow CH_4 + H_2O \qquad (3.26)$$
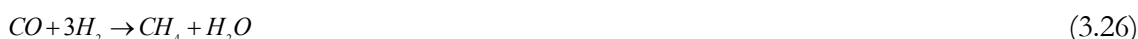
By means of this reaction, the system tends to the thermodynamic equilibrium composition, which is presented in Table 3.2.

Table 3.2 – Equilibrium composition of the product gas for the three experiments of Boukis *et al.* [50]. Gas yields are expressed as moles of gas per mole of feeding methanol.

	CH_3OH 26.2% wt.	CH_3OH 50% wt.	CH_3OH 64% wt.
H_2	0.410	0.196	0.134
CH_4	0.644	0.698	0.714
CO	0.013	0.012	0.012
CO_2	0.343	0.290	0.274

Figure 3.2 shows the same analysis applied to the Brock and Savage's model. First of all, faster kinetics can be observed: the system reaches a first apparent steady state just after approximately 100 s. Here, unlike GRI-Mech 3.0, methane is also expected during the short-time behavior.
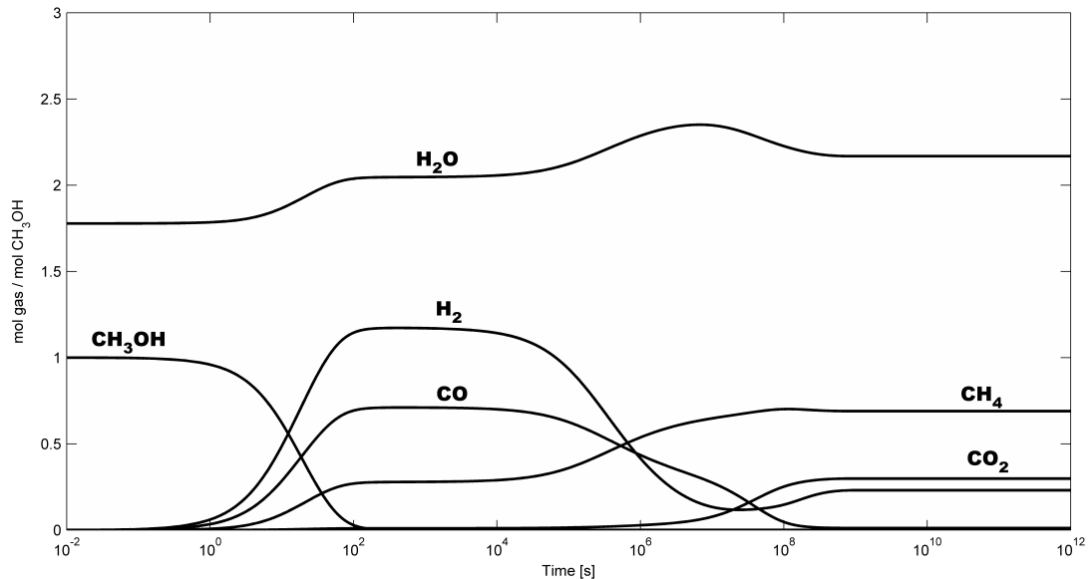
Figure 3.2 – Gas composition vs. time as predicted by Brock and Savage's model. Process conditions: 600°C, 250 bar, CH_3OH 50%wt. in the feed. X-axis in logarithmic scale.

Furthermore, water increases during the first seconds of run time. A more detailed analysis of the reaction mechanism revealed that the water increase is related to methane formation, owing to the following mechanism:

$$CH_3OH + H* \rightarrow CH_3* + H_2O \qquad (3.27)$$

$$CH_3* + H* \rightarrow CH_4 \qquad (3.28)$$
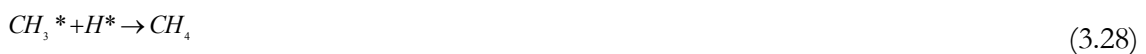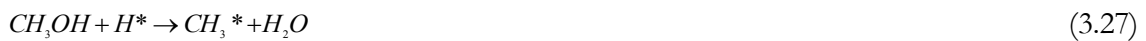
Again, water does not participate in the reaction; in this case, it is even a product. As a consequence of methane formation, H_2 and CO yields are lower with respect to the GRI-Mech 3.0. Moreover, no formaldehyde formation is noted.

On a long-term horizon, hydrogen and carbon monoxide decrease, while water and methane increase. What is also noticeable is the formation of carbon dioxide.

This is the combined effect of water-gas shift [eq. (3.25)] and CO methanation [eq. (3.26)].

The methanation reaction is much slower than methanol decomposition to hydrogen and carbon monoxide. This is also confirmed by a number of experimental works [49, 50, 80, 139]. The effect of methanation is also partially superposed with the water-shift reaction, which starts taking place later on (around 10^7 seconds). The occurrence of water-gas shift is witnessed by the increase in both carbon dioxide and hydrogen; water, after being formed by methanation, is then consumed by water-gas shift. Brock and Savage's model thus considers methanation to be faster than water-gas shift: this causes hydrogen to exhibit a minimum at around 10^7 seconds of run time.

Figure 3.3 shows the results of the analysis for Webley and Tester's model. Here, methanol decomposition kinetics is definitely faster and a complete conversion is achieved in just a few tens of seconds. Water exhibits a behavior similar to the one described above: it acts as a reaction product, since it is produced along with the formation of methane [eq.s (3.27-28)]. Formaldehyde formation is also clearly visible in the first seconds of reaction. This chemical species shows a peak, then it is completely consumed.
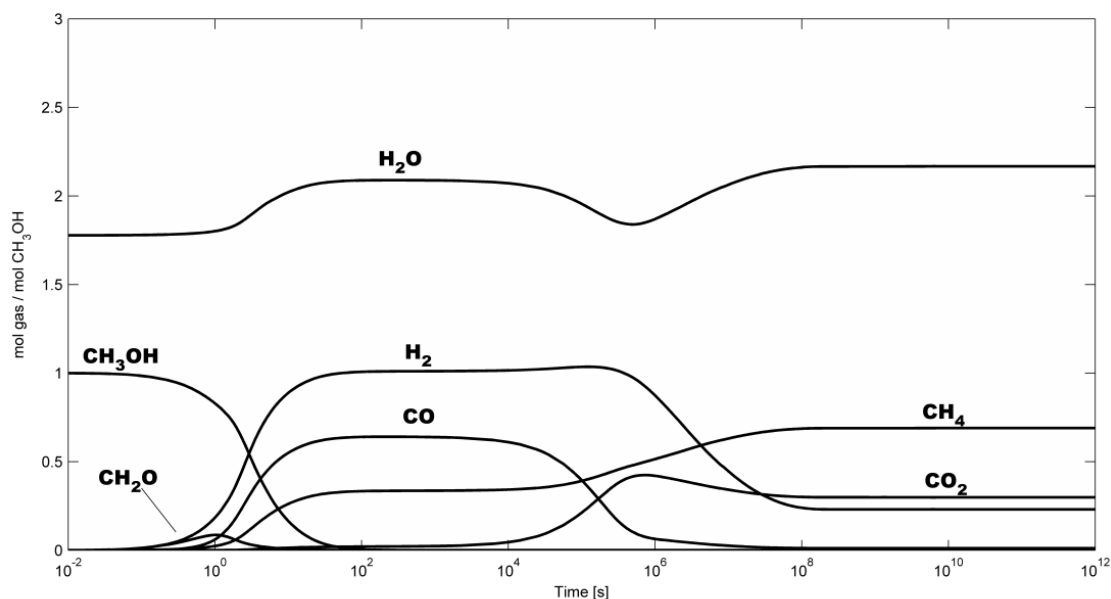
Figure 3.3 – Gas composition vs. time as predicted by Webley and Tester's model. Process conditions: 600°C, 250 bar, CH_3OH 50%wt. in the feed. X-axis in logarithmic scale.

.

After 10^4 s, the effect of water-gas shift and methanation becomes clearly visible. Here, water-gas shift takes place much earlier than methanation. As a result, it is possible to see that water is first consumed, it then reaches a minimum, and eventually it is again produced by means of methanation.

Expectedly, all the models proposed converge to the equilibrium composition, since kinetics expressions are all written in compliance with thermodynamic consistency criteria. The main processes predicted by each model are essentially the same: methanol decomposition, water-gas shift, methanation. However, the different relative velocity of each of these processes determines a different model behavior. Methanol decomposition, the first to occur, always results in CO, H_2 and CH_4. Subsequent reactions re-arrange the amount of each compound towards equilibrium composition.

3.4.2. Methanol conversion

A first comparison among the models was made by contrasting methanol conversion, that is the ratio between the mass of the reacted methanol and its initial amount. The results of this comparison are shown in Figure 3.4.
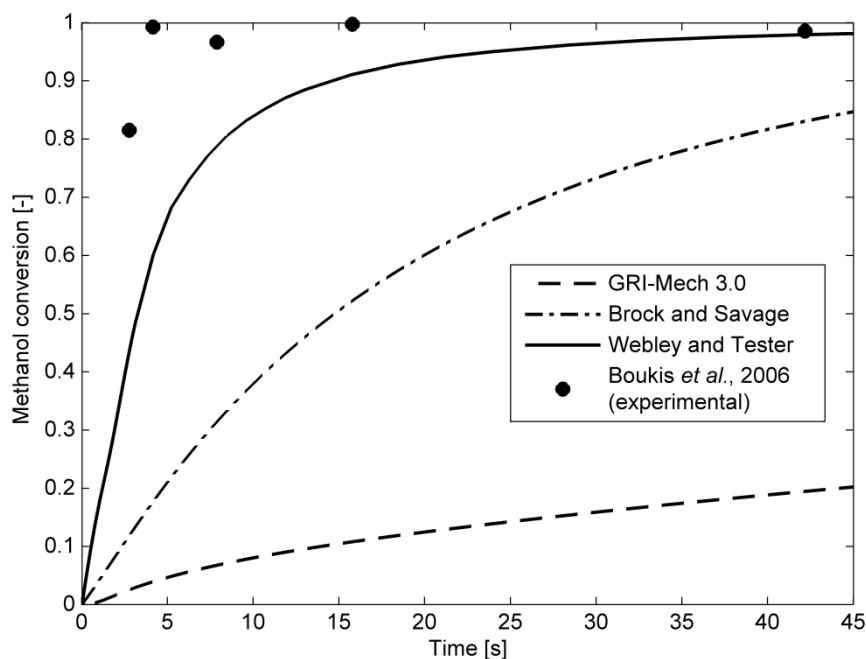
Figure 3.4 – Comparison between the methanol conversion foreseen by the three models and the experimental data of Boukis *et al.* [50]. Process conditions: 600°C, 250 bar, CH_3OH 50% wt. in the feed.

Methanol conversion rates are quite different for each model. Webley and Tester's model is the most effective in predicting methanol conversion, since it is the fastest one. On the other hand, it is still slower with respect to the experimental data. The other models show even slower kinetics. GRI-Mech mechanism is the slowest: in the first 10 seconds, it foresees a conversion lower than 10%.

These results can be explained by analyzing the structures of each model. GRI-Mech, which was designed for methane combustion, was optimized for high temperature reactions. Moreover, some important reactions involving methanol are not foreseen, as they are not significant in the methane combustion context.

Models by Brock and Savage and Webley and Tester present nearly the same key-reactions. However, they use a different approach to pressure-dependent reactions. In Webley and Tester's model, the pressure dependence of such reactions was taken into account by means of the falloff curves method and/or by RRKM calculations [99]. As a result, kinetics parameters are modified to take into account the pressure effect, but the reactions are always considered as first order ones. This does not always apply to Brock and Savage's approach, where the same reactions have reaction orders between 1 and 2, with generally slower rates.

Owing to these results, it was decided to restrict any other comparison to the sole Webley and Tester's model, since the others exhibit too different responses with respect to the experimental data.

3.4.3. Product gas composition

The comparison between the product gas composition predicted by Webley and Tester's model and the experimental findings of Boukis *et al.* [50] is presented in Figure 3.5.
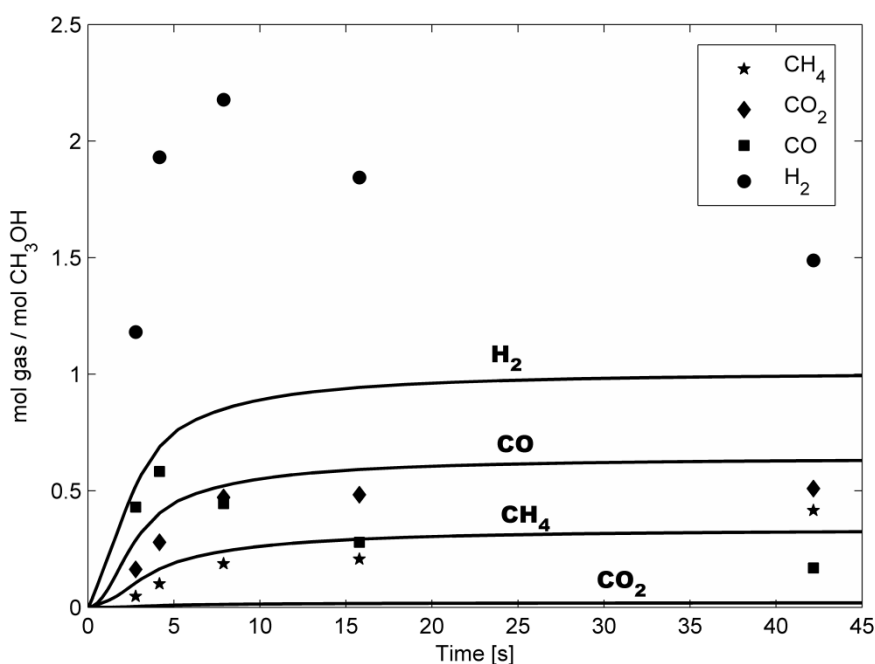
Figure 3.5 – Comparison between the product gas composition foreseen by Webley and Tester's model and the experimental data of Boukis *et al.* [50]. Process conditions: 600°C, 250 bar, CH3OH 50 % wt. in the feed. Points: experimental data. Solid lines: model predictions.

Although the model is able to foresee the methanol decomposition rate in an almost effective way, the product gas composition is not predicted with the same accuracy. Indeed the experimental data show that hydrogen decreases after a peak at around 10 seconds. A similar behavior is found for carbon monoxide, while methane and carbon dioxide show a monotonic increasing trend.

The presence of a peak for CO and H_2 is justified by the fact that the methanation reaction [eq. (3.26)] is much slower than methanol decomposition to CO and H_2. As a consequence, H_2 and CO accumulate in the system until the methanation reaction is able to convert them. The occurrence of such peaks can also be observed in other experimental works, not necessarily concerning supercritical conditions [49, 140].

Webley and Tester's model does not succeed in forecasting these trends. It generally overestimates CO, and the H_2 peak is not present. Carbon dioxide is completely absent from the model results. On the other hand, the model seems to interpret methane correctly. This suggests that direct methanol decomposition to methane is an important reaction pathway, especially for the very-short-time system behavior.

The model was also tested under different conditions, in order to assess its capability to provide meaningful results. It was subsequently run with feeding methanol concentrations of 26.2% and 64% on a weight basis. The experimental results corresponding to these conditions are also present in the work of Boukis *et al.* [14].

The results can be seen in Figure 3.6 and Figure 3.7. The model allows for a methanol conversion which is slower than the experimental data and it does not succeed in forecasting the trends for carbon monoxide and hydrogen, while the fitting is quite good for methane. Previous conclusions can be thus extended to the present cases.
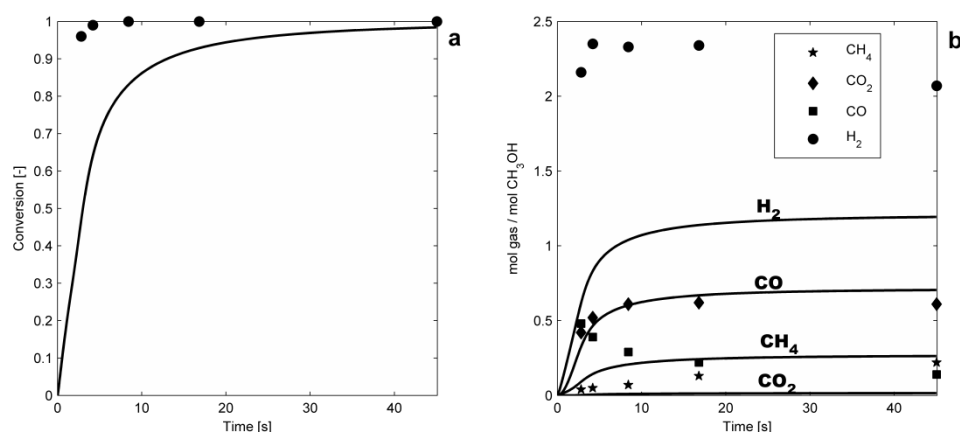
Figure 3.6 – Comparison between methanol conversion (a) and product gas composition (b) foreseen by Webley and Tester's model and the experimental data of Boukis *et al.* [50]. Process conditions: 600°C, 250 bar, CH_3OH 26.2% wt. in the feed. Points: experimental data. Solid lines: model predictions.
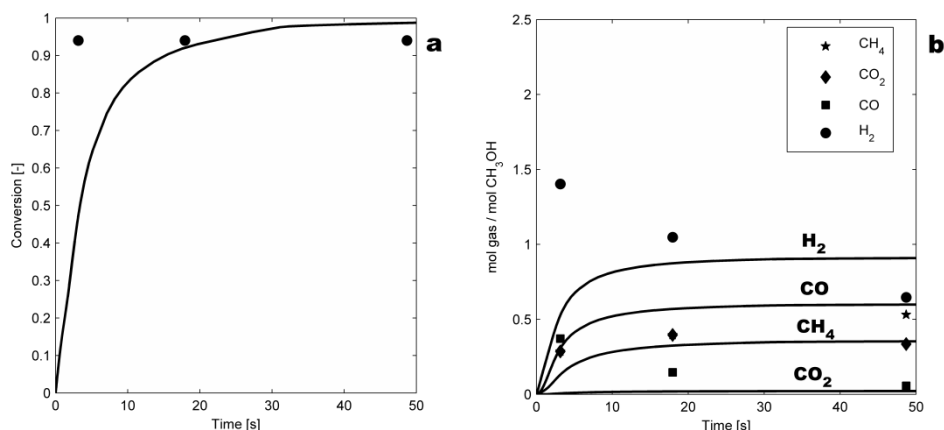
Figure 3.7 – Comparison between methanol conversion (a) and product gas composition (b) foreseen by Webley and Tester's model and the experimental data of Boukis *et al.* [50]. Process conditions: 600°C, 250 bar, CH_3OH 64% wt. in the feed. Points: experimental data. Solid lines: model predictions..

A possible explanation for the experimental trends is the presence of two important reactions: water-gas shift [eq. (3.25)] and methanation [eq. (3.26)]. Both preferably take place through catalytic mechanisms, where a metallic surface is involved. Common catalysts for the WGS reaction are iron, copper, platinum and gold [141], but nickel was also used for this purpose [142]. During the experimental activities, the metallic surface is usually that of the reactor walls, which exerts a significant influence on kinetics according to several authors [143]. It is actually possible to observe the water-gas shift reaction in homogeneous phase (see Paragraph 3.4.4), that is without any catalyst. Anyway, such reaction would be some orders of magnitude slower than the catalyzed one [144].

The same considerations apply to CO methanation. A homogeneous methanation reaction is actually possible. All the three models are able to foresee it in a homogeneous phase but its kinetics is always extremely slow. Methanation is rather carried out on ruthenium and nickel catalysts, with appreciable rates [145]. It is very likely that in real reactors methanation also occurs on some metallic surfaces as a result of this heterogeneous mechanism.

Since the implemented model is developed for homogeneous gas-phase reactions, reactions (3.25) and (3.26) do not show significant kinetics. As a consequence, only methanol decomposition to CO, H_2 and a few CH_4 is predicted in a short time.

The good correspondence between the model results and the methanol decomposition experimental data may suggest that CH_3OH decomposition reactions take place to a significant extent in the homogeneous-phase. On the other hand, the other reactions, through

which the gaseous species rearrange themselves to give the final equilibrium products, are most likely to occur on the surface of a catalyst. An extension of the model with such heterogeneous reactions should help to obtain better results.

3.4.4. Main reaction mechanisms

Webley and Tester's model was more deeply analyzed in order to identify the main reaction pathways it involves, thus trying to acquire a more systematic and critical knowledge about methanol SCWG reactions. It is worth noticing that the reaction schemes drawn for Webley and Tester's model can be generally extended to the other two models.

In order to identify the main reaction pathways, the reactions with the highest rates were considered. However, it should be emphasized that other reaction paths are also possible, though with less importance.

As the proposed mechanism is radicalic, it is necessary to have initiation reactions where radicals form starting from stable species. The initiation mechanism of the analyzed model is the one depicted in Figure 3.8. This mechanism is determined by the formation of the OH* radical from the methanol molecule. Such radical subsequently reacts with another methanol molecule, forming water and CH_2OH^*. The latter will be able to generate H* through reaction 2 in Figure 3.9. H* is the most active in the successive propagation reactions.
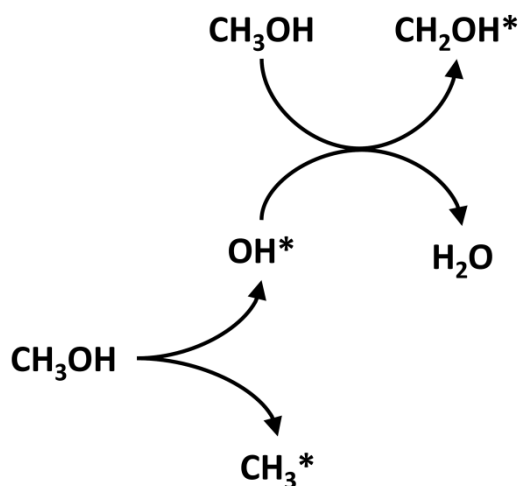
Figure 3.8 – Radicalic initiation reactions involved in Webley and Tester's model.

After initiation, propagation reactions take place. These reactions neither create nor destroy the radicals, but they allow for the transformations from complex molecules to simpler species. Propagation reactions are the most important in the model, since they exhibit the highest rates. Figure 3.9 shows the most important mechanisms.
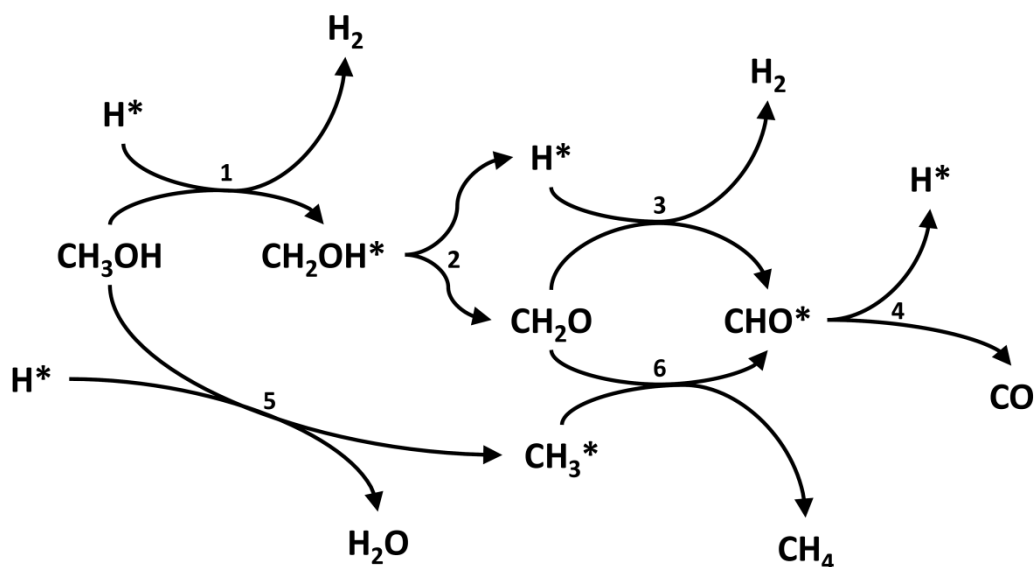
Figure 3.9 – Radicalic propagation reactions for methanol degradation involved in Webley and Tester's model.

In the upper branch of Figure 3.9, it is possible to see that radical H* acts as a sort of catalyst for the reactions converting methanol into hydrogen and carbon monoxide (1-4). This reaction chain can also be divided into two parts, since the reactions leading to the formation of formaldehyde (1-2) are faster than those which convert formaldehyde into CO (3-4). As a result, CH_2O accumulates as a reaction intermediate, as witnessed by Figure 3.3. The occurrence of formaldehyde as a reaction intermediate was also experimentally registered by van Bennekom *et al.* [51]. Radical H* also plays a fundamental role in the conversion of methanol into methane, which is represented by reactions 5 and 6.

Another important mechanism is the one describing the water-gas shift reaction, by which CO reacts with water to form H_2 and CO_2. In gas-phase, this reaction can be expressed by the well-known Bradford's mechanism [146], which is shown in Figure 3.10.
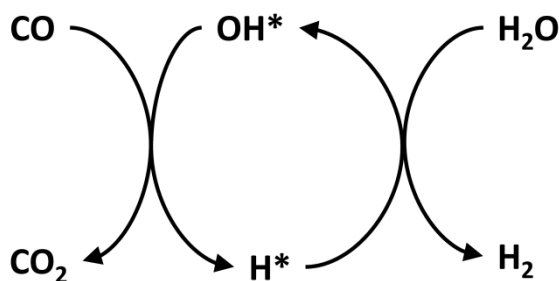
Figure 3.10 – Reaction scheme for homogeneous water-gas shift involved in Webley and Tester's model (Bradford's mechanism).

The WGS mechanism is thus made up of two chained reactions where both radicals OH* and H* are involved. Bradford's mechanism results in very slow reaction rates, which occur in a medium-long time scale, as shown by Figures 3.1-3.

It is worth noticing that in Webley and Tester's model water does not play any role in methanol decomposition. In other words, water only intervenes after the products of methanol decomposition form, in order to adjust the equilibrium between CO and CO_2 through the water-gas shift reaction.

Figure 3.11 describes the mechanism for methanation.
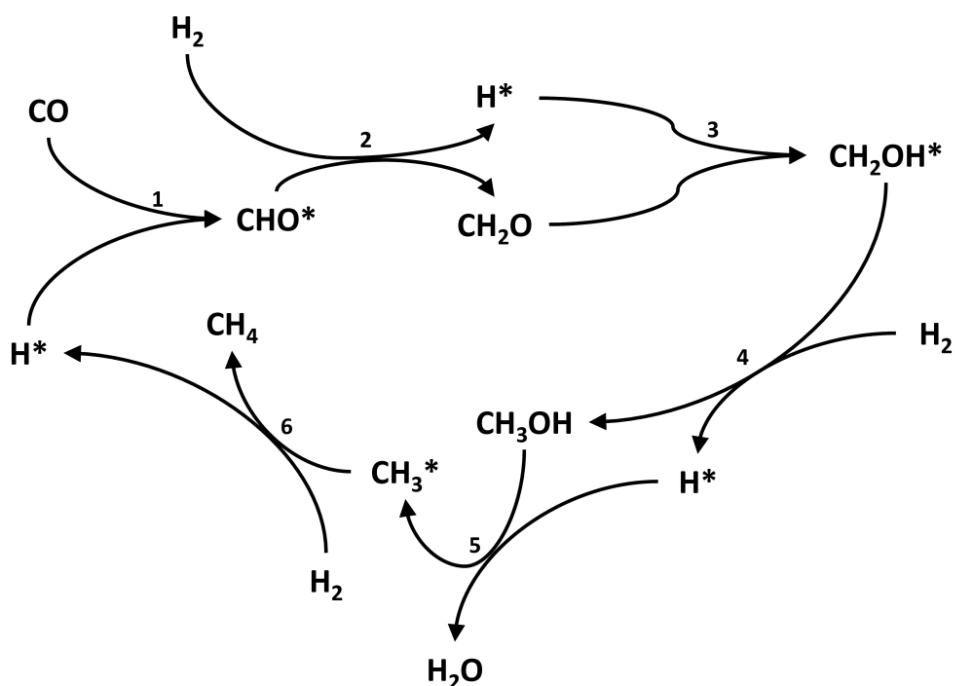
Figure 3.11 – Reaction scheme for homogenous methanation involved in Webley and Tester's model.

Methanation can be considered a cyclic scheme, catalyzed by radical H*. It is interesting to note that many of the reactions involved in this scheme are the same as in the methanol decomposition scheme shown above (Figure 3.9), but they take place in the opposite direction. Moreover, while in Figure 3.9 all the reactions have a non-negative molecularity (they produce a net increase in the total number of moles), in the methanation scheme all the reactions entail a non-positive molecularity (see reactions 1 and 3), thus reducing the total moles of the system. This behavior can be favored when operating at high pressure as in the case of SCWG.

3.4.5. Model improvement

The identification of the most important reaction pathways plays a fundamental role for improving the model in order to comply better with experimental data. Here, a rough attempt of model upgrade was carried out by changing the pre-exponential factors in Webley and Tester's model for the reactions shown in the reaction pathways.

In particular, the k_0 of the reactions in Figure 3.8 and Figure 3.9 (methanol decomposition to H_2, CO and CH_4) were multiplied by a factor of 2.5; the k_0 of the water-gas shift reactions (Figure 3.10) was multiplied by a factor of 10^5. Model results before and after improvement were compared with the experimental data of Boukis *et al.* [50] in parity plots (Figure 3.12). All the experimental data of Figure 3.4 to Figure 3.7 are accounted for in Figure 3.12. Table 3.3 shows the values of the RMSPE (root mean square percentage error, defined by eq. (3.29)) calculated for both the original model and the upgraded one. The last shows far better agreement with experimental data than the original model. This is true for methanol conversion and production of all the gases but methane.

$$RMSPE = 100 \sqrt{\frac{\sum_{h=1}^{N} \left(\frac{q_{h,\exp} - q_{h,\text{mod}}}{q_{h,\exp}} \right)^2}{N}} \tag{3.29}$$
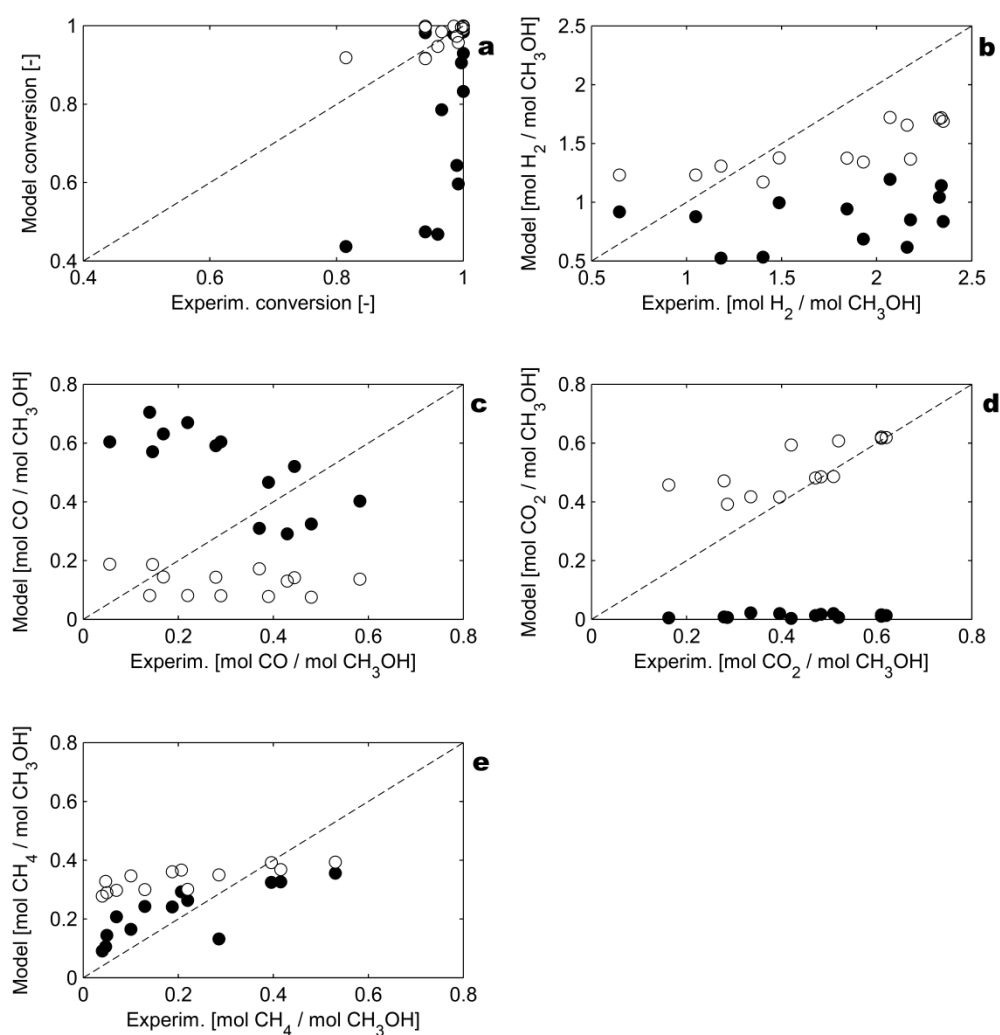
Figure 3.12 – Comparison between model predictions and experimental data of Boukis *et al.* [50]. Filled circles: original Webley and Tester's model. Empty circles: upgraded model. (a) Conversion; (b) Hydrogen; (c) Carbon monoxide; (d) Carbon dioxide; (e) Methane.

Table 3.3 – Root mean square percentage error (RMSPE) for the original Webley and Tester's model and the upgraded model, obtained by comparison with the experimental data of Boukis *et al.* [50].

	Webley and Tester	Model improvement
Conversion	0.2889	0.0453
H_2	0.5342	0.3385
CO	3.2210	0.8810
CO_2	0.9721	0.5638
CH_4	0.9743	2.9470

Though this procedure is just a sort of "exercise", it clearly highlights the contribution of the single reaction pathways. Methanol conversion forecasts improve significantly with only a slight change in the kinetics parameters, showing that, probably, the real reaction mechanism is very close to the modeled one. On the other hand, the water-gas shift mechanism needs a huge multiplier to give a better fit. This suggests that the rate of such mechanism is extremely under-estimated and that, certainly, some catalytic kinetics should be considered.

3.5. Conclusions

In the present work, three different models were implemented to describe methanol gasification in supercritical water. Model results were also compared with experimental data. Although the different models are based nearly on the same set of key-reactions, their results are very different. Webley and Tester's model is the most effective in interpreting methanol conversion experimental data.

The most significant reaction pathways for Webley and Tester's model were obtained and outlined. A fundamental role is played by radical H*, which is able to propagate the radicalic reactions converting methanol into CO and H_2.

The runs of the three models revealed that they can apply almost exclusively to methanol decomposition to CO, H_2 and CH_4. Other important reactions, such as water-gas shift and methanation, show extremely slow kinetics. In our opinion, this is certainly explained by the fact that such reactions usually take place on the surface of a catalyst which, in experimental conditions, is provided by the reactor walls. The three implemented models only address homogeneous gas-phase reactions. A future extension of such models with catalytic kinetics should contribute to an improvement in the results.

3.6. Nomenclature

C   Concentration ($mol\ m^{-3}$)

E_{act} Activation energy ($J\ mol^{-1}$)

F   Broadening parameter

$G°$ Standard Gibbs free energy ($J\ mol^{-1}$)

k   Kinetics constant (dimensions depending on reaction order)

k_0 Pre-exponential factor (dimensions depending on reaction order)

m   Temperature exponent

N   Number of experimental data

P   Pressure (Pa)

q   value of the variable (see eq. (29))

Q   Volumetric flow rate (m^3 s^{-1})

R   Universal gas constant (J mol^{-1} K^{-1})

r   Reaction/generation rate (mol m^{-3} s^{-1})

S   Cross-section (m^2)

T   Temperature (K)

V   Volume (m^3)

Y   Reaction quotient (dimensions depending on reaction order)

Greek symbols

Δ   Variation

ν   Stoichiometric coefficient

ξ   Longitudinal coordinate (m)

τ   Apparent residence time (s)

Subscripts

∞   At extremely high pressure

0   Standard/reference

eff   Effective

i   Index for reaction

-i   Index for backward reaction

j   Index for component

T   Total

Chapter 4[*]

Process modeling

In this Chapter, the supercritical water gasification (SCWG) of biomass for H_2 production is analyzed in terms of process development and energetic self-sustainability. The conceptual design of a plant is proposed and the SCWG process involving several substrates (glycerol, microalgae, sewage sludge, grape marc, phenol) is simulated by means of AspenPlus®. The influence of various parameters – biomass concentration and typology, reaction pressure and temperature – is analyzed. The process accounts for the possibility of exploiting the mechanical energy of compressed syngas, later burned to sustain the SCWG reaction, through expansion in turbines; purified H_2 is fed to fuel cells. Results show that the SCWG reaction can be energetically self-sustained if minimum feed biomass concentrations of 15-25% are adopted. Interestingly, the H_2 yields are found to be maximal at similar feed concentrations. Finally, an energy balance is performed showing that the whole process could provide a net power of about $160 kW_e/(1000 kg_{feed}/h)$.

4.1. Introduction

In the previous Chapters, thermodynamic equilibrium and kinetics models were presented. The importance of these two approaches has been already stated: the first is able to foresee the system composition at equilibrium, while the second gives an insight in the transient state reactions. Though their intrinsic importance, the two approaches merely describe the reaction itself, thus neglecting the engineering aspects of the whole SCWG process. Such aspects include, for instance, the necessity to pump and heat the reacting stream, the energy recovery by means of heat exchangers to guarantee energy self sustainability, syngas treatment and conversion into heat and power, etc. All of these items are of crucial importance, since they allow to determine whether the process is economically feasible or not.

---

[*] Part of the present Chapter has been published as L. Fiori, M. Valbusa, D. Castello, "Supercritical Water Gasification of Biomass for H_2 production: Process Design", Bioresource Technology, vol. 121 (2012), p. 139-147

In this Chapter a comprehensive process aimed at hydrogen production and based on the SCWG of biomass is proposed. Here, the hydrogen-rich syngas is utilized to feed fuel cells for high efficiency energy production. The process scheme is designed to be as simple as possible ahead of the construction of an actual pilot-scale or industrial-scale plant. However, the need for energetic self-sufficiency is also taken into account. The goal is to explore the possibility to have a self-sufficient small-scale plant, which could be a concept for future industrial development.

To our knowledge, the work of Gutierrez Ortiz *et al.* [108] is the first in-depth study aimed at designing and optimizing a complex process scheme for SCWG. The idea is to produce power by expanding the high pressure syngas exiting the SCWG reactor in a turbine. The syngas is then burned with air in a combustor to provide the heat needed to sustain the SCWG reaction. The process accounts for several heat recoveries designed with a view to optimizing the process itself. It is intended to treat a feed stream consisting of a water-glycerol mixture.

The energy needed to sustain the SCWG reactor comes from a furnace powered with the gasification gases, as in [108]. However, this scheme foresees the separation of hydrogen by means of a metallic filter placed upstream of the furnace and its recovery to feed fuel cells. Higher electrical production can be expected with fuel cells, especially if combined with turbines to expand the gasification products. On the other hand, sustaining the process with a less energetic syngas (hydrogen-free) is an issue which has to be carefully investigated.

The process lay-out was implemented by means of the commercial software Aspen Plus® (Aspen Tech, Inc.), which was used to simulate the process at different operating conditions. A wide range of biomass and residual biomass is considered as feedstock for the process: glycerol, phenol, microalga *Spirulina*, sewage sludge and grape marc. This enables to infer some 'general rules' applying to the SCWG of any biomass, specifically with regard to the range of concentration of the biomass in the feed stream allowing for an *autothermal regime* (i.e. all the heat necessary to run the SCWG reactor is furnished by burning the syngas produced by the process itself), the range of hydrogen obtainable per mass unit of feed stream (kg_{H2}/kg_{feed}), the process heat duties, the electric power production.

4.2. Materials and Methods

In this Paragraph, the different biomass substrates used to carry out the simulations are first presented. After that, the proposed process layout for SCWG is shown.

4.2.1. Biomass characterization

Different substrates which are promising candidates for the SCWG process were selected and utilized in the simulations: glycerol, phenol, microalga *Spirulina*, sewage sludge and grape marc.

Over the last few years glycerol has been gaining an increasing importance, since it is the most abundant by-product of bio-diesel industry. 70% of the glycerol production worldwide is due to the bio-diesel industry [133]. The glycerol market cannot accommodate this huge glycerol production and, as a matter of fact, glycerol has become an industrial waste.

Phenol is a well known compound and can be considered representative of the more complex lignin, which is one of the main constituents of woody biomass, along with cellulose and hemicelluloses. Lignin is an extensive by-product of the paper industry, which only employs cellulose in its productive process [147]. In addition, phenol and its derivatives are typically found in a variety of industrial wastewaters. Before such waters can be released into the environment, the phenol concentration must be reduced. Traditional biological wastewater treatment processes (e.g. activated sludge) often fail to treat phenol streams, owing to the bio-tossicity of phenol, which inactivates the bacteria responsible for the depurative process [148]. Partial oxidative gasification of phenol in supercritical water for hydrogen production has been investigated by Guan *et al.* [149].

Microalga *Spirulina* is widely used as food supplement for both humans and animals. Microalgae are biomass with a great potential for exploitation, as they can be grown quite easily and their growth is fast. As a result of their high water content, standard gasification technologies seem to be poorly applicable to them [134]; on the other hand, hydrothermal processes might be a viable way.

Sewage sludge has to be disposed of somehow. Furthermore, as its water content remains significant − higher than 80% [150] − even after dewatering, it is not considered a suitable feedstock for conventional thermo-chemical processes [151].

Finally, grape marc is a residue of the enological industry that includes all grape parts discarded during wine-making. Its world production is estimated at about 7 million tons

[152]. Experimental measures revealed a moisture content in the range of 60-70% [153]. Consequently, even though grape marc can be fed to traditional combustion or gasification plants after a drying pre-treatment [153], the SCWG option seems to be an appealing one.

The representative formula of the various dry substrates is reported as $C_\alpha H_\beta O_\chi S_\delta N_\varepsilon$ in Table 4.1, where the possible presence of ash and the HHV are also indicated. The formulae for microalga *Spirulina*, sewage sludge and grape marc were calculated on the basis of the elementary analyses available in "Phyllis", a database for biomass and waste run by the Energy Research Centre of the Netherlands [135]. The values of pedices α, β, χ, δ and ε assume the mass of one "ideal mole" of these substrates to equal 100 grams, as required by Aspen Plus^{TM}. The HHV values for these substrates were also derived from "Phyllis". The HHV values of glycerol and phenol were calculated on the basis of their enthalpy of formation [154] by using the theoretical combustion reaction.

Table 4.1 - Composition of the various biomass used in the simulations [135].

Biomass	Formula	Ash [%]	HHV$_{dry}$ [MJ/kg]
Glycerol	$C_3H_8O_3$	-	18.01
Phenol	$C_6H_6O_1$	-	32.53
Microalga *Spirulina*	$C_{3.66}H_{6.81}O_{2.16}S_{0.01}N_{0.47}$	7.77	19.82
Sewage sludge	$C_{2.83}H_{4.86}O_{1.25}S_{0.04}N_{0.34}$	35.10	15.10
Grape marc	$C_{4.57}H_{5.78}O_{2.04}S_{0.01}N_{0.15}$	4.3	21.8

4.2.2. Model and simulation

A first objective of this study was to design a possible plant layout for the SCWG of biomass and the production of H_2. The plant is conceived as capable to treat a throughput of 1000 kg/h, but the process design presented here can also suit different plant capacities. The process scheme is designed to be as easy as possible, ahead of a possible implementation. On the other hand, the process must be energetically convenient and its self-sustainability is an important point.

The basic plant scheme is reported in Figure 4.1, where a flow chart developed by means of the software AspenPlus^{TM} is shown.

Figure 4.1 - Schematic flow sheet of the SCWG plant for hydrogen production.

Through AspenPlus™, simulations were performed at various operating conditions, i.e. at different temperatures (500, 700 and 900 °C), pressures (250, 300, 350 bar) and feed concentrations (biomass in the feed stream ranging from 5% to 35%, the rest being water).

In order to explain the process scheme, we report here a description relevant to the SCWG of a feed stream with a 10% glycerol content, where the reaction occurs at 700°C and 300 bar.

The input of the plant is made up of two flows, glycerol (100 kg/h) and water (900 kg/h). Both fluxes are at standard conditions, i.e. 25°C and 1 bar. After being mixed and pumped up to 300 bar, the flow is first heated up by a heat exchanger. This block, HEATX-1, uses the stream exiting from the reactor (SYNGAS) for heat.

The region delimited by the dashed rectangle is the SCWG reactor. It was modeled as a system made of a heat exchanger (HEATX-2) and a reactor (REACTOR1) based on the minimization of Gibbs free energy. This approach was followed because the real-life reactor is conceived as a single vessel or as a countercurrent flow pipe-in-pipe where reaction and heat exchange take place simultaneously. The stream PREHEAT1 is heated up by means of an air burner, combusting the portion of the product gas which does not contain H_2 (thus a mixture of CH_4, CO and CO_2). The burner can also be fed with auxiliary me-

thane, if the gas produced by the SCWG process cannot supply the amount of energy required to keep the reaction temperature (in this case fixed at 700°C) constant.

The process is thus isobaric (300 bar) and isothermal (700°C). A negative Q-REACT thermal flux corresponds to the value of energy the reactor needs to be sustained. In the event of a positive Q-REACT, the reaction is self-sustainable, since it produces a net quantity of thermal energy. Based on a user-defined list, the REACTOR1 block calculates the chemical species minimizing the Gibbs free energy for the thermodynamic conditions given.

The resulting stream, exiting the dashed block, is SYNGAS. It is first cooled in the HEATX-1 heat exchanger, where it serves as heating stream for the incoming feed to the reactor. This heat exchanger is designed in such a way that the vapor fraction of the resulting SYNGAS2 stream is equal to 1. This choice was made to avoid any complications and damage to the equipments due to a two-phase flow.

Subsequently, the SYNGAS2 stream is cooled at 60°C in order to separate water (block SEPAR). In this unit 877.5 kg/h of water can be recovered, meaning that the water consumption due to the reaction amounts to 22.5 kg/h. The most interesting aspect of this unit is the thermal load (stream Q-SEPAR) which must be dissipated. Since it is heat at a relative low temperature, its reuse in the process is quite difficult. Moreover, the dissipation of this waste heat requires energy, as explained in Paragraph 4.3.2.2.

After water separation, hydrogen is separated from the other product gases. This is achieved by means of the Hysep™ [155] palladium filter, which is modeled by the SEPAR2 block. This device is operated at a minimum temperature of 300°C and a pressure of 60 bar: thus, the stream must be heated up (HEAT-AIR heat exchanger) and depressurized (LAMINA1 lamination valve). The heating up followed by the depressurization step enables to avoid problems related to the Joule-Thompson effect. In this specific case, the latter causes the temperature to reduce with the expansion of the gas, possibly leading to the freezing of the mixture. The recovery index of the palladium filter can be reasonably fixed at 1 (that is, all the H_2 of the incoming feed is separated by the filter) in view of its high operating pressure [156].

After hydrogen separation, the resulting stream is further expanded to 1 bar by a lamination valve, for it to be fed to the air burner previously described. The air to the burner is pre-heated in the HEAT AIR 2 heat exchanger.

The scheme of Figure 1 is slightly modified when the possibility of exploiting the mechanical energy of the compressed syngas is analyzed (see Paragraph 4.3.2.3). Furthermore, another slight difference exists between the simulations performed with glycerol or phenol and those with microalgae, sewage sludge or grape marc. Actually, such difference is only fictitious, as it stems from the different way Aspen Plus^{TM} treats simple molecules (such as glycerol and phenol) and pseudo-compounds representative of real biomass (microalgae, sewage sludge and grape marc). It regards the modeling of the reactor (area inside the dashed rectangle), which is modeled as consisting of a heat exchanger and a "Gibbs reactor", as previously explained, for simple molecules. When a pseudo-compound is used, it cannot be fed directly to a "Gibbs reactor". It first needs processing in a devolatilizer, i.e. a reactor breaking up a molecule in its elementary components (C, O_2, H_2, N_2, S). These products can then be fed to the "Gibbs reactor" which calculates the equilibrium composition. Thus, in this case the reactor is modeled as consisting of a heat exchanger, a first reactor (devolatizer), and finally a "Gibbs reactor", with the two reactors being connected through a heat stream. This scheme is reported in the inset A of Figure 4.1.

Given the composition of the biomass used in the simulations (Table 4.1), the chemical species considered as possible reaction products are H_2O, CO, CO_2, N_2, N_2O, NO, NO_2, SO_2, SO_3, H_2, CH_4 and solid carbon (graphite). Higher molecular weight hydrocarbons (C_2H_4, C_2H_6, etc.) are not considered taking into account the results of previous thermodynamic calculations [108, 157] where they were not found among the SCWG products.

To reduce water consumption, the water exiting the separator can be reintegrated into the process, after removing any ash. For the sake of simplicity, the schematization in Figure 4.1 depicts all the ash initially prevailing in the biomass as exiting the process together with the water. In an actual reactor, that would occur to some fly-ash. Larger ash aggregates would collect at the bottom of the SCWG reactor and be occasionally drained out together with precipitated salts [129] and possibly non-equilibrium heavy organic species resulting from the process (char).

In Table 4.2, the values of flow, temperature and pressure of each stream in the plant are reported to exemplify a simulation with microalga *Spirulina*, assuming a feed concentration of 20% and a reaction occurring at 700°C and 300 bar.

Table 4.2 - Flow, temperature and pressure for each stream of Figure 4.1 for a feed consisting of 20% microalga Spirulina and for a SCWG occurring at T=700°C and P=300 bar.

Stream	Flow [kg/h]	Temperature [°C]	Pressure [bar]
H2O	800	25	1
BIOMASS	200	25	1
MIXED	1000	25	1
PUMPED	1000	28.3	300
PREHEAT1	1000	297.1	300
PREHEAT2	1000	953.0	300
IN-REACT	1000	700	300
SYNGAS	1000	700	300
SYNGAS2	1000	350	300
WATER [a]	749.0	60	300
GAS-1	251.0	60	300
GAS-2	251.0	310.4	300
GAS-3	251.0	303.7	60
COMB-1	242.4	303.7	60
H2STREAM	8.56	303.7	3
COMB-2	242.4	295.0	1
CH4	0	-	-
COMB+	242.4	295.0	1
AIR [b]	1063.2	25	1
AIR2	1063.2	217.1	1
FLUE	1305.6	1733.3	1
FLUE2	1305.6	320	1
FLUE3	1305.6	230	1
FLUE4	1305.6	85	1

[a] This stream consists of water (733.5 kg/h) and ash (15.5 kg/h)

[b] The air flow rate is determined considering to operate the combustor with an ER (equivalent ratio) equal to 1.2

4.3. Results and discussion

The model runs resulted in two classes of outputs. First, the model response was observed focusing on the composition of the gaseous products. Then, the process was analyzed in terms of its energy performance.

4.3.1. Syngas and H_2 production

Figure 4.2a shows the syngas production vs. biomass concentration in the feed for the various substrates analyzed, for a SCWG occurring at 700°C and 300 bar. Figure 4.2b and Figure 4.2c evidence the CH_4 and H_2 production at the same operating conditions. While syngas and methane production rises as the biomass concentration increases, the behavior of hydrogen is peculiar: at increasing biomass concentration, the H_2 production first increases, then stabilizes around a maximum, finally starts to decrease. This behavior is shared by all the five substrates analyzed: Figure 4.2c testifies it for phenol, microalga *Spirulina* and grape marc, while for glycerol and sewage sludge this trend is proved by further simulations performed at biomass concentrations equal to 30% and 35% respectively (data not reported in Figure 4.2c). The points of maximal hydrogen production occur at different biomass concentrations for the various substrates: about 13% for phenol, 17% for grape marc, 20% for microalga *Spirulina* and sewage sludge, 25% for glycerol. The maximum in H_2 production can be interpreted as the combined effect of two contrasting phenomena: at increasing biomass concentration the absolute production of gas increases (Figure 4.2a), but according to thermodynamics in this gas the H_2 concentration decreases. This is shown in Figure 4.2d, where the syngas composition is reported as a function of biomass concentration for microalga *Spirulina*.

Figure 4.2e and f show the effect of temperature and pressure on the H_2 production, respectively. An increase in the SCWG temperature causes a significant rise in the H_2 production: this effect is more pronounced at high biomass concentration in the feed (Figure 4.2e). An increase in the SCWG pressure causes a decrease in the H_2 production (Figure 4.2f).
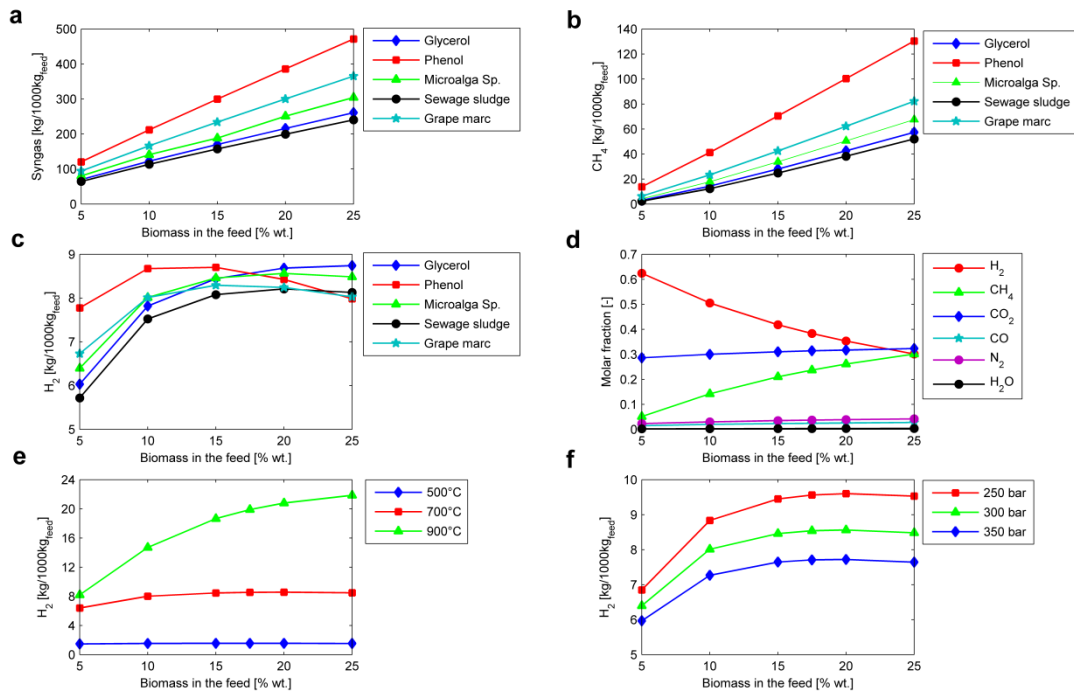
Figure 4.2 - SCWG gaseous products. The indicators represent the simulation outputs, the curves connecting the indicators are intended to help the reader in the comprehension of the figure. (a) Syngas production (after water separation: GAS-1 in Figure 1) vs. biomass concentration in the feed (T=700°C, P=300 bar); (b) methane production vs. biomass concentration in the feed (T=700°C, P=300 bar); (c) hydrogen production vs. biomass concentration in the feed (T=700°C, P=300 bar); (d) syngas composition (after water separation: GAS-1 in Figure 1) vs. biomass concentration in the feed (microalga *Spirulina*, T=700°C, P=300 bar); (e) hydrogen production vs. biomass concentration in the feed at different temperatures (microalga *Spirulina*, P=300 bar); (f) hydrogen production vs. biomass concentration in the feed at different pressures (microalga *Spirulina*, T=700°C).

As far as nitrogen gas species and sulphur oxides are concerned, nitrogen is found as N_2 and sulphur (mainly) as SO_2. Their presence is maximal at 250 bar, 500°C and 25% biomass concentration in the feed. At these operating conditions, as an example, the syngas composition (after water separation: GAS-1 in Figure 4.1) foresees a molar fraction of 0.055 for N_2 and of 0.0026 for SO_2 in the case of microalga *Spirulina*.

Solid carbon is never found as SCWG product for the range of operating conditions simulated.

4.3.2. Energy analysis

An interesting issue arising from process modeling is represented by the analysis of the energy requirements. Looking at the process lay-out in Figure 4.1, two thermal streams are

present, power is required to increase the pressure of the feed stream, hydrogen is produced and, possibly, methane is consumed.

The two thermal streams, Q-SEPAR and Q-REACT, have two different kinds of energy demand. The former results in a cooling request, since the heat arising from separation must be properly dissipated. The latter is the thermal flux arising from the energy balance in the reactor.

4.3.2.1. The reactor

Two scenarios are possible, depending on whether Q-REACT represents an energy demand or an energy production: see Figure 4.3a.
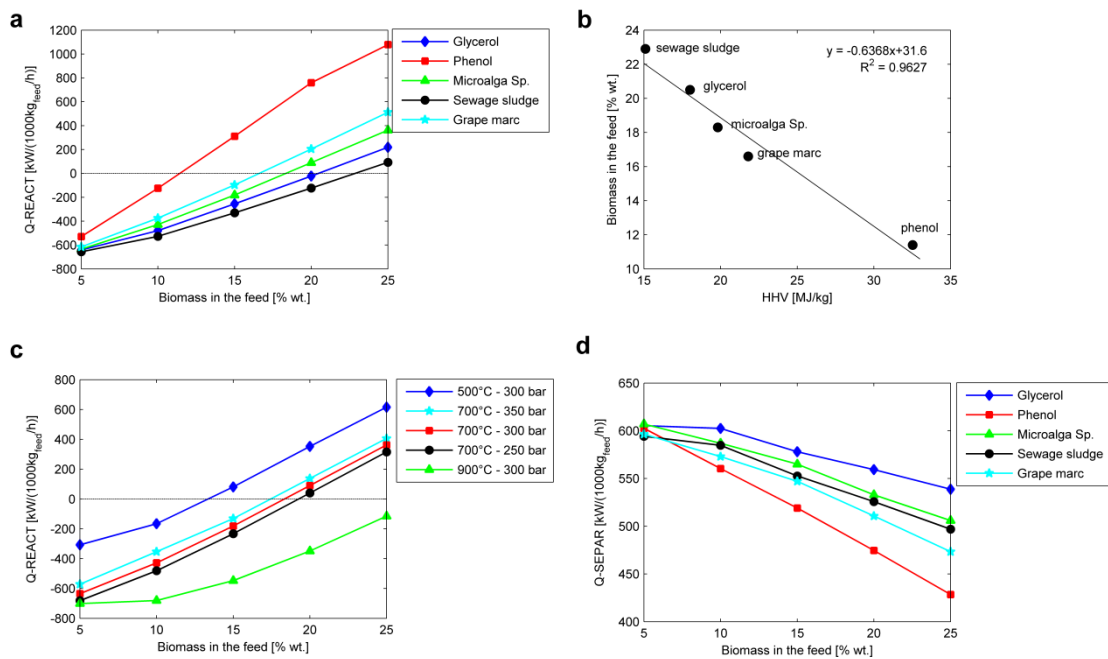
Figure 4.3 - Energy analysis. The indicators represent the simulation outputs, the curves connecting the indicators are intended to help the reader in the comprehension of the figure. (a) Thermal flux Q-REACT as a function of biomass concentration in the feed (from simulations where no CH_4 is supplied to the burner; T=700°C, P=300 bar); (b) relation between the biomass HHV and the auto-thermal concentration (T=700°C, P=300 bar); (c) thermal flux Q-REACT as a function of microalga *Spirulina* concentration in the feed at various temperatures and pressures (from simulations where no CH_4 is supplied to the burner); (d) thermal flux Q-SEPAR as a function of biomass concentration in the feed (from simulations where the reaction step occurs at T=700°C and P=300 bar).

In the first scenario Q-REACT has a negative value, which means that the reactor needs to be sustained by an external source of thermal energy. This gap of energy can be covered by supplying the stream "CH4" to the burner, whose quantity can be easily evaluated (LHV of methane is equal to 50.0 MJ/kg [154].

In the second scenario Q-REACT is positive. There will thus be a production of thermal energy, meaning that the process is self-sustainable. According to our calculations, the process achieves auto-thermal regime (Q-REACT=0) at a biomass concentration in the feed (in what follows referred to as *auto-thermal concentration*) equal to 22.9% for sewage sludge, 20.5% for glycerol, 18.3% for microalga *Spirulina*, 16.6% for grape marc, 11.4% for phenol (for a SCWG occurring at T=700°C and P=300 bar). An almost linear correlation exists between the values of auto-thermal concentration and the HHV of the various substrates, as witnessed by Figure 4.3b.

Gutierrez Ortiz *et al.* [108] calculated a glycerol value of 21.78% in the feed to achieve auto-thermal regime of their SCWG process, occurring at 800°C and 240 bar. This value is close to the value calculated here (20.5% for a reaction step occurring at 700°C and 300 bar). Actually, the two values can be compared to a limited extent, given that the two proposed conceptual designs present a key difference: here H_2 is separated from the syngas for power production; in [108] power production is achieved through syngas expansion in turbine.

Notably, the maximum H_2 production occurs more or less in concurrence with the auto-thermal concentration. Though a theoretical explanation is hard to be found, this fact indicates that working with concentrations of around 15-20% is beneficial for both hydrogen production and process energy sustainability.

Figure 4.3c shows the dependence of the reaction heat duty on the SCWG temperature and pressure. An increase in temperature and a decrease in pressure lead to a rise in the reaction heat duty. The dependence on temperature is particularly significant, while pressure has a lower impact. By contrasting Figure 4.2e and Figure 4.2f with Figure 4.3c, it is possible to notice that the higher is the quantity of hydrogen produced, the higher is the reaction heat duty or, equivalently, the higher is the auto-thermal concentration. Notably, at the temperature of 900°C, which assures the best performances in terms of H_2 production (Figure 4.2e), the process is not thermally self-sufficient in the whole range of biomass concentration analyzed.

Thus, working at 700°C seems to be a good compromise between energy self-sustainability, H_2 production, reactor material resistance and feed stream pumpability, although admittedly no in-depth process optimization is performed. An exercise of process optimization is reported in Appendix B (Paragraph 4.6): the results confirm what stated above.

4.3.2.2. The water separator

Figure 4.3d reports the heat to dissipate (Q-SEPAR) in order to have a temperature of 60°C in the water separator. The cooling request is only slightly dependent on biomass typology, while it is more significantly influenced by biomass concentration.

The decrease of Q-SEPAR is proportional to the increase of the biomass concentration in the feed. This can be easily explained. When the quantity of biomass increases, the amount of water decreases; thus, less energy is needed to perform the cooling down and condense the water. Moreover, the stream SYNGAS2 was imposed to be in vapor phase (see Paragraph 4.2.2). As the biomass concentration increases, the minimum temperature to obtain a one-phase stream decreases on account of the lower water content. This enables to use lower temperature for the stream SYNGAS2, thus achieving a larger heat exchange in the HEATX-1 block.

The dependence of heat dissipation on the SCWG temperature and pressure is not significant (data not reported).

4.3.2.3. Syngas expansion in turbines

A possible improvement to the scheme of Figure 4.1 is the adoption of turbines instead of lamination valves, which is more feasible in large plants. These devices could enable to recover part of the mechanical energy of the high pressure syngas, producing power, thus increasing the global electrical yields.

Thus, referring to Figure 4.1, LAMINA1 and LAMINA2 have been replaced by two turbines through which the syngas expands, respectively, from the SCWG reactor pressure to 60 bar and from 60 to 1 bar.

The expansion processes are considered to have isentropic efficiencies of 90% and mechanical losses are assumed equal to 2% owing to the coupling of turbines with alternators [158]. The expansion occurring in turbines causes a significant reduction of the syngas temperature. To mention an example, in the case of a feed stream to the process consisting of microalga *Spirulina* (20%) and water (80%), the first turbine causes the syngas tempera-

ture to drop by 188°C, while the second turbine prompts a temperature decline of almost 300°C. Thus, considering the minimum working temperature of the H_2 separator, the syngas entering the first turbine (GAS-2, Figure 4.1) should be at a temperature as high as 490°C. Analogous considerations apply to the other biomass analyzed. As a result of the above, when turbines are adopted, the auto-thermal concentrations are slightly higher than the corresponding concentrations calculated in Paragraph 4.3.2.1 and relevant to a process with lamination valves. This data is reported in Table 4.3: the increase in auto-thermal concentration is minimal for phenol (0.8%) and maximal for sewage sludge (1.5%). Table 4.3 also reports the value of the power resulting from the syngas expansion in turbines when working at the new auto-thermal concentrations: it ranges from 49.3 kW/(1000kg_{feed}/h) for glycerol to 54.9 kW/(1000kg_{feed}/h) for grape marc.

Table 4.3 – Data relevant to a SCWG process adopting lamination valves and, alternatively, turbines: maximal H$_2$ production, biomass in the feed allowing for auto-thermal regime, H$_2$ production at auto-thermal point and relevant power obtainable feeding it to fuel cells, power obtainable through expansion of syngas in turbines. SCWG occurring at T=700°C and P=300 bar.

Biomass	Maximal H$_2$ production	SCWG process with lamination valves			SCWG process with turbines			
		auto-thermal concentration	H$_2$ production at auto-thermal concentration	Power through fuel cells	auto-thermal concentration	H$_2$ production at auto-thermal concentration	Power through fuel cells	Power through turbines
	[kg/1000kg$_{feed}$]	[%]	[kg/1000kg$_{feed}$]	[kW/(1000 kg$_{feed}$/h)]	[%]	[kg/1000kg$_{feed}$]	[kW/(1000 kg$_{feed}$/h)]	[kW/(1000 kg$_{feed}$/h)]
Glycerol	8.74	21.5	8.70	130.6	23.9	8.74	131.2	52.8
Phenol	8.74	12.1	8.68	130.4	13.9	8.73	131.1	59.1
Microalga *Spirulina*	8.56	19.3	8.56	128.4	21.6	8.55	128.4	56.0
Sewage sludge	8.21	24.1	8.14	122.2	26.9	8.06	121.0	54.3
Grape marc	8.29	17.6	8.29	124.5	19.7	8.25	123.8	59.5

4.3.2.4. Economy of the process: energy balance

This section aims at analyzing the energy input and output characterizing the process.

First of all, it seems sensible to run the process at auto-thermal concentrations. In this case, no methane has to be supplied when the plant is in normal operation (steady state), as it is only necessary for the start-up operation.

The process produces hydrogen, which can be fed to Proton Exchange Membrane (PEM) fuel cells to produce electric power. Significantly, hydrogen production is virtually the same when working at the auto-thermal concentration for both processes adopting lamination valves and, alternatively, turbines: see Table 4.3. This is due to the "flat behavior" around the maximum of the hydrogen production curve (Figure 4.2c) and to the fact that, as mentioned in Paragraph 4.3.2.1 and testified by the values of Table 4.3, the maximum H_2 production occurs in good approximation in coincidence with the auto-thermal concentrations. The hydrogen is produced in high purity (at a concentration ranging between 99.5% and 99.995% [155]). Nevertheless, to avoid any CO poisoning effect on PEM fuel cells, a small catalytic shift reactor may be foreseen to convert CO into CO_2. The PEM fuel cells efficiency has been conservatively assumed to be equal to 0.45 [159], even though higher efficiencies can be achieved [156].

The power generated through feeding hydrogen to PEM fuel cells results in a range of 122-131 kW/(1000kg_{feed}/h) for all the biomass considered: see Table 4.3.

Considering the low working temperature of the water separator (60°C), this heat is unlikely to be exploitable in any industrial process. Possible uses include, for instance, the warming up of pools or greenhouses. However, should such an end usage not be possible, as is generally the case, this heat would be wasted, thus entailing an extra energy cost.

The energy request depends on the cooling cycle adopted. The power needed to run a typical mechanical refrigeration system can be evaluated by dividing the values of Q-SEPAR (Figure 4.3d) by the coefficient of performance (COP) of the system. A COP of ~ 2.5 could be reasonably adopted [160]. Considering all the substrates and the relevant concentrations at auto-thermal point, the power for cooling results in a range of 190-220 kW/(1000kg_{feed}/h), which is much greater than the power available from fuel cells.

A cycle based on evaporative cooling towers can assure better performances and satisfy the process needs with a consumption lower than 10 kW/(1000kg_{feed}/h). A gross sizing of this cycle is reported in Appendix A (Paragraph 4.5).

Finally, an important issue is the pumping of the feed stream.

Glycerol and phenol are soluble in water and, consequently, the resulting mixture is liquid. Water-glycerol or water-phenol mixtures can be pumped at high pressure with standard process equipment.

Conversely, where the solid is not completely soluble in the liquid but remains in the form of suspended particles, as is the case for microalgae, sewage sludge or grape marc, the pumping of solid-liquid mixtures can become a challenge. If the solids are present in small percentages (0-5%), the pumping can be still performed through standard equipment. If the solids are present in larger percentages, it might be necessary to resort to *ad hoc* pre-treatments [126] or special pumps, such as cement pumps [161]. Kruse reports that their largest plant for hydrothermal biomass gasification is capable of treating a slurry up to 20% (g/g) dry matter, depending on the nature of biomass [39].

In light of the above, we considered increasing the pressure of the various biomass-water mixtures to 250-350 bar with a device having a low efficiency, namely 0.5. Accordingly, the power for pumping ranges between 13.9 and 19.4 $kW/(1000\ kg_{feed}/h)$, depending on the desired reaction pressure.

The energetic sustainability of the proposed process seems assured, and possibly enhanced by exploiting the mechanical energy of the high pressure syngas with turbines. In this case, an additional power of about 49-55 $kW/(1000 kg_{feed}/h)$ is obtained (Table 4.3), provided that a slightly higher concentration of biomass in the feed is supplied.

Making an overall energy balance of the whole process with turbines, its net energy output can be evaluated at 145-157 kW_e per 1000 kg/h of feed stream or, equivalently, 520-565 $MJ_e/1000kg_{feed}$. Although these values are overestimated because no heat and head losses were taken into account, they provide us with an insight into the potential intrinsic in the SCWG of biomass and biomass waste.

In Appendix B (Paragraph 4.6) some results concerning process optimization are reported which confirm the values of net power evaluated above in this section.

Finally, an evaluation of the process's overall electrical efficiency leads to interesting conclusions. Taking into account that the SCWG process is designed for biomass with a high moisture content or waste waters containing a large amount of organic matter, the SCWG electrical efficiency is defined here as the percentage ratio between the net power produced and the low heating value (LHV_{ar}) of the feed stream. If the SCWG process is assumed to be performed with turbines at auto-thermal concentration (Table 4.3), the follow-

ing electrical efficiencies are found: 34.6% for grape marc, 34.2% for glycerol and microalga *Spirulina*, 33.9% for phenol, 33.2% for sewage sludge.

Future work will consist in designing and comparing alternatives processes, for instance by coupling directly the SCWG reactor with high temperature fuel cells. Moreover, a challenging issue for future research will consist in sizing and designing the various equipments and in performing a cost analysis to state the effective convenience and profitability of the SCWG technology.

4.4. Conclusions

A conceptual design for a SCWG plant aimed at H_2 production was developed, and the process was simulated with different biomass types: glycerol, phenol, microalga *Spirulina*, sewage sludge and grape marc. The SCWG reaction can be energetically sustained by burning the syngas produced if a minimum biomass concentration in the feed of 15-25% is adopted. Notably, at this concentration the H_2 production is maximal (around 8.5 kg/1000kg$_{feed}$). An energy balance showed that, by feeding H_2 to fuel cells and expanding the high pressure syngas in turbines, a net power of about 150 kW$_e$/(1000kg$_{feed}$/h) can be achieved.

4.5. Appendix A: Gross sizing of an evaporative cooling tower system

A possible solution to the problem of cooling is offered by the use of an evaporative cooling tower system. Such device is likely to guarantee a minor energy consumption by exploiting the volatilization of water in the air. Since the technology is well known, only a gross sizing is reported in this section.

Referring to standard applications, water can be supplied to the tower at 40°C and recovered at 30°C. Consequently, the tower works with a ΔT of 10°C. Knowing the isobaric heat capacity of water (C_p=4179.3 J/kg K at 35°C) and the heat to dissipate (Q-SEPAR≈550 kW, see Figure 4.3d) the flow of cooling water is found to equal about 47,400 kg/h.

The electric consumption of the evaporative cooling tower is given by two machineries: the water circulation pump and the fan, which creates an air flow from the bottom to the top of the tower. The power consumption of the pump can be evaluated at 6 kW, considering a head loss of 22 m and an efficiency η of 0.5. The nominal power of the fan mo-

tor is equal to 4 kW [162]. According to a conservative estimate, a global power consumption of 10 kW can be assumed.

The evaporative cooling tower evaporates about 820 kg/h of water (ΔH_{evap}=2418 kJ/kg at 35°C). The water reintegrating into the cycle can be estimated at about 1500 kg/h, allowing for a water discharge of around 680 kg/h, which is necessary to avoid an excessive rise in the salinity of the water in the cooling circuit.

4.6. Appendix B: Economy of the process: optimizing the net power produced

The aim of this section is to present an insight in the optimization of the SCWG of microalga *Spirulina*. Reference is done to the scheme of Figure 4.1, both with lamination valves and, alternatively, turbines. A first series of simulations has been performed to calculate the auto-thermal concentration (Q-REACT=0) as a function of the independent variables pressure and temperature: Figures B.1a and b. To construct Figure 4.4, several simulations have been performed considering a matrix temperature/pressure where the temperature varied in the range 500 – 900 °C with step of 20°C and the pressure varied in the range 250 – 350 bar with step of 25 bar. Figure 4.4a and Figure 4.4b report values of auto-thermal concentration varying from a minimum of 13% to a maximum of 25%. Values higher than 25% are not reported because they are out of the range of concentration allowed in an actual plant, where the threshold concentration due to pumpability issues should be around 20% [39], as discussed in Paragraph 4.3.2.4. It is confirmed that at 900°C the process is not thermally self-sufficient. Moreover, by contrasting Figure 4.4a and Figure 4.4b, it can be noticed that utilizing turbines shifts the "iso auto-thermal concentration curves" slightly to the left, i.e. higher concentrations are required for energy sustainability. Just to mention an example, at 250 bar the auto-thermal concentration of 25% occurs at about 825°C with lamination valves (Figure 4.4a) and at about 800°C with turbines (Figure 4.4b). This behavior corresponds to the increase in the auto-thermal concentrations at fixed temperature and pressure occurring when replacing lamination valves with turbines (Table 4.3).
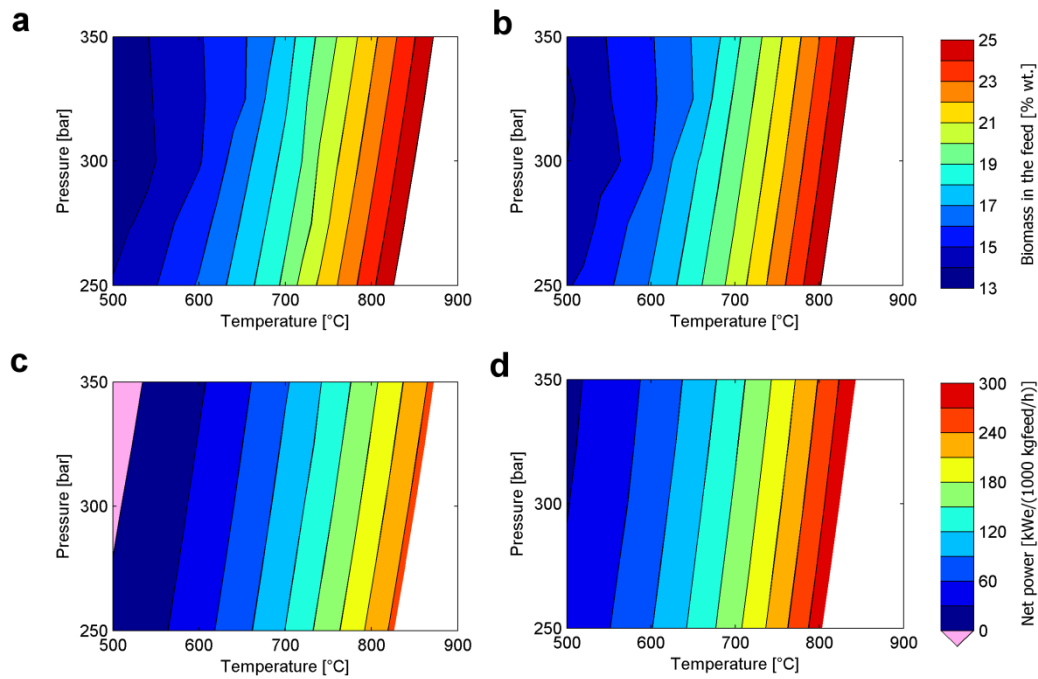
Figure 4.4 - Auto-thermal concentration as a function of temperature and pressure in the case of a process adopting lamination valves (a) and, alternatively, turbines (b). Net power produced in the case of a process adopting lamination valves (c) and, alternatively, turbines (d) when running the process at auto-thermal concentration.

Figure 4.4c and d report the net power produced by the process as a function of temperature and pressure when operating at the auto-thermal concentration shown in Figure 4.4a and Figure 4.4b, respectively. The net power is calculated as the power obtained by feeding hydrogen to fuel cells plus the power generated from turbines (where present) minus the consumption of the cooling circuit and the feed stream pump. The assumptions made to calculate these values are reported in Paragraphs 4.3.2.3, 4.3.2.4 and 4.5 and are not repeated here. Looking at Figure 4.4c, the pink upper-left area testifies a negative value of the net power produced, that is the power necessary to run the process results higher than the power generated by it. At increasing temperature (and biomass in the feed) the net power progressively increases. The maximum value of the net power is of about 250 $kW_e/(1000kg_{feed}/h)$ with lamination valves (Figure 4.4c) and of about 290 $kW_e/(1000kg_{feed}/h)$ with turbines (Figure 4.4d). These values correspond to the maximal auto-thermal concentration allowed for the simulations, i.e. 25%. Considering a more reasonable value of auto-thermal concentration, i.e. 20%, the values of the net power produced change at about 130 $kW_e/(1000kg_{feed}/h)$ with lamination valves (710°C, 250 bar) and

at about 160 $kW_e/(1000kg_{feed}/h)$ with turbines (690°C, 250 bar), confirming the values reported in Paragraph 4.3.2.4.

Interestingly enough, the above analysis furthermore allows to quantify to which extent the process performances can be improved by utilizing turbines to replace lamination valves.

Chapter 5

Batch Gasification of Model Compounds

Starting from this Chapter, experimental activities are presented. Here, experimental tasks are accomplished using simple organic molecules which are able to "simulate" the main components of real biomass. Such molecules are glucose, which is the monomer of cellulose, and phenol, one of the base constituents of lignin. This approach allows to simplify the complex scenario of hydrothermal reactions involved during gasification by considering a feedstock with a precise chemical characterization and whose main reaction pathways are known in the literature. Tests in both sub- and supercritical conditions were performed, with residence times ranging from 1 to 5 hours. Special focus was paid to the role of the reactor material, which can strongly influence the composition of the produced syngas.

5.1. Introduction

In order to perform experimental tests, useful to understand the way supercritical water gasification works, the usage of model compounds offers the possibility to investigate SCWG in a more simplified way than with real biomass.

Unlike real biomass, which exhibits an incredibly high number of organic molecules arranged in a peculiar way, model compounds allow the experimenter to choose a definite material, whose composition is *a priori* known. Moreover, for these simple organic molecules some information is available in the literature, concerning the fundamental reaction pathways at hydrothermal conditions (see Paragraph 1.4.1). This helps in understanding the main reaction pathways and allows acquiring knowledge about how process conditions influence the process outputs.

In this Chapter, two kinds of model compounds were used: glucose and a glucose/phenol mixture. As already explained (see Paragraph 1.4.1), glucose can be assumed as a model compound for cellulose, while phenol is useful to model lignin. The adoption of

glucose/phenol mixture allows to simulate actual biomass, which can be roughly schematized as a set of cellulose and lignin.

The methodology here adopted is based on small-scale 5 ml batch reactors: the so called "micro-autoclaves". They allow performing experimental tests with relative ease of operations and may be manufactured of different materials. Indeed, besides the fundamental gasification behavior of the two model compounds, we tried to answer the question whether catalytic effects due to the metallic reactor walls, are able to affect gasification outputs in a significant way.

Catalysis in SCWG has always been a relevant topic; a comprehensive state of the art can be found in Paragraph 1.4.3. The influence of metal catalysts has been widely investigated. In many works, like [78-81], the presence of the metal is reproduced by adding a wire or a powder inside the reactor. Though such approach allows clearly to understand the influence of a precise metal, it is quite distant from reality, where the metal surface is represented by the whole inner part of the reactor.

Nevertheless, some authors reported that reactor wall effects are not negligible in methanol SCWG [50, 143] and they are also present in biomass gasification [161]. Moreover, in industrial operations the reactor surface is exposed to the reaction conditions for several hours. It would be thus interesting to observe if, even after several runs, the reactor material still plays a catalytic role. Furthermore, all the data available in the literature only evaluates the catalytic effects after a few minutes of operations. It would be useful to understand if such catalytic effects only take place and are evident in the first minutes or they can also play a role on a longer time-scale.

To this purpose, two micro-autoclaves made, respectively, of stainless steel and Inconel® 625 were utilized. Both sub-critical (350°C) and supercritical (400°C) conditions were considered. Tests were conducted at different residence times, ranging between 60 minutes to 300 minutes, in order to evaluate the effect of those reactions and processes taking place at very low rates.

All the experimental activities were conducted at the Karlsruhe Institute of Technology (Germany), Institute of Catalysis Research and Technology (IKFT), under the scientific supervision of prof. A. Kruse.

5.2. Materials and methods

The work performed in this study involves a number of experimental tests performed with small batch reactors. These devices were used to perform more than 80 experimental tests, where solid, liquid and gaseous products were sampled, quantified and analyzed. In order to observe the behavior of the metallic surfaces, tests were executed adding metallic burrs to the reacting mixture and visually observing them with SEM technique.

5.2.1. Micro-autoclaves preparation and reaction

Tests were executed by means of small-scale batch reactors: micro-autoclaves. These devices are small metallic vessels, with a volume of 5 ml, which are able to withstand high pressures. Thanks to their small volume, they can be heated-up quite fast. Moreover, they are very easy to handle and can be used for virtually any type of biomass or model compound, possibly adding catalysts or any other material. The reduced dimensions result in extremely safe operations and the batch configuration avoids clogging issues, common for tubular continuous plants. The micro-autoclaves consisted in two hollow cylindrical elements to be screwed together. The reaction volume was then the internal cavity obtained from screwing up the two parts. This concept of micro-autoclaves has already been successfully used for previous studies in the literature [54, 163]. For each material, two identical micro-autoclaves were adopted in order to exclude that the results were affected by any peculiarities of the specific device, rather than being a general behavior.

Table 5.1 - Average composition of the metal alloys adopted in this study.

	Ni	Cr	Mo	Nb	Mn	Fe	C	Minor
Stainless steel 1.4571	11.5	16.4	2.1	-	1.5	67.8	0.04	0.7
Inconel 625	61.0	21.5	9.0	3.6	-	2.5	0.06	2.3

Two different micro-autoclaves were provided: the former made of stainless steel, the latter manufactured in Inconel® 625. This choice was made to draw a comparison between the two materials and thus to assess the significance of wall effects, due to the specific materials. Stainless steel was chosen since it is one of the most popular manufacturing materials for chemical plants. It is relatively cheap and it can bear the most severe reaction conditions of the present study (400°C and 30 MPa). Stainless steel 1.4571 was used, the main

constituents of which are iron, chromium and nickel, in the amounts exposed in Table 5.1. Inconel® 625 is a non-iron alloy made of nickel, chromium and molybdenum (see Table 5.1 for detailed composition). Nickel-alloys are generally used in hydrothermal processes, since they show great mechanical resistance to harsh reaction conditions, i.e. very high temperature and pressure. Furthermore, they also have sufficient high chemical resistance to corrosion [127]. However, Inconel® 625 is much more expensive than stainless steel, making its usage particularly burdensome.

Tests were performed with two substrates: glucose and a mixture of glucose and phenol. Glucose can be considered a model compound for biomass, since it is the monomer of cellulose, one of the main constituents of vegetal tissues. Moreover, many studies actually schematize biomass as a compound of carbon, hydrogen and oxygen ($C_xH_yO_z$) [93, 157] and this approach is consistent with the actual composition of glucose. Furthermore, glucose has the advantage of a definite composition, which helps in the understanding and interpretation of the results. For this study, glucose monohydrate (Merck KGaA, Darmstadt, Germany) was used; in order to obtain the right amount of glucose, the hydration water of the glucose monohydrate molecule was duly considered.

Besides pure glucose, tests were performed with a mixture of glucose and phenol. The addition of phenol to the reacting mixture is motivated since such compound is one of the "building blocks" of lignin, which is the other important macro-molecule that constitutes ligno-cellulosic biomass. It was thus thought that a mixture of glucose, modeling cellulose, and phenol, modeling lignin, could be more representative of the behavior of real biomass. The mixture was made mixing together 75% wt. glucose (the same reported above) and 25% wt. phenol (Merck-Schuchardt, Hohenbrunn, Germany). The elemental composition of the two obtained substrates is reported in Table 5.2.

Table 5.2 - Elemental compositions (% wt.) of the substrates tested in this study.

	C	H	O
Glucose	40.0	6.7	53.3
Glucose/Phenol	49.1	6.6	44.3

Before performing each series of experiments, the micro-autoclaves first underwent an "aging" treatment. This was done to avoid the possible catalytic effect of clean non-utilized

reactor walls, which is expected to be maximum when the reactor walls are completely new. The aging treatment consists in reacting the micro-autoclaves for a long time with a source of carbon at the same temperature and pressure as the following series of experiments. In this way, the conditions of a real-life reactor were reproduced. The influence of such aging treatment has already been reported, e.g. in the work by Yu et al. [164].

In all performed experiments, both substrates (i.e. pure glucose and the mixture glucose/phenol) were used at 15% wt., the remaining part being constituted by Milli-Q water. This is a relatively high concentration if compared with other studies in the literature, where greater dilutions are usually adopted [30, 31, 42]. Nevertheless, this choice was thought to be more interesting from a technical point of view, since processes with very high water/biomass ratios appear to be hardly energetically self-sustainable [165].

The amount of mixture to be used for reactor loading was determined according to steam tables [166] to ensure that, after the reactor heats up to the desired temperature, the system is able to reach the desired pressure. For this purpose, it was assumed that the reacting mixture had approximately the same density as pure water. At 400 °C and 30 MPa, water was found to have a density of 357.6 g/l. Thus, since the reactor internal volume was 5 ml, the total mixture to be loaded in the autoclave was 1.78 g. In the very same way, when a reaction temperature of 350 °C was selected, the water density of 644.0 g/l leads to a mixture amount of 3.22 g.

After being loaded with the desired reacting mixture, the micro-autoclaves were put in a special closed containment and purged with N_2 to remove oxygen and other atmospheric gases from the inside. By using a dynamometric key, the two parts of the reactor were fastened with a specified momentum (100 Nm) to ensure perfect sealing. Reactors were then put in a hot fixed-temperature oven. To this purpose, a GC oven (HP series) was used, since it allows a very good temperature control. The oven was pre-heated to the reaction temperature and the micro-autoclaves were then put inside it; this choice was made to achieve the fastest reactor heating rate to minimize the effect of thermal transients. After reaction, the reactors were quenched in ice instantaneously to stop any reactions.

5.2.2. Analytic procedure

For sampling operations, a device was adopted (Figure 5.1), constituted by sealed cell connected to a pipe, closed at the opposite side by a valve; in the middle of the tube, a sampling volume with a septum was placed. Once room temperature had been reached, the

reactor was put inside the containment and the device was purged with N_2. The reactor was then opened inside such containment, making the syngas flow into the pipe. There, gas samples were taken from the septum by using a 100 µl syringe and injected into gas-chromatographs.

1. Valve for N_2 purging
2. Containment for micro-autoclaves
3. Movable part
4. Sampling volume with septum
5. Manometer
6. Valve for volume measuring
7. Water vessel
8. Graduated column
9. Valve to the vacuum pump
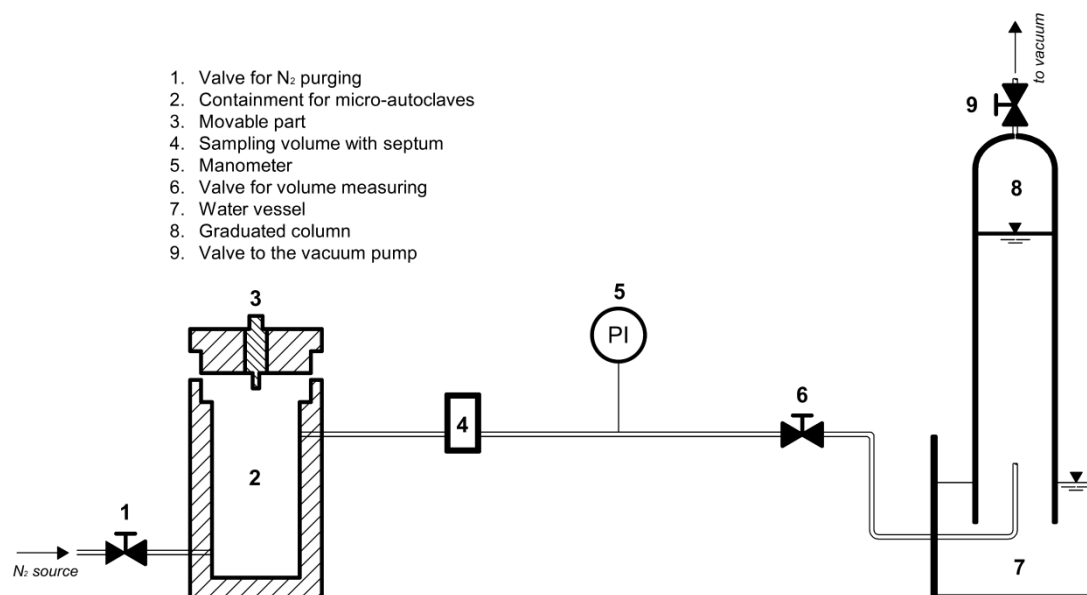
Figure 5.1 – Schematics of the gas sampling equipment.

The sample was first injected into a GC Agilent® 6890A with TCD and FID detectors, helium as a carrier gas, Molsieve® 5A 80/100 and Porapak® Q columns. This apparatus enabled to measure the amounts of: CO, CO_2, CH_4, C_2H_4, C_2H_6, C_3H_6, C_3H_8, C_4H_{10}. The analytical method applied in this device, however, did not allow to determine the presence of small amounts of H_2 (<20%) with adequate accuracy. For this reason, a second injection into another GC was done, an Agilent® 5890 model with TCD detector, nitrogen as a carrier gas, and a packed ShinCarbon® ST 80/100 column.

Once gas sampling had been performed, a gasometer was connected to the pipe. Such device involved a glass column, filled with water, put in a vessel where air was drawn. Once the valve on the pipe was opened, the gas was allowed to bubble inside the gasometer and the water level in the column lowered. By measuring the level of the water meniscus, it was possible to determine the volume production of gas achieved in the experiment.

After gas sampling activities, the reactor was pulled out of the containment and opened to take liquid samples. The liquid inside the reactor was sampled by means of a 2 ml syringe, filtered using a 0.45 µm round filter and collected. The TOC of the liquid sample was

measured to estimate the amount of organic compounds dissolved in water after reaction. A Dimatec® 2000 (Dimatec, Germany) analytical device, based on the principle of thermo-catalytic oxidation with subsequent IR detection, was used to that end.

The solid which had remained inside the reactor was removed by washing the micro-autoclave three times with acetone, carefully stirring with a glass stick. The liquid-solid mixture was thus poured into a beaker, together with the syringe and the filter used for filtration. All these tools had been previously weighted with a Mettler Toledo® balance. Beaker, syringe and filter were then put in a dryer at 105°C overnight, later to be cooled down with hygroscopic salts and weighted again. The solid content was thus determined as the difference between the two weights. The solid sample also underwent elemental analysis, performed using ICP Agilent 7025 ICP-OES.

5.2.3. Surface analysis

To explain why the inner surface of the reactors can still give rise to relevant differences in terms of syngas composition (see Paragraph 5.3.1), even after the aging treatment and many experimental runs, direct observation of the reactor surface was proposed. Anyway, it was not possible to get images of the direct surface of the reactor without destroying it. Alternatively, it was decided to use small pieces of the reactor material, actually burrs provided by the workshop that manufactured the micro-autoclaves themselves.

The metallic burrs, two of stainless steel and two of Inconel® 625, were first washed carefully with acetone, in order to remove the manufacturing oils. After that, they were reacted with a solution of 15% glucose during 7 runs of 16 hours each, for a total duration of 112 hours. After each run, the reactor and the metallic piece were treated exactly in the same way, washing them three times with acetone and drying before the next run.

The four samples were then observed by means of a scanning electron microscope (SEM) FE-SEM DSM 982 Gemini (Carl Zeiss Ltd., Oberkochen, Germany), equipped with an annular high brightness inlens-SE detector for high resolution and true surface imaging. A laterally mounted secondary electron detector (Everhart-Thornley-type) provides topographical contrast.

Additionally, a highly sensitive 4-quadrant solid state back scattered electron (BSE) detector for material contrast and a diode-type transmitted electron (TE) detector for thin specimen (STEM-in-SEM) are available (K.E. Developments Ltd., Cambridge, UK).

The same samples were also observed before the test, in order to provide the blanks for comparison.

5.3. Results

For each biomass, balances are presented showing the mass yields of the gaseous and solid phases, as well as the distribution of carbon between the two; moreover, mass productions of the analyzed permanent gases are shown. Subsequently, the liquid phase is taken into account, highlighting the molar contents of C, H and O: this contributes to understanding the nature of the possible liquid products arising from gasification. Finally, SEM images of the metallic burrs used to simulate the inner reactor surfaces are displayed.

5.3.1. Gasification of glucose

Figure 5.2a and Figure 5.2b show the mass yields of solid and gas products respectively. The yield is defined as the mass of the considered phase divided by the amount of biomass fed. Generally, it is possible to notice that more solid is obtained than gas, at the considered experimental conditions. More solid is obtained at subcritical conditions (~35%) than at supercritical ones (~25%). Vice versa, more gas is yielded at supercritical conditions (~20%) than at subcritical ones (<15%). This witnesses that the increased temperature promotes the selectivity to gaseous products. Anyway, a careful scrutiny of the figures makes it clear that the largest part of organics is actually present in the liquid phase. Moreover, the amount of liquid does not seem to be greatly affected by the reaction conditions, and it always stays at around 50%. The trend in time shows that solid yields are slightly decreasing as the reaction proceeds, while gas yields slightly increase. As far as the reactor material is concerned, Inconel® 625 seems to promote gas production instead of solid formation at both sub- and supercritical conditions.
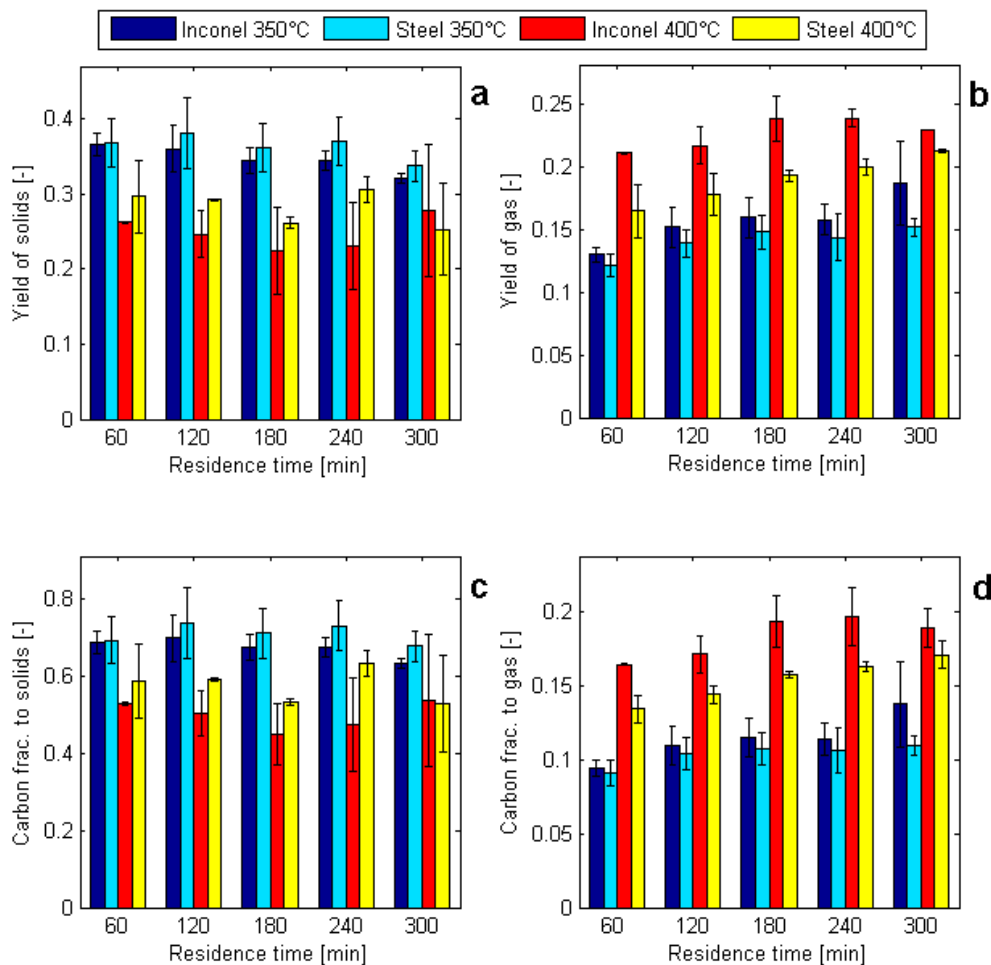
Figure 5.2 - Mass balance for glucose gasification. (a) Mass yields of solid; (b) Mass yields of gas; (c) Carbon balance in the solid; (d) Carbon balance in the gas.

It is interesting to compare the results of the mass balance with those of the sole carbon balance, both in the solid and in the gas, as shown in Figure 5.2c and Figure 5.2d. The first noticeable difference is that, presently, the fraction of fed carbon found in the solid is about 70% for sub-critical experiments and 55-60% for supercritical ones. A comparison with Figure 5.2a highlights that carbon is largely concentrated in the solid phase. The carbon fractions in the gas (Figure 5.2d) nearly reflect those found in the total gas mass (Figure 5.2b). As a consequence, the carbon fraction in the liquid is in the range 20-30%, while the mass fraction, as already stated, is ~50%. Differences among metals are essentially the same as shown in Figure 5.2a and Figure 5.2b.
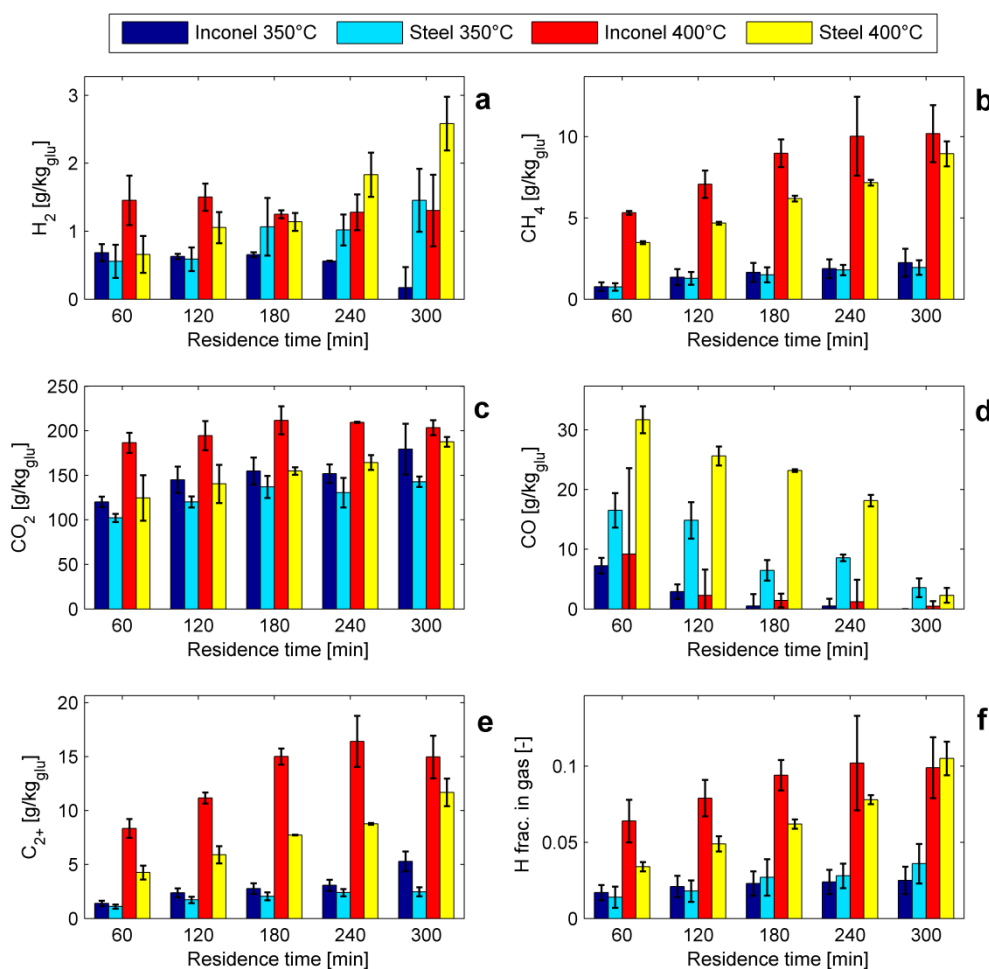
Figure 5.3 - Gas production for glucose gasification. (a) Hydrogen; (b) Methane; (c) Carbon dioxide; (d) Carbon monoxide; (e) C_{2+} hydrocarbons; (f) Hydrogen balance in the gas.

Figure 5.3 presents the yields of single permanent gases. In Figure 5.3a, hydrogen yields are shown. Subcritical conditions generally lead to lower H_2 specific productions than supercritical ones. However, here the reactor material plays a key role. Up to 120 minutes residence time, Inconel® 625 shows a higher hydrogen production than stainless steel at both reaction temperatures. Nonetheless, the trend for stainless steel is always increasing, while in Inconel® it is approximately constant. Starting at 180 min. residence time, H_2 production starts becoming much higher in stainless steel. After 300 min. of reaction, stainless steel at 350°C is even capable of producing more H_2 than Inconel® at 400°C.

Things are completely different when it comes to methane. Figure 5.3b shows that, for both reactor materials, the trend is always increasing in time. On the other hand, while at subcritical conditions the two metals give approximately the same yields, at supercritical conditions Inconel® produces more CH_4 that stainless steel. However, at 400°C and for a

reaction time of 300 min., the spread between the two metals become smaller as the CH_4 production in Inconel® tends to stabilize.

A similar trend can be found in Figure 5.3e, where the hydrocarbons with more than one carbon atoms, the so-called C_{2+}, are displayed. Inconel® 625 reveals a greater attitude to produce hydrocarbons than stainless steel, both at 350°C and 400°C.

Based on these results, stainless steel seems to yield more H_2, while Inconel® promotes the formation of hydrocarbons. It would be therefore interesting to assess which metal is able to transfer more hydrogen to the gas phase. This information can be obtained through a balance on hydrogen, which is presented in Figure 5.3f. Here, the amount of elemental H present in the gas, divided by the total amount of hydrogen fed with the glucose, is reported. It can be observed that, at supercritical conditions, Inconel® is able to shift more hydrogen into the gas than stainless steel despite its generally lower H_2 content. In other words, Inconel® yields more hydrogen in the gas, but preferably in the form of hydrocarbons (methane and other light C_{2+} compounds). Stainless steel enhances selectivity towards H_2.

A useful information is provided by carbon monoxide (Figure 5.3d). Here, a noticeable difference between the two reactors is shown. Stainless steel causes much higher productions of carbon monoxide than Inconel®, at both reaction temperatures; at 400°C, CO productions are higher than at 350°C, and the trend is always decreasing. For Inconel®, CO productions is only remarkable at 60 min. of residence time. After that, the measured amounts often decreased below the detection threshold of the gas-chromatograph. The difference in the CO trend is crucial to understand the different behavior of the two reactors, since CO is involved in both water-gas shift (WGS) and hydrogenation (i.e. methanation) reactions. This will be better explained in Paragraph 5.4.

Finally, Figure 5.3c shows CO_2 production. Here, Inconel® presents higher yields, which generally increase with the residence time. At supercritical conditions, more CO_2 is produced, holding the same reactor material. However, it must be clarified that the increase in the amount produced is essentially due to the larger quantity of gas produced. If the gas volumetric composition is taken into account, it can be proved that Inconel® at 350°C yields a gas with an average CO_2 content of 86%, while at 400°C it is 73.5%. Such analysis also allows to state that stainless steel produces a gas with lower CO_2 concentration: 74.7% at 350°C and 63.2% at 400°C.

5.3.2. Gasification of a mixture of glucose and phenol

The results were compared also with the analogue experiments carried out with the glucose/phenol mixture.
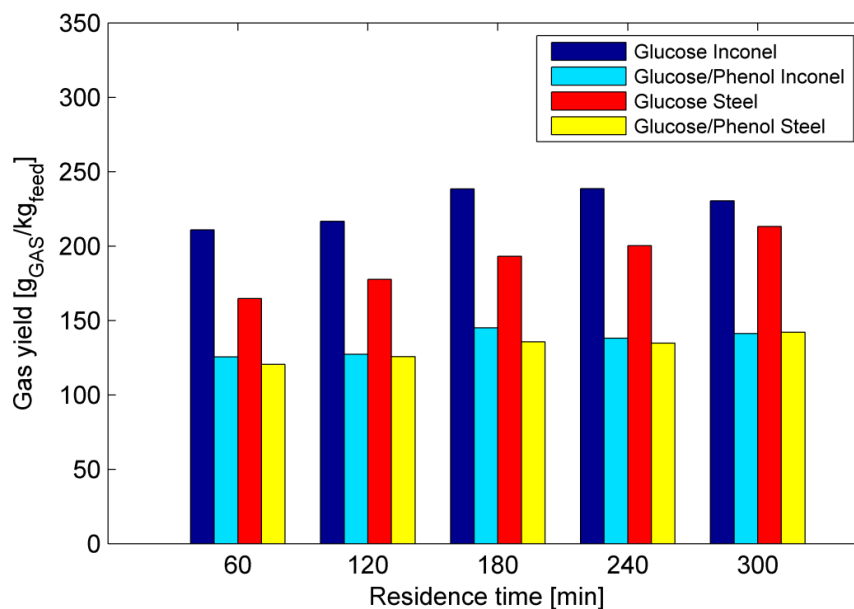
Figure 5.4 – Gas yields for glucose and glucose/phenol mixture supercritical water gasification at 400°C and 30 MPa.

In Figure 5.4, the specific gas production resulting from supercritical water gasification of glucose only and of the glucose-phenol mixture is compared. It is clearly noticeable that the presence of phenol depresses gas formation. The glucose-phenol mixture presents, at the same concentration, a higher carbon content than pure glucose. This would result in higher gas productions, if thermodynamic equilibrium would be achieved. Gas productions are however much lower. This implies to conclude that phenol has a much lower tendency to gasify and it can be considered as a inhibitor of the gasification process. As a consequence, it is also possible to notice that, while for pure glucose there is also a large difference between the stainless steel and the Inconel® reactor, when the glucose-phenol mixture is adopted the discrepancy is less evident.

Figure 5.5 shows the production of the main permanent gases for the gasification of this glucose-phenol mixture. Unlike Figure 5.3, here gas production is reported in terms of volume percentages. This allows to directly compare gas composition, focusing on the nature of the gaseous product, rather than on the extensive amounts.
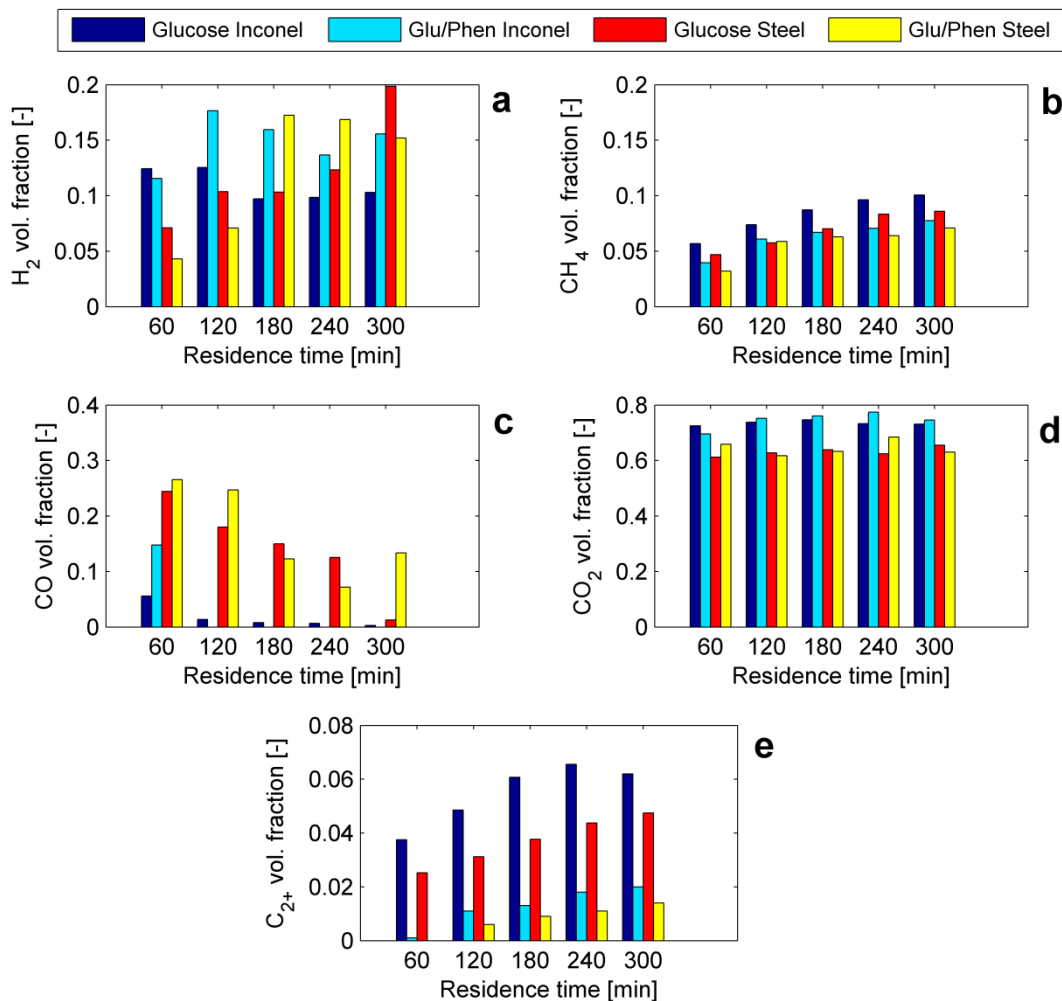
Figure 5.5 – Syngas composition for glucose and glucose/phenol gasification in supercritical water at 400°C and 30 MPa. Volume fractions of (a) hydrogen; (b) methane; (c) carbon monoxide; (d) carbon dioxide; (e) C_{2+} compounds.

The first thing to be noticed is that the glucose/phenol mixture yields a gas much richer in hydrogen than only glucose (Figure 5.5a). Of course, this does not imply that more hydrogen is produced: since overall gas production is lower (Figure 5.4), less hydrogen is produced in terms of mass. Hydrogen volumetric fractions, for the two reactor materials, appear to be comparable in the long-time. For stainless steel, a sudden increase between 120 min. and 180 min. of residence time can be observed.

On the other hand, hydrocarbons production seems to be hampered by the addition of phenol. Results about methane (Figure 5.5b) and especially for C_{2+} (Figure 5.5e) reveal that hydrocarbons in glucose/phenol gasification are far less present than in the corresponding experiments with glucose.

As far as carbon monoxide is concerned, Figure 5.5c shows that, in the same way as for glucose (Figure 5.3d), gasification conducted in a stainless steel reactor leads to higher carbon monoxide productions than Inconel® 625. The frame is reversed when CO_2 is analyzed (Figure 5.5d): now the nickel alloy causes the production of a gas with higher CO_2 content. In this case, only differences related to the reactor material can be seen, while the two substrates seem to behave in a substantially similar way.

As far as the liquid phase is concerned, it can be seen that, when phenol is added, more carbon is stored as liquid compounds. Figure 5.6 shows the fraction of TOC found in the liquid after reaction, referred to the initial amount which, for glucose, is 60.00 g/l and, for the glucose-phenol mixture, is 64.64 g/l (calculated values).

In both cases, the fraction of TOC that is found in the liquid phase after reaction is a much smaller part than the original one, implying that most of carbon is shifted to the solid or the gaseous phase. By the way, it is clearly noticeable that, when the glucose/phenol mixture is gasified, a higher part of TOC is unconverted, which is around 30%. Pure glucose gasification exhibits higher TOC reductions: usually less than 15% of the original TOC is then found in the liquid. As far as materials are concerned, in stainless steel higher TOC conversions are obtained, though data do not testify completely clear trends.
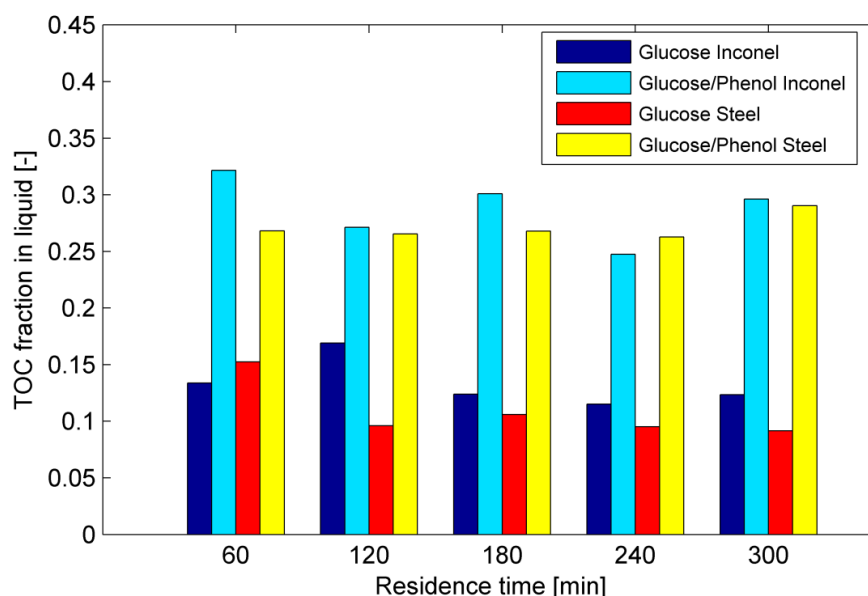
Figure 5.6 – Fraction of TOC remaining in the liquid after gasification of glucose and glucose/phenol mixture at 400°C and 30 MPa.

Differently from the gaseous and liquid products, solids production does not exhibit any significant change when phenol is added to the reacting mixture, as it can be concluded by means of Figure 5.7. Though data exhibit some oscillations, they allow to state that practically no changes can be observed when phenol is added to the reacting mixture. Char production appears to be stable.
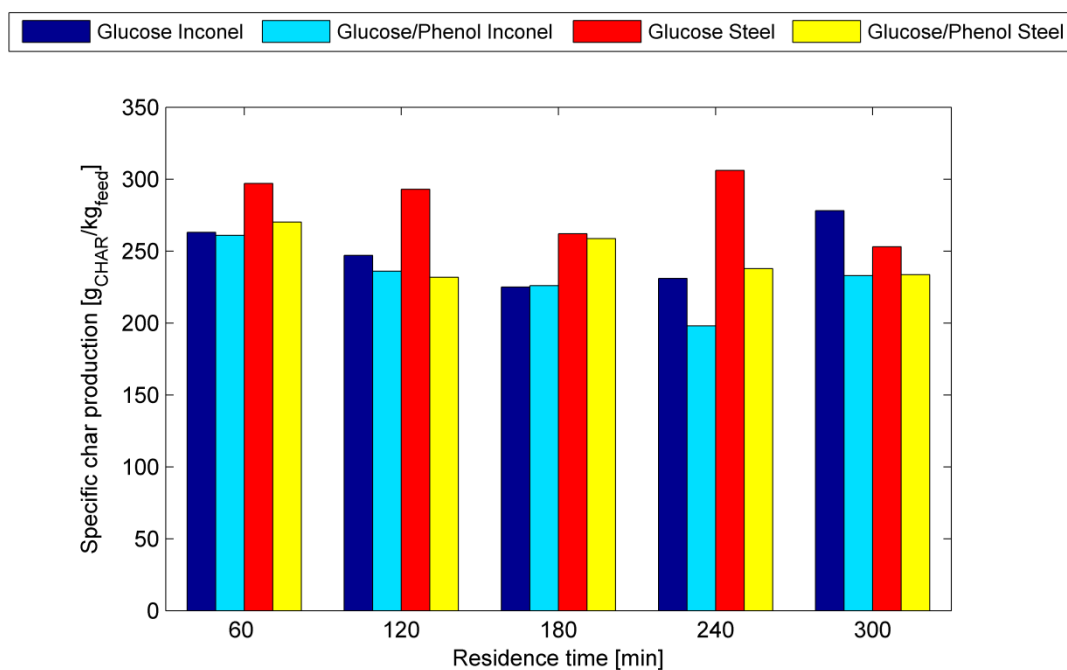
Figure 5.7 – Specific char production for SCWG of glucose and glucose/phenol mixture at 400°C, 30 MPa and biomass concentration of 15% wt.

5.3.3. Metal surface observation

Especially in the case of glucose gasification, the results showed large differences between the two reactor materials. Such differences are extremely significant, since they are present even after the "aging" treatment undergone by the reactors and a very large number of experimental runs. It was thus interesting to understand why catalytic activity is still possible.
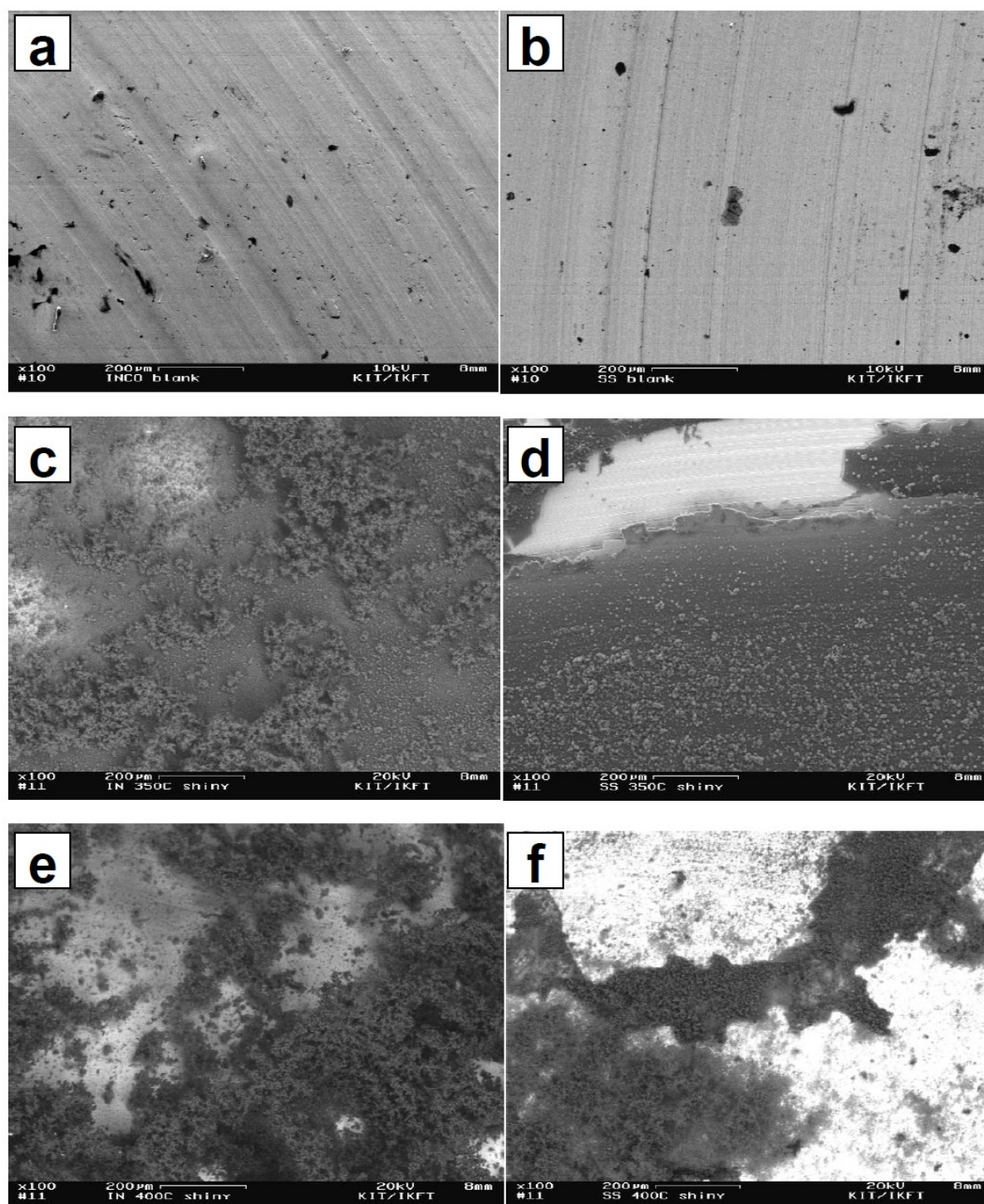
Figure 5.8 - SEM images of the reacted metallic surfaces with glucose 15% wt. after 7 cycles of 16 h reaction each. (a) Inconel® blank; (b) Stainless steel blank; (c) Inconel® at 350°C; (d) Stainless steel at 350°C; (e) Inconel® at 400°C; (f) Stainless steel at 400°C.

Figure 5.8 shows the SEM images of the metallic pieces, which were reacted with glucose (see Paragraph 5.2.3). Figure 5.8a and Figure 5.8b present the metallic pieces before reaction. They appear quite similar. Both surfaces are characterized by very thin stripes,

which are due to the cutting machinery. Figure 5.8c and Figure 5.8d show the surfaces reacted at 350°C for more than 100 hours. In both cases, a black layer deposited on the metal can be noticed. Upon the layer, small carbon spheres can be observed. A more detailed observation revealed that these spheres have a diameter of around 1 µm or less. It can be noticed that the surface coverage by the carbon is not uniform. In the upper-left part of Figure 5.8c, two metal spots can be noticed. In Figure 5.8d, an even more interesting phenomenon is shown. Here, it is clearly visible that the carbon layer detaches from the bottom metal and a shiny metal region becomes evident.

Figure 5.8e and Figure 5.8f represent the surfaces after reaction at 400°C. Now, the carbon layer is less uniform than at 350°C. Carbon tends to form more aggregates of smaller spheres, which leave more "exposed" metal regions. This tendency seems to be more pronounced in stainless steel than in Inconel® 625.

Despite the differences between the two metal surfaces, the latter are not covered uniformly with carbon material and some metallic spots are still exposed to the reactive environment, thus exerting a catalytic activity that persists in the longer run.

5.4. Discussion

A number of observations can be made by analyzing the experimental results more in depth. A noticeable difference between the two materials resides in the composition of the produced gas. Especially at 400°C, stainless steel seems to yield more hydrogen than Inconel®. Vice versa, the nickel-alloy is more effective in methane production, especially in the case of glucose conversion. To account for these differences, it is useful to focus on the different ways through which hydrogen can be produced.

There are mainly three ways to produce H_2 through hydrothermal processing: *(a)* direct production from small organic compounds, *(b)* water dissociation induced by metal, *(c)* water-gas shift (WGS) reaction.

Direct production is generally achieved by dissociating small organic molecules into permanent gases: mainly H_2, CO, CO_2, CH_4. A possible pathway is, for example, de-carboxylation of formic acid:

$$HCOOH \rightarrow H_2 + CO_2 \tag{5.1}$$

or de-carbonylation of formaldehyde, which results in:

$$HCHO \rightarrow H_2 + CO \tag{5.2}$$

In both reactions 5.1 and 5.2, hydrogen as well as CO and CO_2 are directly produced

through the thermal decomposition of small organic molecules, originating from the hydro-thermal degradation reactions of biomass. In these reactions, water plays a limited role and mostly does not intervene as a reactant.

Under certain conditions, hydrogen can also be produced directly from water, through the action of a metal catalyst. Resende and Savage, for example, reported H_2 formation when some metals were exposed to supercritical water at 500°C [81]. This pathway does not seem to be relevant for the present study, since temperatures are too low to allow for a significant contribution of the water dissociation reaction.

Finally, hydrogen can be produced through gas-phase reactions, whereby the previous-ly formed permanent gases are allowed to re-arrange by reacting among them. The most important reaction is WGS, taking place in compliance with the following pattern:

$$CO + H_2O \rightarrow CO_2 + H_2 \qquad (5.3)$$

Here, water acts as a reactant and, as a result of hydrothermal conditions and their large water excess, the reaction equilibrium should be shifted to the right side. WGS is a key-reaction in hydrothermal conditions. It has been reported that H_2 production from hydro-thermal biomass gasification is mainly due to the WGS reaction [167]. The reaction tem-peratures considered in this study fall inside to the so-called "high temperature WGS", which includes the range between 310°C and 450°C [168]. At these conditions, "ferro-chrome" catalysts are commonly used, that is to say catalysts whose main constituents are iron (Fe_2O_3) and chromium (Cr_2O_3) oxides [141]. Indeed, chromium oxide acts as a stabi-lizer and prevents iron oxide sintering, thus enhancing the catalytic activity of iron oxide. Stainless steel, which is mainly an iron-chromium alloy, can act as a good catalyst for WGS, as is easily proved. Nonetheless, WGS can also be effectively catalyzed by nickel to some extent [142].

Another key-reaction that occurs during hydrothermal processing is CO methanation, which belongs to the family of hydrogenations. Through this reaction, CO reacts with H_2 to produce methane:

$$CO + 3H_2 \rightarrow CH_4 + H_2O \qquad (5.4)$$

Similar reactions could be envisaged for the formation of higher hydrocarbons. They all be-long to the well-known Fischer-Tropsch chemistry.

In the tests with Inconel® 625, lower CO, lower H_2 and higher CH_4 concentrations are measured after reaction, with comparison to stainless steel. All these elements corroborate the hypothesis that Inconel® 625 enhances CO methanation reaction. Nickel is the most

widely used CO methanation catalyst. In the literature several studies can be found where CO methanation is achieved using Ni- or Ru-based catalysts, possibly doped with noble metals [145, 169, 170]. Owing to its high nickel content, Inconel® 625 can effectively serve as a CO methanation catalyst.

By observing the experimental results, it can be stated that the solid produced is almost constant during time, as it does not decrease significantly even after several hours of run. It is known that solid char is far less reactive than biomass. Once it is formed, it is hardly reconverted into liquid intermediate or gases, thus representing a sort of "kinetic sink". This is a consequence of the lower polarity of char because of the lower oxygen content. Water as polar compounds preferably reacts with polar bonds, therefore coke is relatively inert.

Indeed, the role of char as a kinetic sink is widely confirmed by other studies in the literature. In a work by Chuntanapum and Matsumura, who studied and modeled glucose gasification in both sub- and supercritical water [30], no reaction involving char as a reactant is present. Therefore, it can be deduced that, once char is formed, its further conversion is assumed to be negligible. Furthermore, the same assumption of a non-reacting char was also made in the work by Resende and Savage [104], who modeled the SCWG of cellulose and lignin. It is thus evident that a strategy to improve gasification efficiency cannot go without an *a priori* prevention of char formation, which constitutes a permanent loss in gasification efficiency.

Interesting pieces of information are offered by the comparison between glucose and glucose/phenol gasification. The comparison of gas production yields allows to conclude that phenol acts as an inhibitor for gasification. When phenol is added to the reacting mixture, in fact, gas yields are sensibly lower than with pure glucose. It could be hypothesized that phenol forms a structure that inhibits organic molecules from gasification. In the literature, it has been reported about the so-called "free-radical scavenger" effect of phenol [47]. It consists in the formation of relatively stable free-radicals that are able to stop radicalic reactions chains, thus resulting in lower gasification yields.

The refractoriness of phenol towards SCWG can be also taken as a possible explanation of the gas composition achieved. As it was mentioned in Paragraph 5.3.2, hydrogen is relatively more present than hydrocarbons (CH_4 and C_{2+}). It is known from thermodynamic modeling that hydrogen is the preferred product at lower biomass concentrations, while methane is preferred when higher biomass/water ratios are involved (see Chapter 2 and

[157]). If phenol is considered as an inert, the consequence is that the real water/biomass ratio is higher. This would provide some justification about the experimental results.

Consistently, the presence of organic compounds in the liquid phase is higher, as witnessed by the data about TOC (Figure 5.6). This suggests that phenol molecules are probably more refractory to gasification and tend to stay in the liquid phase. The action of phenol could be that of stabilizing the organics intermediates, that is to prevent organic compounds from undergoing any further reactions, neither to form smaller gas species nor to aggregate into more complex macro-molecules.

To some extent, this theory can be supported by an analysis of the data about solid production. The experimental results, indeed, tend to exclude that the presence of phenol could imply higher polymerization rates. Figure 5.7 testifies that the measured amounts of solid obtained after gasification of glucose and glucose/phenol mixture are comparable. In other words, though the gasification of organic molecules is inhibited, their polymerization to solid products is equally not favored: organic molecules mostly stay in the liquid phase.

Probably, phenol itself is refractory to both gasification and polymerization. Phenol could also prevent other organic molecules from gasification/polymerization, as well. Although a study by Weiss-Hortala *et al.* [47] supports this thesis, no conclusion can be drawn based on the present data. However, the problem will be further discussed in Chapter 7, where different glucose/phenol mixtures will be gasified in a continuous reactor.

5.5. Conclusions

In this study, several tests of supercritical water gasification were performed with glucose and glucose/phenol as model compounds. An experimental methodology based on metallic micro-autoclaves was used and easily allowed to obtain results for many different experimental conditions. Supercritical and subcritical conditions were explored, as well as the influence of the reactor material.

The study highlighted that, in the considered experimental conditions, some of the reactions take place over quite long time scales. These are essentially gas phase reactions, which are mainly represented by water-gas shift and CO methanation.

As far as the effect of material is concerned, the adoption of a nickel alloy resulted in slightly higher gas productions. Inconel® 625 promotes hydrogenation reaction, as CO methanation, which consumes CO and hydrogen producing methane and other light hydrocarbons. On the other hand, stainless steel shows higher hydrogen yields, which can be

attributed to its ability to catalyze water-gas shift reaction. This is strictly true for supercritical conditions, while at subcritical conditions the two materials appear to give almost the same results. Tests at 400 °C showed significantly higher gas yields than those at 350 °C.

Based on these results, it can be suggested that at 400°C a stainless steel reactor can be a viable choice for many applications, since it is cheaper than Inconel® 625 and it is able to enhance H_2 production.

Gasification tests with a glucose/phenol mixture allowed to understand that phenol is an inhibitor for supercritical water gasification. Its addition to the reacting mixture results in considerably lower gas production, higher concentrations of organics in the liquid and almost equal solid yields. Extending these results to real biomass, it can be inferred that a higher lignin content depresses gasification yields and enhances the production of liquid products, at least at the considered reaction conditions.

Chapter 6

Batch Gasification of Real Biomass

In the present Chapter, batch experimental tests with real biomasses are reported. Real biomass is considerably different from model compounds, involving a more complex structure and the presence of other elements beyond carbon, oxygen and hydrogen. The experimental tests which were executed can be grouped into three main lines. First, batch experiments were conducted on beech sawdust, in order to compare the results with those of the previous Chapter concerning glucose. Then, the focus was moved on the analysis of supercritical water gasification conducted with the solid product arising from hydrothermal carbonization process (HTC). Finally, long-time tests were performed by reacting biomass for 16h in reactors made of different materials, possibly using K_2CO_3 as a catalyst.

6.1. Introduction

In the previous Chapter, the attention was focused on the gasification of model compounds: glucose and phenol were used to schematize cellulose and phenol, which are the main constituents of biomass. As it has been already stated, this methodology involves several advantages, since it allows to provide ease of reasoning. Model compounds have, in fact, a precise composition, since they are characterized by a precise molecular formula. Moreover, for these simple organic molecules some information is available in the literature, concerning the fundamental reaction pathways at hydrothermal conditions. This helps in understanding the main reaction pathways and allows to acquire information about how process conditions influence the process outputs.

On the other hand, such approach also shows its intrinsic limits. First of all, glucose and phenol can be only considered as the monomers of more complex organic macromolecules. The reaction steps leading from polymers to monomers are reasonably very important, and they can influence the kinetics of the process in an outstanding way. The model compounds approach actually neglects this crucial depolymerization step, where hydrolysis plays a fundamental role. Additionally, cellulose, hemicellulose and lignin in real

biomass are arranged in a peculiar way, that differs from one vegetal species to another. As a consequence, each substrate is intrinsically different from another, even with a similar composition.

Another weakness point of processing model compounds like glucose and phenol is the fact they can only schematize ligno-cellulosic biomass. In this category, mostly traditional biomasses are included: for example, trees and some types of agriculture residues (i.e. straw). On the other hand, supercritical water gasification can potentially deal with non-conventional types of biomass, like municipal waste or algae. These substrates do not present a ligno-cellulosic structure, thus the schematization with glucose-phenol has only limited value.

An important thing that differentiates real biomass from the model compounds approach is that biomass cannot be described only in terms of CHO-based components. It is well known that biomass is also constituted also by heteroatoms, like nitrogen and sulfur, which are parts of some organic molecules (e.g. proteins). Another important difference is represented by the presence of the so-called "ashes". This term is usually employed to indicate those compounds that are found after burning biomass: it is substantially the mineral part of biomass. Despite their apparent inertia, ashes may exert a crucial role in hydrothermal reactions, since they can act as catalysts for important reactions, like water-gas shift (WGS) [39].

In the present Chapter, batch SCWG of real biomass is treated. The experimental tests which were executed can be grouped into three main lines. First, batch experiments with beech sawdust were executed. The aim was to compare the results with those obtained for glucose in the previous Paragraph 5.3.1, trying to find analogies and differences between the investigated substrate and the model compound.

Then, the gasification of the solid product from hydrothermal carbonization (HTC) process was studied, in order to understand the reaction behavior of a material deriving from another hydrothermal process, which could have interesting practical applications (Paragraph 6.4). An insight on the processes involved during SCWG was made through the observation of SEM images of the solid products.

Finally, long-time tests (16 hours) were performed by reacting different types of biomass (beech sawdust, HTC char, municipal waste and malt spent grains) for 16h in reactors made of different materials, eventually using K_2CO_3 as a catalyst. The aim of this activity

was to compare different substrates in terms of gasification yields and to investigate about the combined catalytic effects of reactor walls and added catalyst (Paragraph 6.5).

As for the previous Chapter, the experimental activities were conducted at the Karlsruhe Institute of Technology (Germany), Institute of Catalysis Research and Technology (IKFT), under the scientific supervision of prof. A. Kruse.

6.2. Materials and methods

The experimental activities presented in this Chapter consisted in batch experiments made with different real biomasses. The methodologies for the experimental procedure and for gas, liquid and solid products analysis are the same as the ones reported in Chapter 5. In this paragraph, their description will be consequently briefer: all the required details can be found in Paragraph 5.2.

6.2.1. Biomass typologies

For this work, four types of real biomass were selected. The way they were chosen is related to the availability of the specific substrate and to its significance. The selected materials were: beech sawdust, municipal waste, malt spent grains and hydrothermal char deriving from corn silage. Each material was first analyzed by means of ICP (Agilent® 7025 ICP-OES) in order to obtain its elemental composition (Table 6.1).

Table 6.1 – Elemental composition of the selected biomass and model compounds (% wt.).

Biomass	C	H	O	N	S
Glucose	40.0	6.7	53.3	-	-
Beech sawdust	48.9	6.2	40.6	1.0	0.1
Municipal waste	45.2	6.6	41.8	2.1	0.2
Hydrothermal char	64.2	5.6	20.0	2.3	0.2
Malt spent grains	49.7	6.9	34.3	4.3	0.3

The first type of biomass chosen was beech sawdust. This substrate is indicative of ligno-cellulosic biomass, which is the category of biomass which has been usually adopted in bio-energy applications. Such material is characterized by the fact its composition involves cellulose, hemicelluloses and lignin. In this study, sawdust was used with an average

granulometry of 0.7 mm. It can be said that this material is of relative importance, since it is usually produced as a by-product, for example, of the furniture industry.

On the other hand, ligno-cellulosic biomass is not the sole that can be of interest for bioenergy production. Many other types of biomass are not actually included in this class, since their composition involves different organic constituents. The huge domain of non-ligno-cellulosic biomass is very extended, and it can be said that it represents the largest part of world available biomass, usually present as waste or by-product.

To this purpose, municipal waste were chosen. To obtain this substrate, a mixture of an average kitchen waste was built, using different wastes: egg shells, fruit skins, food rests, etc. The obtained material was dried and then crushed, obtaining a powder. Municipal waste is very interesting for supercritical water gasification, since this material is also naturally very wet, thus traditional technologies are not the most recommended for its energy valorization. The problem of an efficient treatment of municipal waste, in an economic feasible way, is of particular interest since it represents a huge cost for the whole collectivity and hydrothermal processes could be the right answer.

Another waste biomass is represented by malt spent grains. This is a by-product of bier industry. Malt spent grains are the residue that is obtained in a brewery after the mashing of malt. It is constituted by a mixture of grain husks, pericarp and fragments of endosperm. From a composition point of view, this residue involves a quite high protein content, along with vitamins. These characteristics has allowed this material to be very popular for the production of animal feed or as a soil fertilizer. On the other hand, this is an interesting substrate for hydrothermal processing, since, after the mashing process, this material presents a natural high water content.

Finally, hydrothermal char was considered for analyses. This substrate is the product of another hydrothermal process, that is hydrothermal carbonization (HTC), which is aimed at producing a carbonaceous solid material from biomass through reaction in hot pressurized water (see Paragraph 1.2.2). In this work, hydrothermal char obtained through carbonization of corn silage was used. The original feedstock, corn silage, is obtained through the fermentation of the whole corn plants in silos, through a process called "ensilage". The product of such process can be stored for longer times than the original plant and is commonly used as a feed for cud-chewing animals. Corn silage underwent a hydrothermal carbonization treatment for 2 h at 200°C.

6.2.2. Experimental plan

The experimental activities of this chapter can be summarized into three typologies. First, beech sawdust was tested at both subcritical and supercritical conditions. For this biomass, the very same tests as for glucose were performed (see Paragraph 5.2), using the same reaction conditions and methodology. In this way, comparison could be provided.

A second experimental task involved hydrothermal char gasification. Tests were conducted at 400°C and 30 MPa, with a substrate concentration of 15% wt. This activity was performed in order to acquire information about the possibility to treat a product that had already undergone a hydrothermal process. Tests were repeated in stainless steel and Inconel® 625 reactors, with residence times ranging from 1 hour to 5 hours. Liquid, solid and gaseous samples were analyzed as for the previous point. Moreover, the solid product was also considered and it was analyzed for both structure and composition. In particular, SEM images of the char products were taken for each reacted sample. The elemental composition was then obtained through a microanalysis unit, connected to the SEM instrument, and constituted by an Energy Dispersive X-ray (EDX) analyzer with a Si(Li) detector INCA PentaFET-x3 (Oxford Instruments, UK).

Finally, all the considered biomasses were used for long-time tests, involving 16 hours of reaction, again using both stainless steel and Inconel® 625 micro-autoclaves. This kind of tests were aimed at understanding what is the behavior of different biomass in the long-time, also comparing the experimental results with the equilibrium predictions of the previously proposed thermodynamic model (see Chapter 2).

Besides the already presented 5 ml metallic micro-autoclaves, another reactor was employed in this activity. Such device consisted of an external containment of stainless steel and of an interior inlay of aluminum oxide (alumina, Al_2O_3), whose volume was 23.59 ml. This apparatus is shown in Figure 6.1. The ceramic inlay was put inside the containment, but a small gap was ensured between the metallic and the ceramic walls. This allowed a pressure balancing that prevented the ceramic inlay from rupture; ceramics have, indeed, poor tensile strength and thus they are not indicated for the manufacturing of pressurized vessels.

Figure 6.1 – Metallic containment and ceramic inlay manufactured in alumina (Al_2O_3).

The reactor was closed on the top by a flange, which could be screwed in and off to allow reactor loading. On the top of the flange, two sampling ports were present: one, closed with a valve, allowed gas sampling; the other was used to plug a manometer, in order to measure the actual reactor pressure.

Tests with such ceramic reactor were made for two main reasons: *(a)* to provide results less affected by the catalytic activity of metallic walls, since alumina is commonly referred as inert; *(b)* to test a reactor solution.

Long-time tests were also repeated adding a catalyst to the reacting mixture. The used catalyst was potassium carbonate (K_2CO_3). It was added in a ratio 1:4 to the reacting biomass, which was then reacted in the very same way. K_2CO_3 is known as a catalyst for biomass gasification, which is able to increase the gaseous yields [73]. Moreover, it is a quite inexpensive material, thus its usage as a possible industrial catalyst appears to be reasonably feasible. The possibility to have results that can better deal with equilibrium was considered.

6.3. Beech sawdust gasification

The same analyses carried out for glucose were repeated for beech sawdust. In this case, biomass was initially present in the reacting mixture as solid phase. Thus, a prior step of dissolution into liquid should be hypothesized to happen before gasification. Moreover, in this case heteroatoms like N and S, but also potential catalysts like alkali ions, are present.

6.3.1. Gaseous products
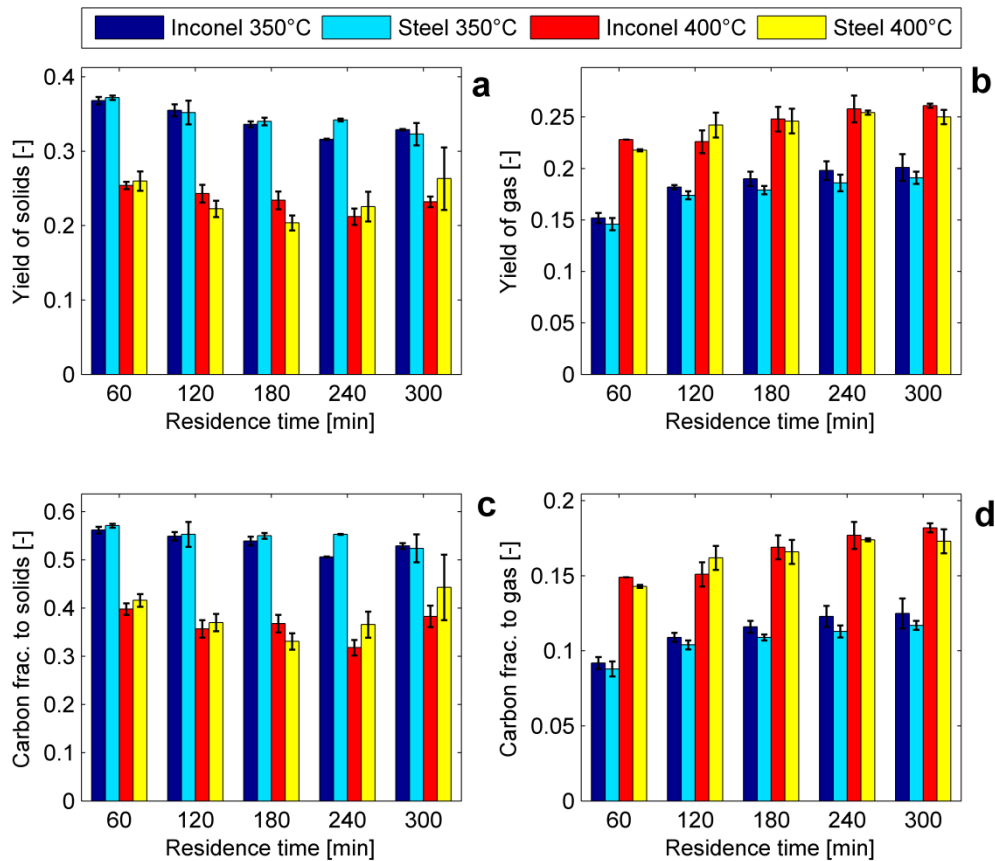
Figure 6.2 - Mass balance for beech sawdust gasification. (a) Mass yields of solid; (b) Mass yields of gas; (c) Carbon balance in the solid; (d) Carbon balance in the gas.

Figure 6.2a and Figure 6.2b report the mass balance which highlights how biomass gets parted between solid and gas phases. As for glucose, Inconel® 625 appears to yield more gas than stainless steel, even though the difference is extremely low. Solid yields tend to slightly decrease in time, but it can be stated they are essentially constant.

Carbon balance (Figure 6.2c and Figure 6.2d) also does not show an evident difference between the two materials. It can be noticed, however, that the carbon fraction found in the gas is approximately the same as for glucose (Figure 5.2d). On the other hand, the fraction found in the solid is generally lower: this allows to conclude that more carbon is found in the liquid phase.
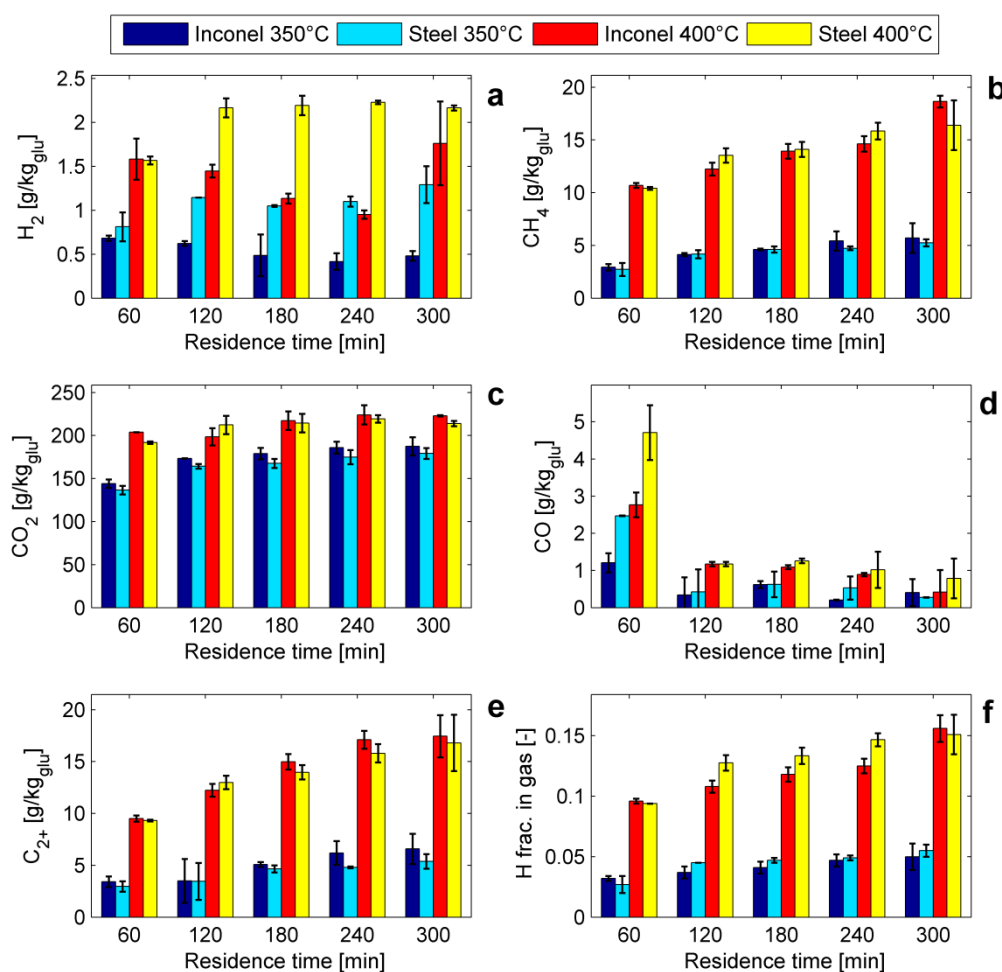
Figure 6.3 - Gas production for beech sawdust gasification. (a) Hydrogen; (b) Methane; (c) Carbon dioxide; (d) Carbon monoxide; (e) C_{2+} hydrocarbons; (f) Hydrogen balance in the gas.

Gas composition obtained with beech sawdust is shown in detail in Figure 6.3. Following the same way of thinking as in Paragraph 5.3.1, the first noticeable thing is the greater H_2 production measured in the stainless steel micro-autoclaves, especially at 400°C, with respect to Inconel® 625. The production trend highlights that, after an initial equivalence at 60 mins residence time, H_2 production in stainless steel booms from 1.5 to 2.2 mg/g biomass and it holds approximately constant. On the other hand, H_2 produced by the Inconel® 625 reactor seems to decrease in time, except for the last point, at 300 mins, where it increases again. Since Figure 6.3b shows that the total gas production in Inconel® and stainless steel is substantially the same (the former even yields something more) it can be said that H_2 is somehow reacted to form some other gaseous species.

Moving to methane, generally higher productions are achieved with respect to glucose. At 400°C an average production of ~12 mg/g can be appreciated. The differences between the two materials are not so evident in the case of beech wood. The same way of reasoning can be applied for the C_{2+} hydrocarbons (Figure 6.3e) and also for the hydrogen fraction in the gas (Figure 6.3f). It is worth-noticing the behavior of CO (Figure 6.3d). The tendency that has been already reported for glucose (Figure 5.3d) can be appreciated again, thus stainless steel is able to yield more CO, especially at higher temperatures. However, the amount produced is now much lower (maximum 4.5 mg/g, while it used to be well over 30 mg/g for glucose). On the other hand, it must be said that CO is only found in significant amounts at 60 min. residence time. After then, CO is decreasing (thus it reacts with other molecules) but the amount is very small and it falls under the detection threshold of the measuring instrument. It can be thus affirmed that practically no CO, or at least, no significant amount of CO is detected from 120 min. ahead.

The differences between the two reactor materials are also quite negligible in the case of CO_2 (Figure 6.3c). The trends are the same as for glucose, but the amounts of CO_2 are higher, probably as a consequence of the higher carbon content in the biomass fed.

6.3.2. Liquid phase

An interesting result is represented by the amount of carbon, hydrogen and oxygen, originating from feedstock, which are found in the liquid phase. This information can be acquired through the elemental balances, since the elemental composition of feedstock (Table 6.1), gas and solid, as well as the carbon content in the liquid, are known. The amounts of oxygen and hydrogen transferred to the liquid phase were calculated by difference. Through the analysis of the elemental molar ratios, it is possible to have an idea of which kind of compounds are present in the liquid phase.

In order to establish a useful comparison, the same results were calculated on the basis of the experiments with glucose, carried out in Chapter 5.

Table 6.2 reports the milli-moles of C, H and O, originating from glucose and beech sawdust, which are found in the liquid phase. For glucose, C, H and O are approximately in the molar ratio 1:12:6, while the feedstock has 1:2:1. For beech sawdust, the ratio is approximately 1:6:2, and the initial biomass has 1:1.5:0.6. In both cases, a high number of hydrogen and oxygen atoms for each atom of carbon was found. The "excess" in hydrogen and oxygen is more pronounced for glucose than for beech sawdust. These results allow to

formulate the hypothesis that, at the considered experimental conditions, water is formed among the liquid products and, thus, H_2O is a product rather than being a reactant. This thesis will be better debated in the subsequent Paragraph 6.4.

Table 6.2 - Milli-moles of C, H and O, derived from glucose and beech sawdust, present in the liquid phase (averaged values).

Reactor material and conditions	Glucose			Beech sawdust		
	C	H	O	C	H	O
Inconel® 625 350°C	2.1	25.5	11.8	3.6	20.0	6.7
Stainless steel 350°C	2.0	25.4	12.1	3.7	20.1	6.9
Inconel® 625 400°C	1.0	12.7	5.6	1.7	12.0	3.4
Stainless steel 400°C	0.8	13.5	6.1	1.7	11.8	3.7

At this stage, focusing on the role of water in hydrothermal reactions is appropriate. If the data concerning carbon balance and total mass balance in the liquid phase is considered (see Figure 5.2 and Figure 6.2), high liquid mass yields are measured, although with a much lower carbon fraction. Moreover, the data in Table 6.3 shows that most of the hydrogen and oxygen originally contained in the biomass is found in the liquid phase. As a result, C:H:O molar ratios of approximately 1:12:6 and 1:5:1.5 are observed for glucose and beech sawdust, respectively.

Especially in the case of glucose, it is very unlikely that these molar ratios can be entirely imputed to organic compounds. Indeed, small organic molecules, which are often found in the liquid, have very different molar ratios. In formaldehyde, for example, the C:H:O ratio is 1:2:1, in formic acid 1:2:2, in pentane 1:2.4:0, and in 5-HMF 1:1:0.5. Evidently, the observed C:H:O ratios cannot be achieved, not even by combining such possible organic products, since H and O are far higher than C. This gives value to the hypothesis that water (whose ratio is 0:2:1) is formed during feedstock hydrothermal degradation. Water thus seems to be a product, rather than a reactant, as would be expected under high water excess conditions.

A possible source for water formation can be represented by glucose degradation steps. As reported in [40], glucose gives different products when degraded at hydrothermal conditions. A number of these reaction steps actually take place through dehydration, with the production of water. Examples of this pathway are the dehydration of glucose to

levoglucosan, or the formation of 5-HMF ($C_6H_6O_3$) from fructose [171]:

$$C_6H_{12}O_6 \rightarrow C_6H_6O_3 + 3H_2O \qquad (6.1)$$

Such reaction is of outstanding importance, since 5-HMF is considered the main precursor of char/coke [52]. If 5-HMF is not subsequently hydrolyzed, it undergoes polymerization reactions leading to solid products formation. Therefore, water formation is compatible with the observed occurrence of coke in our experimental results.

The production of water during feedstock hydrothermal degradation was also highlighted in Chapter 3, where methanol SCWG was kinetically modeled (see also [172]). In that work, it was predicted that water is only consumed through the water-gas shift reaction. Indeed, the reactions leading to the "direct" formation of the small permanent gas molecules (CO, CO_2, H_2, CH_4) occurred with a net water production. The comparison of results shows an influence of the type of metal stronger for glucose than for beech sawdust. The explanation might be that the small ash content with alkali salts leads to a catalysis of the WGS, which is superimposed on the metal surface catalysis effect.

Looking at the molar ratios in the obtained liquid, it can be affirmed that water is produced in a higher amount for glucose than for beech sawdust. This could be explained by considering that, as beech sawdust is a biomass composed of cellulose and lignin, it needs a prior dissolution step, occurring with the hydrolysis process [173]. Hydrolysis involves the reaction of bio-macromolecules with water for them to de-polymerize to form smaller oligomers or monomer units. For example, hydrolysis of cellulose is of the form:

$$[C_6H_{10}O_5]_{n+1} + H_2O \rightarrow [C_6H_{10}O_5]_n + C_6H_{12}O_6 \qquad (6.2)$$

Thus, water actively takes part in the hydrolysis process, which implies that real biomass has a higher "water demand" than model compounds. In other words, water is still a product in beech sawdust, but a lower quantity is formed because a part was previously employed for hydrolysis.

As stated when discussing Eq. (6.1), the production of water is directly linked to the formation of solid char. Since the solid phase is much richer in carbon than the original feedstock, hydrogen and oxygen must be released in the other phases, which causes water formation. It was observed that char formation is greatly enhanced by biomass concentration, since its reaction order is around 3÷4 [52, 61]. It can be concluded that, along with char, water is formed as well and its amount becomes higher as the biomass concentration in the feed increases.

Importantly, thermodynamic equilibrium actually foresees that water acts as a reactant,

which means that, at equilibrium, less water than that present in the fed would be expected. The fact that water is formed evidently reveals that equilibrium is not achieved under the experimental conditions considered. Non-equilibrium can also be promptly deduced by observing that solid and liquid products are formed: at thermodynamic equilibrium, only gaseous products should be present [157]. Equilibrium is not achieved even after several hours of operations: this reveals the existence of strong kinetics constraints.

6.4. Hydrothermal Char (HTC) gasification

The results concerning the gasification of hydrothermal char are reported in this paragraph. They are presented distinguishing those about products yields and gas composition and the observation of the solids arising from the gasification operations.

6.4.1. Products yields and gas composition

The very same analyses carried out for glucose and beech sawdust were also performed for hydrothermal char. Figure 6.4 shows the yields of solids and gas and the carbon balance.
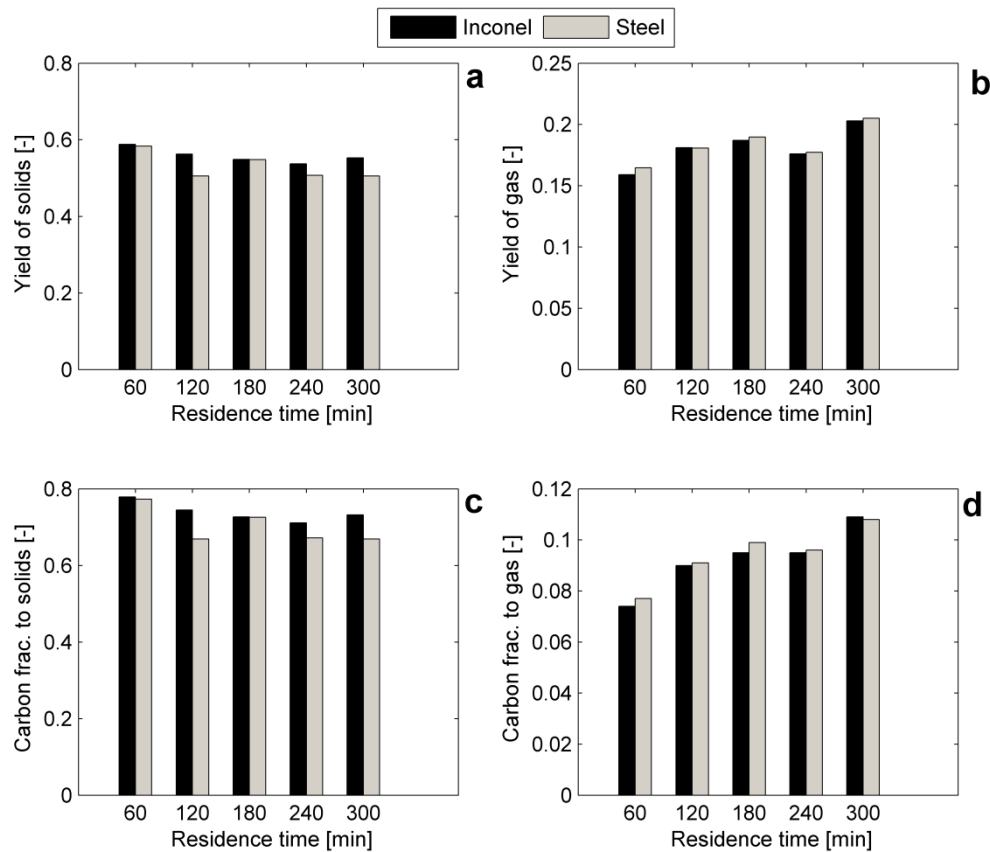
Figure 6.4 – Mass balance for hydrothermal char gasification. (a) Mass yields of solid; (b) Mass yields of gas; (c) Carbon balance in the solid; (d) Carbon balance in the gas.

Also in this case, most of the initial feed (around 60%) is converted to solid products. Gas yields are again quite low, ranging from 15% to 20% wt. Compared with Figure 6.2, higher solid yields and slightly lower gas yields are shown. This is indicative of the lower tendency of hydrothermal char to gasify, due to the lower content in volatile organic matter. No evident differences between the two reactor materials can be seen.

Data about the carbon balance, show that the largest part of the original carbon is still contained in the solid phase. The comparison with beech sawdust data clearly shows that, in the case of HTC, around 20% more carbon is found in the solid. At the same time, Figure 6.4d shows that the part of carbon passing to gas phase is lower than for beech sawdust, but the effect is less evident. This implies that the part of carbon going to the liquid phase should be much more reduced.
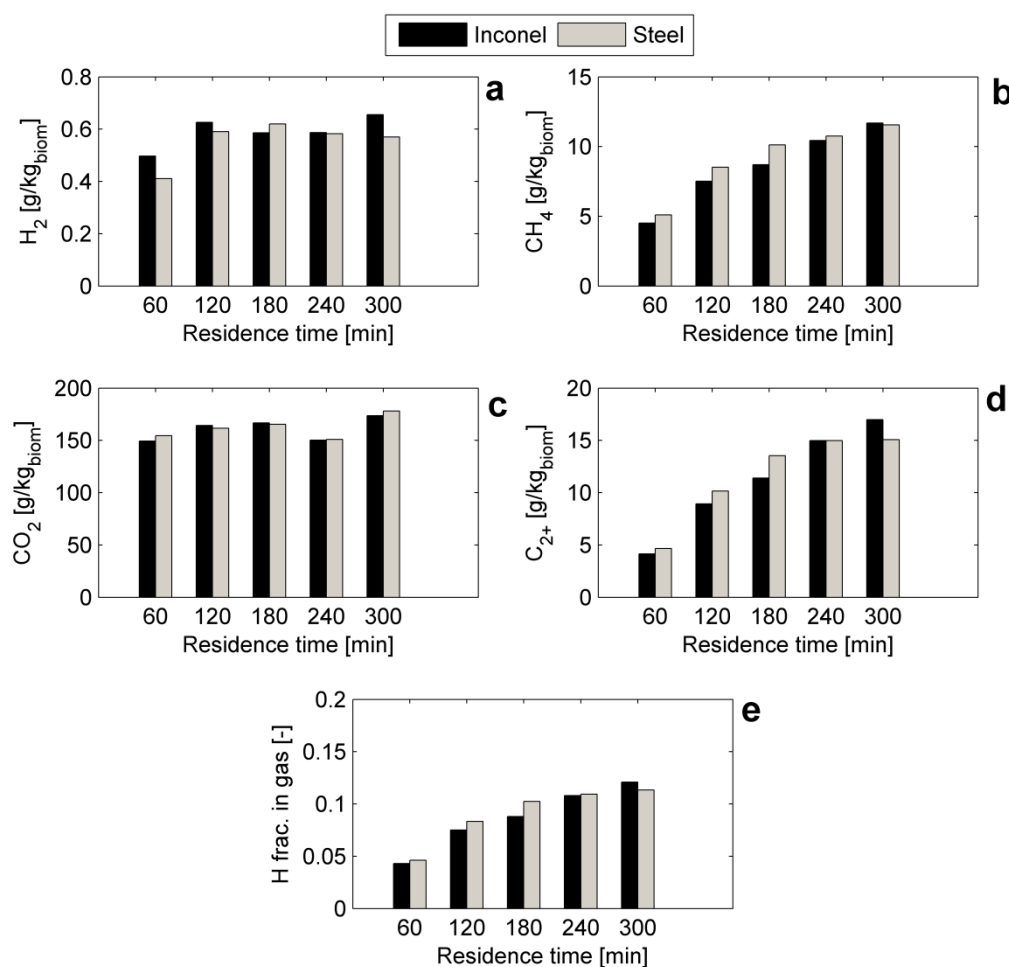
Figure 6.5 – Gas production for hydrothermal char gasification. (a) Hydrogen; (b) Methane; (c) Carbon dioxide; (d) C_{2+} hydrocarbons; (e) Hydrogen balance in the gas.

Figure 6.5 presents the production of the main permanent gases obtained through HTC gasification. It is possible to see that hydrogen seem to be increasing only at the beginning (60 minutes test). After that, from 120 to 300 minutes of residence time, it appears to be steady, also without any significant difference between the two materials. A similar trend is shown by carbon dioxide (Figure 6.5c), with a stable gas production of around 150 g/kg.

On the other hand, the production of hydrocarbon species differs considerably. Gas production is, indeed, always increasing for both methane (Figure 6.5b) and C_{2+} (Figure 6.5d) species. The trend is also confirmed by the H fraction found in the gas, which is always increasing. This reveals that HTC is preferably gasified into methane. However, this should be foreseeable, since thermodynamics affirms that a higher carbon content results in higher methane productions (see Chapter 2).

It can be also noticed that, in Figure 6.5, no chart concerning carbon monoxide was reported. This was done since, in all the performed experiments, CO was never found among the reaction products. Also when discussing about beech sawdust, it was highlighted how, practically, no CO was measured except for the lowest residence time (60 minutes). The fact CO is here completely absent tends to confirm the hypothesis that in real biomass gasification CO is not produced due to lower de-carbonlyation (Eq. 5.2) or to higher consumption for methanation (Eq. 5.4) or water-gas shift (Eq. 5.3).

6.4.2. Solid products observation

An interesting aspect concerning hydrothermal char gasification is represented by the direct observation of solids. In Figure 6.6, SEM images of the solid products deriving from HTC are shown after 1 hour and 5 hours of gasification. The images of the blank sample are shown as well.

The observation of the blank samples shows the nature of the material being gasified. HTC char is in the form of an intimately porous solid, with a very rough surface. This texture is typical of hydrothermal carbonization process, which enhances porosity. When a higher magnification is adopted (Figure 6.6b), it is possible to distinguish how the porous structure is obtained. The surface of the material is practically composed by several grains of char, with different dimension, resembling sort of "chips".
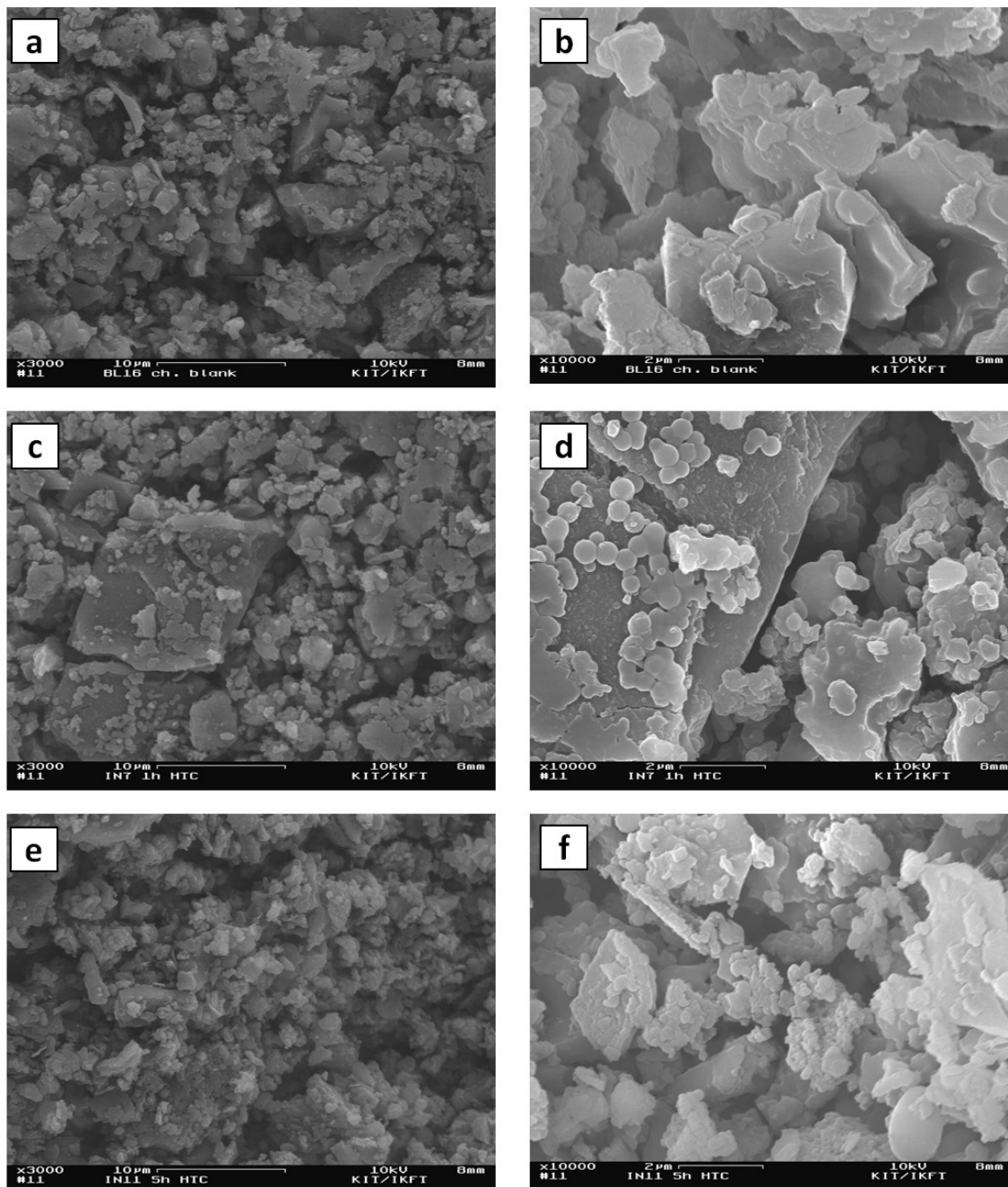
Figure 6.6 – SEM observation of the solid gasification products deriving from HTC char SCWG at 400°C, 30 MPa, 15% wt. (a) blank sample at 3000x magnification; (b) same at 10000x; (c) after 1 h reaction at 3000x; (d) same at 10000x; (e) after 5 h reaction at 3000x; (f) same at 10000x.

After 1 h reaction, some changes can be observed. The image taken at 3000x magnification does not differ from the homologue previous one in a significant way. The same structure as the blank material can be, indeed, observed. Things change when a 10000x magnification is adopted. In Figure 6.6d the already observed char structure can be seen.

However, it can be noticed that, on the pre-existent surface, many small spheres are now present, whose radius is extremely small (less than 1 μm).

The last couple of images report the situation after 5 h of reaction. Now, significant changes can be detected at both magnification scales. At 3000x (Figure 6.6e), the surface appears to be more "messy". In other words, unlike in the other figures some larger structures could be recognized, now the scene is dominated by very small char aggregates. Figure 6.6f shows, at higher magnification, the material structure. Small char "chips" are observed and the presence of the small spheres is even more enhanced than before.

In the literature, two forms of solids are usually distinguished when dealing with hydrothermal treatment. A first category is represented by "char". This expression, used in its strict sense, applies to those solid products originated by solid-solid reactions. Through these reactions, the solid material looses oxygen and hydrogen and, consequently, its carbon content increases. Char usually retains the structure of the initial biomass, eventually shrinking its dimensions. On the other hand, another class of solid products can be found, and they are referred as "coke". By this term, compounds deriving from polymerization of liquid intermediates are commonly indicated. According to its origin, coke is found as particles, since polymerization proceeds through a process of nucleation and successive growth [163].

Such conclusions apply also in the case here considered. Coke particles are produced and they stick on the surface of char. This one acts like a scaffold: the surface of char seems able to attach coke particles, perhaps through physical or chemical adsorption.

It can be also hypothesized another way of formation of the coke spheres, which comes from reactor quenching. During reaction, it is very probable that all the organic compounds are present in a single supercritical phase. If polymerization takes place to a large extent, solid particles can precipitate; otherwise, if the attained molecular mass is not enough high, they still keep dissolved in supercritical phase. As the system is quenched, their solubility is suddenly decreased, inducing precipitation. In other words, what we now observe as a solid could be present in the homogenous phase, at reaction conditions.

Furthermore, the solid surface was characterized by means of elemental composition. Through this technique, the relative carbon to oxygen ratio (C/O) was obtained for all the tests. The results are reported in Figure 6.7.
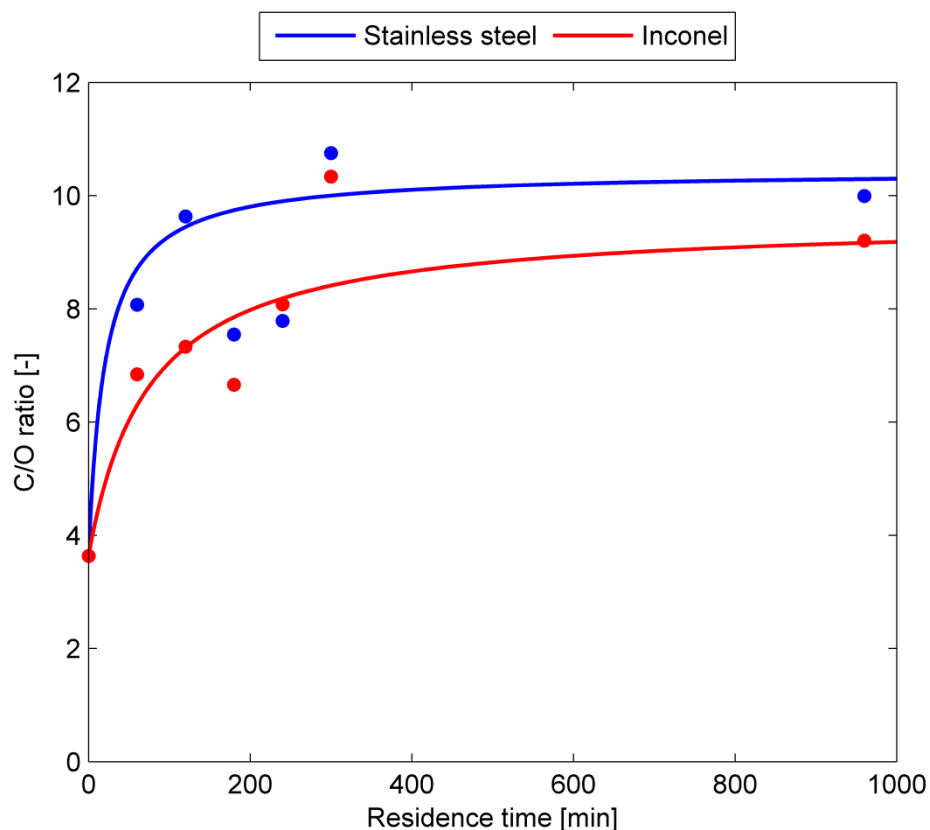
Figure 6.7 – Carbon to oxygen ratio in the produced solids from supercritical water gasification of corn silage hydrothermal char at 400°C and 25 MPa.

Apart from experimental errors, data show that, at the beginning of the SCWG treatment, C/O increases from an initial value of 3.63 to values well over 10 As long as the process proceeds, char gets more and more enriched in carbon.

A slight difference between the materials can be observed. The Inconel® reactor, indeed, seems to produce a char with higher carbon content. Although this effect is very contained, substantial agreement can be found if the carbon balance in the gas is considered (Figure 6.4d). Indeed, stainless steel gives rise to higher carbon yields in the gaseous phase than Inconel® 625. As a consequence, more carbon is held in the solid phase when Inconel® is present in the reaction environment.

6.5. Long-time testing

The four considered biomasses were all processed through long-time tests, involving 16 hours of reaction. These experimental runs were effectuated for two main reasons. First, it was interesting to understand what is the behavior of supercritical water gasification after

very long time, which is quite unknown in the literature. Moreover, by considering very long reaction times, it is possible to understand if the reactions involved in SCWG achieve the equilibrium conditions predicted by thermodynamics, or at least approach them. To this purpose, the possibility of adding a low cost catalyst (potassium carbonate) was tested.

6.5.1. Reaction products analysis

In Figure 6.8 the specific gas production is shown for each considered biomass, with and without catalyst, for both stainless steel and Inconel® 625 reactors. Non-catalytic tests with the ceramic reactor were also conducted (see Paragraph 6.2.2).
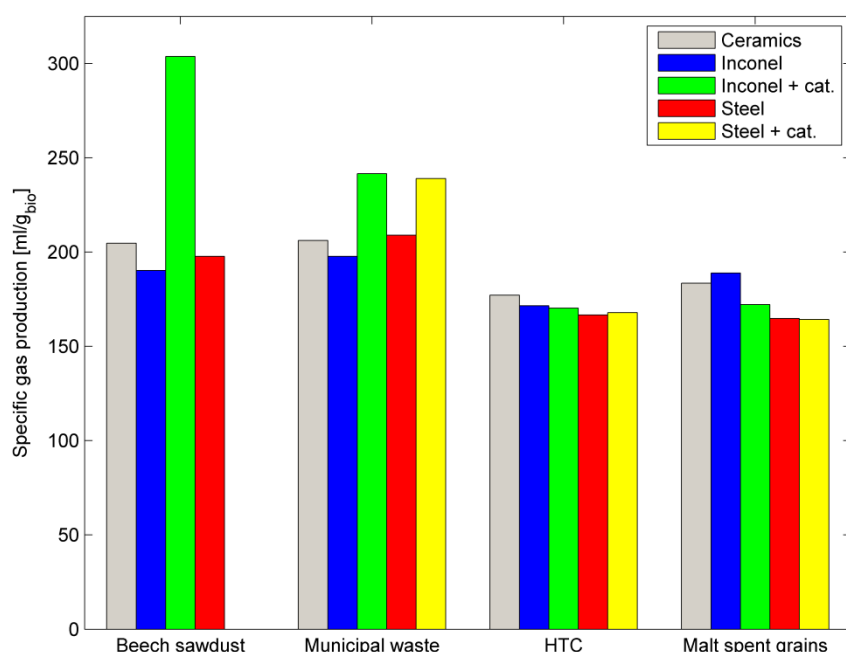
Figure 6.8 – Specific gas production for the supercritical water gasification of different biomasses. Temperature: 400°C, pressure: 300 bar, biomass concentration 15 % wt., residence time: 16 h.

Tests with the ceramic reactor showed that gasification yields obtained in such device are comparable to those measured in the Inconel® and stainless steel microautoclaves: no significant differences can be observed.

As far as the role of the catalyst is concerned, the frame that is depicted is quite peculiar. It was foreseeable that the addition of potassium carbonate to the reacting mixture could have the effect of increasing gas production. Anyway, such effect is evident only for some of the considered biomasses. In beech sawdust, it is possible to notice the large in-

crease, of ca. 50%, in gas production with respect to the non-catalyzed case. Unfortunately, it was not possible to obtain the datum for the catalyzed stainless steel experiment, since the reactor got broken twice while performing the tests. This was due probably to a particularly strong corrosive environment or to a large pressure increase caused by a large gas production. The situation is similar when municipal waste is taken into account. Here, the effect of the catalyst is less evident, but an increase in gas production in the order of 20% can still be noticed.

Generally, in the non-catalyzed case, stainless steel appears to yield more gas than Inconel®, even though such effect is very limited. On the other hand, when the catalyst is added the differences between the two materials almost tend to disappear.

Hydrothermal char and malt spent grains seem to behave in a different way. Here, the addiction of a catalyst to the reacting mixture does not appear to have any visible effect. The gas production is indeed constant: for malt spent grains it seems even to be smaller.

This apparent contradiction can be explained if the data about the production of the single gas species is observed. The specific production of hydrogen, methane and carbon dioxide are shown in Figure 6.9.
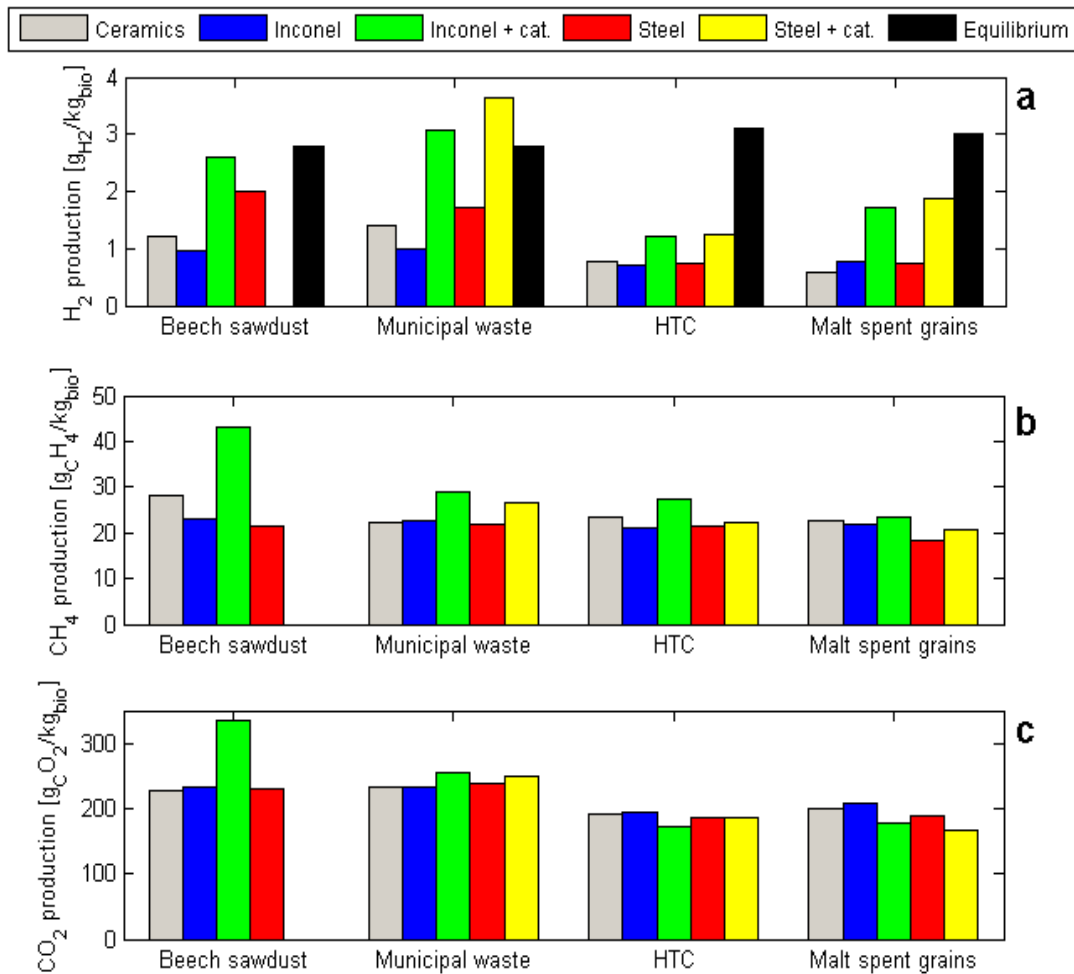
Figure 6.9 – Gas production for 16 h biomass supercritical water gasification. (a) Hydrogen; (b) Methane; (c) Carbon dioxide.

Now it is possible to have a clearer frame on the effect of catalysis during real biomass gasification, for both reactor wall effect and potassium carbonate addiction. Figure 6.8a shows the specific hydrogen production. The effect of K_2CO_3 is evident: when this salt is used, hydrogen production dramatically increases and is often doubled. The effect of the reactor material is now more evident, but only for beech sawdust and municipal waste. For the other two biomasses, no significant differences can be envisaged. Comparing the results of the ceramics reactor, it can be more evidently observed the specific effect of stainless steel in catalyzing hydrogen production. Hydrogen production in this typology of reactor appears to be slightly higher than Inconel®, perhaps due to two possible reasons: *(a)* the fact that Inconel® catalyzes methanation, thus consuming H_2; *(b)* a possible catalytic activity

played by aluminum oxide. The former hypothesis seems to be more plausible, since alumina is usually referred as an inert material at such conditions

The situation is substantially confirmed for methane (Figure 6.9b). Also in this case, the catalyst boosts gas production, though to a lower extent. Again, the effect is maximum for beech sawdust, then municipal waste and the others. It is interesting to notice that, as far as the reactor material is concerned, Inconel® 625 allows to have higher methane productions than stainless steel. This contributes to support the validity of the conclusions drawn for the case of glucose gasification: Inconel® favors methanation reactions, while stainless steel seems to be more effective in promoting water-gas shift.

Figure 6.9c shows the specific production of carbon dioxide. The general trends of Figure 6.8 are here confirmed: indeed, carbon dioxide is generally the most abundant product in the considered reaction conditions. The CO_2 trend thus "dominates" gas production and it is clearly reflected on the total gas production chart. For beech sawdust and municipal waste, potassium carbonate also increases CO_2 yields For the other two biomasses, the effect is neutral or even opposite.

The other permanent gases are here neglected, since they are produced in very low amount. It is worthy to state that carbon monoxide was not found in the final products, both with and without catalyst. This is quite reasonable, since the other tests conducted in batch micro-autoclaves clearly showed that, already after 4-5 hours of reaction, no CO can be found among the gaseous products (see Paragraphs 6.3.1 and 6.4.1)

Table 6.3 – Equilibrium yields of permanent gases for SCWG of 15% wt. biomasses at 400°C and 30 MPa ($g_{GAS}/g_{BIOMASS}$).

	Beech sawdust	Municipal waste	HTC	Malt spent grains
H_2	2.8	2.8	3.1	3
CH_4	358.3	345.4	539.5	415.7
CO_2	967.7	894	1238	938.3

An interesting aspect is represented by the comparison with the equilibrium data, obtained from a thermodynamic model based on Gibbs' free energy minimization [157] and reported in Table 6.3. It is possible to notice that equilibrium conditions are not achieved, even after 16 h experiments. This could be imputed to char formation, which represents an intermediate of very low reactivity under the experimental conditions applied and therefore

difficult to gasify once produced [104].

6.5.2. Ceramic reactor surface observation

An interesting information to be acquired is the direct observation of the surface of the ceramics reactor. This information is important, since it allows to understand if a ceramic inlay can resist the harsh reaction conditions typical of SCWG. Moreover, it can give an interesting insight about the physical-chemical phenomena involved in the process.

The SEM images of the ceramic inlay are shown in Figure 6.10. The blank sample (Figure 6.10a) shows the intimate structure of alumina: it looks like a sort of mosaic, with many irregular grains merged together. After reaction, the ceramic surface visually appeared black. SEM picture (Figure 6.10b) shows that very small spheres of char are present and they cover the surface almost uniformly.

After cleaning the reactor, we found that the carbon layer got detached in some points of the surface, which appeared bright white; these fragments were also observed with SEM. The surface (Figure 6.10c) exhibits the same structure as the blank sample, and no significant changes can be noticed. This suggests that alumina can resist to the experimental conditions considered. In the picture, anyway, ceramic grains are now more evident than before: their borders are, indeed, more accentuated and definite. Though no clear evidence could be deduced, it could be inferred that, over very long time scales, inter-grain corrosion could take place.

Figure 6.10d shows the carbon layer with higher magnification (3000x). It is possible to appreciate that the covering of the surface is represented by a lot of microspheres, with very regular shape. Though different dimensions could be observed, most of the spheres have a sub-micrometric diameter.
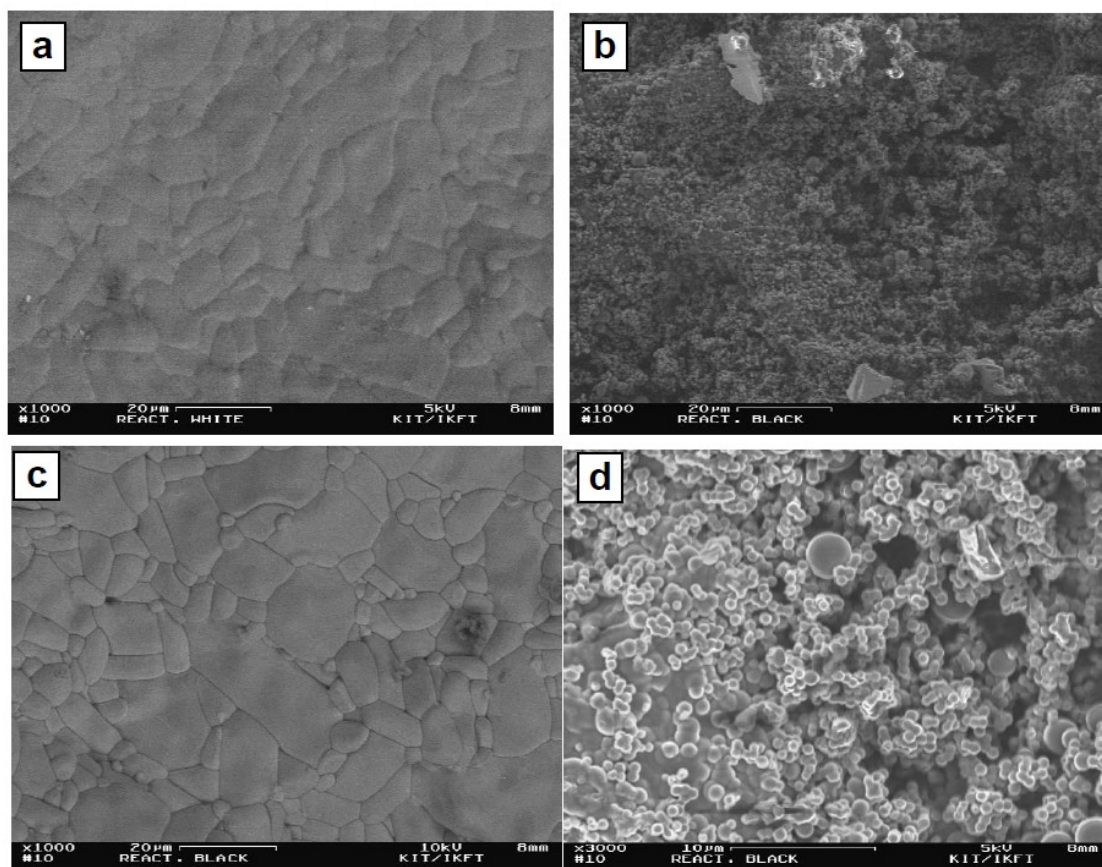
Figure 6.10 – SEM images of the ceramic inlay: (a) blank; (b) black area after reaction; (c) white area after reaction; (d) Higher magnification of char microspheres.

6.6. Conclusions

Real biomass gasification was carried out in this Chapter, providing different experimental tests.

First, the same methodology as Chapter 5 was applied to beech sawdust, analyzing the differences between this substrate and glucose. The analyses pointed out that the large differences of behavior between Inconel® 625 and stainless steel reactors are less evident in the case of beech sawdust. This was attributed to the higher complexity of real biomass compared to a model compound. In beech sawdust, indeed, lignin is also present; furthermore, minor ions, usually present in the ashes, can play a significant role in catalyzing some reactions, like water-gas shift, thus hiding the catalytic effect of the reactor walls.

Through an analysis of mass balances, it was found that water is here a reaction product rather than being a reactant. Furthermore, an important difference between glucose and beech sawdust gasification was found: the former produces significantly more water than

the latter during gasification. This was attributed to the process of hydrolysis, required to dissolve cellulose, which is absent for glucose, being it already solubilized.

Gasification of hydrothermal char is a new perspective in hydrothermal processing. Hydrothermal carbonization could be seen as a pretreatment for a subsequent supercritical water gasification. The results showed lower gas yields if compared to other biomass, due to the lower volatility of such kind of biomass. The observation of the solid residues after gasification gave important information about the way gasification proceeds. Further work should investigate the real profitability of such process as a competitive pretreatment in biomass gasification.

Finally, long-time tests showed that, even with very long reaction times, equilibrium composition are not achieved in the analyzed experimental conditions. This evidenced the presence of kinetics constraints which limit the production of gas from the considered biomasses. The role of K_2CO_3 as an effective catalyst for gasification was tested. Its relevance appeared to be decisive in boosting gas and hydrogen yields, especially for beech sawdust and municipal waste. In the other two biomasses, the effect of the catalyst was considerably lower. This suggests further investigations about the effectiveness of catalysis for non lignocellulosic and/or highly proteic biomass.

Chapter 7

Gasification in a Continuous Tubular Reactor

In the present Chapter, glucose/phenol mixtures were gasified in a continuous tubular reactor. This rector configuration allows overcoming some limitations of batch reactor testing, such as the impossibility to perform tests with a very short residence time and the scarcity of the sample gathered. Four solutions with increasing amounts of phenol, but with the same overall organic content (5% wt.), were tested over residence times ranging from 10 to 240 seconds. Results showed that the addition of phenol causes less gas production. The question whether this should be attributed to the minor glucose amounts fed or to an actual inhibition behavior of phenol is addressed. A reaction scheme for glucose SCWG is proposed, in order to explain the large amounts of methanol measured in the liquid phase.

7.1. Introduction

In the previous chapters, several experiments with model compounds and real biomass gasification were conducted in batch reactors. As it was possible to see, this methodology allows a great flexibility and is able to give important results with a relative ease of experimenting. Batch reactors are, thus, a very versatile methodology to carry out laboratory experiments. They can be very effective, for example, to understand how certain process parameters influence the products yields, what is the effect of a certain catalyst, and so on.

On the other hand, batch reactors also present important disadvantages. One of them is the transient state which, for such typology of apparatuses, cannot be eliminated in any way. Operations with batch autoclaves, indeed, require to load the reactor and then to heat it up to the desired temperature. The system is thus subjected to a thermal ramp, from room temperature to the final reaction conditions, which is variable according to reactor and heater geometries. This can affect results in a significant way, since the rapidity of heat transfer is an important factor in determining gasification yields [63].

Furthermore, during the thermal transient the system experiences several reaction conditions, starting subcritical, crossing the critical point and then arriving at supercritical state. It is very plausible that all these changes could affect the final results to some extent.

This transient state also makes difficult to state when reactions are really starting. Even though time measuring is started from the instant when the reactor has reached the desired temperature, reactions have already started before, at lower temperatures. This problem can be overcome if long residence times are considered, so that the transient state can be considered as negligible. On the contrary, if very short reaction times are required, it is impossible to perform experiments with meaningful results.

Operating with very small reactors can be an advantage, since reduced volumes translate into short heating up times. However, this also implies that very small amounts of reacting mixture must be loaded inside the reactor. Thus, very small amounts of samples are available and the analytic procedure is much more complicated: experimental errors are potentially higher and there is not enough sample to make a large number of analytical chemistry investigations and to check for measures reproducibility.

Moreover, batch processing is also quite distant from real-scale industrial processes, which most of times are carried out in continuous plants. In the previous Chapter 4, it was pointed out that the application of an industrial process for hydrogen production through SCWG should be a continuous plant. Thus, though batch experiments are extremely useful to understand many aspects of the process functioning, tests in a continuous plant are potentially able to give more interesting results.

It was decided to investigate the behavior of glucose/phenol mixtures. As it has been reported in the state of the art (Paragraph 1.4.1), the behavior of such mixtures is very important, being them representative for cellulose and lignin. In the literature, only a few works deal with the effects of phenol on carbohydrates gasification in supercritical water. One work was performed by Goodwin and Rorrer [48], who tested the influence of phenol on xylose (main constituent of hemicelluloses) gasification at 750°C, finding that phenol is very refractory to gasification. Another work was carried out by Weiss-Hortala *et al.* [47], who gasified glucose/phenol mixtures at 600°C. They noticed that phenol acts as an inhibitor for glucose gasification: when phenol was added to the mixture, glucose yielded less gas than when it was gasified alone.

In the present Chapter, the effect of phenol on glucose gasification was tested at 400°C and 25 MPa. Four different aqueous solutions were prepared, each with 5% wt. of feedstock. However, in each solution an increasing phenol content was adopted, from 0 (pure glucose) to 30%. This methodology was selected in order to understand how the presence of phenol affects gasification, without changing the total amount of organics fed

to the mixture, which would affect overall equilibria. Furthermore, the utilized glucose/phenol mixtures can be considered as models for real biomass, since the relative amounts of glucose and phenol reflect those of cellulose and lignin in a reasonable way. Liquid and gaseous products were sampled and analyzed, allowing obtaining useful information about phenol reactivity and reaction mechanisms in supercritical water.

7.2. Materials and methods

Experimental activities were performed in a continuous tubular plant operated at 400°C and 25 MPa. In this Paragraph, details concerning the experimental plant, preparation of the mixtures and analytical methods are provided.

7.2.1. Experimental apparatus

The experimental apparatus which was adopted for the research work is a continuous system for supercritical water gasification. A schematics of the plant is depicted in Figure 7.1.
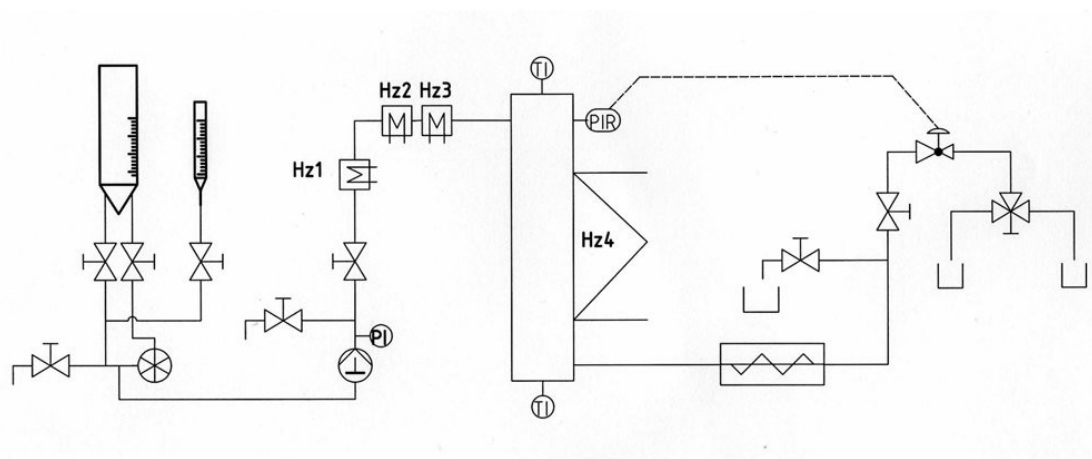
Figure 7.1 – Flowsheet of the experimental continuous plant.

The plant was fed by means of two bottles containing, respectively, de-mineralized water and the water solution to be gasified (glucose and phenol in different relative concentrations). The liquid was pumped by means of an HPLC (high performance liquid chromatography) pump to the desired pressure of 25 MPa and passed through a pre-heater, constituted by three electrical resistors of 250 W each (Hz1-3 in Figure 7.1), which were set at the constant temperature of 250°C.

After the pre-heater, the reacting mixture entered the reactor, constituted by a tube of stainless steel (length: 320 mm; internal diameter: 8.2 mm). The reactor was put inside a heater constituted by a ceramic shell with four electrical resistors of 500 W each. This heating element was able to increase the temperature of the fluid up to the reaction conditions. Inside the tube, a K-type thermocouple, located at approximately 150 mm along the axis of the reactor, was used to read the inner temperature.

After reaction, the reaction products were cooled down to room temperature by means of a cooling system constituted by a heat exchanger with a solution of water and ethylene-glycol at -1.0°C powered by a refrigeration cycle. Then, a back-pressure regulator TESCOM® 26-1721-24A was used to expand the products to room pressure. This apparatus was used to keep the pressure at the desired value in all the units upstream the valve itself. The valve was dynamically controlled by a compressed air regulator which received the inline measure of the reactor pressure through a digital manometer and drove the head of the back-pressure valve in order to keep the pressure constant at the desired set-point (25 MPa).

After expansion, a three-way valve allowed to select the desired output (liquid or gaseous) for sampling (see Paragraph 7.2.2).

Four different water/glucose/phenol mixtures were considered for gasification experiments. All of them presented a feedstock concentration of 5% on weight basis, the remaining part being Milli-Q water. However, the composition of the feedstock in each mixture was varied, with increasing phenol contents. Table 7.1 reports the composition of the mixtures used for the experiments.

Table 7.1 – Composition of the water/glucose/phenol mixtures used in the experiments (% wt.).

Mixture	Water	Glucose	Phenol
Glucose	95	5.0	0.0
Glu/Phen 10%	95	4.5	0.5
Glu/Phen 20%	95	4.0	1.0
Glu/Phen 30%	95	3.5	1.5

For preparation, glucose monohydrate (Merck KGaA, Germany) and phenol for synthesis, with purity higher than 99% (Merck-Schuchardt, Germany) were adopted.

7.2.2. Sampling procedure and analytics

The plant was started only with water, put under pressure, and then very slowly heated to the desired reaction temperature. This procedure was adopted in order to prevent the risk that during the heat up phase biomass could polymerize, causing rapid reactor clogging.

Only after the temperature had been reached (usually after 1-2 h), the feeding was switched from water to glucose/phenol solution by means of a three-way valve. After that, a waiting time between 20 and 150 minutes, depending on the flow rate, was observed before sampling, in order to reach steady-state conditions.

First, gas flow rate was measured by means of a water gasometer. Such measuring device was constituted by a bottle, filled with water, where another transparent pipe, open at one side and closed on the opposite one, was immerged. Gas was able to bubble inside this transparent pipe, starting to accumulate in the upper part of it and lowering the level of the liquid meniscus, in the very same way as the apparatus used in Paragraph 5.2.2 (see Figure 5.1). The time required to produce a fixed volume of gas was measured with a chronometer, allowing to obtain gas flow rate. For each experimental run, such measure was repeated at least four times in order to ensure reproducibility and to get a reasonable experimental error.

Through the same device, gas was also sampled for subsequent analyses. A gas trap, previously purged with nitrogen, was indeed connected to the aforementioned plastic tube. The gas stored in its upper part flew into the trap, from where it was taken by means of syringe and injected in GC apparatuses. The analytic procedure of the gas is the same procedure already presented in Paragraph 5.2.2.

After that, the three-way valve was switched and the liquid started dropping inside a sampling vial, allowing a straightforward sampling. The sample underwent several analyses to determine the amounts of several organic species, as well as other useful parameters such as phenol index, COD and TOC. Table 7.2 summarizes all the performed measurements and reports details about the analytical devices used to the purpose.

7.3. Results

In this Section, the results of the measuring operations are presented for both gaseous and liquid phases. In some cases, data were fitted by means of mathematical functions, in order to achieve useful quantitative information.

Table 7.2 – Measuring devices adopted to analyze the liquid phase deriving from SCWG of glucose/phenol mixtures in a continuous tubular plant.

Parameter	Measuring device
Phenol	HPLC VWR-Hitachi®
	Column: Phenomenex Kinetex PFP
	Detector DAD
	Eluent: 7.6 ml H_3PO_4 85% and 12 ml $NaHPO_4$
Furfural	HPLC Merck-Hitachi®
	Column: Merck LiChroCART® 250-4
	Detector UV 290 nm
	Eluent: water/acetonitrile 90/10
Organic acids - alcohols	HPLC Rezex ROA-Organic acids H+
	Detector UV 110 nm (organic acids) and RI-Detector L-7490 (alcohols)
	Eluent: 10^{-4} M H_2SO_4
Phenol index	Test LCK 346 by Hach Lange®
Glucose, fructose	Enzymatic test by R-Biopharm® according to DIN 10381
COD	Test LCK 314 by Hach-Lange® (Germany)
TOC	TOC analyzer DimaTOC® 2000 (Dimatec, Germany)

7.3.1. Gas phase

In Figure 7.2a, specific gas production per unit feedstock fed is shown. Results show that, evidently, as far as phenol is added to the reacting mixture, less gas is formed. For instance, if results at 180 s reaction time are considered, gas yields go from around 80 ml/g for pure glucose to around 50 ml/g when phenol constitutes the 30% of the feed.

Moreover, an observation of the experimental points trends allows distinguishing two main phases through which gasification takes place. A first phase up to, approximately, 60 seconds, where gas production increases approximately linearly. After that, gas production becomes more steady and the trend become substantially constant or only slightly increasing.
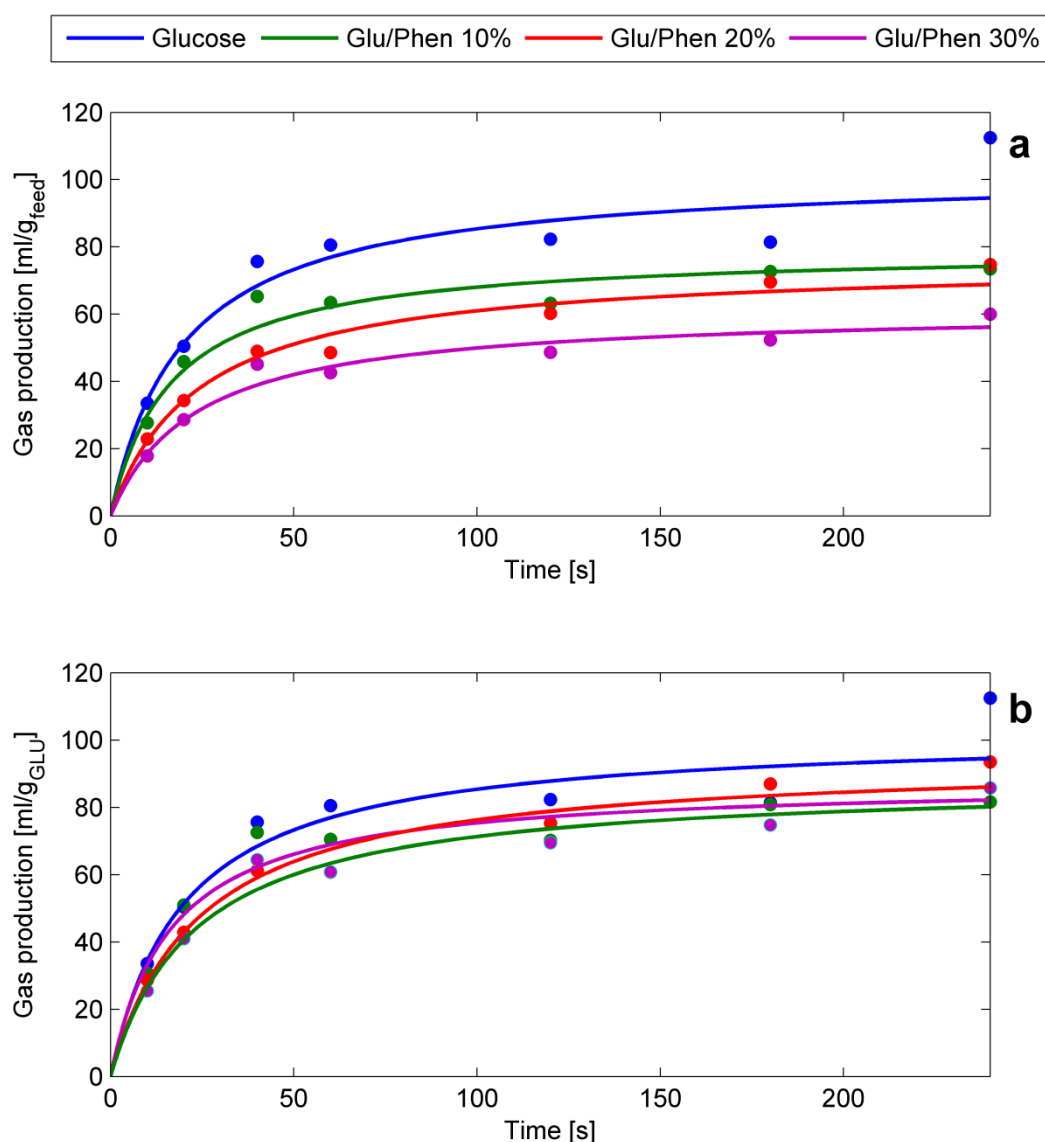
Figure 7.2 – Specific gas production for the supercritical water gasification of glucose/phenol mixtures at 400°C and 25 MPa. Points: experimental measures. Lines: fitting curves. (a) Gas production per unit feedstock; (b) Gas production per unit glucose fed.

In Figure 7.2b data of gas production are reported on a different scale. Rather than considering gas production per unit feedstock, now gas production was divided by the mass of glucose fed, thus neglecting phenol. Obviously, this leads to the same output for pure glucose, but it increases the values for the other mixtures. The rationale behind this choice is the hypothesis that only glucose contributes to gas production or, at least, it is the major contributor.

It can be seen that, though experimental points practically follow the same trend as in Figure 7.2a, now the differences among the points are extremely reduced. Despite quite small differences, different gas yields are conserved up to 60 seconds residence time. After then, the experimental points become very close to each other and they start to overlap.

By observing the trends of the experimental points, it was decided to fit them through a function of the form:

$$y = a\frac{bx}{c + bx}$$ (7.1)

Such function tends to zero as x tends to 0; when x tends to infinite, y tends to the constant value a, which is thus the maximum achievable gas yield. Curve fitting was performed by means of the software Microsoft Excel® through the minimization of the root of the mean squared percentage error (RMSPE). The results of this fitting are reported in Table 7.3.

Table 7.3 – Results of the fitting for specific gas production (per unit mass of organics fed) from supercritical water gasification of glucose/phenol mixtures at 400°C and 25 MPa.

Feedstock	a [ml g^{-1}]	b [s^{-1}]	c [-]	RMSPE [%]	Initial slope [ml g^{-1} s^{-1}]
Glucose	120.3	5.55E-4	0.011	9.21	5.163
Glu/Phen 10%	79.3	5.27E-5	8.74E-4	7.57	4.787
Glu/Phen 20%	75.7	-4.3E-4	-0.010	5.93	3.140
Glu/Phen 30%	61.6	-2.16	-50.50	6.71	2.641

A comparison among the values of the coefficient a allows to reproduce all the considerations made: the addition of phenol causes lower gas productions. In particular, for "Glu/Phen 30%" the maximum gas production is approximately half the one obtained for pure glucose experiments. Moreover, the derivative of equation 7.1 gives:

$$\frac{dy}{dx} = \frac{abc}{(c + bx)^2}$$ (7.2)

which tends to zero when x tends to infinite, but tends to ab/c when x tends to zero. This value represents the initial slope of the curve, that is the initial gas production rate. The initial slope is always decreasing as far as phenol concentration increases, testifying that gas production occurs with lower rates when less glucose is present in the mixture.

The same elaboration was performed for the gas productions referred to only glucose, thus without considering the phenol fed along with the mixture. The results are reported in Table 7.4.

Table 7.4 - Results of the fitting for gas production (per unit mass of glucose fed) from supercritical water gasification of glucose/phenol mixtures at 400°C and 25 MPa.

Feedstock	a [ml g^{-1}]	b [s^{-1}]	c [-]	RMSPE [%]	Initial slope [ml g^{-1} s^{-1}]
Glucose	102.3	5.54E-4	1.10E-2	9.22	5.163
Glu/Phen 10%	87.8	-2.87	-47.22	7.57	5.332
Glu/Phen 20%	94.7	-3.98E-3	-9.59E-2	5.93	3.927
Glu/Phen 30%	88.0	-2.17	-50.69	6.71	3.772

This time, looking at the values of *a*, it can be seen that less differences are found. Pure glucose still continues to yield the highest maximum amounts of gases, though now the difference is much lower than it used to be when results were referred to the whole organics fed. As far as the initial slope is concerned, glucose and the mixture at 10% phenol show similar values. The remaining two mixtures exhibit lower values.

In Figure 7.3 the measured gas composition is reported for each analyzed mixture, showing only the most significant permanent gases: H_2, CO, CH_4 and CO_2. Other gaseous species were not reported since their amounts were minimal.
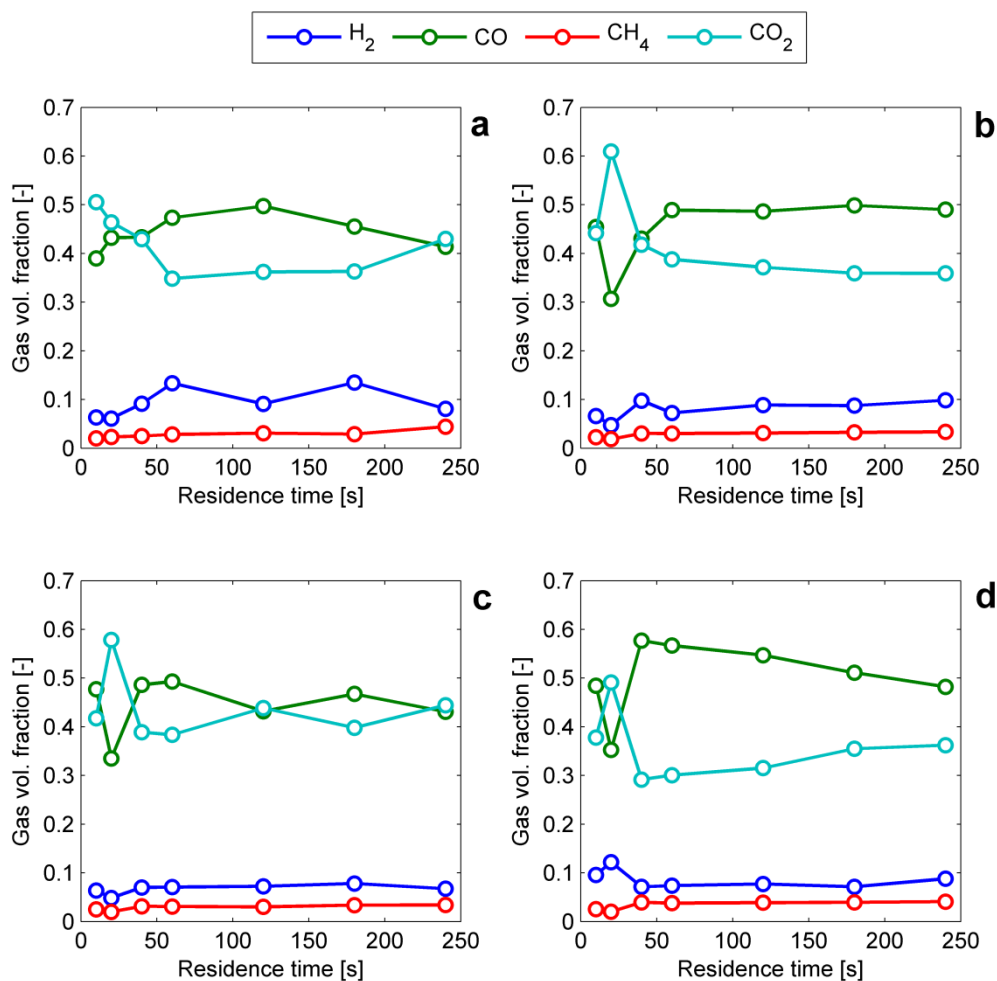
Figure 7.3 – Volume fractions of the gas produced in supercritical water gasification experiments at 400°C and 25 MPa. (a) Glucose; (b) Glu/Phen 10%; (c) Glu/Phen 20%; (d) Glu/Phen 30%.

A result which is immediately observable is that the produced gas is mainly composed by carbon monoxide and carbon dioxide. Taken together, they represent up to 90% of the whole volume sampled. However, their mutual ratios vary throughout the test. At very low residence times, the preferred product seems to be CO_2. Then, as long as the reaction takes place, CO is measured in increasing amounts, which overcome those of CO_2. CO trend appears approximately steady, unless for Glu/Phen 30% (Figure 7.3d). Here, CO trend is clearly decreasing and CO_2 appears to be symmetrical to it. A decreasing trend can be also observed in Figure 7.3a for pure glucose, for the highest residence times points. The trends of both CO and CO_2 show relatively large variations in the first part of the test, that is up to approximately 60 seconds and, then, they become almost constant. This tendency is in

line with what already said when commenting Figure 7.2, where higher gas production rates were observed during the first minute of reaction.

As far as hydrogen and methane are concerned, their sum is approximately 10% of the total gas volume. A trend for hydrogen can be only seen in Figure 7.3a, where H_2 is increasing in the first 60 seconds of reaction. An opposed tendency is shown in Figure 7.3d, with hydrogen concentration decreasing over time.

7.3.2. Liquid phase

Interesting results can be obtained through the analysis of the liquid phase. A first worth-noticing result is the conversion of phenol, which is defined according to the expression:

$$X = \frac{C_0 - C(t)}{C_0}$$

(7.3)

where $C(t)$ is the concentration of phenol at time t and C_0 is the initial phenol concentration. Results are displayed in Figure 7.4
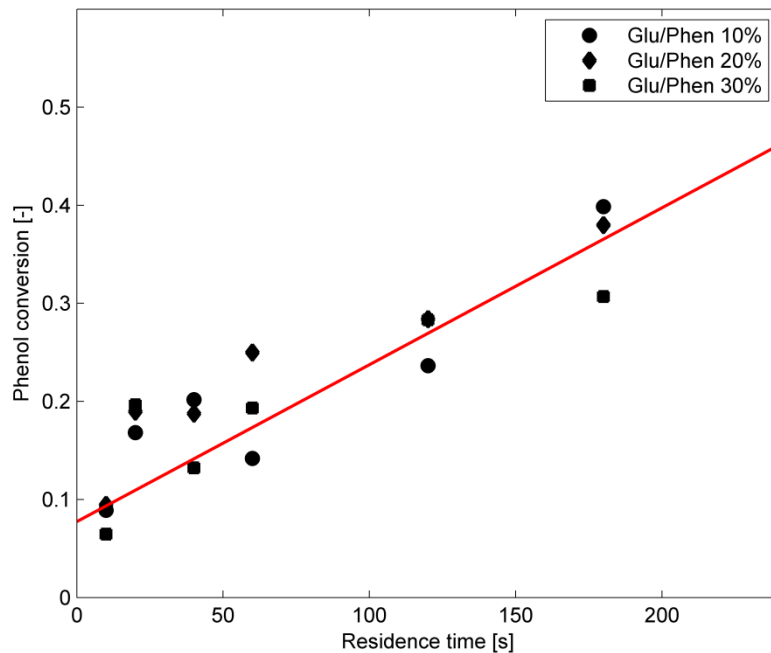
Figure 7.4 – Conversion of phenol as a function of residence time for supercritical water gasification of glucose/phenol mixture (T = 400°C, P = 25 MPa).

When increasing phenol concentrations are used in the reacting solution, this does not change phenol conversion in any way. Trends are indeed substantially coincident, thus al-

lowing to conclude that phenol concentration does not play any effect on phenol conversion. In other words, it can be affirmed that, at the considered experimental conditions, the reaction is zero-order with respect to phenol.

Data were fitted by means of a straight line, whose equation is:

$$X = 0.016t + 0.0775 \tag{7.4}$$

The slope of this line represents the reaction rate of phenol. Thus, phenol conversion rate can be estimated in 0.016 s^{-1}. However, such fitting would give phenol conversion of around 8% at time zero, which is obviously not possible. This implies that, in the first seconds of reaction, significant higher conversion rates are obtained.
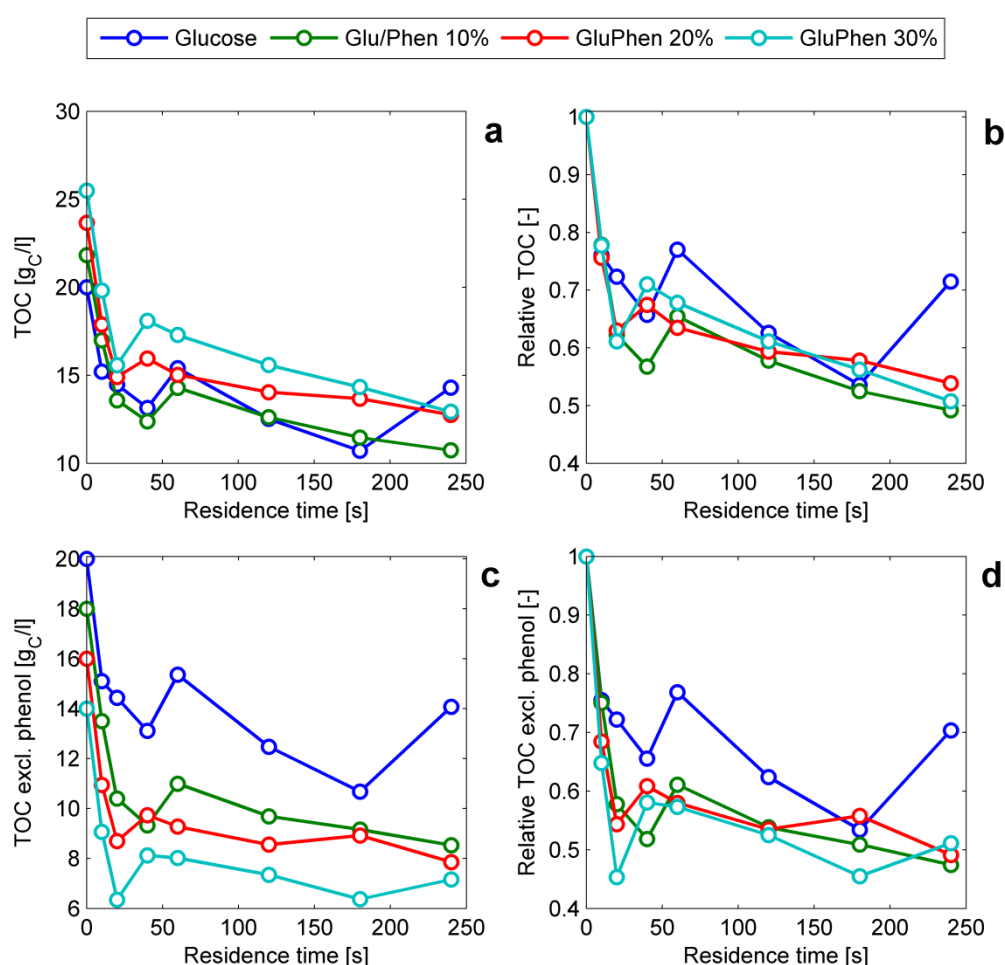
Figure 7.5 – Total organic carbon (TOC) measured in the liquid after supercritical water gasification of glucose/phenol mixtures at 400°C and 25 MPa. (a) Measured TOC; (b) Relative TOC; (c) TOC without phenol; (d) Relative TOC without phenol.

An important parameter in the liquid phase is represented by the total organic carbon (TOC). Through such parameter, it is possible to have an overall estimate of the organics present in the liquid phase, although it does not allow to define which substances are actually present.

In Figure 7.5a the trend of the measured TOC is reported. The trends are always decreasing and the measured values appear to be increasing as far as higher phenol concentrations are fed within the mixture. Figure 7.5b reports the same data but in relative form, that is after normalizing them by the TOC of the original solution fed. The three curves now appear to be much more grouped, showing similar TOC conversions. It is worth-noticing that TOC conversion exhibits two different slopes. Up to about 40 seconds, the trend is linear and quite steep, indicating very high removal rates. Then, for higher residence times, lower TOC removal rates are shown.

As witnessed by Figure 7.4, phenol conversion throughout the experiment is not very high, and it does not exceed 50%. As a result, high quantities of phenol are present in the liquid, deriving from the original feed. It was therefore decided to subtract the TOC due to phenol from the total TOC, thus obtaining a new parameter, which was plotted in Figure 7.5c. Now, much more difference is obtained: if the unreacted phenol is subtracted from TOC, the four curves are clearly distinguished. This can be a clear consequence of the fact that, if phenol is subtracted, less feedstock is fed as long as phenol concentration in the mixtures increases (and, as a consequence, glucose concentration decreases).

However, Figure 7.5d reports the same data normalized by the initial TOC without phenol. Results are quite different from the analogue non-dimensional parameter of Figure 7.5b. Here, the trends still look differentiated, even though normalization was performed. TOC removals are generally higher as far as phenol concentrations are increased. The solution with only glucose shows the lowest TOC removals conversion with respect to the other ones. Whenever this would suggest that more organic feedstock was gasified, a comparison with Figure 7.2 clearly shows that this higher TOC conversion does not imply higher gas productions, even if such productions are referred per unit glucose (Figure 7.2b). It is quite reasonable, thus, that the presence of phenol results in production of organic substances which were not considered in TOC and, possibly, created different phases not sampled with the liquid.

Finally, in Figure 7.6 the concentrations of some compounds found in the liquid are reported. The most significant compounds were selected, in order to show the possible reaction pathways.

In Figure 7.6a, b and c, 5-hydroxymethylfurfural (5-HMF), furfural and methylfurfural are shown. These compounds all belong to the family of furfurals, heterocyclic compounds with four atoms of carbon and one atom of oxygen, which are commonly produced from glucose gasification [40]. 5-HMF and furfural have similar trends. They are both decreasing with reaction time and the concentrations found in the liquid are proportional to glucose concentration in the feed. On the other hand, methylfurfural presents an opposite behavior, being it produced as far as the reaction takes place. However, concentrations of methylfurfural are much lower than those of the two previously considered compounds.

Figure 7.6d and Figure 7.6e show the trends of glyceraldehyde and glycolic acid. They are both intermediates of glucose decomposition in supercritical water, as it is possible to observe in Figure 1.7 and in [40, 43]. In particular, the mechanism of glucose degradation would foresee that glyceraldehyde is first produced from glucose hydrolysis and, then, glycolic acid is produced from its further degradation. The observed trends seem to confirm this hypothesis. Indeed, it is possible to notice that glyceraldehyde has a decreasing trend, and it tends to zero at higher residence times. On the other hand, glycolic acid shows an opposite behavior, as it is produced when glyceraldehydes is consumed. Some relevant differences can be observed among the different reacting mixtures. Again, the trends follow the glucose concentrations in the feed (except for Glu/Phen 10% in Figure 7.6d). By the way, it is remarkable observing that, in the experiments with only glucose, sensibly higher concentrations of both compounds were observed.

Figure 7.6f presents the production of methanol. First of all, it can be noticed that much higher concentrations are observed with respect to all the other compounds considered, even one order of magnitude greater. Methanol is thus the most present compound in the liquid phase, if phenol is not considered. Looking at the trend, the shape of the curve exhibits a maximum point occurring at around 60 seconds. Methanol is thus formed during the first phase of gasification and is consumed afterwards. Again, more methanol is produced when more glucose is present, but when pure glucose is adopted considerably higher methanol amounts are obtained, up to 22 g/l.
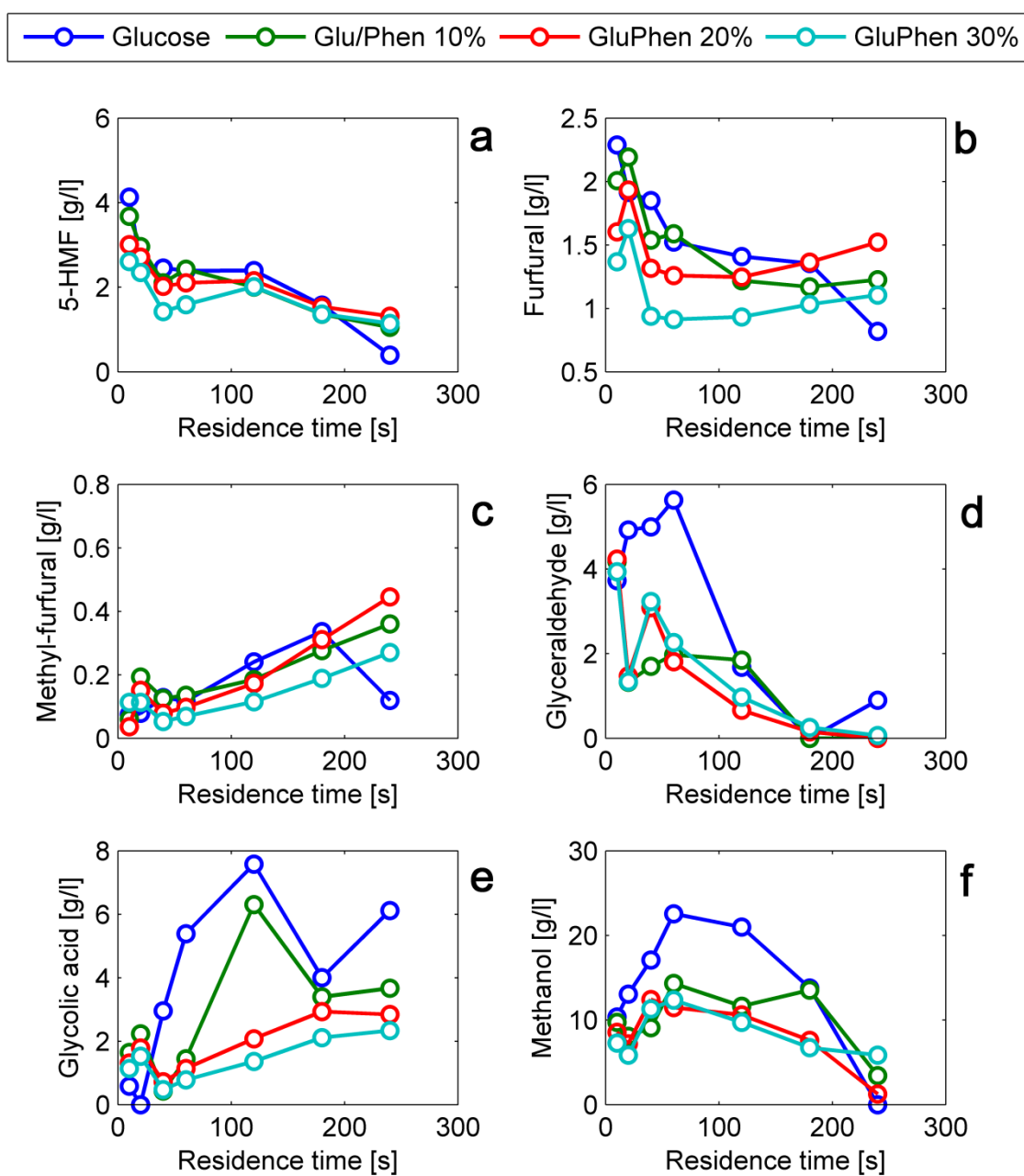
Figure 7.6 – Concentration of some compounds found in the liquid phase after supercritical water gasification of glucose/phenol mixtures at 400°C and 25 MPa. (a) 5-Hydroxymethylfurfural; (b) Furfural; (c) Methylfurfural; (d) Glyceraldehyde; (e) Glycolaldehyde; (f) Methanol.

7.4. Discussion

The results presented in Paragraph 7.3 enable to make some considerations about glucose and phenol gasification in supercritical water at 400°C. Such discussion involves the role of phenol as well as the general mechanism of glucose gasification.

A first thing to be discussed concerns quantitative gas production. It was shown that, by adding phenol to the reacting mixture, the amounts of gas produced become smaller. There are two possible ways to explain this phenomenon. A first possibility could be that phenol plays an active role in inhibiting gasification. Therefore, glucose conversion is not able to take place to the same extent as it would happen without phenol. On the other hand, the lower amounts of gas produced could be merely explained because less glucose is fed. In this case, phenol would not play any real inhibition role, but it should be only regarded as a sort of inert. Of course, the two approaches are not mutually exclusive.

Figure 7.2 would allow to say that the latter hypothesis has a higher weight. Indeed, when phenol is simply not considered and the results are referred only to the glucose fed (Figure 7.2b), the four series of experiments give much similar results, especially for longer reaction times. The inhibition effect is also present and it can also be appreciated (see Paragraph 7.3.1 and Table 7.4), but its effect appears to be smaller. This hypothesis is also supported by gas composition (Figure 7.3), which is practically the same for all the four considered feeds.

According to this theory, phenol is thus only an inert, not influencing gasification at all, or, at least, to a limited extent. It is not necessary that it is an inert in the strict sense of the word, i.e. a compounds not reacting at all. This definition would be contradicted by Figure 7.4, where it is clearly shown that phenol reacts, though with very low rates. Phenol could be considered as an inert only with respect to the gas formation, meaning that its reaction does not result in gaseous products.

However, the observation of TOC reveals that the addition of phenol causes an increase in phenol-free-TOC relative conversion (Figure 7.5d): organics are removed from the liquid phase with higher percentages. On the other hand, the specific production of gas does not show any higher gas production for glucose/phenol mixtures when compared to pure glucose. A possible explanation is that phenol actually interacts with some intermediates from glucose gasification to form some products which are not found in the liquid phase anymore. It could be that the interaction with such products is responsible for the formation of tar and char, which could have stick on the reactor and pipelines walls and, sometimes, were also visually observed (e. g. during reactor washing).

Besides the role of phenol, other considerations concern the general behavior of glucose gasification. First of all, all the performed tests showed that two periods can be distinguished. In a first period, up to until 40-60 seconds, very high reaction rates are observed.

Gas is produced with very high rates and, at the same time, TOC in the liquid is converted. During this phase, glucose is completely consumed.

A quite surprising result among those presented in Paragraph 7.3.2 is the high concentration of methanol that was measured in the liquid. It is known from the literature that the degradation of biomass and model compounds first results in small organic molecules (alcohols, aldehydes, carboxylic acids, etc.), which are later further converted into permanent gases or can polymerize to form tar and char [30, 174, 175]. To our knowledge, no work has reported that, at the considered reaction conditions, methanol is the most present compound in the liquid phase.
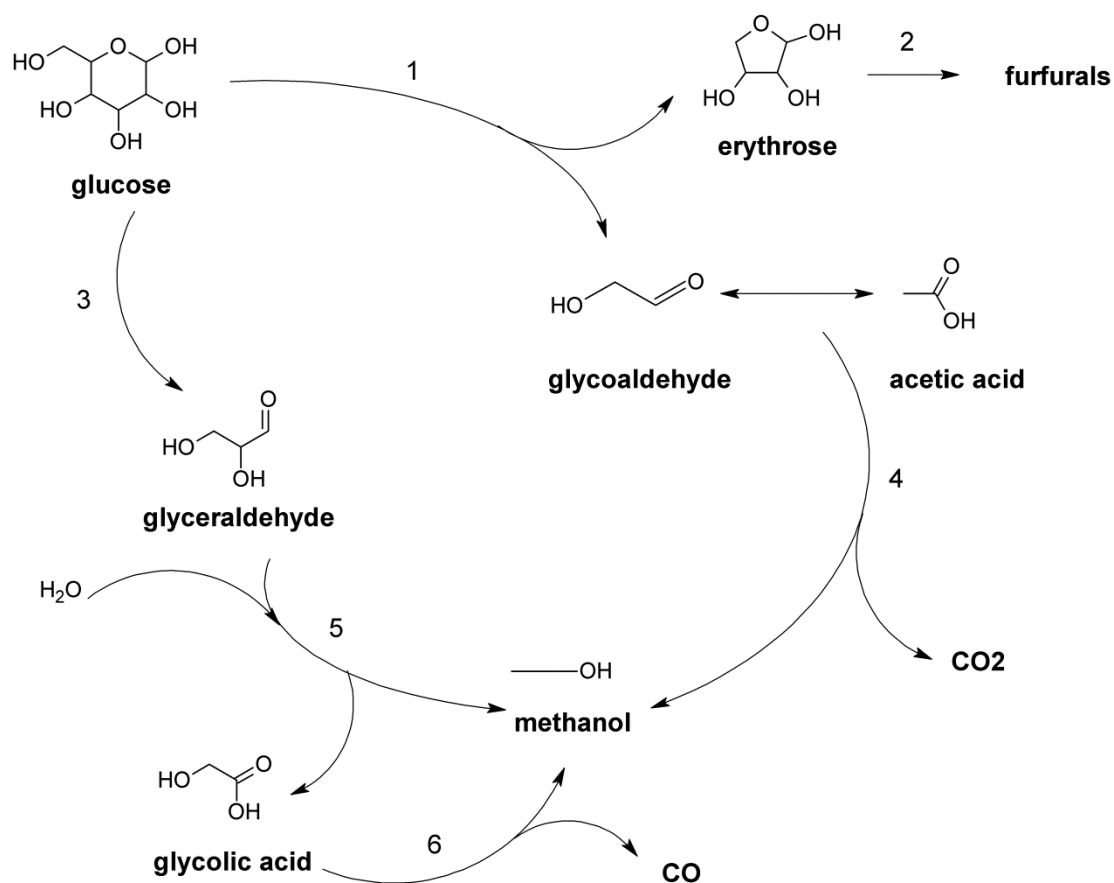
Figure 7.7 – Postulated mechanism for glucose decomposition in supercritical water and formation of methanol.

Methanol can be formed through different pathways. In Figure 7.7 a mechanism for glucose decomposition in supercritical water is reported. The formation of compounds deriving from glucose decomposition, such as glyceraldehyde, glycoaldehyde, erythrose and

glycolic acids (reactions 1, 2 and 3), was taken from the existing literature [40, 43, 44]. The other reactions were postulated, accounting for the typical reactions taking pa lace in hydrothermal environment. Three possible ways for methanol production are individuated. Methanol could be formed from reaction number 4, that is by decarboxylation of acetic acid (or glycoaldehyde), where such acid loses its carboxyl group producing CO_2. Another pathway is shown by reaction number 5, that is the hydrolysis of glyceraldehyde, forming methanol and one molecule of glycolic acid. Such compound can undergo a decarbonylation reaction, producing another molecule of methanol and CO. As it can be seen, methanol represents a very important node of the decomposition mechanism of glucose.

Formation of large amounts of methanol could be a possible explanation to the fact that reaction rates become very low after the first 40-60 seconds. Methanol, indeed, is known to be very difficult to gasify at 400°C. Boukis *et al.* report that, after 100 seconds at 400°C, a conversion of less than 22% was obtained by gasifying a methanol solution at 26.2% wt. [50]. Methanol gasification is usually performed at much higher temperatures (600-700°C), where very high rates are established and approximately total conversions can be achieved.

By the way, methanol refractoriness to gasification would suggest that its concentration should remain stable. Vice versa, the experimental trend shows a typical intermediate behavior, with an evident peak. This means that methanol, after being formed through the aforementioned reactions, is somehow depleted. Since TOC, from 60 seconds of residence times ahead, does not change in a relevant way and, at the same time, gas production is unchanged, the only conclusion can be that methanol is transformed into other soluble compounds, contributing to TOC.

In particular, it can be hypothesized that methanol interacts with other compounds, for example allowing them to polymerize. Since all the molecules of simplest organics were measured, and no increase was registered for them, methanol could have been involved in the formation of polymers. To this purpose, it is relevant to cite the studies of Chuntanapum and Matsumura, who gasified 5-HMF, a precursor of char [52, 53]. The authors observed that 5-HMF alone does not produce any char when gasified at supercritical conditions. They thus concluded that char is likely formed through the interaction of 5-HMF with small organic molecules in the liquid phase. Turning back to the present study, methanol could have been involved in polymerization reactions with 5-HMF (which is

consumed) and with other molecules. Further analyses are needed to proof this hypothesis in a rigorous way.

The fact that methanol is one of the most important intermediates opens new perspectives in the design of SCWG plants. The mechanisms of methanol reactions in supercritical water are indeed already known (see Chapter 3 and [51, 121, 172]). This would help finding the appropriate reaction conditions to enhance gasification yields. To this purpose, further research is needed, with special concern to the study of the interactions between methanol and other organic compounds originating from biomass degradation.

7.5. Conclusions

In the present Chapter, supercritical water gasification of glucose/phenol mixtures was executed in a continuous tubular plant at 400°C and 25 MPa. Four different mixtures with increasing phenol contents were tested over a range of reaction time between 10-240 seconds and both gaseous and liquid products were sampled and analyzed.

Results showed that phenol actually plays an inhibition role on glucose gasification, but this effect seems to be quite small. At the considered reaction conditions, it is more likely to think that phenol acts as a sort of inert with respect to gasification, being it converted mainly to liquid products. Phenol probably interacts with other organic molecules in the liquid phase also derived from glucose degradation. Further analyses are required to determine which compounds are actually formed.

The analysis of the liquid products revealed that methanol is a key intermediate in glucose SCWG at these experimental conditions. A reaction mechanism for glucose SCWG was postulated which stated that it could derive from many reaction pathways. This information could help to better understand the way SCWG works and to increase gasification yields, e. g. by using appropriate catalysts. Further work should be carried out to describe the reactions of methanol with other compounds that compete with gasification in the considered experimental conditions.

Final remarks

This work considered several aspects of supercritical water gasification of biomass, taking into account both mathematical modeling and experimental aspects.

The first part was devoted to mathematical modeling activities about SCWG, involving equilibrium, kinetics and process modeling.

A thermodynamic equilibrium model was developed for the supercritical water gasification of biomass, following the approach of non-stoichiometric modeling, based on Gibbs free energy minimization. The model was able to deal with the formation of two phases at equilibrium: solid and gas. The model allowed to foresee how the process parameters influence gasification outputs. A specific issue was to state if solid carbon can be foreseen at equilibrium. The model stated that, though this possibility can be realized for some kinds of biomass and for some operating conditions, carbon formation at equilibrium appears quite unlikely. Indeed, for most biomasses, relatively high concentrations would be required, while, in practice, much lower biomass-to-water ratios are adopted (usually up to 30% wt.). Since solids are actually formed, as the experiments reported in this thesis work clearly showed, it must be concluded that kinetics constraints prevent from achieving thermodynamic equilibrium.

The same thermodynamic model allowed performing an energy analysis of the SCWG of glycerol. Isothermal operations were considered, thus helping to quantify only the amount of energy needed to sustain the reaction itself. Results proved that SCWG can be an exothermal process. These results were very encouraging, since they revealed that SCWG can be an effective process and paved the way for the subsequent process modeling activities. The obtained results were the first to show SCWG energy behavior through a non-stoichiometric model and were published in [157].

On the basis of these results, a more comprehensive modeling activity was established, developing and simulating a possible layout for a full-scale SCWG plant. In this way not only the (exothermal) SCWG reaction was taken into account, but all the other unit operations, such as pumps, heat exchangers and separators, were considered. The results proved that a SCWG process aimed at hydrogen production can be self-sustainable, when biomass

concentrations above 15-25% wt. are adopted. This piece of information is very important for engineering the process, in order to go from its current laboratory scale application to a future possible industrial exploitation. The results of this study were published in [165].

Moreover, the analysis enabled to find the process bottlenecks. One of them is constituted by the heat exchangers, whose efficiency is crucial to ensure process sustainability and whose design should be thus carefully optimized for this application. Another point which revealed to be very important, is the energy demand for cooling down the reaction products, which turned out to be very significant. In the considered case a cooling tower was proposed, but the necessity to think about cooling is a new and original issue that has not been addressed by the existing literature. Other technical issues are those related to the pumpability of a solid-liquid mixture at high pressures, which could be technically difficult, and to ashes collection and disposal. All these possible bottlenecks should be further studied: their overcome would allow SCWG to be proposed as an effective way to produce hydrogen from waste biomass in a very efficient way.

Modeling activities were also performed in the field of kinetics. To this purpose, a novel approach was adopted, by considering elementary reaction models developed for combustion and supercritical water oxidation and applying them to SCWG of methanol. Though some discrepancies with the experimental data, possibly due also to unaccounted catalytic effects, one of the investigated models (the one by Webley and Tester) was able to describe methanol conversion in a quite satisfactory way. An analysis of such model revealed the possible reaction mechanisms involved in methanol SCWG, which were substantially confirmed by other experimental works. Furthermore, an upgrade of Webley and Tester's model was proposed, based on increasing the rates of certain groups of elementary reactions, obtaining a significant better agreement with the experimental results. Although this was only a sort of "exercise", this is a clue to address further efforts in methanol SCWG kinetics modeling, which, in the future, should also account for a better description of water-gas shift and methanation reactions, possibly including catalytic kinetics. The results of kinetics modeling were published in [172].

Though some relevant achievements were obtained in the field of SCWG modeling, many further outputs can be envisaged for future studies. In the field of thermodynamic modeling, it would be very interesting to pursue the so-called stoichiometric approach, thus hypothesizing a small number of reactions and calculating the equilibrium for them. This would help to understand the role of the single reaction steps involved in SCWG at varying

operating conditions. For kinetics modeling, much work should be still done, trying to describe the mechanisms of gasification of other organic compounds and real biomass. A useful tool would be to combine a simplified lumped model for the more complex substances and a more detailed approach to describe the transformations of the simpler ones, which could constitute a good tradeoff for technical purposes. Kinetics modeling could be also combined with computational fluid dynamics (CFD) techniques, thus creating a tool for reactor design. In this way, also process modeling could be upgraded, considering other issues like non-equilibrium conversions and thermal losses. Moreover, such approach would allow an estimate for plant costs, that is a parameter of outstanding importance for a practical realization of SCWG.

The second part of the work dealt with experimental tests. The activities were all conducted at 350-400°C with pressures of 25-30 MPa, that is in subcritical and slightly supercritical conditions. Tests were performed with different typologies of biomass and model compounds, using both continuous and discontinuous reactors.

Batch tests with glucose were carried out, using micro-reactors made of different metals: stainless steel and Inconel® 625. This allowed to test the catalytic effects of reactor walls, which turned out to have a significant influence on gasification yields. Stainless steel, indeed, tends to promote hydrogen production, while Inconel® is effective in catalyzing CO hydrogenation reactions leading to CH_4 and higher hydrocarbons. Moreover, at supercritical conditions much higher gas productions were recorded. Direct observation of metallic surfaces allowed to clarify the possible reasons why catalytic effects are still present even after several hours of exposure to the reaction environment.

The same tests were carried out with beech sawdust. Results confirmed the catalytic effects of the reactor walls, but the differences between stainless steel and Inconel® experiments were much slighter. An interesting analysis was the one conducted by performing the elemental balances. This procedure showed that gasification operations caused the production of water, which is thus a product rather than a reactant at the considered experimental conditions. However, higher water production resulted from glucose than from beech sawdust: this was attributed to the water uptake for cellulose hydrolysis.

Other real biomasses were also tested, possibly not belonging to the ligno-cellulosic ones. One of them is hydrothermal char (HTC) that is the product of another process based on hot compressed water: hydrothermal carbonization. Its usage as a gasification

feedstock is completely novel in the literature. Results showed that hydrothermal char from corn silage can be gasified, though with lower gas yields.

The batch reactor technology also allowed performing experiments with very long reaction times. This is useful in order to acquire data to be compared with the forecast of thermodynamic equilibrium models. A series of tests lasting for 16 hours was established, involving different substrates: beech sawdust, hydrothermal char, municipal waste and malt spent grains, a byproduct of brewery industry. Results showed that much lower gas productions than equilibrium are achieved. Differences between Inconel® and stainless steel were also highlighted, though they occurred at a different extent for each substrate. Potassium carbonate (K_2CO_3) was also tested as a catalyst and it caused higher gas productions. Its catalytic activity was mainly explicated in hydrogen production, where values comparable to equilibrium were achieved. Further work should be undertaken in order to better understand the catalytic mechanism and how this interacts with the nature of the biomass fed.

A perspective that was sketched out is the possibility to use a ceramic reactor, that is a vessel with an inner ceramic inlay, for supercritical water gasification of biomass. Such choice would allow to reduce corrosion issues which are common for hydrothermal processes and, consequently, the cost of the plants. Observation of the ceramic surface exposed to reactions in supercritical water did not show any significant change or corrosion phenomena, though a more systematic study should be established.

Turning back to model compounds, the behavior of glucose/phenol mixtures was tested. Such practice is very important, since glucose and phenol are the model compounds of cellulose and lignin, respectively. Such two macromolecules are the main constituents of ligno-cellulosic biomass, thus tests with glucose/phenol may help to understand the behavior of real biomass. To this purpose, both batch and continuous tests were conducted. Batch tests were performed with mixtures at 15% wt. (overall concentration of organics in water), whereof 75% was constituted by glucose and 25% by phenol. If compared with gasification of pure glucose, results showed a general reduction in gas yields and an increase in liquid organic products (TOC), though solid char productions were found to be substantially similar.

Glucose/phenol mixtures were also investigated in a continuous tubular reactor. Such configuration, indeed, is more similar to a possible real scale process and it allows reproducing short residence times, useful to investigate the reaction kinetics in the first minutes of reaction. Mixtures at 5% wt. of organic compounds, with increasing phenol concentra-

tions (up to 30%), were used. Results showed that the addition of phenol causes less gas production. Though a real inhibition effect is actually present, this phenomenon was attributed to the lower availability of glucose, assuming that phenol is substantially inert, with regard to gas production. Phenol actually gets converted, but with very low rates.

An interesting point resulting from these experiments was the analysis of the liquid species. Through it, it was possible to observe that methanol is one of the most abundant products in glucose SCWG at 400°C. A reaction mechanism, partly based on the existing literature and partly postulated, was proposed in order to justify methanol production. Further work is required to better prove these assumptions and to validate the model. On the other hand, the fact that methanol is an important node in glucose degradation mechanism enables to produce an even more detailed reaction scheme. In this work, indeed, methanol degradation pathways have been already explored through mathematical modeling and thus they are known. Combining the two models would allow producing a powerful mathematical tool to describe glucose degradation reactions in a more satisfactory way.

In conclusion, this work has presented several aspects of SCWG and it has shown that such technology is potentially very effective. Nevertheless, it is also quite complex, since there are many aspects to be considered at the same time. SCWG actually needs much more scientific and technical work in order to be fully developed and applied to real scale. My personal wish is that, in the future, further research could be devoted to supercritical water gasification, as well as to other hydrothermal processes for biomass energy valorization. Biomass can be the oil of tomorrow: refining it into energy means to ensure next generations the possibility of a clean and sustainable development, not depending on fossil resources anymore. Doubtless, this is a big challenge. A challenge that, in my opinion, we can win. One day.

References

[1]   Biomass Energy Centre of the UK. Available from: http://www.biomassenergycentre.org.uk/. Accessed on: January 2013.

[2]   E. Johnson, *Goodbye to carbon neutral: Getting biomass footprints right.* Environmental Impact Assessment Review, 2009. 29 (3): p. 165-168.

[3]   D.L. Klass, *Biomass for Renewable Energy, Fuels and Chemicals*. 1998, San Diego, California: Academic Press.

[4]   G. Maggio, G. Cacciola, *When will oil, natural gas, and coal peak?* Fuel, 2012. 98: p. 111-123.

[5]   C. Panoutsou, J. Eleftheriadis, A. Nikolaou, *Biomass supply in EU27 from 2010 to 2030.* Energy Policy, 2009. 37 (12): p. 5675-5686.

[6]   A.V. Bridgwater, *Renewable fuels and chemicals by thermal processing of biomass.* Chemical Engineering Journal, 2003. 91: p. 87-102.

[7]   L. Zhang, C. Xu, P. Champagne, *Overview of recent advances in thermo-chemical conversion of biomass.* Energy Conversion and Management, 2010. 51 (5): p. 969-982.

[8]   S. Hurley, H. Li, C. Xu, *Effects of impregnated metal ions on air/CO2-gasification of woody biomass.* Bioresource Technology, 2010. 101 (23): p. 9301-9307.

[9]   R.R. Davda, J.W. Shabaker, G.W. Huber, R.D. Cortright, J.A. Dumesic, *A review of catalytic issues and process conditions for renewable hydrogen and alkanes by aqueous-phase reforming of oxygenated hydrocarbons over supported metal catalysts.* Applied Catalysis B: Environmental, 2005. 56 (1-2): p. 171-186.

[10]   R.D. Cortright, R.R. Davda, J.A. Dumesic, *Hydrogen from catalytic reforming of biomass-derived hydrocarbons in liquid water.* Nature, 2002. 418: p. 964-967.

[11]   A. Tanksale, J.N. Beltramini, G.M. Lu, *A review of catalytic hydrogen production processes from biomass.* Renewable and Sustainable Energy Reviews, 2010. 14 (1): p. 166-182.

[12]   F. Bergius, *Die Anwendung hoher Drücke bei chemischen Vorgängen und eine Nachbildung des Entstehungsprozesses der Steinkohle*. 1913, Halle/Saale: Knapp.

[13]   S.M. Heilmann, H.T. Davis, L.R. Jader, P.A. Lefebvre, M.J. Sadowsky, F.J. Schendel, M.G. von Keitz, K.J. Valentas, *Hydrothermal carbonization of microalgae.* Biomass and Bioenergy, 2010. 34 (6): p. 875-882.

[14]   Z. Liu, A. Quek, S. Kent Hoekman, M.P. Srinivasan, R. Balasubramanian, *Thermogravimetric investigation of hydrochar-lignite co-combustion.* Bioresource Technology, 2012. 123: p. 646-652.

[15]   Z. Liu, A. Quek, S. Kent Hoekman, R. Balasubramanian, *Production of solid biochar fuel from waste biomass by hydrothermal carbonization.* Fuel, 2013. 103: p. 943-949.

[16]   M.-M. Titirici, M. Antonietti, *Chemistry and materials options of sustainable carbon materials made by hydrothermal carbonization.* Chemical Society Reviews, 2010. 39 (1): p. 103.

[17]   S.S. Toor, L. Rosendahl, A. Rudolf, *Hydrothermal liquefaction of biomass: A review of subcritical water technologies.* Energy, 2011. 36 (5): p. 2328-2342.

[18]   S. Xiu, A. Shahbazi, *Bio-oil production and upgrading research: A review.* Renewable and Sustainable Energy Reviews, 2012. 16 (7): p. 4406-4414.

[19]   Y. Kahn, G.K. Anderson, D.J. Elliott, *Wet oxidation of activated sludge.* Water Research, 1999. 33 (7): p. 1681-1687.

[20]   K.-H. Kim, S.-K. Ihm, *Heterogeneous catalytic wet air oxidation of refractory organic pollutants in industrial wastewaters: A review.* Journal of Hazardous Materials, 2011. 186 (1): p. 16-34.

[21]   B. Veriansyah, J.-D. Kim, *RETRACTED: Supercritical water oxidation for the destruction of toxic organic wastewaters: A review.* Journal of Environmental Sciences, 2007. 19 (5): p. 513-522.

[22]   M.D. Bermejo, M.J. Cocero, F. Fernández-Polanco, *A process for generating power from the oxidation of coal in supercritical water.* Fuel, 2004. 83 (2): p. 195-204.

[23]   M.J. Cocero, E. Alonso, M.T. Sanz, F. Fdz-Polanco, *Supercritical water oxidation process under energetically self-sufficient operation.* The Journal of Supercritical Fluids, 2002. 24: p. 37-46.

[24]   D. Knezevic, W.P.M. van Swaaij, S.R.A. Kersten, *Hydrothermal Conversion of Biomass: I, Glucose Conversion in Hot Compressed Water.* Industrial & Engineering Chemistry Research, 2009. 48: p. 4731-4743.

[25]   D. Knezevic, W. Van Swaaij, S. Kersten, *Hydrothermal conversion of biomass. II. Conversion of wood, pyrolysis oil, and glucose in hot compressed water.* Industrial & Engineering Chemistry Research, 2010. 49: p. 104-112.

[26]   P. Azadi, K.M. Syed, R. Farnood, *Catalytic gasification of biomass model compound in near-critical water.* Applied Catalysis A: General, 2009. 358 (1): p. 65-72.

[27]   P. Hasler, T. Nussbaumer, *Gas cleaning for IC engine applications from fixed bed biomass gasification.* Biomass and Bioenergy, 1999. 16: p. 385-395.

[28]   A.F. Kirkels, G.P.J. Verbong, *Biomass gasification: Still promising? A 30-year global overview.* Renewable and Sustainable Energy Reviews, 2011. 15 (1): p. 471-481.

[29]   A. Kruse, E. Dinjus, *Hot compressed water as reaction medium and reactantProperties and synthesis reactions.* The Journal of Supercritical Fluids, 2007. 39 (3): p. 362-380.

[30]   A. Chuntanapum, Y. Matsumura, *Char formation mechanism in supercritical water gasification process: a study of model compounds.* Industrial & Engineering Chemistry Research, 2010. 49: p. 4055-4062.

[31]   X.H. Hao, L.J. Guo, X. Mao, X.M. Zhang, X.J. Chen, *Hydrogen production from glucose used as a model compound of biomass gasified in supercritical water.* International Journal of Hydrogen Energy, 2003. 28: p. 55-64.

[32]   D. Bröll, C. Kaul, A. Krämer, P. Krammer, T. Richter, M. Jung, H. Vogel, P. Zehner, *Chemistry in supercritical water.* Angewandte Chemie International Edition, 1999. 38: p. 2999-3014.

[33]   M. Uematsu, E.U. Franck, *Static dielectric constant of water and steam.* Journal of Physical and Chemical Reference Data, 1980. 9 (4): p. 1291-1306.

[34]   H. Weingärtner, E.U. Franck, *Supercritical Water as a Solvent.* Angewandte Chemie International Edition, 2005. 44 (18): p. 2672-2692.

[35]   W.L. Marshall, E.U. Franck, *Ion product of water substance, 0-1000°C, 1-10,000 bars. New international formulation and its background.* Journal of Physical and Chemical Reference Data, 1981. 10 (2): p. 295-304.

[36]   M. Modell, *Gasification and liquefaction of forest products in supercritical water*, in *Fundamentals of Thermochemical Biomass*, R.P. Overend and T.A. Milne, Editors. 1985, Elsevier Applied Science Publisher: London, UK. p. 95.

[37]   Y. Matsumura, T. Minowa, B. Potic, S. Kersten, W. Prins, W. Vanswaaij, B. Vandebeld, D. Elliott, G. Neuenschwander, A. Kruse, M.J. Antal Jr, *Biomass gasification in near- and super-critical water: Status and prospects.* Biomass and Bioenergy, 2005. 29 (4): p. 269-292.

[38]   A. Loppinet-Serani, C. Aymonier, F. Cansell, *Current and Foreseeable Applications of Supercritical Water for Energy and the Environment.* ChemSusChem, 2008. 1 (6): p. 486-503.

[39]   A. Kruse, *Hydrothermal biomass gasification.* The Journal of Supercritical Fluids, 2009. 47 (3): p. 391-399.

[40]   B.M. Kabyemela, T. Adschiri, R.M. Malaluan, K. Arai, *Glucose and fructose decomposition in subcritical and supercritical water: Detailed reaction pathway, mechanisms, and kinetics.* Industrial & Engineering Chemistry Research, 1999. 38: p. 2888-2895.

[41]   X. Hao, L. Guo, X. Mao, X. Zhang, X.J. Chen, *Hydrogen production from glucose used as a model compound of biomass gasified in supercritical water.* International Journal of Hydrogen Energy, 2003. 28: p. 55-64.

[42]   I.-G. Lee, M.-S. Kim, S.-K. Ihm, *Gasification of glucose in supercritical water.* Industrial & Engineering Chemistry Research, 2002. 41: p. 1182-1188.

[43]   P. Williams, J. Onwudili, *Composition of products from the supercritical water gasification of glucose: A model biomass compound.* Industrial & Engineering Chemistry Research, 2005. 44: p. 8739-8749.

[44]   Y. Matsumura, S. Yanachi, T. Yoshida, *Glucose decomposition kinetics in water at 25 MPa in the temperature range of 448-673 K.* Industrial & Engineering Chemistry Research, 2006. 45: p. 1875-1879.

[45]   D. Hendry, C. Venkitasamy, N. Wilkinson, W. Jacoby, *Exploration of the effect of process variables on the production of high-value fuel gas from glucose via supercritical water gasification.* Bioresource Technology, 2011. 102 (3): p. 3480-3487.

[46]   R.F. Susanti, L.W. Dianningrum, T. Yum, Y. Kim, B.G. Lee, J. Kim, *High-yield hydrogen production from glucose by supercritical water gasification without added catalyst.* International Journal of Hydrogen Energy, 2012. 37 (16): p. 11677-11690.

[47]   E. Weiss-Hortala, A. Kruse, C. Ceccarelli, R. Barna, *Influence of phenol on glucose degradation during supercritical water gasification.* The Journal of Supercritical Fluids, 2010. 53 (1-3): p. 42-47.

[48]   A.K. Goodwin, G.L. Rorrer, *Conversion of xylose and xylose-phenol mixtures to hydrogen-rich gas by supercritical water in an isothermal microtube flow reactor.* Energy & Fuels, 2009. 23: p. 3818-3825.

[49]   J.B. Gadhe, R.B. Gupta, *Hydrogen production by methanol reforming in supercritical water: Suppression of methane formation.* Industrial & Engineering Chemistry Research, 2005. 44: p. 4577-4585.

[50]   N. Boukis, V. Diem, U. Galla, E. Dinjus, *Methanol reforming in supercritical water for hydrogen production.* Combustion Science and Technology, 2006. 178: p. 467-485.

[51]   J.G. van Bennekom, R.H. Venderbosch, D. Assink, H.J. Heeres, *Reforming of methanol and glycerol in supercritical water.* The Journal of Supercritical Fluids, 2011. 58 (1): p. 99-113.

[52]   A. Chuntanapum, Y. Matsumura, *Formation of tarry material from 5-HMF in subcritical and supercritical water.* Industrial & Engineering Chemistry Research, 2009. 48: p. 9837-3846.

[53]   A. Chuntanapum, T.L.-K. Yong, S. Miyake, Y. Matsumura, *Behavior of 5-HMF in Subcritical and Supercritical Water.* Industrial & Engineering Chemistry Research, 2008. 47: p. 2956-2962.

[54]   J.B. Müller, F. Vogel, *Tar and coke formation during hydrothermal processing of glycerol and glucose. Influence of temperature, residence time and feed concentration.* The Journal of Supercritical Fluids, 2012. 70: p. 126-136.

[55]   M.J. Antal, Jr., S.G. Allen, D. Schulman, X. Xu, R.J. Divilio, *Biomass gasification in supercritical water.* Industrial & Engineering Chemistry Research, 2000. 39: p. 4040-4053.

[56]   Y. Lu, L. Guo, C. Ji, X. Zhang, X. Hao, Q. Yan, *Hydrogen production by biomass gasification in supercritical water: A parametric study.* International Journal of Hydrogen Energy, 2006. 31 (7): p. 822-831.

[57]   L. Guo, Y. Lu, X. Zhang, C. Ji, Y. Guan, A. Pei, *Hydrogen production by biomass gasification in supercritical water: A systematic experimental and analytical study.* Catalysis Today, 2007. 129 (3-4): p. 275-286.

[58]   M.B. García Jarana, J. Sánchez-Oneto, J.R. Portela, E. Nebot Sanz, E.J. Martínez de la Ossa, *Supercritical water gasification of industrial organic wastes.* The Journal of Supercritical Fluids, 2008. 46 (3): p. 329-334.

[59]   A.G. Chakinala, D.W.F. Brilman, W.P.M. van Swaaij, S. Kersten, *Catalytic and non-catalytic supercritical water gasification of microalgae and glycerol.* Industrial & Engineering Chemistry Research, 2010. 49: p. 1113-1122.

[60]   A. Kruse, T. Henningsen, A. Sinag, J. Pfeiffer, *Biomass gasification in supercritical water: influence of the dry matter content and the formation of phenols.* Industrial & Engineering Chemistry Research, 2003. 42: p. 3711-3717.

[61]   A. Kruse, M. Faquir, *Hydrothermal Biomass Gasification – Effects of Salts, Backmixing and Their Interaction.* Chemical Engineering & Technology, 2007. 30 (6): p. 749-754.

[62]   J. Yanik, S. Ebale, A. Kruse, M. Saglam, M. Yuksel, *Biomass gasification in supercritical water: Part 1. Effect of the nature of biomass.* Fuel, 2007. 86 (15): p. 2410-2415.

[63]   Y. Matsumura, M. Harada, K. Nagata, Y. Kikuchi, *Effect of Heating Rate of Biomass Feedstock on Carbon Gasification Efficiency in Supercritical Water Gasification.* Chemical Engineering Communications, 2006. 193 (5): p. 649-659.

[64]   M. Mozaffarian, E.P. Deurwaarder, S.R.A. Kersten. *"Green gas" (SNG) production by supercritical gasification of biomass.* 2004. ECN. Report n. ECN-C--04-081.

[65]   C. Di Blasi, C. Branca, A. Galgano, D. Meier, I. Brodzinski, O. Malmros, *Supercritical gasification of wastewater from updraft wood gasifiers.* Biomass and Bioenergy, 2007. 31 (11-12): p. 802-811.

[66]   A. Demirbas, *Hydrogen-rich gas from fruit shells via supercritical water extraction.* International Journal of Hydrogen Energy, 2004. 29 (12): p. 1237-1243.

[67]   P.T. Williams, J. Onwudili, *Subcritical and supercritical water gasification of cellulose, starch, glucose and biomass waste.* Energy & Fuels, 2006. 20: p. 1259-1265.

[68] H. Schmieder, J. Abeln, N. Boukis, E. Dinjus, A. Kruse, M. Kluth, G. Petrich, E. Sadri, M. Schacht, *Hydrothermal gasification of biomass and organic wastes.* The Journal of Supercritical Fluids, 2000. 17: p. 145-153.

[69] Z.R. Xu, W. Zhu, M. Li, *Influence of moisture content on the direct gasification of dewatered sludge via supercritical water.* International Journal of Hydrogen Energy, 2012. 37 (8): p. 6527-6535.

[70] J. Penninger, M. Rep, *Reforming of aqueous wood pyrolysis condensate in supercritical water.* International Journal of Hydrogen Energy, 2006. 31 (11): p. 1597-1606.

[71] T. Minowa, F. Zhen, T. Ogi, *Cellulose decomposition in hot-compressed water with alkali or nickel catalyst.* The Journal of Supercritical Fluids, 1998. 13: p. 253-259.

[72] A. Kruse, D. Meier, P. Rimbrecht, M. Schacht, *Gasification of pyrocatechol in supercritical water in the presence of potassium hydroxide.* Industrial & Engineering Chemistry Research, 2000. 39: p. 4842-4848.

[73] A. Sinag, A. Kruse, V. Schwarzkopf, *Key compounds of the hydropyrolysis of glucose in supercritical water in the presence of K_2CO_3.* Industrial & Engineering Chemistry Research, 2003. 42: p. 3516-3521.

[74] J. Yanik, S. Ebale, A. Kruse, M. Saglam, M. Yüksel, *Biomass gasification in supercritical water: II. Effect of catalyst.* International Journal of Hydrogen Energy, 2008. 33 (17): p. 4520-4526.

[75] I. Rönnlund, L. Myréen, K. Lundqvist, J. Ahlbeck, T. Westerlund, *Waste to energy by industrially integrated supercritical water gasification – Effects of alkali salts in residual by-products from the pulp and paper industry.* Energy, 2011. 36 (4): p. 2151-2163.

[76] Y. Guan, A. Pei, L. Guo, *Hydrogen production by catalytic gasification of cellulose in supercritical water.* Frontiers of Chemical Engineering in China, 2008. 2 (2): p. 176-180.

[77] D. Xu, S. Wang, Y. Guo, X. Tang, Y. Gong, H. Ma, *Catalyzed Partial Oxidative Gasification of Phenol in Supercritical Water.* Industrial & Engineering Chemistry Research, 2011. 50 (8): p. 4301-4307.

[78] B. Potic, S. Kersten, W. Prins, W.P.M. Van Swaaij, *A high-throughput screening technique for conversion in hot compressed water.* Industrial & Engineering Chemistry Research, 2004. 43 (16): p. 4580-4584.

[79] S.R.A. Kersten, B. Potic, W. Prins, W.P.M. Van Swaaij, *Gasification of Model Compounds and Wood in Hot Compressed Water.* Industrial & Engineering Chemistry Research, 2006. 45 (12): p. 4169-4177.

[80] G.J. DiLeo, P.E. Savage, *Catalysis during methanol gasification in supercritical water.* The Journal of Supercritical Fluids, 2006. 39 (2): p. 228-232.

[81] F.L.P. Resende, P.E. Savage, *Effect of metals on supercritical water gasification of cellulose and lignin.* Industrial & Engineering Chemistry Research, 2010. 49: p. 2694-2700.

[82]   E.A. Youssef, E. Elbeshbishy, H. Hafez, G. Nakhla, P. Charpentier, *Sequential supercritical water gasification and partial oxidation of hog manure.* International Journal of Hydrogen Energy, 2010. 35 (21): p. 11756-11767.

[83]   Z. Fang, *Catalytic hydrothermal gasification of cellulose and glucose.* International Journal of Hydrogen Energy, 2008. 33 (3): p. 981-990.

[84]   A. Byrd, K. Pant, R. Gupta, *Hydrogen production from glycerol by reforming in supercritical water over Ru/Al₂O₃ catalyst.* Fuel, 2008. 87 (13-14): p. 2956-2960.

[85]   A.J. Byrd, S. Kumar, L. Kong, H. Ramsurn, R.B. Gupta, *Hydrogen production from catalytic gasification of switchgrass biocrude in supercritical water.* International Journal of Hydrogen Energy, 2011. 36 (5): p. 3426-3433.

[86]   A. May, J. Salvadó, C. Torras, D. Montané, *Catalytic gasification of glycerol in supercritical water.* Chemical Engineering Journal, 2010. 160 (2): p. 751-759.

[87]   Y. Lu, S. Li, L. Guo, X. Zhang, *Hydrogen production by biomass gasification in supercritical water over Ni/γAl₂O₃ and Ni/CeO₂-γAl₂O₃ catalysts.* International Journal of Hydrogen Energy, 2010. 35 (13): p. 7161-7168.

[88]   T. Sato, K. Inda, N. Itoh, *Gasification of bean curd refuse with carbon supported noble metal catalysts in supercritical water.* Biomass and Bioenergy, 2011. 35 (3): p. 1245-1251.

[89]   J. Gadhe, R. Gupta, *Hydrogen production by methanol reforming in supercritical water: Catalysis by in-situ-generated copper nanoparticles.* International Journal of Hydrogen Energy, 2007. 32 (13): p. 2374-2381.

[90]   D.C. Elliott, *Catalytic hydrothermal gasification of biomass.* Biofuels, Bioproducts and Biorefining, 2008. 2 (3): p. 254-265.

[91]   Y. Guo, S.Z. Wang, D.H. Xu, Y.M. Gong, H.H. Ma, X.Y. Tang, *Review of catalytic supercritical water gasification for hydrogen production from biomass.* Renewable and Sustainable Energy Reviews, 2010. 14: p. 334-343.

[92]   P. Azadi, R. Farnood, *Review of heterogeneous catalysts for sub- and supercritical water gasification of biomass and wastes.* International Journal of Hydrogen Energy, 2011. 36 (16): p. 9529-9541.

[93]   S. Letellier, F. Marias, P. Cezac, J.P. Serin, *Gasification of aqueous biomass in supercritical water: A thermodynamic equilibrium analysis.* The Journal of Supercritical Fluids, 2010. 51 (3): p. 353-361.

[94]   F. Marias, S. Letellier, P. Cezac, J.P. Serin, *Energetic analysis of gasification of aqueous biomass in supercritical water.* Biomass and Bioenergy, 2011. 35 (1): p. 59-73.

[95]   H. Tang, K. Kitagawa, *Supercritical water gasification of biomass: thermodynamic analysis with direct Gibbs free energy minimization.* Chemical Engineering Journal, 2005. 106 (3): p. 261-267.

[96]   Q. Yan, L. Guo, Y. Lu, *Thermodynamic analysis of hydrogen production from biomass gasification in supercritical water.* Energy Conversion and Management, 2006. 47 (11-12): p. 1515-1528.

[97]   F.A.P. Voll, C.C.R.S. Rossi, C. Silva, R. Guirardello, R.O.M.A. Souza, V.F. Cabral, L. Cardozo-Filho, *Thermodynamic analysis of supercritical water gasification of methanol, ethanol, glycerol, glucose and cellulose.* International Journal of Hydrogen Energy, 2009. 34 (24): p. 9737-9744.

[98]   J. Tester, P. Webley, H.R. Holgate, *Revised global kinetic measurements of methanol oxidation in supercritical water.* Industrial & Engineering Chemistry Research, 1993. 32: p. 236-239.

[99]   P. Webley, J. Tester, *Fundamental kinetics of methane oxidation in supercritical water.* Energy & Fuels, 1991. 5: p. 411-419.

[100]   P. Webley, *Kinetics of simple compounds in supercritical water.* PhD thesis. Massachussets Institute of Technology (MIT), 1990. Supervisor: J. Tester.

[101]   E.E. Brock, P.E. Savage, *Detailed chemical kinetics model for supercritical water oxidation of C_1 compounds and H_2.* AIChE Journal, 1995. 41 (8): p. 1874-1888.

[102]   H.J. Ederer, A. Kruse, C. Mas, K.H. Ebert, *Modelling of the pyrolysis of tert-butylbenzene in supercritical water.* The Journal of Supercritical Fluids, 1999. 15: p. 191-204.

[103]   W. Bühler, E. Dinjus, H.J. Ederer, A. Kruse, C. Mas, *Ionic reactions and pyrolysis of glycerol as competing reaction patways in near- and supercritical water.* The Journal of Supercritical Fluids, 2002. 22: p. 37-53.

[104]   F.L.P. Resende, P.E. Savage, *Kinetic model for noncatalytic supercritical water gasification of cellulose and lignin.* AIChE Journal, 2010. 56 (9): p. 2412-2420.

[105]   W. Feng, *Phase equilibria for biomass conversion processes in subcritical and supercritical water.* Chemical Engineering Journal, 2004. 98 (1-2): p. 105-113.

[106]   W. Feng, H. Vanderkooi, J. Deswaanarons, *Biomass conversions in subcritical and supercritical water: driving force, phase equilibria, and thermodynamic analysis.* Chemical Engineering and Processing, 2004. 43 (12): p. 1459-1467.

[107]   Y. Lu, L. Guo, X. Zhang, Q. Yan, *Thermodynamic modeling and analysis of biomass gasification for hydrogen production in supercritical water.* Chemical Engineering Journal, 2007. 131 (1-3): p. 233-244.

[108]   F.J. Gutiérrez Ortiz, P. Ollero, A. Serrera, S. Galera, *An energy and exergy analysis of the supercritical water reforming of glycerol for power production.* International Journal of Hydrogen Energy, 2012. 37 (1): p. 209-226.

[109]   T. Yoshida, Y. Matsumura, *Reactor development for supercritical water gasification of 4.9 wt% glucose solution at 673 K by using Computational Fluid Dynamics.* Industrial & Engineering Chemistry Research, 2009. 48: p. 8381-8386.

[110] A.K. Goodwin, G.L. Rorrer, *Modeling of Supercritical Water Gasification of Xylose to Hydrogen-Rich Gas in a Hastelloy Microchannel Reactor*. Industrial & Engineering Chemistry Research, 2011. 50 (12): p. 7172-7182.

[111] Y. Matsumura, Y. Shimizu, Y. Yamamura, T. Nakamura, H. Kiyonaga, T. Minowa, Y. Noda, *Biomass gasification power generation system*. 2008. Patent n. JP2008246343 (A).

[112] Y. Matsumura, Y. Shimizu, Y. Yamamura, T. Nakamura, H. Kiyonaga, T. Minowa, Y. Noda, *Biomass gasification method and biomass gasification system*. 2009. Patent n. JP2009149773 (A).

[113] Z. Wang, R. Yang, *Method for using sludge in supercritical water for preparing hydrogen-rich gas by continuous catalysis gasification*. 2008. Patent n. CN101327908 (A).

[114] L. Guo, J. Chen, X. Zhang, Y. Lu, P. Xiao, *Biomass supercritical water gasification hydrogen production system and method thermally driven by focusing solar energy*. 2009. Patent n. CN101597026 (A).

[115] L. Guo, Y. Lu, X. Zhang, *Biomass supercritical water gasification and multi-plate focusing heat supply coupling hydrogen production device and method* 2009. Patent n. CN101597027 (A).

[116] L. Guo, J. Chen, X. Zhang, Y. Lu, *Biomass supercritical water gasification hydrogen production absorption reactor thermally driven by solar energy* 2009. Patent n. CN101597025 (A).

[117] R.F. Susanti, B. Veriansyah, J.-D. Kim, J. Kim, Y.-W. Lee, *Continuous supercritical water gasification of isooctane: A promising reactor design*. International Journal of Hydrogen Energy, 2010. 35 (5): p. 1957-1970.

[118] N. Dahmen, E. Dinjus, A. Kruse, *De-gassing of biomasses with suppression of coke and tar formation and achievement of high hydrogen yields is achieved in a two-stage process using supercritical water*. 2006. Patent n. DE10259928 (B4).

[119] Y. Matsumura, *Fundamental design of a continuous biomass gasification process using a supercritical water fluidized bed*. International Journal of Hydrogen Energy, 2004. 29 (7): p. 701-707.

[120] Y. Lu, H. Jin, L. Guo, X. Zhang, C. Cao, X. Guo, *Hydrogen production by biomass gasification in supercritical water with a fluidized bed reactor*. International Journal of Hydrogen Energy, 2008. 33 (21): p. 6066-6075.

[121] J. Taylor, *Hydrogen production in a compact supercritical water reformer*. International Journal of Hydrogen Energy, 2003. 28 (11): p. 1171-1178.

[122] B. Potic, *Gasification of biomass in supercritical water*. PhD thesis. University of Twente, 2006. Supervisor: W.P.M. van Swaaij.

[123] B. Potic, S. Kersten, M. Ye, M. Vanderhoef, J. Kuipers, W. Vanswaaij, *Fluidization with hot compressed water in micro-reactors*. Chemical Engineering Science, 2005. 60 (22): p. 5982-5990.

[124] A.K. Goodwin, G.L. Rorrer, *Conversion of glucose to hydrogen-rich gas by supercritical water in a microchannel reactor.* Industrial & Engineering Chemistry Research, 2008. 47: p. 4106-4114.

[125] A.K. Goodwin, G.L. Rorrer, *Reaction rates for supercritical water gasification of xylose in a micro-tubular reactor.* Chemical Engineering Journal, 2010. 163 (1-2): p. 10-21.

[126] Y. Matsumura, *Evaluation of supercritical water gasification and biomethanation for wet biomass utilization in Japan.* Energy Conversion and Management, 2002. 43: p. 1301-1310.

[127] P.A. Marrone, G.T. Hong, *Corrosion control methods in supercritical water oxidation and gasification processes.* The Journal of Supercritical Fluids, 2009. 51 (2): p. 83-103.

[128] T. Richard, J. Poirier, C. Reverte, C. Aymonier, A. Loppinet-Serani, G. Iskender, E.-B. Pablo, F. Marias, *Corrosion of ceramics for vinasse gasification in supercritical water.* Journal of the European Ceramic Society, 2012. 32 (10): p. 2219-2233.

[129] A. Kruse, D. Forchheim, M. Gloede, F. Ottinger, J. Zimmermann, *Brines in supercritical biomass gasification: 1. Salt extraction by salts and the influence on glucose conversion.* The Journal of Supercritical Fluids, 2010. 53 (1-3): p. 64-71.

[130] L. Myréen, I. Rönnlund, T. Westerlund, *Integration of supercritical water gasification (SCWG) in pulp and paper production - A feasibility study of integration options.* Chemical Engineering Transactions, 2011. 25: p. 429-434.

[131] B.J. McBride, S. Gordon, M.A. Reno. *Coefficients for calculating thermodynamic and transport properties of individual species.* 1993. National Aeronautics and Space Administration (NASA). Report n. NASA TM-4513.

[132] M.A. McHugh, V.J. Krukonis, *Supercritical Fluid Extraction: Principles and Practice.* 1994, Stoneham, MA: Butterworth-Heinemann.

[133] M.-C. Henard. *Bio-Fuels. Impacts on Oilseed Industry following Biofuel Boom.* 2007. USDA Foreign Agricultural Service.

[134] U. Jena, K.C. Das, J.R. Kastner, *Effect of operating conditions of thermochemical liquefaction on biocrude production from Spirulina platensis.* Bioresource Technology, 2011. 102 (10): p. 6221-6229.

[135] ECN. *Phyllis, database for biomass and waste.* Available from: http://www.ecn.nl/phyllis. Accessed on: March 2011.

[136] N. Gao, A. Li, C. Quan, *A novel reforming method for hydrogen production from biomass steam gasification.* Bioresource Technology, 2009. 100 (18): p. 4271-4277.

[137] G.A. Olah, *Beyond Oil and Gas: The Methanol Economy.* Angewandte Chemie International Edition, 2005. 44 (18): p. 2636-2639.

[138] G.P. Smith, G.D. M., M. Frenlach, N.W. Moriarty, B. Eiteneer, M. Goldenberg, T. Bowman, R.K. Hanson, S. Song, W.C. Gardiner, V.V. Lissianski, Z. Qin. *GRI-Mech 3.0*. Available from: http://www.me.berkeley.edu/gri_mech.

[139] J.D. Taylor, C.M. Herdman, B.C. Wu, K. Wally, S.F. Rice, *Hydrogen production in a compact supercritical water reformer*. International Journal of Hydrogen Energy, 2003. 28 (11): p. 1171-1178.

[140] P.K. De Bokx, A.R. Balkenende, J.W. Geus, *The mechanism and kinetics of methane formation by decomposition of methanol on a Ni/SiO₂ catalyst*. Journal of Catalysis, 1989. 117: p. 467-484.

[141] C. Ratnasamy, J. Wagner, *Water Gas Shift Catalysis*. Catalysis Reviews, 2009. 51 (3): p. 325-440.

[142] K.-R. Hwang, C.-B. Lee, J.-S. Park, *Advanced nickel metal catalyst for water-gas shift reaction*. Journal of Power Sources, 2011. 196: p. 1349-1352.

[143] F. Vogel, J.L. DiNaro Blanchard, P.A. Marrone, S.F. Rice, P.A. Webley, W.A. Peters, K.A. Smith, J.W. Tester, *Critical review of kinetic data for the oxidation of methanol in supercritical water*. The Journal of Supercritical Fluids, 2005. 34 (3): p. 249-286.

[144] T. Sato, S. Kurosawa, R. Smith, T. Adschiri, K. Arai, *Water gas shift reaction kinetics under noncatalytic conditions in supercritical water*. The Journal of Supercritical Fluids, 2004. 29 (1-2): p. 113-119.

[145] E.D. Park, D. Lee, H.C. Lee, *Recent progress in selective CO removal in a H₂-rich stream*. Catalysis Today, 2009. 139: p. 280-290.

[146] B.W. Bradford, *The water-gas reaction in low-pressure explosions*. Journal of Chemical Society, 1933: p. 1557-1563.

[147] S. Sahoo, M.Ö. Seydibeyoğlu, A.K. Mohanty, M. Misra, *Characterization of industrial lignins for their utilization in future value added applications*. Biomass and Bioenergy, 2011. 35 (10): p. 4230-4237.

[148] K. Watanabe, S. Hino, N. Takahashi, *Responses of Activated Sludge to an Increase in Phenol Loading*. Journal of Fermentation and Bioengineering, 1996. 82 (5): p. 522-524.

[149] Q. Guan, C. Wei, H. Shi, C. Wu, X.-S. Chai, *Partial oxidative gasification of phenol for hydrogen in supercritical water*. Applied Energy, 2011. 88 (8): p. 2612-2616.

[150] Y. Watanabe, K. Tanaka, *Innovative sludge handling through pelletization/thickening*. Water Research, 1999. 33 (15): p. 3245-3252.

[151] L. Zhang, C. Xu, P. Champagne, *Energy recovery from secondary pulp/paper-mill sludge and sewage sludge with supercritical water treatment*. Bioresource Technology, 2010. 101 (8): p. 2713-2721.

[152] L. Fiori, M. Valbusa, D. Lorenzi, L. Fambri, *Modeling of the devolatilization kinetics during pyrolysis of grape residues.* Bioresource Technology, 2012. 103 (1): p. 389-397.

[153] L. Fiori, L. Florio, *Gasification and Combustion of Grape Marc: Comparison Among Different Scenarios.* Waste and Biomass Valorization, 2010. 1 (2): p. 191-200.

[154] R.H. Perry, D.W. Green, *Perry's Chemical Engineers' Handbook.* 6th Edition ed. 1984: McGraw Hill.

[155] ECN. *HYSEP, Hydrogen Separation Modules.* Available from: http://www.hysep.com. Accessed on: March 2012.

[156] A. Brunetti, G. Barbieri, E. Drioli, *A PEMFC and H_2 membrane purification integrated plant.* Chemical Engineering and Processing: Process Intensification, 2008. 47 (7): p. 1081-1089.

[157] D. Castello, L. Fiori, *Supercritical water gasification of biomass: Thermodynamic constraints.* Bioresource Technology, 2011. 102 (16): p. 7574-7582.

[158] M.J. De Kam, R. Vance Morey, D.G. Tiffany, *Biomass Integrated Gasification Combined Cycle for heat and power at ethanol plants.* Energy Conversion and Management, 2009. 50 (7): p. 1682-1690.

[159] EG&G Technical Services Inc. U.S. Department of Energy, Office of Fossil Energy. National Energy Technology Laboratories. *Fuel Cells Handbook.*

[160] The Energy Research Institute Departmente of Mechanical Engineering University of Cape Town. *Handbook - Refrigeration.* Available from: http://www.scribd.com/doc/16538132/Handbook-Refrigeration. Accessed on: March 2012.

[161] M.J. Antal Jr., S.G. Allen, D. Schulman, X. Xu, R.J. Divilio, *Biomass gasification in supercritical water.* Industrial & Engineering Chemistry Research, 2000. 39: p. 4040-4053.

[162] T.E. Boldrocchi. *Cooling Towers.* Available from: http://www.btetorri.com. Accessed on: March 2012.

[163] T. Karayıldırım, A. Sınağ, A. Kruse, *Char and Coke Formation as Unwanted Side Reaction of the Hydrothermal Biomass Gasification.* Chemical Engineering & Technology, 2008. 31 (11): p. 1561-1568.

[164] D. Yu, M. Aihara, M.J. Antal Jr., *Hydrogen Production by Steam Reforming Glucose in Supercritical Water.* Energy & Fuels, 1993. 7: p. 574-577.

[165] L. Fiori, M. Valbusa, D. Castello, *Supercritical water gasification of biomass for H2 production: Process design.* Bioresource Technology, 2012. 121: p. 139-147.

[166] W. Wagner, A. Pruß, *The IAPWS formulation 1995 for the thermodynamic properties of ordinary water substance for general and scientific use.* Journal of Physical and Chemical Reference Data, 2002. 31 (2): p. 387-535.

[167]   R. Muangrat, J.A. Onwudili, P.T. Williams, *Influence of alkali catalysts on the production of hydrogen-rich gas from the hydrothermal gasification of food processing waste.* Applied Catalysis B: Environmental, 2010. 100 (3-4): p. 440-449.

[168]   B. Smith R J, M. Loganathan, M.S. Shanta, *A Review of the Water Gas Shift Reaction Kinetics.* International Journal of Chemical Reactor Engineering, 2010. 8.

[169]   M. Kramer, M. Duisberg, K. Stowe, W. Maier, *Highly selective CO methanation catalysts for the purification of hydrogen-rich gas mixtures.* Journal of Catalysis, 2007. 251 (2): p. 410-422.

[170]   L.C. Loc, N.M. Huan, N.A. Gaidai, H.S. Thoang, Y.A. Agafonov, N.V. Nekrasov, A.L. Lapidus, *Kinetics of carbon monoxide methanation on nickel catalysts.* Kinetics and Catalysis, 2012. 53 (3): p. 384-394.

[171]   M. Watanabe, Y. Aizawa, T. Iida, C. Levy, T.M. Aida, H. Inomata, *Glucose reactions within the heating period and the effect of heating rate on the reactions in hot compressed water.* Carbohydrate Research, 2005. 340 (12): p. 1931-1939.

[172]   D. Castello, L. Fiori, *Kinetics modeling and main reaction schemes for the supercritical water gasification of methanol.* The Journal of Supercritical Fluids, 2012. 69: p. 64-74.

[173]   M. Sasaki, B.M. Kabyemela, R.M. Malaluan, S. Hirose, N. Takeda, T. Adschiri, K. Arai, *Cellulose hydrolysis in subcritical and supercritical water.* The Journal of Supercritical Fluids, 1998. 13: p. 261-268.

[174]   C. Promdej, Y. Matsumura, *Temperature Effect on Hydrothermal Decomposition of Glucose in Sub- And Supercritical Water.* Industrial & Engineering Chemistry Research, 2011. 50 (14): p. 8492-8497.

[175]   Z. Fang, R.L. Smith, J.A. Kozinski, T. Minowa, K. Arai, *Reaction of d-glucose in water at high temperatures (410°C) and pressures (180MPa) for the production of dyes and nano-particles.* The Journal of Supercritical Fluids, 2011. 56 (1): p. 41-47.